

# Advances

## in Clinical and Experimental Medicine

MONTHLY ISSN 1899-5276 (PRINT) ISSN 2451-2680 (ONLINE)

[www.advances.umw.edu.pl](http://www.advances.umw.edu.pl)

2022, Vol. 31, No. 6 (June)

Impact Factor (IF) – 1.727

Ministry of Science and Higher Education – 70 pts

Index Copernicus (ICV) – 166.39 pts



WROCLAW  
MEDICAL UNIVERSITY

Advances  
in Clinical and Experimental  
Medicine



# Advances in Clinical and Experimental Medicine

ISSN 1899-5276 (PRINT)

ISSN 2451-2680 (ONLINE)

[www.advances.umw.edu.pl](http://www.advances.umw.edu.pl)

**MONTHLY 2022**  
**Vol. 31, No. 6**  
**(June)**

Advances in Clinical and Experimental Medicine (*Adv Clin Exp Med*) publishes high-quality original articles, research-in-progress, research letters and systematic reviews and meta-analyses of recognized scientists that deal with all clinical and experimental medicine.

## Editorial Office

ul. Marcinkowskiego 2–6  
50-368 Wrocław, Poland  
Tel.: +48 71 784 12 05  
E-mail: [redakcja@umw.edu.pl](mailto:redakcja@umw.edu.pl)

## Publisher

Wrocław Medical University  
Wybrzeże L. Pasteura 1  
50-367 Wrocław, Poland

Online edition is the original version  
of the journal

## Editor-in-Chief

Prof. Donata Kurpas

## Deputy Editor

Prof. Wojciech Kosmala

## Managing Editor

Marek Misiak, MA

## Statistical Editors

Wojciech Bombała, MSc  
Katarzyna Giniewicz, MSc Eng.  
Anna Kopszak, MSc  
Dr. Krzysztof Kujawa

## Manuscript editing

Marek Misiak, MA, Jolanta Krzyżak, MA

## Scientific Committee

Prof. Sabine Bährer-Kohler  
Prof. Antonio Cano  
Prof. Breno Diniz  
Prof. Erwan Donal  
Prof. Chris Fox  
Prof. Naomi Hachiya  
Prof. Carol Holland  
Prof. Markku Kurkinen  
Prof. Christos Lionis

Prof. Raimundo Mateos  
Prof. Zbigniew W. Ras  
Prof. Jerzy W. Rozenblit  
Prof. Silvina Santana  
Prof. James Sharman  
Prof. Jamil Shibli  
Prof. Michal Toborek  
Prof. László Vécsei  
Prof. Cristiana Vitale

## Section Editors

### Anesthesiology

Prof. Marzena Zielińska

### Basic Sciences

Prof. Iwona Bil-Lula  
Prof. Bartosz Kempisty  
Dr. Anna Lebedeva  
Dr. Mateusz Olbromski  
Dr. Maciej Sobczyński

### Clinical Anatomy, Legal Medicine, Innovative Technologies

Prof. Rafael Boscolo-Berto

### Dentistry

Prof. Marzena Dominiak  
Prof. Tomasz Gedrange  
Prof. Jamil Shibli

### Dermatology

Prof. Jacek Szepietowski

### Emergency Medicine, Innovative Technologies

Prof. Jacek Smereka

### Gynecology and Obstetrics

Prof. Olimpia Sipak-Szmigiel

### Histology and Embryology

Prof. Marzena Podhorska-Okołów

### Internal Medicine

#### Angiology

Dr. Angelika Chachaj

#### Cardiology

Prof. Wojciech Kosmala  
Dr. Daniel Morris

### Endocrinology

Prof. Marek Bolanowski

### Gastroenterology

Prof. Piotr Eder

Assoc. Prof. Katarzyna Neubauer

### Hematology

Prof. Andrzej Deptała

Prof. Dariusz Wołowicz

### Nephrology and Transplantology

Assoc. Prof. Dorota Kamińska

Assoc. Prof. Krzysztof Letachowicz

### Pulmonology

Prof. Anna Brzecka

### Microbiology

Prof. Marzenna Bartoszewicz

Assoc. Prof. Adam Junka

### Molecular Biology

Dr. Monika Bielecka

Prof. Jolanta Saczko

### Neurology

Assoc. Prof. Magdalena Koszewicz

Assoc. Prof. Anna Pokryszko-Dragan

Dr. Masaru Tanaka

### Neuroscience

Dr. Simone Battaglia

### Oncology

Prof. Andrzej Deptała

Dr. Marcin Jędryka

### Gynecological Oncology

Dr. Marcin Jędryka

### Orthopedics

Prof. Paweł Reichert

### Otolaryngology

Assoc. Prof. Tomasz Zatoński

### Pediatrics

#### Pediatrics, Metabolic Pediatrics, Clinical Genetics, Neonatology, Rare Disorders

Prof. Robert Śmigiel

#### Pediatric Nephrology

Prof. Katarzyna Kiliś-Pstrusińska

#### Pediatric Oncology and Hematology

Assoc. Prof. Marek Ussowicz

### Pharmaceutical Sciences

Assoc. Prof. Marta Kepinska

Prof. Adam Matkowski

### Pharmacoeconomics, Rheumatology

Dr. Sylwia Szafraniec-Buryło

### Psychiatry

Prof. Istvan Boksay

Prof. Jerzy Leszek

### Public Health

Prof. Monika Sawhney

Prof. Izabella Uchmanowicz

### Qualitative Studies, Quality of Care

Prof. Ludmiła Marcinowicz

### Radiology

Prof. Marek Szaśniadek

### Rehabilitation

Prof. Jakub Taradaj

### Surgery

Assoc. Prof. Mariusz Chabowski

Prof. Renata Tabała

### Telemedicine, Geriatrics, Multimorbidity

Assoc. Prof. Maria Magdalena

Bujnowska-Fedak

---

## Editorial Policy

Advances in Clinical and Experimental Medicine (Adv Clin Exp Med) is an independent multidisciplinary forum for exchange of scientific and clinical information, publishing original research and news encompassing all aspects of medicine, including molecular biology, biochemistry, genetics, biotechnology and other areas. During the review process, the Editorial Board conforms to the "Uniform Requirements for Manuscripts Submitted to Biomedical Journals: Writing and Editing for Biomedical Publication" approved by the International Committee of Medical Journal Editors ([www.ICMJE.org](http://www.ICMJE.org)). The journal publishes (in English only) original papers and reviews. Short works considered original, novel and significant are given priority. Experimental studies must include a statement that the experimental protocol and informed consent procedure were in compliance with the Helsinki Convention and were approved by an ethics committee.

For all subscription-related queries please contact our Editorial Office:

[redakcja@umw.edu.pl](mailto:redakcja@umw.edu.pl)

For more information visit the journal's website:

[www.advances.umw.edu.pl](http://www.advances.umw.edu.pl)

Pursuant to the ordinance No. 134/XV R/2017 of the Rector of Wrocław Medical University (as of December 28, 2017) from January 1, 2018 authors are required to pay a fee amounting to 700 euros for each manuscript accepted for publication in the journal Advances in Clinical and Experimental Medicine.

Indexed in: MEDLINE, Science Citation Index Expanded, Journal Citation Reports/Science Edition, Scopus, EMBASE/Excerpta Medica, Ulrich's™ International Periodicals Directory, Index Copernicus

Typographic design: Piotr Gil, Monika Kołęda

DTP: Wydawnictwo UMW

Cover: Monika Kołęda

Printing and binding: Soft Vision Mariusz Rajski

## Contents

### Meta-analyses

- 583 Sian Alexandra Bradley, Ivica Smokovski, Sonu Menachem Maimonides Bhaskar  
**Impact of diabetes on clinical and safety outcomes in acute ischemic stroke patients receiving reperfusion therapy: A meta-analysis**
- 597 Wanlu Nie, Lili Zhu, Ping Yan, Jie Sun  
**Thyroid nodule ultrasound accuracy in predicting thyroid malignancy based on TIRADS system**

### Original papers

- 607 Hanna Gerber, Tomasz Gedrange, Piotr Szymor, Anna Leszczyszyn, Marcin Kubiak, Monika Rutkowska, Michał Sarul, Sylwia Hnitecka  
**Oral cancer awareness among patients at 3 university hospitals in Poland and Germany: A survey research**
- 615 Michał Szymon Nowak, Bożena Romanowska-Dixon, Iwona Grabska-Liberek, Michał Żurek  
**Incidence and survival of ocular melanoma in National Cancer Registry of Poland in 2010–2017**
- 623 Dongya Chen, Jingfang Xiong, Hui Feng, Yihui Liu, Jianjun Xu, Hong Xu  
**The influence of mosapride on gut microbiota of carbon tetrachloride-induced cirrhosis rats based on 16S rRNA gene sequencing**
- 635 Raied Fagehi, Gamal A. El-Hiti, Abdulaziz Alanazi, Mohammed A. Aldawood, Ali Abusharha, Mana A. Alanazi, Ali M. Masmali, Turki Almubrad  
**Improving tear ferning patterns collected from goats and camels after adding various electrolyte solutions**
- 643 Marianna Tyczewska, Marta Szyszka, Karol Jopek, Marcin Ruciński  
**Effects of Galp and alarin peptides on HPA axis gene expression and adrenal function: In vivo experiments**
- 655 Jun Yang, De Zhi Li, Yu Pang, Tao Zhou, Jia Sun, Xian Yi Cheng, Wei V. Zheng  
**MicroRNA-139-5p negatively regulates NME1 expression in hepatocellular carcinoma cells**
- 671 Hui Luo, Fangyan Zhong, Xiang Jing, Hong Lin, Yong Li  
**miRNA profiling of human nasopharyngeal carcinoma cell lines HONE1 and CNE2 after X-ray therapy**
- 689 Xiaopeng Xia, Xiaojian Zhu, Shu Zhang, Xiaoxia Zhang, Yan Wang  
**Effect of different expression patterns of HAX-1 on the proliferation and apoptosis of human astrocyte**

### Research letters

- 701 Jarosław Olech, Bartosz Koczyński, Łukasz Tomczyk, Grzegorz Konieczny, Krystian Kazubski, Piotr Morasiewicz  
**The functional and radiographic outcomes following distal radius fracture treatment in a cast for 4 and 6 weeks in the elderly: A randomized trial**
- 707 Jarosław Czyż, Łukasz Szukalski, Adriana Szukalska, Bożena Katarzyna Budziszewska, Ewa Lech-Marańda, Joanna Zdziarska, Tomasz Sacha  
**Eculizumab treatment in pregnant women with paroxysmal nocturnal hemoglobinuria: A Polish experience**



# Impact of diabetes on clinical and safety outcomes in acute ischemic stroke patients receiving reperfusion therapy: A meta-analysis

Sian Alexandra Bradley<sup>1,2,A–D,F</sup>, Ivica Smokovski<sup>4,A,D–F</sup>, Sonu Menachem Maimonides Bhaskar<sup>1,2,3,5,6,A–F</sup>

<sup>1</sup> Global Health Neurology and Translational Neuroscience Laboratory, Sydney and Neurovascular Imaging Laboratory, Clinical Sciences Stream, Ingham Institute for Applied Medical Research, Sydney, Australia

<sup>2</sup> South Western Sydney Clinical School, University of New South Wales, Australia

<sup>3</sup> New South Wales Brain Clot Bank, New South Wales Health Pathology, Sydney, Australia

<sup>4</sup> Clinic of Endocrinology, Diabetes and Metabolic Disorders Skopje, Faculty of Medical Sciences, The Goce Delčev University of Štip, North Macedonia

<sup>5</sup> Stroke and Neurology Research Group, Ingham Institute for Applied Medical Research, Liverpool, Australia

<sup>6</sup> Department of Neurology and Neurophysiology, Comprehensive Stroke Center, Liverpool Hospital and South Western Sydney Local Health District, Australia

A – research concept and design; B – collection and/or assembly of data; C – data analysis and interpretation;

D – writing the article; E – critical revision of the article; F – final approval of the article

Advances in Clinical and Experimental Medicine, ISSN 1899–5276 (print), ISSN 2451–2680 (online)

*Adv Clin Exp Med.* 2022;31(6):583–596

## Address for correspondence

Sonu Menachem Maimonides Bhaskar

E-mail: [Sonu.Bhaskar@reproprogramglobal.org](mailto:Sonu.Bhaskar@reproprogramglobal.org)

## Funding sources

Funding for the New South Wales Brain Clot Bank (chief investigator: Dr. S.M.M. Bhaskar) from the New South Wales Ministry of Health (2019–2022). The funding body had no role in the study design, data collection, analysis, interpretation of findings, or manuscript preparation. The content is solely the responsibility of the authors and does not necessarily represent the official views of the affiliated/funding organization/s.

## Conflict of interest

None declared

Received on September 24, 2021

Reviewed on January 17, 2022

Accepted on January 31, 2022

Published online on February 25, 2022

## Cite as

Bradley SA, Smokovski I, Bhaskar SMM. Impact of diabetes on clinical and safety outcomes in acute ischemic stroke patients receiving reperfusion therapy: A meta-analysis.

*Adv Clin Exp Med.* 2022;31(6):583–596.

doi:10.17219/acem/146273

## DOI

10.17219/acem/146273

## Copyright

Copyright by Author(s)

This is an article distributed under the terms of the Creative Commons Attribution 3.0 Unported (CC BY 3.0)

(<https://creativecommons.org/licenses/by/3.0/>)

## Abstract

**Background.** Patients with diabetes are known to have worse outcomes after an acute ischemic stroke (AIS) relative to those without diabetes. However, the impact of diabetes on the outcomes after the reperfusion therapy is poorly understood.

**Objectives.** This study investigated prognostic accuracy of diabetes and its association with clinical and safety outcomes in AIS patients receiving intravenous thrombolysis (IVT), endovascular thrombectomy (EVT), or both.

**Materials and methods.** Studies were identified from PubMed, Embase and Cochrane databases, using the following inclusion criteria: (a) AIS patients receiving reperfusion therapy, (b) age  $\geq$  18 years, (c) hemispheric stroke, and (d) the availability of comparative data between diabetic and nondiabetic groups and relevant poststroke outcomes. Random effects modelling was used to study the association of diabetes with functional outcome at discharge and at 90 days, mortality at 90 days, recanalization status, and postreperfusion safety outcomes, including rates of symptomatic intracerebral hemorrhage (sICH) and hemorrhagic transformation (HT). Forest plots of odds ratios (ORs) were generated.

**Results.** Of a total cohort of 82,764 patients who received reperfusion therapy, 16,877 had diabetes. Diabetes significantly increased the odds of poor functional outcome at discharge (OR 1.310; 95% confidence interval (95% CI): [1.091; 1.574];  $p = 0.0037$ ) and at 90 days (OR 1.487; 95% CI: [1.335; 1.656];  $p < 0.00010$ ), mortality at 90 days (OR 1.709; 95% CI: [1.633; 1.788];  $p < 0.0001$ ), sICH (OR 1.595; 95% CI: [1.301; 1.956];  $p < 0.0001$ ), and HT (OR 1.276; 95% CI: [1.055; 1.543];  $p = 0.0118$ ).

**Conclusions.** Our meta-analysis demonstrates that diabetes is significantly associated with poor functional outcome, increased mortality and poor postprocedural safety outcomes, including sICH and HT.

**Key words:** diabetes, stroke, meta-analysis, cerebrovascular disease, reperfusion therapy

## Background

Diabetes is known to be an important risk factor for stroke.<sup>1</sup> The advent of reperfusion treatment, intravenous thrombolysis (IVT) and endovascular thrombectomy (EVT) offers the opportunity to significantly improve the outcomes after acute ischemic stroke (AIS).<sup>2</sup> Moreover, since 2015, in the era of EVT, an increasing attention has been paid to identifying patients or stratifying them based on the clinical profiles or imaging factors,<sup>3,4</sup> who are more likely to benefit from time-critical therapies.<sup>5–9</sup> As such, it is of clinical relevance to fully delineate the role of diabetes in AIS, in the setting of reperfusion therapy.<sup>10</sup> Diabetes is known to be associated with worse functional outcomes and mortality after AIS,<sup>11,12</sup> largely due to its effect on endothelial dysfunction, fibrosis and vascular remodeling.<sup>13</sup> Furthermore, diabetes may also influence recanalization efficacy following IVT or EVT.<sup>14</sup>

## Objectives

This study sought to estimate the prognostic accuracy of diabetes and investigate its association with clinical outcomes in AIS patients receiving IVT, EVT and/or both, by performing a meta-analysis. Our underlying questions concerning AIS patients receiving reperfusion therapy are as follows:

1. What is the prognostic accuracy of diabetes?
2. Is diabetes associated with functional outcomes at 90 days?
3. Is diabetes associated with functional outcomes at discharge?
4. Is diabetes associated with increased mortality at 90 days?
5. Is diabetes associated with safety profile (defined in terms of symptomatic intracerebral hemorrhage (sICH)<sup>15</sup> or any hemorrhagic transformation (HT))?
6. Is diabetes associated with recanalization status?

## Materials and methods

### Literature search: Identification and selection of studies

Studies were identified from PubMed, Embase and Cochrane Central Register of Controlled Trials (CENTRAL) databases for the period between January 1, 2005, and September 2021. The search terms included: “stroke”, or “ischemic stroke”, or “cerebrovascular accident”, or “brain ischemia”, or “brain infarction”, or “anterior circulation”, or “middle cerebral artery (MCA) stroke”, or “internal carotid artery (ICA) stroke”, or “MCA occlusion”, or “large vessel occlusion” and “reperfusion”, or “endovascular thrombectomy”, or “thrombolysis”, or “thrombolytic

therapy”, or “tissue plasminogen activator”, or “clot retrieval” and “diabetes”, or “diabetes mellitus” and “clinical outcome”, or “tissue outcome”, or “mortality”, or “morbidity”, or “death”, or “adverse outcome”, or “NIHSS (National Institute of Health Stroke Scale/Score)”, or “clinical severity”, or “discharge outcome”, or “infarct volume”, or “disability score”, or “modified Rankin Score”, or “prognosis”. The full search term/strategy is provided in the Online Supplementary Information (Search Strategy). Studies written in a language other than English and not including human subjects were excluded by applying additional limits. Moreover, reference lists of relevant articles, systematic reviews and meta-analyses were also searched manually in order to retrieve additional articles. The Preferred Reporting Items for Systematic Reviews and Meta-Analyses (PRISMA) flowchart shows the search strategy, included studies and various subgroup analyses performed in the meta-analysis (Fig. 1). The following reporting frameworks adhered to and were reported: the Meta-analysis of Observational Studies in Epidemiology (MOOSE) checklist (Supplementary Table 5), PRISMA 2020 checklist (Supplementary Table 6), and Standards for Reporting of Diagnostic Accuracy Studies (STARD) 2015 checklist (Supplementary Table 7); all available in Online Supplementary Information.

### Inclusion and exclusion criteria

Studies were eligible if they met the following criteria: (a) AIS patients receiving reperfusion therapy (IVT or EVT); (b) age  $\geq 18$  years; (c) hemispheric stroke; (d) availability of comparative data between diabetic and nondiabetic groups and relevant poststroke outcome data; and (e) studies with correct methodological design (studies with sufficient sample size, determined to be  $\geq 20$  patients in each group). The exclusion criteria were as follows: 1) patients with posterior circulation stroke; 2) animal studies; 3) duplicated publications; 4) full-text of the article not available; 5) thrombolytic agent other than tissue plasminogen activator (tPA) used; 6) intra-arterial thrombolysis used; 7) systematic reviews, meta-analyses, letters, and case reports or case series; and 8) studies presented in the abstract form, with relevant data on diabetes not available or no relevant postreperfusion clinical outcome measured.

### Data extraction

First, the titles and abstracts were reviewed in Endnote (Clarivate Analytics, London, UK) to rule out the articles mismatched to the eligibility criteria. The remaining articles were examined thoroughly to determine whether they should be included in the systematic review or meta-analysis, according to the eligibility criteria. The screening was conducted independently by 2 authors. The disagreements were discussed and final decisions were reached



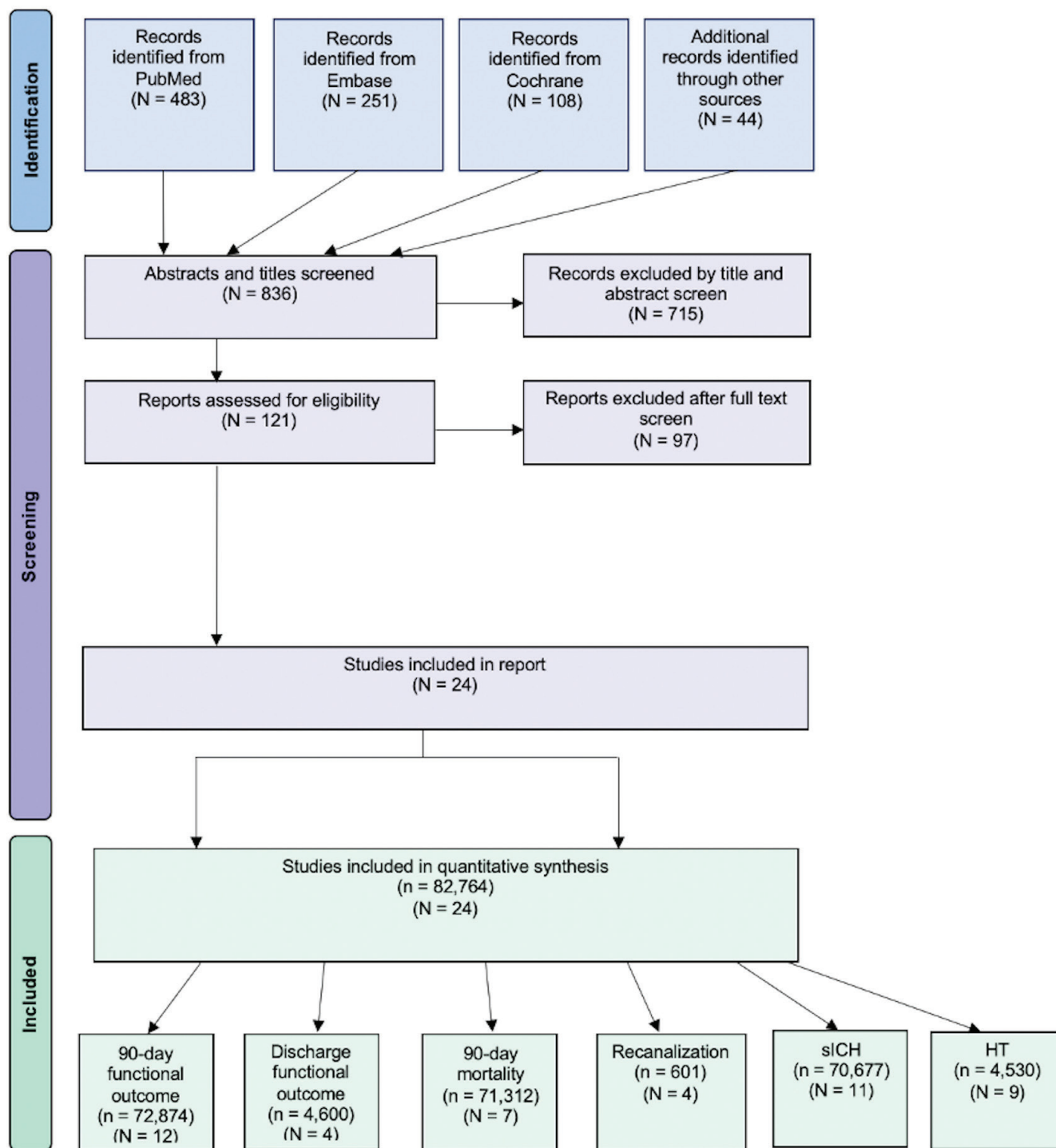


Fig. 1. The Preferred Reporting Items for Systematic Reviews and Meta-Analyses (PRISMA) flowchart showing the studies included in the meta-analysis n – cohort size; N – number of studies; sICH – symptomatic intracerebral hemorrhage; HT – hemorrhagic transformation.

by consensus. The data from each study/trial were extracted independently using a data extraction sheet to obtain the following information: 1) baseline demographics: author, country and year of publication; 2) study population: age of patients, sample size, characteristics of acute stroke patients, presence or absence of diabetes; 3) type and time window of the treatments; and 4) outcome measures: the functional outcome at 90 days, the functional outcome

at discharge, mortality at 90 days, sICH, HT, and the recanalization status. The functional outcome was measured using the modified Rankin Scale (mRS) score. The sICH was determined using Safe Implementation of Thrombolysis in Stroke-Monitoring Study (SITS-MOST), the Second European-Australasian Acute Stroke Study (ECASS-II) or the Third European Cooperative Acute Stroke Study (ECASS-III) criteria, and HT was defined as any hemorrhage

observed on follow-up imaging. If a study reported more than one type of sICH, SITS-MOST results were used.

## Methodological quality assessment of included studies

The methodological quality assessment using the modified Jadad analysis (MJA) scale of all studies included in the meta-analysis was performed independently by 2 researchers.<sup>16</sup> Moreover, the risk of bias in the results owing to funding was also evaluated, based on the declaration of funding sources and conflicts of interest obtained from individual studies.<sup>17</sup>

## Statistical analyses

All statistical analyses were performed using STATA v. 13.0 (StataCorp, College Station, USA). The baseline characteristics of the overall cohort included in the meta-analysis were derived from all included studies. Means and standard deviations (SDs) were calculated from the medians and interquartile ranges (IQRs) using the method of Wan et al., where appropriate.<sup>18</sup>

The prognostic utility of diabetes was evaluated by estimating the pooled sensitivity (SENS) and specificity (SPEC), positive and negative predictive values, positive and negative likelihood ratios, and area under the curve (AUC) (a global measure of prognostic accuracy obtained from summary receiver operating characteristic (SROC) curves), by performing a meta-analysis for each prognostic outcome.<sup>19</sup> Moreover, the prognostic model was characterized using the goodness-of-fit test. The Deeks' funnel plot asymmetry test was used to assess the publication bias.

To examine the impact of diabetes on postreperfusion sICH and HT, functional outcomes at discharge, and functional outcomes and mortality at 90 days, a random effects meta-analysis designed by DerSimonian and Laird (DL) was used. Summary effects and heterogeneity measures obtained for each prognostic outcome from the meta-analysis were tabulated. For the odds ratios (ORs), 95% confidence intervals (95% CIs), percentage weights, and the heterogeneity across studies included in the meta-analysis, forest plots were created (Fig. 2). The heterogeneity between the studies was assessed using the  $I^2$  statistics and  $p$ -value (<40% = low, 30–60% = moderate, 50–90% = substantial, 75–100% = considerable).<sup>20</sup> The random effects model was used across all subgroup analyses. The subgroup analyses for IVT or EVT studies were also performed. The presence of publication bias was visually detected using Begg's funnel plot. In the funnel plot, any asymmetry on either side indicated the presence of publication bias. We have also computed meta-analysis estimates when a specific study was excluded, to account for the influence of the individual study on the overall meta-analysis (Supplementary Fig. 5 in Online Supplementary Information). The value of  $p < 0.05$  was considered statistically significant.

## Results

### Description of included studies

A total of 24 studies, comprising 82,764 patients, were included in this meta-analysis. Eighteen studies included patients who primarily received IVT, with or without EVT; 6 studies included patients who primarily received EVT, with or without IVT. Nine studies were excluded from this meta-analysis because they had cohort sizes that were too small, 5 were excluded for having the same cohort (or part of the same cohort) as later studies and 1 was excluded because of the use of intra-arterial thrombolysis as the treatment.

Of all patients included in this meta-analysis, 16,877 had diabetes (20.4%). The mean age  $\pm$  standard deviation (SD) of all included studies was 69.5  $\pm$  33.4 years ( $n = 77,319$ ). With regard to clinical history, 22.8% of patients had atrial fibrillation ( $n = 78,804$ ), 37.5% had dyslipidemia ( $n = 74,551$ ), 67.6% had hypertension ( $n = 64,064$ ), 18.4% had prior stroke and/or transient ischemic attack (TIA) ( $n = 75,242$ ), and 18.6% were prior or current smokers ( $n = 62,208$ ). The description of the clinical characteristics and outcomes of the studies included in the meta-analysis can be found in Table 1 and Table 2, respectively.

Summary effects and heterogeneity from the meta-analysis on the association of diabetes are provided in Table 3. Supplementary Table 1 also provides the summary of the level of significance of the association of diabetes with various clinical and/or safety outcomes. There were variations in definitions of sICH and recanalization status across studies. The findings of the assessment of methodological quality and funding bias of the included studies are given in Supplementary Table 3. Effect size analyses for the functional outcome, sICH, HT, mortality, and recanalization status are also presented (Supplementary Fig. 6). Two studies demonstrated a moderate potential for funding bias and 1 study demonstrated a significant potential (Supplementary Table 3). The publication bias assessment, using the Egger's test, of the included studies is summarized in Supplementary Table 4. The subgroup analysis was conducted to address the prognostic ( $n = 24$  studies) capability of diabetes in AIS.

### Prognostic capability of diabetes in acute ischemic stroke

The SROC curves for diabetes to predict the outcomes are shown in Fig. 3. A summary of prognostic summary estimates is provided in Supplementary Table 2 and Supplementary Fig. 3. Supplementary Fig. 4 illustrates the likelihood ratio scatter matrix (all supplementary materials are available in Online Supplementary Information). Twenty-four studies investigated the prognostic capability of diabetes in AIS. The meta-analysis demonstrated that the prognostic accuracy of diabetes for poor functional outcome at 90 days

Table 1. Clinical characteristics of studies included in the meta-analysis

Author	Year	Country	Study type	Cohort (number of patients)	Age (years $\pm$ SD)	Male (%)	Reperfusion	sICH criteria	Recanalization criteria
Ahmed et al. <sup>29</sup>	2010	more than 1	prospective	15,787	68.19 $\pm$ 12.83	58.86	IVT	SITS-MOST	–
Bauza et al. <sup>46</sup>	2018	USA	retrospective	645	NR	51.78	IVT	–	–
Borggrefe et al. <sup>26</sup>	2018	Germany	retrospective	317	70 $\pm$ 14.5	48.58	EVT	ECASS-II	–
Chen et al. <sup>47</sup>	2019	China	retrospective	160	63.2 $\pm$ 12.2	67.5	EVT	–	–
Cucchiara et al. <sup>48</sup>	2009	more than 1	retrospective	965	68 $\pm$ 13	56.99	IVT	SITS-MOST	–
Fang et al. <sup>34</sup>	2020	China	retrospective	1084	63.44 $\pm$ 11.39	60.89	IVT	SITS-MOST	–
Filipov et al. <sup>49</sup>	2018	Germany	retrospective	527	72.22 $\pm$ 14.07	50.66	IVT	SITS-MOST	–
Fuentes et al. <sup>50</sup>	2014	Spain	prospective	261	67.59 $\pm$ 12.59	57.09	IVT	–	–
Kim et al. <sup>51</sup>	2019	South Korea	retrospective	125	68.1 $\pm$ 13.5	55.2	EVT	–	–
Lansberg et al. <sup>52</sup>	2007	USA	retrospective	74	70.76 $\pm$ 14.86	55.41	IVT	$\geq$ 2-point change in NIHSS associated with any degree of hemorrhage on CT or MR	–
Mishra et al. <sup>30</sup>	2010	more than 1	retrospective	1585	NR	NR	IVT	–	–
Montalvo et al. <sup>53</sup>	2019	USA	retrospective	578	72.55 $\pm$ 15.06	47.75	EVT	ECASS-III	–
Ngiam et al. <sup>54</sup>	2022	Singapore	retrospective	666	64.9 $\pm$ 14.3	60.66	IVT	–	–
Nikneshan et al. <sup>55</sup>	2013	Canada	retrospective	1689	NR	NR	IVT	SITS-MOST	–
Nowak et al. <sup>56</sup>	2020	Poland	retrospective	291	66 $\pm$ 15	50.86	EVT	–	–
Reiter et al. <sup>42</sup>	2014	Austria	retrospective	2158	matched analysis		IVT	NR	–
Ribo et al. <sup>35</sup>	2005	Spain	prospective	139	71 $\pm$ 11.4	56.83	IVT	–	TCD ultrasound
Tang et al. <sup>36</sup>	2016	China	retrospective	419	67.12 $\pm$ 13.08	63.25	IVT	NR	TIMI
Tsivgoulis et al. <sup>32</sup>	2019	more than 1	retrospective	54,206	70.13 $\pm$ 13.21	54.60	IVT	SITS-MOST	–
Wang et al. <sup>57</sup>	2019	China	retrospective	403	67.01 $\pm$ 31.88	66.25	IVT	–	–
Wnuk et al. <sup>31</sup>	2020	Poland	retrospective	181	66.15 $\pm$ 9.5	51.38	EVT	–	mTICI
Xu et al. <sup>58</sup>	2017	China	retrospective	162	65.6 $\pm$ 10.6	63.58	IVT	–	–
Yoo et al. <sup>59</sup>	2014	South Korea	retrospective	207	70.6 $\pm$ 11.11	61.35	IVT	–	–
Zhang et al. <sup>60</sup>	2019	China	prospective	135	64.2 $\pm$ 5.5	57.78	IVT	–	NR

SD – standard deviation; EVT – endovascular thrombectomy; IVT – intravenous thrombolysis; ST – systemic thrombolysis; mRS – modified Rankin Scale; sICH – symptomatic intracerebral hemorrhage; ECASS-II – the Second European-Australasian Acute Stroke Study; ECASS-III – the Third European Cooperative Acute Stroke Study; SITS-MOST – Safe Implementation of Thrombolysis in Stroke-Monitoring Study; NR – not reported; HT – hemorrhagic transformation; NIHSS – National Institutes of Health Stroke Scale; TIMI – Thrombolysis in Myocardial Infarction; TCD – transcranial Doppler; mTICI – modified Thrombolysis in Cerebral Infarction; CT – computed tomography; MR – magnetic resonance.

Table 2. Clinical outcomes of studies included in the meta-analysis

Author	Poor functional outcome at 90 days		Poor functional outcome at discharge		Mortality outcome at 90 days		sICH		HT		Poor recanalization	
	diabetes (n, %)		diabetes (n, %)		diabetes (n, %)		diabetes (n, %)		diabetes (n, %)		diabetes (n, %)	
	yes	no	yes	no	yes	no	yes	no	yes	no	yes	no
Ahmed et al. <sup>29</sup>	1335 (57.39)	4970 (44.7)	–	–	515 (21.81)	1467 (13)	69 (2.59)	89 (1.48)	–	–	–	–
Bauza et al. <sup>46</sup>	90 (55.21)	275 (58.64)	–	–	–	–	–	–	–	–	–	–
Borggreve et al. <sup>26</sup>	33 (76.74)	151 (60.4)	–	–	13 (30.23)	54 (21.6)	5 (12.82)	10 (3.8)	–	–	–	–
Chen et al. <sup>47</sup>	17 (58.62)	72 (54.96)	–	–	–	–	–	–	–	–	–	–
Cucchiara et al. <sup>48</sup>	–	–	–	–	–	–	10 (5.18)	44 (5.7)	52 (23.53)	141 (18.95)	–	–
Fang et al. <sup>34</sup>	81 (42.41)	356 (39.87)	–	–	25 (13.09)	83 (9.29)	7 (3.66)	13 (1.46)	–	–	–	–
Filipov et al. <sup>49</sup>	–	–	120 (63.16)	170 (50.30)	–	–	11 (5.82)	5 (1.48)	42 (22.22)	50 (14.79)	–	–
Fuentes et al. <sup>50</sup>	–	–	22 (38.6)	57 (33.93)	–	–	–	–	8 (12.9)	16 (8.04)	–	–
Kim et al. <sup>51</sup>	27 (69.23)	48 (55.81)	–	–	–	–	–	–	–	–	–	–
Lansberg et al. <sup>52</sup>	–	–	–	–	–	–	3 (15)	4 (7.41)	–	–	–	–
Mishra et al. <sup>30</sup>	221 (64.62)	681 (54.79)	–	–	69 (20.18)	184 (14.8)	–	–	–	–	–	–
Montalvo et al. <sup>53</sup>	–	–	–	–	–	–	8 (5.93)	11 (2.48)	–	–	–	–
Ngiam et al. <sup>54</sup>	65 (51.59)	240 (44.44)	–	–	–	–	–	–	–	–	–	–
Nikneshan et al. <sup>55</sup>	–	–	252 (75.68)	934 (68.88)	–	–	25 (7.51)	92 (6.8)	42 (12.61)	169 (12.46)	–	–
Nowak et al. <sup>56</sup>	50 (62.5)	87 (41.23)	–	–	22 (27.5)	41 (19.43)	–	–	–	–	–	–
Reiter et al. <sup>42</sup>	–	–	691 (64.04)	658 (60.98)	–	–	53 (4.91)	38 (3.52)	–	–	–	–
Ribo et al. <sup>35</sup>	–	–	–	–	–	–	–	–	–	–	21 (72.41)	74 (67.27)
Tang et al. <sup>36</sup>	–	–	–	–	–	–	2 (2.04)	13 (4.05)	–	–	31 (91.18)	84 (75)
Tsivgoulis et al. <sup>32</sup>	5637 (51.72)	17,626 (40.7)	–	–	2608 (23.93)	6794 (15.69)	280 (2.57)	702 (1.62)	–	–	–	–
Wang et al. <sup>57</sup>	–	–	–	–	–	–	–	–	5 (10)	41 (11.61)	–	–
Wnuk et al. <sup>31</sup>	25 (59.52)	60 (43.17)	–	–	–	–	–	–	21 (50)	58 (41.73)	15 (35.71)	48 (34.53)
Xu et al. <sup>58</sup>	–	–	–	–	–	–	–	–	3 (7.69)	17 (13.82)	–	–
Yoo et al. <sup>59</sup>	29 (65.91)	101 (61.96)	–	–	9 (20.45)	24 (14.72)	–	–	23 (52.27)	62 (38.04)	–	–
Zhang et al. <sup>60</sup>	–	–	–	–	–	–	–	–	4 (5.71)	3 (4.62)	45 (64.29)	19 (29.23)

sICH – symptomatic intracerebral hemorrhage; HT – hemorrhagic transformation.

**Table 3.** Summary effects and heterogeneity obtained from the meta-analysis of the association of diabetes with clinical outcomes in acute ischemic stroke patients

Outcome	Reperfusion therapy	Effect measure	Summary Effects	Heterogeneity <sup>†</sup>		Heterogeneity variance estimates			
			REDL	tests of overall effect	Cochran's Q	H	I <sup>2</sup> ≤*	p-value	τ <sup>2</sup> ≤ <sup>†</sup>
			OR (95% CI)						
Functional outcome at 90 days	overall	OR	1.487 [1.335; 1.656]	p < 0.0001 z = 7.225	22.05	1.416 (95% CI: [1.000; 1.916])	50.1% (95% CI: [0.0; 72.7])	0.024	0.0100
	IVT	OR	1.430 [1.270; 1.611]	p < 0.0001 z = 5.885	17.91	–	66.5%	0.006	–
	EVT	OR	1.941 [1.424; 2.646]	p < 0.0001 z = 4.199	2.21	–	0.0%	0.697	–
Functional outcome at discharge	overall (IVT)	OR	1.310 [1.091; 1.574]	p = 0.004 z = 2.896	4.43	1.215 (95% CI: [1.000; 2.163])	32.3% (95% CI: [0.0; 78.6%])	0.219	0.0114
Mortality at 90 days	overall	OR	1.709 [1.633; 1.788]	p < 0.0001 z = 23.111	4.24	0.840 (95% CI: [1.000; 1.552])	0.0% (95% CI: [0.0; 58.5%])	0.644	0.0000
	IVT	OR	1.713 [1.629; 1.801]	p < 0.0001 z = 20.934	4.11	–	2.7%	0.391	–
	EVT	OR	1.573 [0.994; 2.489]	p = 0.053 z = 1.933	0.00	–	0.0%	1.000	–
Recanalization	overall	OR	2.059 [0.963; 4.400]	p = 0.062 z = 1.863	9.13	1.774 (95% CI: [1.000; 2.729])	67.1% (95% CI: [0.0; 86.6%])	0.028	0.3938
	IVT	OR	2.693 [1.204; 6.027]	p = 0.016 z = 2.411	4.42	–	54.7%	0.110	–
	EVT	OR	1.053 [0.512; 2.167]	p = 0.888 z = 0.141	0.00	–	–	–	–
sICH	overall	OR	1.595 [1.301; 1.956]	p < 0.0001 z = 4.586	15.07	1.228 (95% CI: [1.000; 1.723])	33.7% (95% CI: [0.0; 66.3])	0.129	0.0310
	IVT	OR	1.524 [1.245; 1.866]	p < 0.0001 z = 4.079	11.98	–	33.2%	0.152	–
	EVT	OR	2.917 [1.421; 5.990]	p = 0.004 z = 2.917	0.30	–	0.0%	0.585	–
HT	overall	OR	1.276	p = 0.012 z = 2.517	6.67	0.918 (95% CI: [1.000; 1.480])	0.0% (95% CI: [0.0; 54.4])	0.564	0.0000
	IVT	OR	1.267	p = 0.019 z = 2.348	6.67	–	0.0%	0.464	–
	EVT	OR	1.397 [0.699; 2.791]	p = 0.344 z = 0.945	0.00	–	–	–	–

EVT – endovascular thrombectomy; IVT – intravenous thrombolysis; sICH – symptomatic intracerebral hemorrhage; HT – hemorrhagic transformation; REDL – DerSimonian and Laird random effects method; OR – odds ratio; Q – heterogeneity measures were calculated from the data with 95% confidence intervals (95% CIs), based on noncentral  $\chi^2$  (common effect) distribution for Cochran's Q test; H – relative excess in Cochran's Q over its degrees of freedom; I<sup>2</sup> – proportion of total variation in effect estimate due to between study heterogeneity (based on Cochran's Q test);  $\tau^2$  – between-study variance to test the comparisons of heterogeneity among subgroups; \* values of I<sup>2</sup> are percentages; <sup>†</sup> – heterogeneity measures were calculated from the data with 95% CIs based on gamma (random effects) distribution for Q; <sup>†</sup> – heterogeneity variance estimates (tau<sup>2</sup>) were derived from the DerSimonian and Laird method.

was 56% (AUC: 0.56; 95% CI: [0.03; 0.98]). The pooled prognostic sensitivity of diabetes for poor functional outcome at 90 days was 59% (SENS: 0.59; 95% CI: [0.54; 0.64]; p < 0.0001). The test of heterogeneity revealed a considerable heterogeneity for diagnostic sensitivity (I<sup>2</sup> = 99.87) and specificity (I<sup>2</sup> = 99.93). The prognostic accuracy of diabetes for poor functional outcome at discharge was 56% (AUC: 0.56; 95% CI: [0.04; 0.98]). The pooled prognostic sensitivity of diabetes for poor functional outcome at discharge was 61% (SENS: 0.61; 95% CI: [0.47; 0.73]; p < 0.0001). The test of heterogeneity revealed a considerable heterogeneity

for the diagnostic sensitivity (I<sup>2</sup> = 99.81) and specificity (I<sup>2</sup> = 99.45). The prognostic accuracy of diabetes for mortality at 90 days was 54% (AUC: 0.54; 95% CI [0.01; 0.99]). The pooled prognostic sensitivity of diabetes for mortality at 90 days was 23% (SENS: 0.23; 95% CI: [0.20; 0.26]; p < 0.0001). The test of heterogeneity revealed a considerable heterogeneity for the diagnostic sensitivity (I<sup>2</sup> = 94.13) and specificity (I<sup>2</sup> = 98.85). The prognostic accuracy of diabetes for poor recanalization was 61% (AUC: 0.61; 95% CI: [0.06; 0.98]). The pooled prognostic sensitivity of diabetes for poor recanalization was 70% (SENS: 0.7;

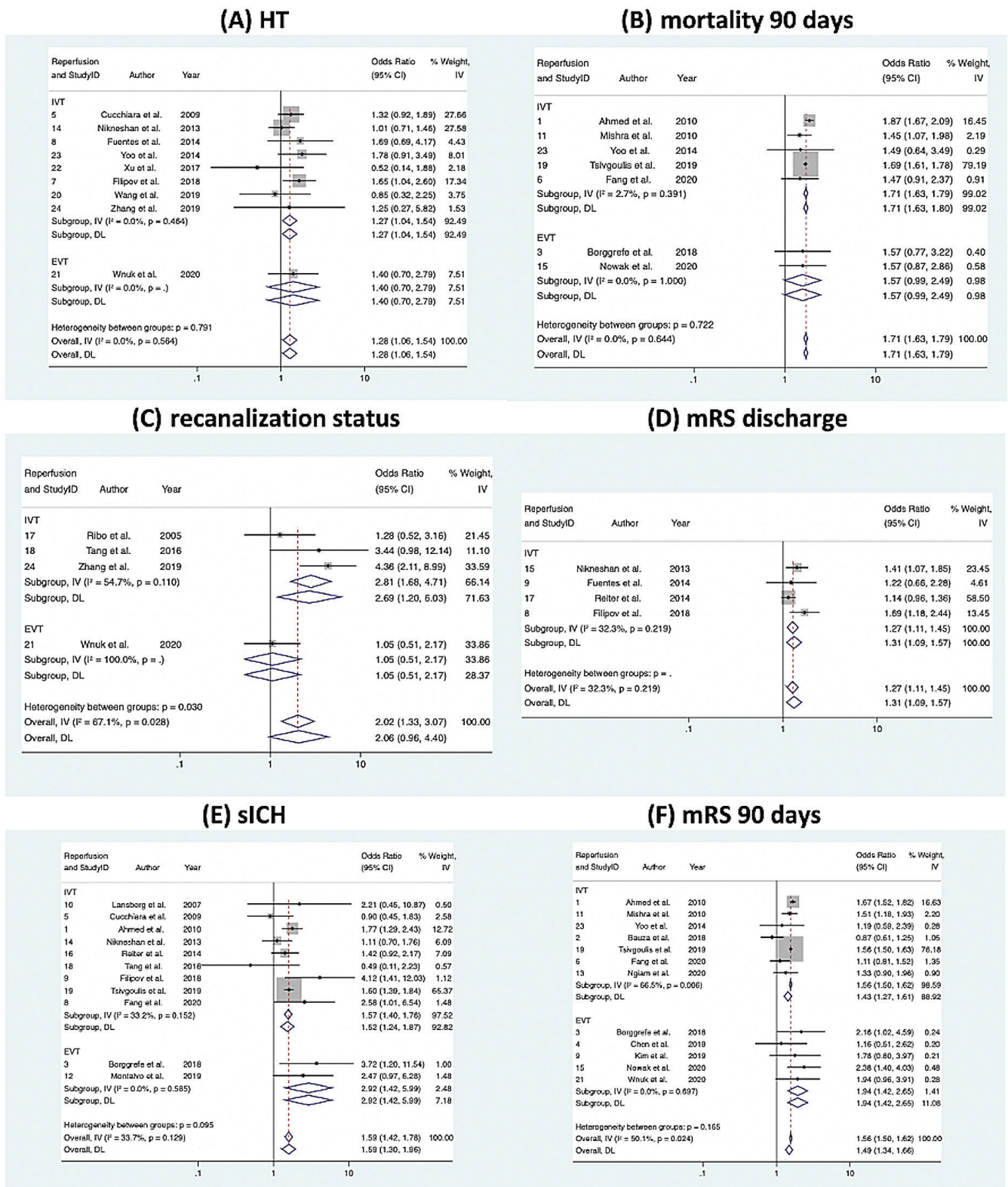


Fig. 2. Forest plot of estimated effect for the association of diabetes with: A. hemorrhagic transformation (HT); B. mortality at 90 days; C. recanalization status; D. functional outcome at discharge (mRS discharge); E. symptomatic intracerebral hemorrhage (sICH); and F. functional outcome at 90 days (mRS 90 days) in acute ischemic stroke patients receiving reperfusion therapy. Odds ratio of meta-analysis for the association of diabetes with poor functional outcome at 90 days, mortality at 90 days, symptomatic intracerebral hemorrhage, hemorrhagic transformation, recanalization status, and functional outcome at discharge. IVT – all patients received IVT; EVT – all patients received EVT.

mRS – modified Rankin scale score; IVT – intravenous thrombolysis; EVT – endovascular thrombectomy.

95% CI: [0.45; 0.86];  $p < 0.0001$ ). The test of heterogeneity revealed a considerable heterogeneity for diagnostic sensitivity ( $I^2 = 98.16$ ) and specificity ( $I^2 = 96.72$ ). The prognostic accuracy of diabetes for sICH was 42% (AUC: 0.42; 95% CI: [0.00; 1.00]). The pooled prognostic sensitivity of diabetes for sICH was 4% (SENS: 0.04; 95% CI: [0.03; 0.06];  $p < 0.0001$ ). The test of heterogeneity revealed considerable heterogeneity for diagnostic sensitivity ( $I^2 = 99.84$ ) and specificity ( $I^2 = 99.99$ ). The prognostic accuracy of diabetes for HT could not be determined.

## Association of diabetes with the functional outcome at 90 days

Overall, 12 studies were included in the final meta-analysis of the association of diabetes with the poor functional outcome at 90 days, comprising a total of 72,874 patients. Poor functional outcome at 90 days was defined as mRS score of 3–6 in all studies. Diabetes was associated with significantly increased odds of poor functional outcome at 90 days (OR 1.487; 95% CI: [1.335; 1.656];  $p < 0.0001$ ) (Fig. 2F). Moderate to substantial heterogeneity was found between the studies ( $I^2 = 50.1\%$ ,  $p = 0.024$ ). There was the evidence of publication bias, observed by visual inspection of the funnel plot (Supplementary Fig. 1), revealed by Egger's test (Supplementary Fig. 2; all supplementary materials are available in Online Supplementary Information). There was a significant association of diabetes with mRS at 90 days, observed in patients receiving IVT (OR 1.430; 95% CI: [1.270; 1.611];  $p < 0.0001$ ) and in patients receiving EVT (OR 1.941; 95% CI: [1.424; 2.646];  $p < 0.0001$ ).

## Association of diabetes with mortality at 90 days

Seven studies were included in the final meta-analysis of the association of diabetes with mortality at 90 days, comprising a total of 71,312 patients. Diabetes was significantly associated with mortality at 90 days (OR 1.709; 95% CI: [1.633; 1.788];  $p < 0.0001$ ) (Fig. 2B). A low heterogeneity was found between the studies ( $I^2 = 0.0\%$ ,  $p = 0.644$ ). There was the evidence of publication bias, observed by visual inspection of the funnel plot (Supplementary Fig. 1) and revealed by Egger's test (Supplementary Fig. 2; all supplementary materials are available in Online Supplementary Information). A significant association of diabetes with mortality at 90 days was observed in patients receiving IVT (OR 1.713; 95% CI: [1.629; 1.801];  $p < 0.0001$ ). No significant association of diabetes with mortality at 90 days was observed in patients receiving EVT (OR 1.573; 95% CI: [0.994; 2.489];  $p = 0.0532$ ) (Fig. 2B).

## Association of diabetes with sICH

Overall, 11 studies were included in the final meta-analysis of the association of diabetes with sICH, comprising

a total of 70,677 patients. The sICH was defined by SITS-MOST<sup>21</sup> criteria in 6 studies, ECASS-II<sup>22</sup> criteria in 1 study, National Institute of Neurological Disorders and Stroke (NINDS) criteria in 1 study, ECASS-III<sup>23</sup> criteria in 1 study, as  $\geq 2$  point change in National Institutes of Health Stroke Scale (NIHSS) score associated with any degree of hemorrhage on computed tomography (CT) or magnetic resonance (MR) in 1 study, and not defined in 2 studies. Overall, diabetes was significantly associated with an increased sICH rate (OR 1.595; 95% CI: [1.301; 1.956];  $p < 0.0001$ ) (Fig. 2E). A low to moderate heterogeneity was found between the studies ( $I^2 = 33.7\%$ ,  $p = 0.129$ ). Some evidence of publication bias was observed by the visual inspection of the funnel plot (Supplementary Fig. 1) and by Egger's test (Supplementary Fig. 2; all supplementary materials are available in Online Supplementary Information). A significant association between diabetes and the odds of sICH was observed in patients receiving IVT (OR 1.524; 95% CI: [1.245; 1.866];  $p < 0.0001$ ) and those receiving EVT (OR 2.917; 95% CI: [1.421; 5.99];  $p = 0.0035$ ) (Fig. 2E).

## Association of diabetes with HT

Nine studies were included in the final meta-analysis of the association of diabetes with HT, comprising a total of 4530 patients. Overall, diabetes was associated with increased odds of HT (OR 1.276; 95% CI: [1.055; 1.543];  $p = 0.0118$ ) (Fig. 2A). A low heterogeneity was found between the studies ( $I^2 = 0.0\%$ ,  $p = 0.564$ ). There was the evidence of publication bias, observed by a visual inspection of the funnel plot (Supplementary Fig. 1), and revealed by Egger's test (Supplementary Fig. 2; all supplementary materials are available in Online Supplementary Information). There was also a significant association of diabetes with HT in patients specifically receiving IVT (OR 1.267; 95% CI: [1.040; 1.543];  $p = 0.0188$ ) (Fig. 2A).

## Association of diabetes with recanalization status

The meta-analysis of the association of diabetes with recanalization status included 4 studies encompassing 601 patients. A poor recanalization outcome was defined as a Thrombolysis in Myocardial Infarction (TIMI) score  $< 3$  in 1 study, a modified Thrombolysis in Cerebral Infarction (mTICI) score  $< 2b$  in 1 study and incomplete recanalization on transcranial Doppler ultrasound in 1 study, while it was not defined in 1 study. Although diabetes was associated with increased odds of incomplete recanalization status, the association failed to reach statistical significance (OR 2.059; 95% CI: [0.963; 4.400];  $p = 0.0624$ ) (Fig. 2C). A moderate to substantial heterogeneity was reported ( $I^2 = 67.1\%$ ,  $p = 0.028$ ). There was no evidence of publication bias, observed by a visual inspection of the funnel plot (Supplementary Fig. 1) and revealed by Egger's test (Supplementary Fig. 2; all supplementary materials are available

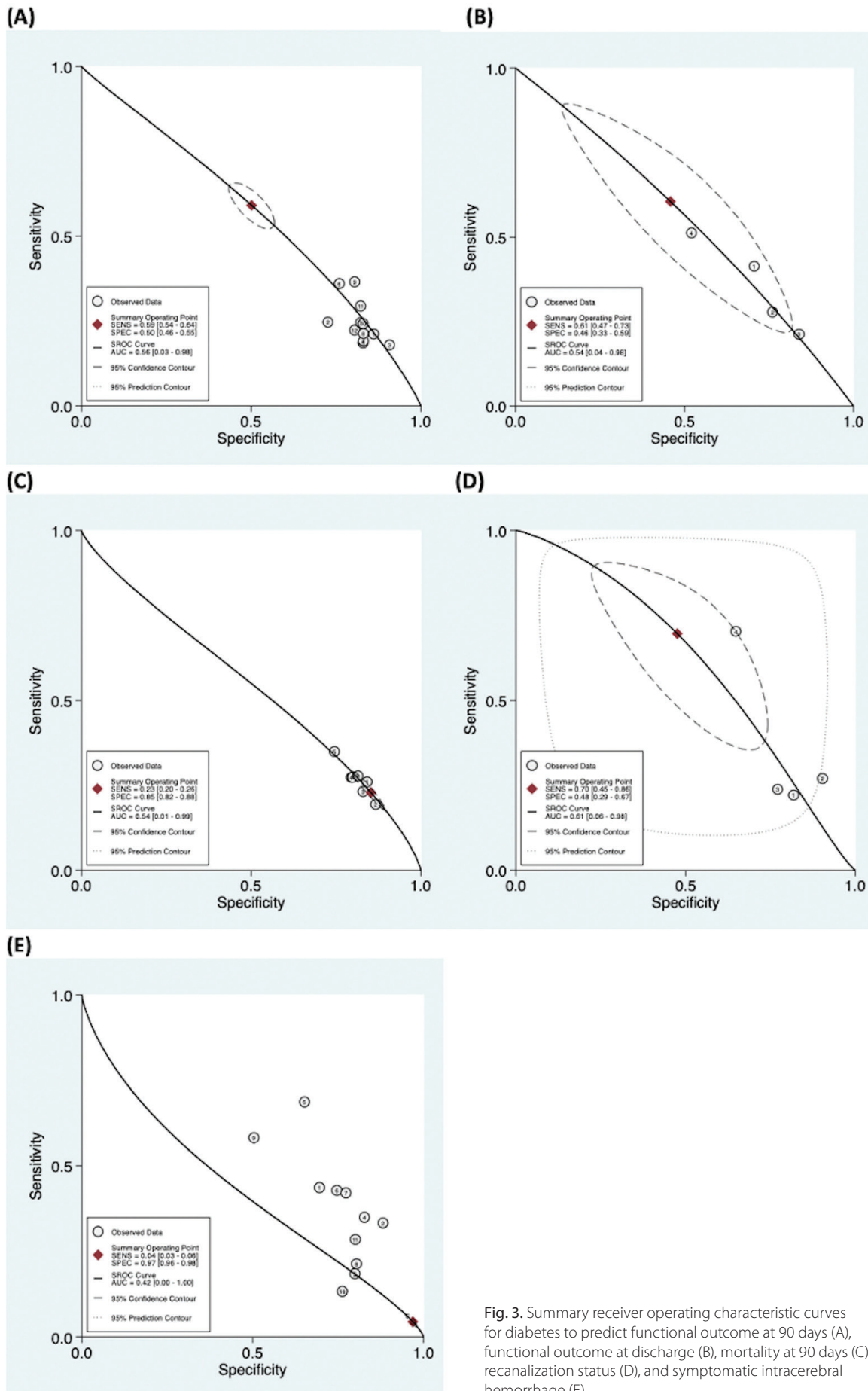


Fig. 3. Summary receiver operating characteristic curves for diabetes to predict functional outcome at 90 days (A), functional outcome at discharge (B), mortality at 90 days (C), recanalization status (D), and symptomatic intracerebral hemorrhage (E)



in Online Supplementary Information). There was, however, a significant association of diabetes with incomplete recanalization status in IVT patients (OR 2.693; 95% CI: [1.204; 6.027];  $p = 0.0159$ ).

## Association of diabetes with the functional outcome at discharge

Four studies were included in the meta-analysis of the association of diabetes with poor functional outcome at discharge, defined as mRS score of 3–6 at discharge. A total of 4600 patients were included, and patients in all included studies received IVT. Diabetes was associated with a significantly increased odds of poor functional outcome at discharge (OR 1.310; 95% CI: [1.091; 1.574];  $p = 0.0037$ ) (Fig. 2D). Low to moderate heterogeneity was found ( $I^2 = 32.3\%$ ,  $p = 0.219$ ). There was the evidence of publication bias, observed by visual inspection of the funnel plot (Supplementary Fig. 1) and revealed by Egger's test (Supplementary Fig. 2; all supplementary materials are available in Online Supplementary Information).

## Discussion

The results of this meta-analysis demonstrate that diabetes is associated with increased mortality and poor clinical and safety outcomes in AIS patients receiving reperfusion therapy. Specifically, diabetes was associated with poor functional outcome at discharge and at 90 days, as well as mortality at 90 days. The IVT and EVT subgroup analysis revealed similar outcomes; however, the association of diabetes with mortality at 90 days in EVT patients was not significant. With regard to postprocedural outcomes, AIS patients with pre-existing diabetes were associated with significantly increased odds of any HT or sICH after the reperfusion therapy. In particular, there was a strong association between diabetes and sICH in IVT patients. Although patients with diabetes were at increased odds of incomplete recanalization after the reperfusion therapy, the association failed to reach statistical significance overall. However, the association of diabetes with incomplete recanalization was significant for the IVT subgroup.

Identifying biomarkers or phenotypes associated with poor or better clinical profiles in AIS patients receiving reperfusion therapy is important in order to stratify patients for an optimal therapy.<sup>10</sup> Furthermore, given the rising prevalence of diabetes in the increasingly developing world, the proportion of AIS patients with diabetes is also expected to increase, warranting public health and clinical attention.<sup>24</sup> Within the AIS population with diabetes, patients with acute hyperglycemia are at an even increased risk of poor outcome profiles, as acute hyperglycemia is associated with an increased risk of infarct growth – by potentially impairing the vulnerability of penumbra.<sup>25</sup> Therefore, patients with diabetes, especially those

with acute hyperglycemia, need urgent attention and rapid reperfusion treatment. Previous studies have indicated longer times to reperfusion in diabetes patients, owing to the additional need for medical care for hyperglycemia or diabetes management, prior to the reperfusion therapy.<sup>26,27</sup> On a systemic level, this warrants establishing specialized pathways to identify AIS patients with a high risk of poor outcomes.<sup>9,28</sup>

Current evidence on functional outcome at 90 days for patients with diabetes who have undergone reperfusion therapy is mixed.<sup>5,26,29–31</sup> Most of the studies included in this meta-analysis did not individually find a significant relationship between diabetes and the odds of poor functional outcome. Tsivgoulis et al.,<sup>32</sup> with the largest cohort of any study ( $n = 54,206$ ), did find a significant relationship. However, the study was of retrospective design. De Silva et al.,<sup>33</sup> Fang et al.<sup>34</sup> and Tsivgoulis et al.<sup>32</sup> all found a significant relationship between the glucose level at admission and a poor functional outcome, in patients with or without diabetes, indicating that a poor functional outcome may be associated more with acute hyperglycemia seen in AIS patients. Our meta-analysis demonstrated a significant association between diabetes and a poor functional outcome at discharge and at 3 months. It also found a significant association between diabetes and increased 90 days mortality after the reperfusion therapy. A further investigation is needed in order to determine whether factors such as acute hyperglycemia and prior stroke play a role in these findings. Our meta-analysis found a significant association, although in a limited sample size drawn from 4 studies, between diabetes and unsuccessful recanalization, which contrasted with the individual findings of most of the included studies.<sup>14,31,35–37</sup>

With regard to safety outcomes, our meta-analysis revealed significantly increased odds of sICH and HT for AIS patients with diabetes who have undergone reperfusion therapy, compared to those without diabetes. This corroborates previous meta-analyses stating that diabetes and tPA independently increase the risk of hemorrhagic events after a stroke.<sup>14,38</sup> This meta-analysis considers the impact of diabetes across all reperfusion therapies. From a pathophysiological perspective, rodent models have demonstrated that increased MMP-9, the receptor for advanced glycation end products (RAGE) and vascular endothelial growth factor (VEGF) in diabetic mice are associated with increased blood–brain barrier (BBB) leakage, hemorrhage and impaired functional outcome.<sup>37,39</sup> The IVT may further exacerbate BBB leakage through BBB disruption.<sup>40</sup> Factors such as delayed onset-to-reperfusion time and leukoaraiosis have also been implicated.<sup>3,41</sup> Regardless, studies have shown that reperfusion therapy is safe for patients with diabetes and leads to better outcomes compared to patients who did not receive reperfusion therapy.<sup>30,42</sup>

During the current coronavirus disease 2019 (COVID-19) pandemic, an increasing attention is being paid to the disproportionate burden on patients with

pre-existing diabetes.<sup>43–45</sup> Furthermore, studies also indicate that patients with diabetes may be at an increased risk of COVID-19 infection.<sup>44</sup> This highlights the need for comprehensive and tailored management of patients with diabetes during the pandemic and beyond,<sup>43</sup> as well as in stroke patients with pre-existing diabetes who are at risk of poor outcomes after AIS.<sup>46–60</sup>

## Limitations

This study has several limitations. Most studies included in the meta-analysis were retrospective, and thus inherently limited in their design. This also resulted in most of the included studies relying on a history of diabetes diagnosis or diabetes treatment as criteria for inclusion in the treatment group. This means that there may be some patients in the control group with undiagnosed diabetes. The inclusion of case-controlled studies may cause spectrum bias or random error. However, most of the studies reported that all consecutive acute ischemic stroke patients receiving reperfusion therapy were included; this may minimize the selection bias. Furthermore, certain parameters such as diabetic severity, duration and type were either minimally reported or not reported at all. Due to its large sample size, the study by Tsvigoulis et al.<sup>32</sup> had a disproportionate effect on the overall results. Supplementary Fig. 5 (Online Supplementary Information) displays the results with the exclusion of that study. The outcomes of poor recanalization and functional outcome at discharge had relatively small cohorts and were therefore not highly powered. Last, not all studies clearly defined the number of patients who received both thrombolysis and thrombectomy. Findings should be interpreted on methodological design and the study population. However, given the fact that we performed a random effects model, some of these variabilities and heterogeneities will be accounted for.

## Conclusions

Diabetes is an important clinical consideration in AIS patients receiving reperfusion therapy. Our meta-analysis demonstrates that diabetes is associated with poor outcomes such as poor functional outcome, mortality, and poor safety outcomes, including sICH and HT. These results are mostly consistent across reperfusion treatment subgroups.

## Data availability statement

The original contributions presented in the study are included in the article Online Supplementary Information; further inquiries can be directed to the corresponding author. The Online Supplementary Information is available online at <https://doi.org/10.5281/zenodo.5930131>.

## ORCID iDs

Sonu Menachem Maimonides Bhaskar

 <https://orcid.org/0000-0002-9783-3628>

## References

- Roth GA, Mensah GA, Johnson CO, et al. Global burden of cardiovascular diseases and risk factors, 1990–2019: Update From the GBD 2019 study. *J Am Coll Cardiol.* 2020;76(25):2982–3021. doi:10.1016/j.jacc.2020.11.010
- Bhaskar S, Stanwell P, Cordato D, Attia J, Levi C. Reperfusion therapy in acute ischemic stroke: Dawn of a new era? *BMC Neurol.* 2018;18(1):8. doi:10.1186/s12883-017-1007-y
- Rastogi A, Weissert R, Bhaskar SMM. Emerging role of white matter lesions in cerebrovascular disease. *Eur J Neurosci.* 2021;54(4):5531–5559. doi:10.1111/ejn.15379
- Rastogi A, Weissert R, Bhaskar SMM. Leukoaraiosis severity and post-reperfusion outcomes in acute ischaemic stroke: A meta-analysis. *Acta Neurol Scand.* 2022;145(2):171–184. doi:10.1111/ane.13519
- Lu GD, Ren ZQ, Zhang JX, Zu QQ, Shi HB. Effects of diabetes mellitus and admission glucose in patients receiving mechanical thrombectomy: A systematic review and meta-analysis. *Neurocrit Care.* 2018;29(3):426–434. doi:10.1007/s12028-018-0562-4
- Katyal A, Bhaskar S. CTP-guided reperfusion therapy in acute ischemic stroke: A meta-analysis. *Acta Neurol Scand.* 2021;143(4):355–366. doi:10.1111/ane.13374
- Bhaskar S, Bivard A, Stanwell P, et al. Baseline collateral status and infarct topography in post-ischaemic perilesional hyperperfusion: An arterial spin labelling study. *J Cereb Blood Flow Metab.* 2017;37(3):1148–1162. doi:10.1177/0271678X16653133
- Ravindran AV, Killingsworth MC, Bhaskar S. Cerebral collaterals in acute ischaemia: Implications for acute ischaemic stroke patients receiving reperfusion therapy. *Eur J Neurosci.* 2021;53(4):1238–1261. doi:10.1111/ejn.14955
- Santana Baskar P, Cordato D, Wardman D, Bhaskar S. In-hospital acute stroke workflow in acute stroke: Systems-based approaches. *Acta Neurol Scand.* 2021;143(2):111–120. doi:10.1111/ane.13343
- Bradley SA, Spring KJ, Beran RG, Chatzis D, Killingsworth MC, Bhaskar SMM. Role of diabetes in stroke: Recent advances in pathophysiology and clinical management. *Diabetes Metab Res Rev.* 2021;38(2):e3495. doi:10.1002/dmrr.3495
- Forti P, Maioli F, Nativio V, Maestri L, Coveri M, Zoli M. Association of prestroke glycemic status with stroke mortality. *BMJ Open Diabetes Res Care.* 2020;8(1):e000957. doi:10.1136/bmjdr-2019-000957
- Lau LH, Lew J, Borschmann K, Thijs V, Ekinici EI. Prevalence of diabetes and its effects on stroke outcomes: A meta-analysis and literature review. *J Diabetes Investig.* 2019;10(3):780–792. doi:10.1111/jdi.12932
- Bhaskar S. Impact of obesity-induced type 2 diabetes on long-term outcomes following stroke. *Clin Sci (Lond).* 2019;133(14):1603–1607. doi:10.1042/CS20190492
- Desilles JP, Meseguer E, Labreuche J, et al. Diabetes mellitus, admission glucose, and outcomes after stroke thrombolysis: A registry and systematic review. *Stroke.* 2013;44(7):1915–1923. doi:10.1161/STROKEAHA.111.000813
- Rao NM, Levine SR, Gornbein JA, Saver JL. Defining clinically relevant cerebral hemorrhage after thrombolytic therapy for stroke: Analysis of the National Institute of Neurological Disorders and Stroke tissue-type plasminogen activator trials. *Stroke.* 2014;45(9):2728–2733. doi:10.1161/STROKEAHA.114.005135
- Jadad AR, Moore RA, Carroll D, et al. Assessing the quality of reports of randomized clinical trials: Is blinding necessary? *Control Clin Trials.* 1996;17(1):1–12. doi:10.1016/0197-2456(95)00134-4
- Saunders R, Struys M, Pollock RF, Mestek M, Lightdale JR. Patient safety during procedural sedation using capnography monitoring: A systematic review and meta-analysis. *BMJ Open.* 2017;7(6):e013402. doi:10.1136/bmjopen-2016-013402
- Wan X, Wang W, Liu J, Tong T. Estimating the sample mean and standard deviation from the sample size, median, range and/or interquartile range. *BMC Med Res Methodol.* 2014;14(1):135. doi:10.1186/1471-2288-14-135

19. Kataly A, Calic Z, Killingsworth M, Bhaskar SMM. Diagnostic and prognostic utility of computed tomography perfusion imaging in posterior circulation acute ischemic stroke: A systematic review and meta-analysis. *Eur J Neurol*. 2021;28(8):2657–2668. doi:10.1111/ene.14934
20. Deeks J, Higgins J, Altman D. In: *Cochrane Handbook for Systematic Reviews of Interventions*. Cochrane; 2021. www.training.cochrane.org/handbook.
21. Wahlgren N, Ahmed N, Davalos A, et al. Thrombolysis with alteplase for acute ischaemic stroke in the Safe Implementation of Thrombolysis in Stroke-Monitoring Study (SITS-MOST): An observational study. *Lancet*. 2007;369(9558):275–282. doi:10.1016/S0140-6736(07)60149-4
22. Hacke W, Kaste M, Fieschi C, et al. Randomised double-blind placebo-controlled trial of thrombolytic therapy with intravenous alteplase in acute ischaemic stroke (ECASS II). Second European-Australasian Acute Stroke Study Investigators. *Lancet*. 1998;352(9136):1245–1251. doi:10.1016/s0140-6736(98)08020-9
23. Yaghi S, Eisenberger A, Willey JZ. Symptomatic intracerebral hemorrhage in acute ischemic stroke after thrombolysis with intravenous recombinant tissue plasminogen activator: A review of natural history and treatment. *JAMA Neurol*. 2014;71(9):1181–1185. doi:10.1001/jamaneurol.2014.1210
24. Bradley SA, Varghese FM, Menon B, Mehndiratta MM, Bhaskar SMM. Stroke in patients with diabetes: Is it time to expand public health priority to encompass high-risk patients with increased insulin resistance? *EMJ Diabet*. 2021;9(1):84–91. doi:10.33590/emjdiabet/21-00171
25. Rosso C, Pires C, Corvol JC, et al. Hyperglycaemia, insulin therapy and critical penumbral regions for prognosis in acute stroke: Further insights from the INSULINFARCT trial. *PLoS One*. 2015;10(3):e0120230. doi:10.1371/journal.pone.0120230
26. Borggrefe J, Gluck B, Maus V, et al. Clinical outcome after mechanical thrombectomy in patients with diabetes with major ischemic stroke of the anterior circulation. *World Neurosurg*. 2018;120:e212–e220. doi:10.1016/j.wneu.2018.08.032
27. Kamal N, Sheng S, Xian Y, et al. Delays in door-to-needle times and their impact on treatment time and outcomes in get with the guidelines-stroke. *Stroke*. 2017;48(4):946–954. doi:10.1161/STROKEAHA.116.015712
28. Baskar PS, Chowdhury SZ, Bhaskar SMM. In-hospital systems interventions in acute stroke reperfusion therapy: A meta-analysis. *Acta Neurol Scand*. 2021;144(4):418–432. doi:10.1111/ane.13476
29. Ahmed N, Davalos A, Eriksson N, et al. Association of admission blood glucose and outcome in patients treated with intravenous thrombolysis: Results from the Safe Implementation of Treatments in Stroke International Stroke Thrombolysis Register (SITS-ISTR). *Arch Neurol*. 2010;67(9):1123–1130. doi:10.1001/archneurol.2010.210
30. Mishra NK, Davis SM, Kaste M, Lees KR; VISTA Collaboration. Comparison of outcomes following thrombolytic therapy among patients with prior stroke and diabetes in the Virtual International Stroke Trials Archive (VISTA). *Diabetes Care*. 2010;33(12):2531–2537. doi:10.2337/dc10-1125
31. Wnuk M, Popiela T, Drabik L, et al. Fasting hyperglycemia and long-term outcome in patients with acute ischemic stroke treated with mechanical thrombectomy. *J Stroke Cerebrovasc Dis*. 2020;29(5):104774. doi:10.1016/j.jstrokecerebrovasdis.2020.104774
32. Tsvigoulis G, Katsanos AH, Mavridis D, et al. Association of baseline hyperglycemia with outcomes of patients with and without diabetes with acute ischemic stroke treated with intravenous thrombolysis: A propensity score-matched analysis from the SITS-ISTR registry. *Diabetes*. 2019;68(9):1861–1869. doi:10.2337/db19-0440
33. De Silva DA, Ebinger M, Christensen S, et al. Baseline diabetic status and admission blood glucose were poor prognostic factors in the EPI-THET trial. *Cerebrovasc Dis*. 2010;29(1):14–21. doi:10.1159/000255969
34. Fang HJ, Pan YS, Wang YJ, Wang CX, Wang YL, Zhong LY. Prognostic value of admission hyperglycemia on outcomes of thrombolysis in ischemic stroke patients with or without diabetes. *Chin Med J (Engl)*. 2020;133(18):2244–2246. doi:10.1097/CM9.0000000000001005
35. Ribo M, Molina C, Montaner J, et al. Acute hyperglycemia state is associated with lower tPA-induced recanalization rates in stroke patients. *Stroke*. 2005;36(8):1705–1709. doi:10.1161/01.STR.0000173161.05453.90.9f
36. Tang H, Zhang S, Yan S, et al. Unfavorable neurological outcome in diabetic patients with acute ischemic stroke is associated with incomplete recanalization after intravenous thrombolysis. *J Neurointerv Surg*. 2016;8(4):342–346. doi:10.1136/neurintsurg-2014-011643
37. Zhang ZG, Zhang L, Jiang Q, et al. VEGF enhances angiogenesis and promotes blood–brain barrier leakage in the ischemic brain. *J Clin Invest*. 2000;106(7):829–838. doi:10.1172/JCI9369
38. Hao Z, Yang C, Xiang L, Wu B, Liu M. Risk factors for intracranial hemorrhage after mechanical thrombectomy: A systematic review and meta-analysis. *Expert Rev Neurother*. 2019;19(10):927–935. doi:10.1080/14737175.2019.1632191
39. Ning R, Chopp M, Yan T, et al. Tissue plasminogen activator treatment of stroke in type-1 diabetes rats. *Neuroscience*. 2012;222:326–332. doi:10.1016/j.neuroscience.2012.07.018
40. Hayakawa M. Reperfusion-related intracerebral hemorrhage. *Front Neurol Neurosci*. 2015;37:62–77. doi:10.1159/000437114
41. Laredo C, Renu A, Llull L, et al. Elevated glucose is associated with hemorrhagic transformation after mechanical thrombectomy in acute ischemic stroke patients with severe pretreatment hypoperfusion. *Sci Rep*. 2020;10(1):10588. doi:10.1038/s41598-020-67448-x
42. Reiter M, Teuschl Y, Matz K, Seyfang L, Brainin M; Austrian Stroke Unit Registry C. Diabetes and thrombolysis for acute stroke: A clear benefit for diabetics. *Eur J Neurol*. 2014;21(1):5–10. doi:10.1111/ene.12263
43. Bradley SA, Banach M, Alvarado N, Smokovskii I, Bhaskar SMM. Prevalence and impact of diabetes in hospitalized COVID-19 patients: A systematic review and meta-analysis. *J Diabetes*. 2021. doi:10.1111/1753-0407.13243
44. Singh AK, Gillies CL, Singh R, et al. Prevalence of co-morbidities and their association with mortality in patients with COVID-19: A systematic review and meta-analysis. *Diabetes Obes Metab*. 2020;22(10):1915–1924. doi:10.1111/dom.14124
45. Sinha A, Bhaskar SMM. In-hospital prevalence of mucormycosis among coronavirus disease 2019 (COVID-19) patients and COVID-19 in mucormycosis: A systematic review and meta-analysis [published online ahead of print on October 11, 2021]. *Int Forum Allergy Rhinol*. 2021. doi:10.1002/alr.22906
46. Bauza C, Yeatts SD, Borg K, et al. Determining the joint effect of obesity and diabetes on functional disability at 3-months and on all-cause mortality at 1-year following an ischemic stroke. *BMC Endocr Disord*. 2018;18(1):40. doi:10.1186/s12902-018-0255-1
47. Chen X, Liu Z, Miao J, et al. High stress hyperglycemia ratio predicts poor outcome after mechanical thrombectomy for ischemic stroke. *J Stroke Cerebrovasc Dis*. 2019;28(6):1668–1673. doi:10.1016/j.jstrokecerebrovasdis.2019.02.022
48. Cucchiara B, Kasner SE, Tanne D, et al. Factors associated with intracerebral hemorrhage after thrombolytic therapy for ischemic stroke: Pooled analysis of placebo data from the Stroke-Acute Ischemic NXY Treatment (SAINT) I and SAINT II Trials. *Stroke*. 2009;40(9):3067–3072. doi:10.1161/STROKEAHA.109.554386
49. Filipov A, Ebert AD, Neumaier-Probst E, Alonso A. The burden of diabetes and the chance of a previous stroke: Thrombolysis for recurrent stroke in diabetics. *J Stroke Cerebrovasc Dis*. 2018;27(5):1343–1349. doi:10.1016/j.jstrokecerebrovasdis.2017.12.027
50. Fuentes B, Cruz-Herranz A, Martinez-Sanchez P, et al. Acute ischemic stroke patients with diabetes should not be excluded from intravenous thrombolysis. *J Thromb Thrombolysis*. 2014;38(4):522–527. doi:10.1007/s11239-014-1110-5
51. Kim JM, Bae JH, Park KY, et al. Incidence and mechanism of early neurological deterioration after endovascular thrombectomy. *J Neurol*. 2019;266(3):609–615. doi:10.1007/s00415-018-09173-0
52. Lansberg MG, Thijs VN, Bammer R, et al. Risk factors of symptomatic intracerebral hemorrhage after tPA therapy for acute stroke. *Stroke*. 2007;38(8):2275–2278. doi:10.1161/STROKEAHA.106.480475
53. Montalvo M, Mistry E, Chang AD, et al. Predicting symptomatic intracranial haemorrhage after mechanical thrombectomy: The TAG score. *J Neurol Neurosurg Psychiatry*. 2019;90(12):1370–1374. doi:10.1136/jnnp-2019-321184
54. Ngiam JN, Cheong CWS, Leow AST, et al. Stress hyperglycaemia is associated with poor functional outcomes in patients with acute ischaemic stroke after intravenous thrombolysis. *QJM*. 2022;115(1):7–11. doi:10.1093/qjmed/hcaa253
55. Nikneshan D, Raptis R, Pongmoragot J, et al. Predicting clinical outcomes and response to thrombolysis in acute stroke patients with diabetes. *Diabetes Care*. 2013;36(7):2041–2047. doi:10.2337/dc12-2095
56. Nowak K, Włodarczyk E, Porębska K, et al. Mechanical thrombectomy for acute ischaemic stroke during therapeutic anticoagulation: Long-term outcomes. *Neurol Neurochir Pol*. 2020;54(6):538–543. doi:10.5603/PJNNS.a2020.0088

57. Wang R, Zeng J, Wang F, Zhuang X, Chen X, Miao J. Risk factors of hemorrhagic transformation after intravenous thrombolysis with rt-PA in acute cerebral infarction. *QJM*. 2019;112(5):323–326. doi:10.1093/qjmed/hcy292
58. Xu X, Li C, Wan T, et al. Risk factors for hemorrhagic transformation after intravenous thrombolysis in acute cerebral infarction: A retrospective single-center study. *World Neurosurg*. 2017;101:155–160. doi:10.1016/j.wneu.2017.01.091
59. Yoo DS, Chang J, Kim JT, et al. Various blood glucose parameters that indicate hyperglycemia after intravenous thrombolysis in acute ischemic stroke could predict worse outcome. *PLoS One*. 2014;9(4):e94364. doi:10.1371/journal.pone.0094364
60. Zhang Z, Qian M, Ge Z, Zhou P, Liu J, Chen J. Effects of blood glucose and glycosylated hemoglobin levels on intravenous thrombolysis in patients with acute cerebral infarction and type 2 diabetes mellitus. *Pak J Med Sci*. 2019;35(3):862–867. doi:10.12669/pjms.35.3.8-

# Thyroid nodule ultrasound accuracy in predicting thyroid malignancy based on TIRADS system

Wanlu Nie<sup>1,A</sup>, Lili Zhu<sup>2,C</sup>, Ping Yan<sup>1,B</sup>, Jie Sun<sup>1,E,F</sup>

<sup>1</sup> Department of Ultrasound, Penglai People's Hospital, Yantai, China

<sup>2</sup> Department of Endocrinology, Penglai People's Hospital, Yantai, China

A – research concept and design; B – collection and/or assembly of data; C – data analysis and interpretation; D – writing the article; E – critical revision of the article; F – final approval of the article

Advances in Clinical and Experimental Medicine, ISSN 1899–5276 (print), ISSN 2451–2680 (online)

*Adv Clin Exp Med.* 2022;31(6):597–606

## Address for correspondence

Wanlu Nie

E-mail: niewanlu1979@sina.com

## Funding sources

None declared

## Conflict of interest

None declared

Received on December 21, 2021

Reviewed on December 30, 2021

Accepted on February 17, 2022

Published online on May 4, 2022

## Cite as

Nie W, Zhu L, Yan P, Sun J. Thyroid nodule ultrasound accuracy in predicting thyroid malignancy based on TIRADS system. *Adv Clin Exp Med.* 2022;31(6):597–606. doi:10.17219/acem/146776

## DOI

10.17219/acem/146776

## Copyright

Copyright by Author(s)

This is an article distributed under the terms of the Creative Commons Attribution 3.0 Unported (CC BY 3.0) (<https://creativecommons.org/licenses/by/3.0/>)

## Abstract

**Background.** A frequent prevalence of thyroid nodules in patients prioritizes the need for an accurate method that characterizes them as benign or malignant. Fine-needle aspiration biopsy (FNAB) and thyroid ultrasonography (USG) are currently used for this purpose. However, since FNAB is complicated, time-consuming and expensive, thyroid USG, a fast and highly sensitive method, is preferably used. Although USG is reported as a suitable method for characterization of thyroid nodules, there are some contrasting studies available which report its limited use in the differentiation of benign and malignant thyroid nodules.

**Objectives.** This meta-analysis aims to assess the accuracy of ultrasound in predicting thyroid cancer in terms of sensitivity, specificity and diagnostic odds ratios (ORs) for positive and negative results.

**Materials and methods.** Systematic and extensive literature search on the use of ultrasound (US) to predict thyroid cancer was conducted in the databases of Scopus, CINAHL (via EBSCO), MEDLINE (via PubMed), and Web of Science, covering the period from 2010 till 2021. The morphological features of thyroid nodules observed during the USG were analyzed based on Thyroid Imaging Reporting And Data System (TIRADS) guidelines. The accuracy of thyroid US was determined using parameters such as sensitivity, specificity, positive likelihood ratio (PLR), negative likelihood ratio (NLR), and diagnostic ORs. Moreover, the respective forest plot and hierarchical summary receiver operating characteristics (HSROC) curve were plotted.

**Results.** A total of 2765 reference studies were examined, and among them, 15 relevant references were selected. The selected studies were heterogeneous and included retrospective and prospective studies. The risk of publication bias is low as the p-value for both Egger's and Begg's tests is  $>0.05$ . The overall sensitivity of 92.53% (95% confidence interval (95% CI): [84.55%; 96.33%]), specificity of 33.88% (95% CI: [23.16%; 45.53%]) and diagnostic OR of 12.36 (95% CI: [3.90%; 54.11%]) are achieved. These results were statistically significant with a p-value  $< 0.001$  and are predictive of US accuracy in detecting cancer.

**Conclusions.** The present meta-analysis, on the basis of statistically significant results, demonstrated the high accuracy of thyroid ultrasound in detection of malignant nature of nodules in patients suspected with a worrisome thyroid nodule.

**Key words:** ultrasound, thyroid nodule, fine-needle aspiration biopsy (FNAB), thyroid imaging – reporting and data system (TIRADS), benign and malignant nodule

## Introduction

All cancers are tumors, but not all tumors are cancerous. Therefore, it is imperative to have a concrete diagnosis in patients with thyroid nodules in order to differentiate between benign and malignant nodules. With a rapid rise in the number of patients with suspicious thyroid nodules, it is a medical emergency to characterize the nature of these nodules as either malignant or benign. In order to assess the malignancy and cancerous nature of the suspected thyroid nodule, fine-needle aspiration biopsy (FNAB) is performed.<sup>1</sup> However, it is a high cost and time-consuming invasive surgical procedure and it is not an easy diagnostic procedure for patients. Therefore, to simplify the nodule diagnosis, current thyroid guidelines (Thyroid Imaging Reporting And Data System (TIRADS)) advocate the use of ultrasonography (USG) as a preliminary test for all patients suspected of having thyroid nodule.<sup>2,3</sup>

Clinical variables and ultrasound (US) findings as per the TIRADS guidelines are recommended as a primary criterion to assess the benign and malignant nature of a nodule. Based on these results, the clinician further advises an additional confirmatory testing (FNAB) or simple

routine US follow-up. A surgical procedure is considered based on both US and FNAB results with cytology (FNAC).

Currently, different TIRADS guidelines<sup>4–8</sup> are available, including American College of Radiology (ACR) – TIRADS, American Thyroid Association (ATA) – TIRADS, American Association of Clinical Endocrinology/American Clinical Endocrinology/American Medical Endocrinology (AACE/ACE/AME) – TIRADS, Korean Society of Thyroid Radiology (KSR)/(KSThR) – TIRADS, and European Thyroid Association (ETA)/(EU) – TIRADS. These TIRADS provide a list of notable morphological features reported in the US images as a gold standard to classify a suspected nodule as malignant or benign. These features are internal calcifications, hypoechogenicity, vascularity, shape, and nodule size.

As per these guidelines (Fig. 1), if the nodule is round to ovoid with no solid portion, isoechoic, spongiform, grows across the normal tissue plane in a parallel fashion, has smooth margins and increased peripheral blood flow, and either has no calcification or egg-shell calcification, it is considered as benign. In contrast, if the nodule is solid, non-oval, taller than wider cells with irregular margins, and has an increased central blood flow with marked hypoechogenicity and microcalcifications,

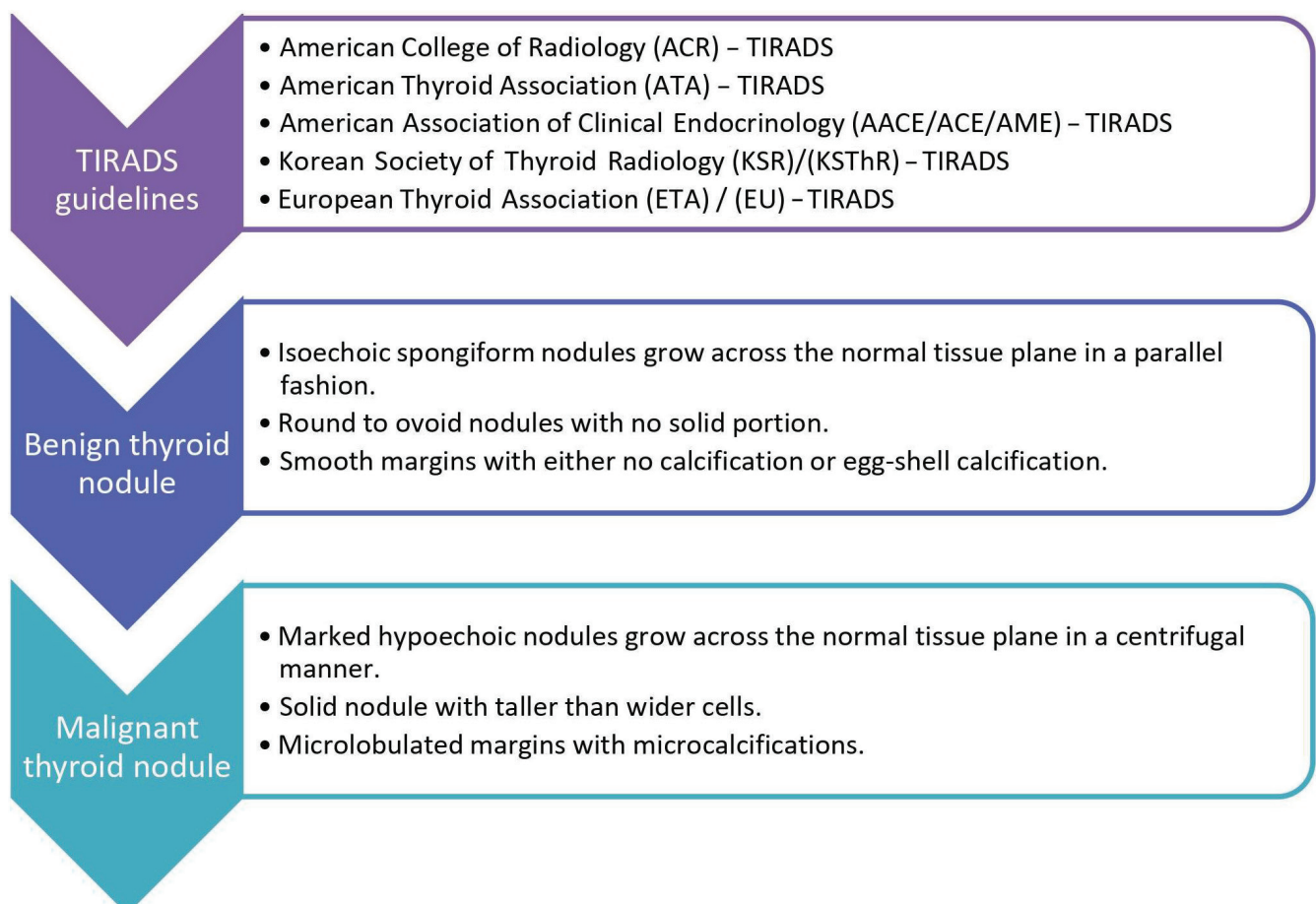


Fig. 1. Thyroid Imaging Reporting and Data System (TIRADS) guidelines

it is believed to be malignant and considered for further analysis.

Among these morphological features of the thyroid, USG and solid nodule are the most preferred criteria for assessing nodular malignancy. Therefore, many random clinical trials were performed to assess similar US and FNAB results in predicting nodular malignancy in terms of sensitivity and specificity. As a result, the sensitivity and specificity of various randomized controlled trials (RCTs) were reported in the range of 98% and 30%, respectively. These results align with the sensitivity and specificity values in the range of 98% and 70%, respectively, reported for FNAB.<sup>9–11</sup>

Based on these studies, the use of US examination has become widely accepted as a significant diagnostic step in stratifying the risk of malignancy in the patients; still, the diagnostic accuracy of several of examined sonographic parameters is a subject of much debate. Therefore, this meta-analysis was performed to understand the traits of US that help in establishing the diagnosis of a thyroid nodule, either benign or malignant. The positive outcomes suggest its accuracy and comparable diagnostic efficiency to FNAB, and highly recommend its use in the medical practice. The US examination enables patients to get their nodule tested in a short time with no surgical procedures. In addition, it could save their money on confirmatory tests and thus, have a significant impact on both clinical practice and guideline recommendations.

## Objectives

The current study is an attempt to analyze thyroid US results according to TIRADS guidelines and the associated nodule management, in order to establish this method as reliable for predicting thyroid cancer in terms of sensitivity and specificity for positive and negative US results.

## Materials and methods

This study, with the registration No. SUYP#/IRB/2021/1254, followed the normative requirements of Preferred Reporting Items for Systematic Reviews and Meta-Analyses (PRISMA).

### Search strategy

From 2010 until the end of March 2021, an exhaustive search was undertaken in MEDLINE (through PubMed), CINAHL (via EBSCO), Scopus, and Web of Science databases. Keywords like [ultrasonography], [FNAB], [thyroid nodules, malignancy], [TIRADS recommendations], [US-based risk stratification methods] and [diagnostic accuracy] were used in this search. The PRISMA criteria were used to assess all of the papers. The language,

publication status and prospective or retrospective nature of the study had no bearing on the study selection. Table 1 presents the demographic features of the studies included in the MEDLINE database search query along with the evaluated factors.<sup>12–26</sup>

The main goal of this study was to evaluate the effectiveness of USGat detecting thyroid nodules in people of various ages. In order to assess the efficiency of US for nodule examination, patients of varied age groups were studied, and statistical parameters such as sensitivity, specificity, positive likelihood ratio (PLR), negative likelihood ratio (NLR), and diagnostic odds ratios (ORs) were calculated with the help of true positive (TP), false positive (FP), true negative (TN), and false negative (FN) values.

Two authors (WN and LZ) independently searched the sources for similar studies. Full-text articles were collected, and abstracts were analyzed if sufficient information could be retrieved. Obsolete references were removed, and only valuable studies were included. Data from the included research were obtained separately by 2 researchers (PY and JS).

## Inclusion and exclusion criteria

Studies from the years 2010–2021 that examined the diagnostic accuracy of USG for thyroid nodule assessment in the individuals of all ages with a suspected thyroid nodule and subsequent nodule therapy were included in the study. Only full-text data were included in this analysis; publications with inadequate data, reference standards other than US/FNAB report and comparable studies published before 2010 were all excluded, as shown in Fig. 2.

## Evaluation of the analytical standard

Two authors (WN and LZ) independently examined the methodological validity of the included studies using the quality evaluation of diagnostic accuracy test assessment instrument to establish their methodological quality (QUADAS-2). One author (JS) was also in charge of addressing any issues that arose among other co-authors of this study.

## Statistical analyses

A 2 × 2 table was created to determine the pooled sensitivity, specificity and diagnostic OR using the DerSimonian and Laird approach. A higher diagnostic OR number suggests that the test is more accurate in its diagnosis. The I<sup>2</sup> index and the Cochran's Q statistic were used to determine the heterogeneity of the studies. MedCalc software (MedCalc Software Ltd., Ostend, Belgium) was used to create the forest plots. The sensitivity and specificity data from the various studies are displayed in a hierarchical summary receiver operating characteristics (HSROC) curve with their respective 95% confidence intervals (95% CIs).

**Table 1.** Demographic summary of included studies with thyroid ultrasound in suspected cases of thyroid malignancy

Study ID and year	Study type	Study duration	Total sample size	Age [years]	Gender M/F	Type of US probe
Arpana et al. 2018 <sup>12</sup>	cross-sectional	1 year	85	14–70	15/70	NR
Al-Ghanimi et al. 2020 <sup>13</sup>	retrospective	2 years	68	8–82	20/48	Esaote US machine (MyLab™ ClassC, Esaote, Genoa, Italy) and electronically focused near-field probes with a bandwidth of 7–12 MHz
Smith-Bindman et al. 2013 <sup>14</sup>	retrospective	5 years	11618	30–70	2277/9341	NR
Liu et al. 2019 <sup>15</sup>	retrospective	5 years	1568	18–80	412/1156	IU22 device (Philips Medical Systems, Bothell, USA; 5–12 MHz linear probe) or the S3000 device (Siemens Medical Solutions, Mountain View, USA; 5–14 MHz linear probe)
Luo et al. 2020 <sup>16</sup>	retrospective	2 years	296	30–50	54/168	The Mylab™ 90 (Esaote SpA, Genoa, Italy) ultrasound image system was used for US examination, the L522 probe (4–9 MHz; Esaote SpA) for CEUS and the L523 probe (7.5–13.0 MHz, Esaote SpA) for conventional gray-scale US, CDUS and ES.
Kwak et al. 2011 <sup>17</sup>	retrospective	8 months	1638	11–81	265/1373	5–12 MHz linear-array transducer (iU22; Philips Medical Systems).
Srinivas et al. 2016 <sup>18</sup>	prospective	4 years	365	18–68	22/334	GE VOLUSON 730 PRO machine (GE Healthcare, Milwaukee, USA) equipped with a 7.5–12 MHz high-frequency linear array transducer with color and power Doppler capability.
Mohanty et al. 2019 <sup>19</sup>	prospective	1 year	50	40–50	10/40	GE Logic F8 ultrasound machine with a 6–12 MHz linear array transducer and Samsung HS70A ultrasound machine with 4–18 MHz linear array transducer (Samsung Neurologica Corp., Danvers, USA)
Nabahati et al. 2019 <sup>20</sup>	cross-sectional	2 years	718	14–83	NR	Samsung H60 ultrasound machine, with a 3–14 MHz linear array transducer (Samsung Neurologica Corp.)
Ghani et al. 2018 <sup>21</sup>	retrospective	2 years	91	27–80	21/83	linear array transducer (5–12 MHz) on ultrasound scanners HD11/HD11 XE/iU22 (Phillips Medical Systems) or Toshiba Xario200 (Toshiba Corp., Tokyo, Japan)
Ram et al. 2015 <sup>22</sup>	cross-sectional	2 years	101	15–73	20/81	High frequency linear probe with 7.5 MHz bandwidth (models Zario and Nemio; Toshiba Corp.)
Wettasinghe et al. 2019 <sup>23</sup>	prospective	1.5 years	263	16–74	16/247	NR
Azizi et al. 2021 <sup>24</sup>	prospective	1 year	355	40–50	45/310	virtual organ computer-aided analysis; (VOCAL; GE Healthcare) and a 3-D multi-planar display with rendering in HDLive and HDLive Silhouette (GE Healthcare).
Zayadeen et al. 2016 <sup>25</sup>	retrospective	3 years	1466	11–96	265/1201	5–12 MHz linear probe (iU22, Philips Healthcare) or a 6–15-MHz linear probe (Logiq E9, GE Healthcare)
Richie and Mellonie 2021 <sup>26</sup>	retrospective	2 years	226	18–62	39/187	NR

US – ultrasound; NR – not reported; CEUS – contrast-enhanced ultrasound; CDUS – color Doppler ultrasonography; ES – elastosonography.

## Analysis of sensitivity

Excluding individuals with equivocal results might cause diagnostic test accuracy to be overestimated. As a result, the sensitivity analysis was carried out, with uninterpretable data factored into the analysis. Finally, we compared the outcomes of the primary analysis, which excluded uninterpretable data, to those of the diagnostic precision analysis, which included all uninterpretable results.

## Investigation of sources of heterogeneity

Meta-regression was used to investigate heterogeneity of the included experiments, introducing various sources of heterogeneity as covariates and fitting a bivariate model. To assess the covariate effect on the sensitivity and precision, probability ratio test was used. A p-value <0.05 was considered statistically significant for any of the subgroups. Full-text publications compared to abstracts, high compared to low risk of bias (RoB) in included studies, prospective compared to retrospective studies, studies that



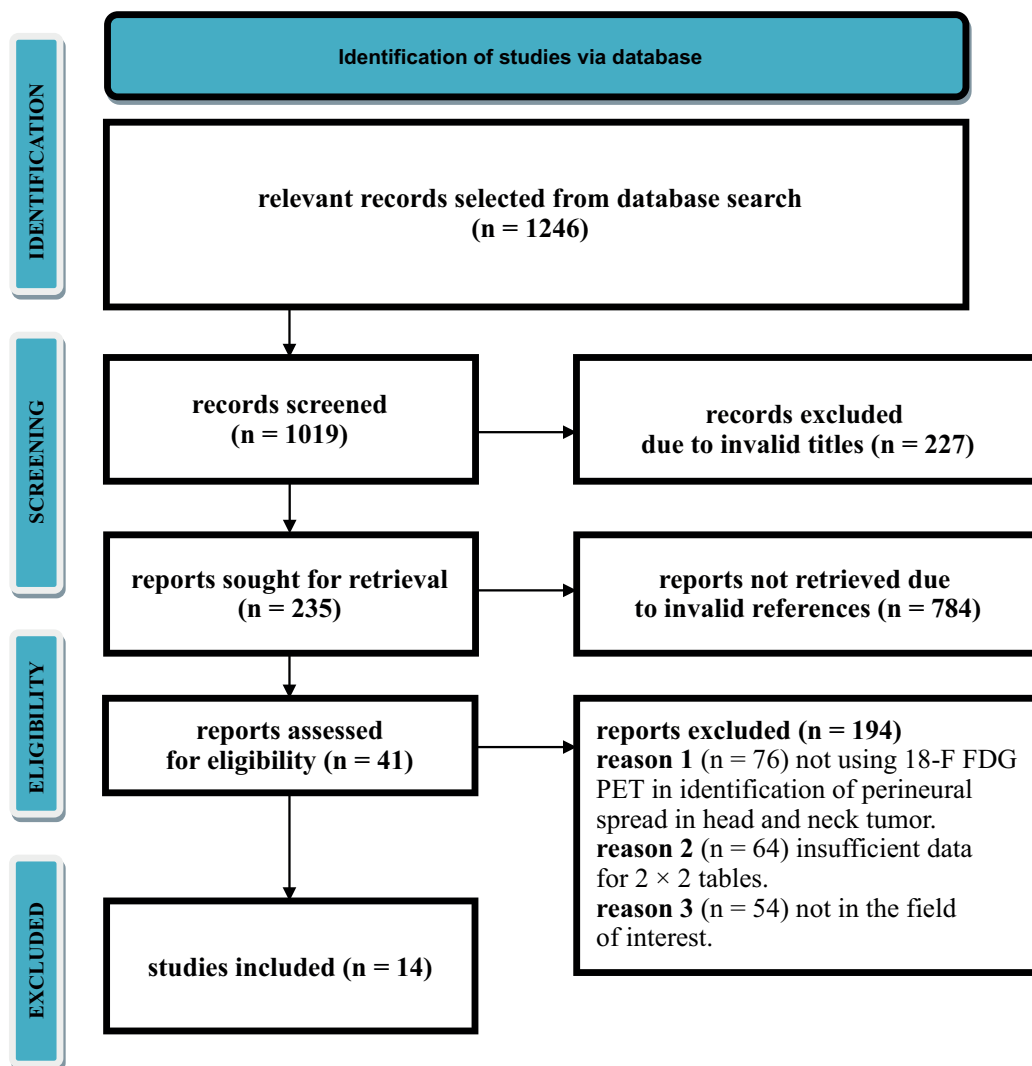


Fig. 2. Preferred Reporting Items for Systematic Reviews and Meta-Analyses (PRISMA) diagram

TIRADS – Thyroid Imaging Reporting And Data System; 18-FDG PET – 18-fluorodeoxyglucose, positron emission tomography.

included only adults compared to mixed adult and pediatric population studies, the proportion of female participants, the proportion of obese patients, type of US probe, and ultrasonographer experience were among the investigated heterogeneity sources.

## Results

### Literature search results

Through computerized scanning, a total of 2765 studies were retrieved. We eliminated 745 articles based on their titles and abstracts, and 1825 papers due to faulty references. Owing to duplicity, about 165 out of the remaining 195 studies were removed. Finally, 30 full-text publications were screened. Among these, 15 were eliminated due to inclusion requirements. As a result, as shown in Fig. 2, this meta-analysis included 15 papers that satisfied the inclusion criteria, namely morphological characteristics of thyroid USG as per TIRADS standards. The main grounds for omission were inadequate evidence and improper comparison criteria needed for creating 2 × 2 tables for review.

The demographic details of the studies included in this meta-analysis are shown in Table 1. It describes the authors of each included study, year of publication, type of study, duration of the study, total sample size, type of US probe used in the study, age, gender, and the total number of nodules on which US was conducted. In addition, the morphological features of the thyroid nodule, as suggested by TIRADS guidelines (Fig. 1), are set as a gold standard for its characterization. A total of 18,908 patients were included in all analyzed studies. Four of the studies were prospective, 8 were retrospective and 3 were cross-sectional, and they were all published as full-text publications. The participants' age ranged from 8 to 80 years, and the information regarding the type of utilized US probe was provided.

### Risk of bias assessment

The estimated sensitivity value ranged from 74% to 98%, whereas the estimated specificity value ranged from 8% to 84%. According to the QUADAS-2 tool, all of the included experiments had a low likelihood of bias, as indicated in Table 2. Figure 3 shows a Duke funnel plot used to assess the possibility of publication bias.

### Meta-analysis results

The overall sensitivity of the US scan for thyroid nodule was 92.53% (95% CI: [84.55%; 96.33%]) and overall specificity was 33.88% (95% CI: [23.16%; 45.53%]) with  $p < 0.001$ , indicative of statistical significance. The value of the overall PLR was 6.90 (95% CI: [2.66; 23.8]), and the overall NLR value was 0.71 (95% CI: [0.59; 0.85]), as shown in Table 3. These results proved the high accuracy of US scan in detecting only positive nodules as malignant. The summary receiver operating characteristic (SROC) plot showing an estimate of sensitivity compared to specificity and area under the SROC curve, as shown in Fig. 4, indicates its positive efficiency. The box and whisker plot (Fig. 5) clearly shows that the diagnostic accuracy of thyroid US is high, as the number of TP results is high, similarly to the results of FNAB, while number of FP results is low. The diagnostic OR was 12.36 (95% CI: [3.90; 54.11]), as shown in Table 4. As reported, the diagnostic OR higher than 10 indicates the positive outcome of a test, as shown in the forest plot in Fig. 6. Our results are congruent with those reports and suggest a greater accuracy of thyroid US in diagnosing thyroid cancer.

### Discussion

Accurate diagnosis of a worrisome thyroid nodule for malignancy has always been challenging because initial symptoms of both nodules, either benign or malignant, are

**Table 2.** Exploration of heterogeneity sources; the impact of sample subgroups or participant characteristics on overall sensitivity and specificity

Subgroup	p-value
Full texts compared to abstracts	NA
High compared to low risk of bias	NA
Prospective compared to retrospective studies	0.024*
Adults compared to mixed population	0.924
Proportion of female participants	0.05*
Proportion of obese participants	NA
Type of ultrasound probe	0.034*
Ultrasonographer experience	0.001*
Clinical probability of TC	0.001*

TC – thyroid cancer; NA – not available. The details could not be retrieved from the report, or only one party was present; \*significant impact of the subgroup on summary results.

usually the same.<sup>9,10</sup> Therefore, early nodule characterization is of extreme importance since a benign nodule can be easily cured, but treating a malignant nodule is complex and depends on its stage. Therefore, the early detection of malignant nodules increases a patient’s chances of treatment and survival rate; otherwise, thyroid cancer can be fatal.

Fine-needle aspiration biopsy is the gold standard<sup>1,2,9–11</sup> for accurately detecting malignancy in thyroid nodule patients, with a substantial sensitivity of 98%, according to numerous studies.<sup>12–26</sup> It is, however, rarely chosen since

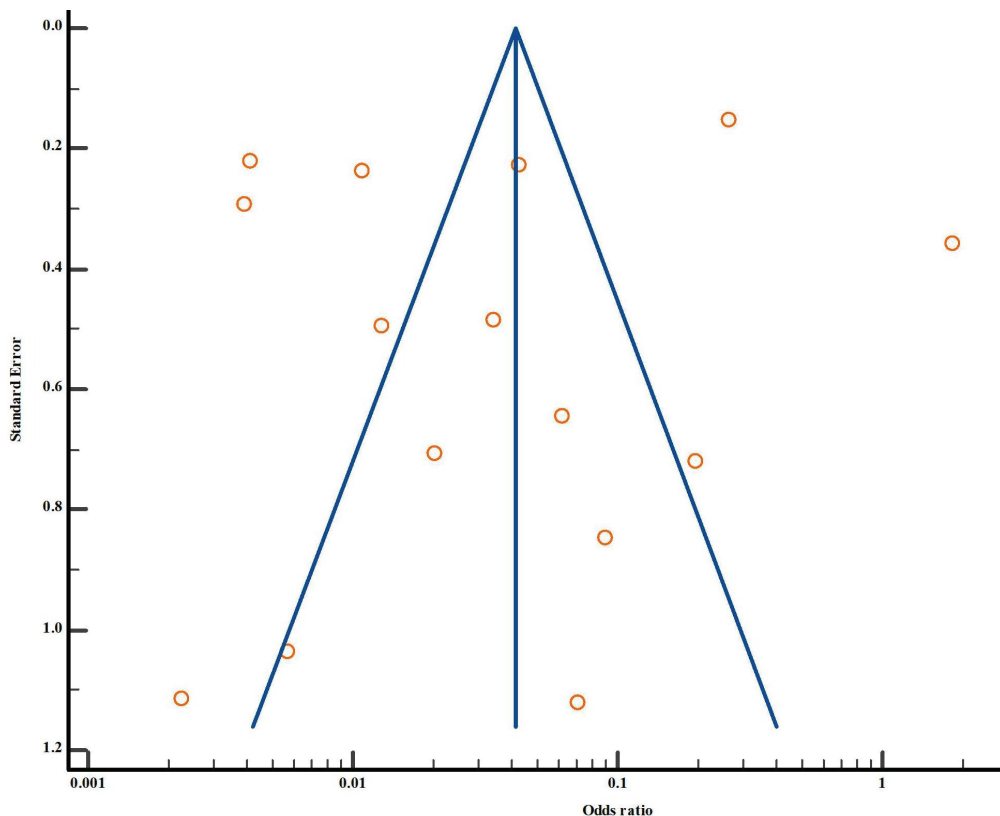


**Fig. 3.** Duke funnel plot test for publication bias

<b>Egger's test</b>	
<b>Significance level</b>	P = 0.5952
<b>Begg's test</b>	
<b>Kendall's Tau</b>	0.04762
<b>Significance level</b>	P = 0.8046

Table 3. Sensitivity and specificity of different studies

Study ID and year	Specificity [%]	95% CI upper limit	95% CI lower limit	Sensitivity [%]	95% CI upper limit	95% CI lower limit
Kwak et al. 2011 <sup>17</sup>	24.06	21.51	26.75	96.66	94.88	97.95
Smith-Bindman et al. 2013 <sup>14</sup>	23.61	18.83	28.95	87.94	83.56	91.50
Ram et al. 2015 <sup>22</sup>	8.06	2.67	17.83	97.50	86.84	99.94
Zayadeen et al. 2016 <sup>25</sup>	14.25	11.98	16.78	97.57	96.46	98.41
Srinivas et al. 2016 <sup>18</sup>	48.15	28.67	68.05	96.45	93.88	98.15
Ghani et al. 2018 <sup>21</sup>	23.08	11.13	39.33	93.62	82.46	98.66
Arpana et al. 2018 <sup>12</sup>	32.35	17.39	50.53	88.57	73.26	96.80
Wettasinghe et al. 2019 <sup>23</sup>	13.68	9.55	18.75	96.55	82.24	99.91
Luo et al. 2020 <sup>16</sup>	84.52	77.84	89.82	74.63	62.51	84.47
Liu et al. 2019 <sup>15</sup>	57.93	55.12	60.71	84.00	79.89	87.56
Nabahati et al. 2019 <sup>20</sup>	8.98	6.37	12.21	96.18	94.09	97.68
Mohanty et al. 2019 <sup>19</sup>	60.00	36.05	80.88	95.45	77.16	99.88
Azizi et al. 2021 <sup>24</sup>	14.08	10.21	18.74	92.65	83.67	97.57
Al-Ghanimi et al. 2020 <sup>13</sup>	50.00	15.70	84.30	91.67	81.61	97.24
Richie and Mellonie 2021 <sup>26</sup>	45.45	24.39	67.79	98.53	95.76	99.70

95% CI – 95% confidence interval.

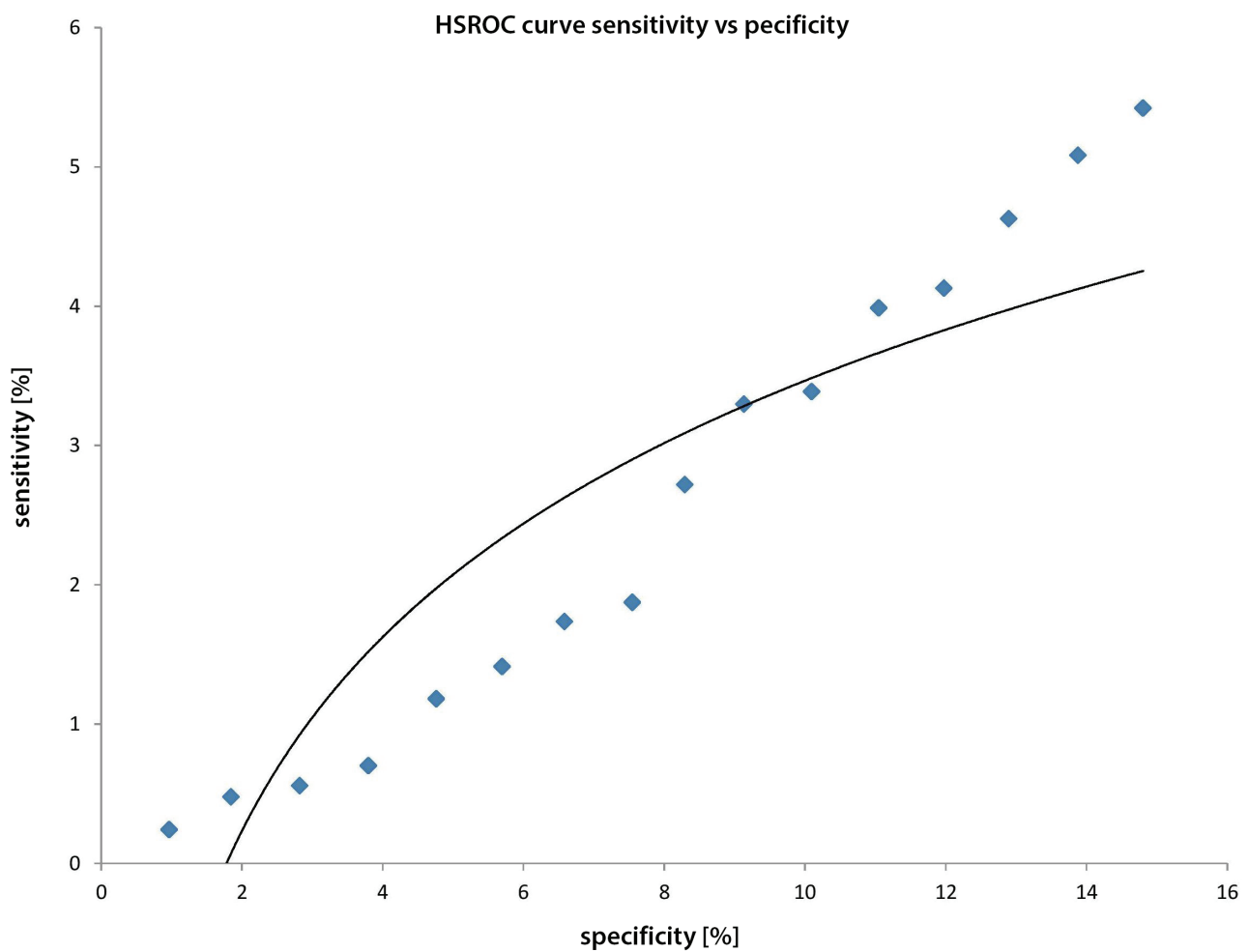


Fig. 4. Hierarchical summary receiver operating characteristics (HSROC) curve sensitivity compared to specificity

Table 4. Diagnostic OR of cases studied

Study ID and year	Benign nodule (simple cyst)	Benign nodule (solid cyst)	Malignant nodule (solid cyst)	Malignant nodule (simple/mixed cyst)	Diagnostic odds ratio	95% CI upper limit	95% CI lower limit
Kwak et al. 2011 <sup>17</sup>	578.00	805.00	255.00	20.00	9.15	5.74	14.61
Bindmann et al. 2013 <sup>14</sup>	248.00	220.00	68.00	34.00	2.25	1.44	3.54
Ram et al. 2015 <sup>22</sup>	39.00	57.00	5.00	1.00	3.42	0.38	30.43
Zayadeen et al. 2016 <sup>25</sup>	1043.00	734.00	122.00	26.00	6.67	4.32	10.29
Srinivas et al. 2016 <sup>18</sup>	326.00	14.00	13.00	12.00	25.23	9.76	65.20
Ghani et al. 2017 <sup>21</sup>	44.00	30.00	9.00	3.00	4.40	1.09	17.60
Arpana et al. 2018 <sup>12</sup>	31.00	23.00	11.00	4.00	3.71	1.05	13.13
Wettasinghe et al. 2019 <sup>23</sup>	28.00	202.00	32.00	1.00	4.44	0.58	33.75
Luo et al. 2020 <sup>16</sup>	50.00	24.00	131.00	17.00	16.05	7.50	32.37
Liu et al. 2019 <sup>15</sup>	315.00	517.00	712.00	60.00	7.23	5.36	9.74
Nabahati et al. 2019 <sup>20</sup>	478.00	365.00	36.00	19.00	2.48	1.40	4.39
Mohanty et al. 2019 <sup>19</sup>	21.00	8.00	12.00	1.00	31.50	3.50	283.30
Azizi et al. 2021 <sup>24</sup>	63.00	238.00	39.00	5.00	2.06	0.78	5.45
Ghanimi et al. 2021 <sup>13</sup>	55.00	4.00	4.00	5.00	11.00	2.08	57.91
Richi et al. 2021 <sup>26</sup>	201.00	3.00	10.00	12.00	55.80	13.50	229.90

OR – odds ratio; 95% CI – 95% confidence interval.

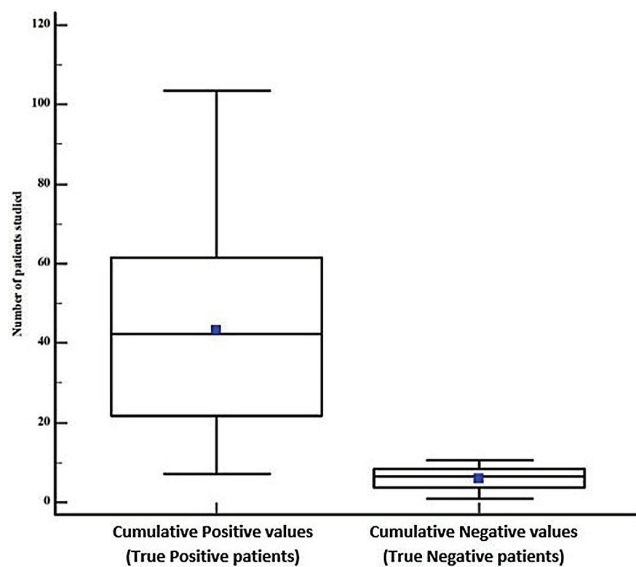


Fig. 5. Box and whisker plot for cumulative positive value (CPV) compared to cumulative negative value (CNV) of samples studied

it is time-consuming, intrusive and costly. The current meta-analysis is an excellent step in simplifying the nodule characterization technique by demonstrating that thyroid USG and FNAB are equally effective in diagnosing probable thyroid cancer in patients of all ages.

In this meta-analysis, a total of 15 publications were chosen to predict the specificity, sensitivity, PLR, NLR, and diagnostic ORs. Overall sensitivity of 92.53% (95% CI: [84.55%; 96.33%]) and specificity of 33.88% (95% CI: [23.16%; 45.53%]) were found in this study. The diagnostic OR was found to be 12.36 (95% CI: [3.90; 54.11]).

The studies covered a wide range of sensitivity, ranging from 74% to 95% with a 95% CI of [60%; 95%], while included studies revealed a wide specificity range ranging from 8% to 85% (95% CI: [2%; 90%]). Latif et al., in a research similar to ours, evaluated FNAB and USG to diagnose benign and malignant thyroid nodules.<sup>27</sup> The gold standard in this investigation was surgery or follow-up.

In this study, the combined sensitivity and specificity in the adult population were 90% and 77%, respectively, supporting the use of US in diagnosing thyroid cancer. Similarly, Ghani et al.<sup>21</sup> showed a sensitivity of 100% and specificity of 91.4%, Wettasinghe et al.<sup>23</sup> calculated sensitivity and specificity of 0.13% and 0.95%, respectively, Luo et al.<sup>16</sup> showed a sensitivity and specificity of 0.72% and 0.83%, respectively, and Richi and Mellonie showed the high specificity of 45%.<sup>12,23,16,26</sup> All these studies, similarly to the present study, are in support of the application of US imaging for the detection of the malignant tumor. However, in contrast to the present analysis, Jiang et al.<sup>28</sup> observed different results and concluded that the US should not be used for diagnosing thyroid cancer cases.

Thyroid USG was very accurate when combined with FNAB by Salam et al., although, unlike the current study, that study did not employ any reference standards (morphological properties of the nodule) to limit the chances of FN results.<sup>4</sup> The positive and negative probability ratios were 6.90 (95% CI: [2.66; 23.8]) and 0.71 (95% CI: [2.66; 23.8]), respectively. The diagnostic OR in this research was 12.36 (95% CI: [3.90; 54.11]), indicating that thyroid USG has a substantial accuracy rate in predicting thyroid cancer. The SROC curve of the current study indicates

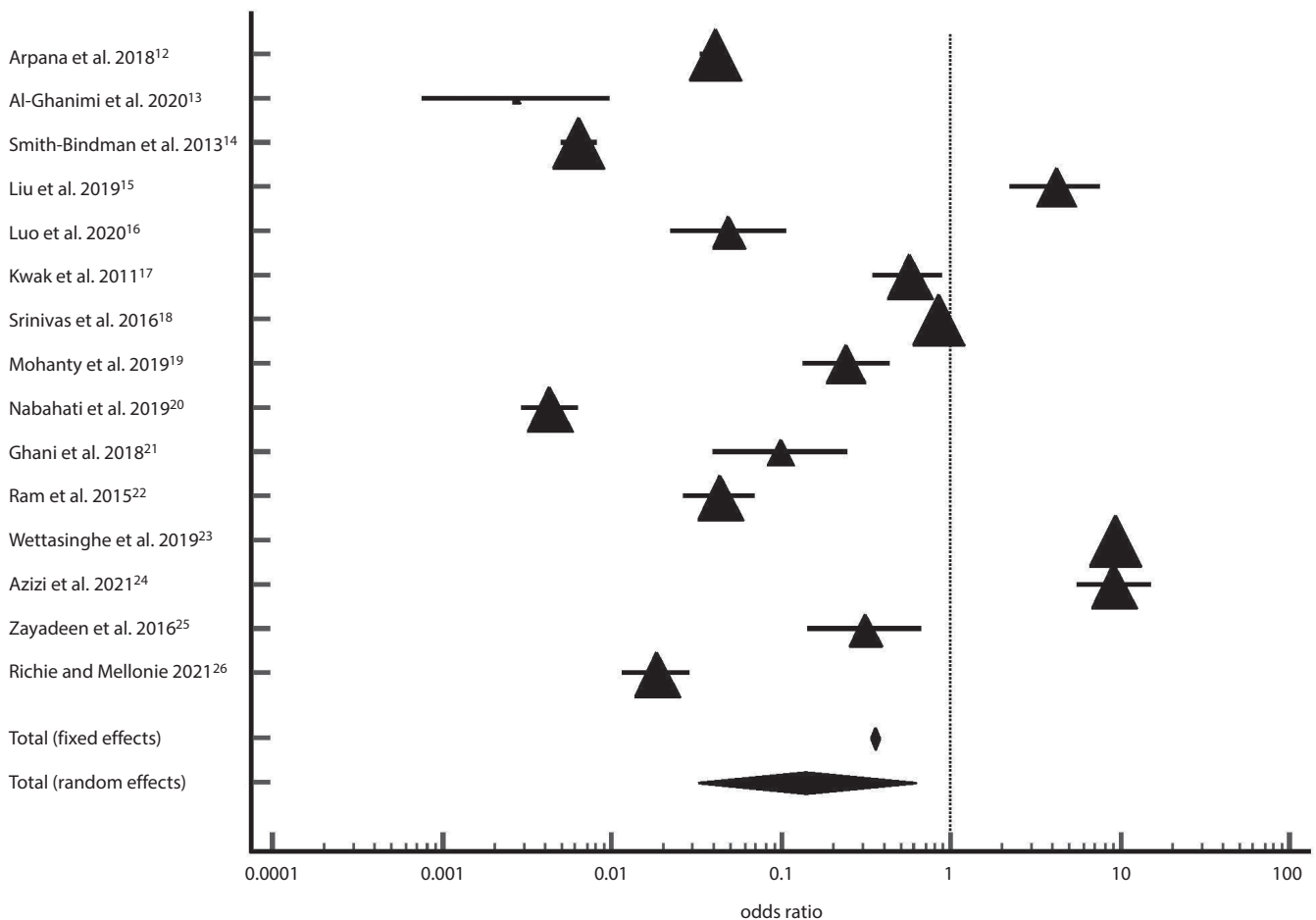


Fig. 6. Forest plot for the diagnostic odds ratio (OR) of case studies100100

the combined effect of sensitivity and specificity, with an inclination of the curve towards the upper left, showing high quality of thyroid US diagnostic accuracy.

Azizi et al. investigated the hypothesis stating that three-dimensional ultrasound (3-D-US) allows for distinguishing benign from malignant thyroid nodules with better sensitivity and specificity than two-dimensional ultrasound (2-D-US).<sup>24</sup> They used both 2-D-US and 3-D-US to examine 344 thyroid nodules, followed by a FNAB. Based on the appearance of the margins in 3-D-US, TNs were categorized into 4 categories. The researchers employed bivariate and multivariate analyses. In 40 individuals, surgical pathology revealed 44 thyroid malignancies. In malignant TNs, uneven margins and microcalcifications ( $p < 0.001$ ) were more common on 2-D-US. The sensitivity and specificity of irregular margins on 2-D-US were 61.4% and 79.3%, respectively.<sup>27</sup> The sensitivity and specificity of irregular margins on 3-D-US were 86.4% and 83.3%, respectively. Microcalcifications and irregular margins on 2-D-US had better sensitivity, specificity, as well as positive and negative predictive values than irregular margins on 3-D-US. The 3-D-US evaluation of TN margins had higher sensitivity and specificity than 2-D-US in distinguishing benign TNs from malignant ones.

### Limitations

The diversity of US equipment utilized and tests performed by various sonographers influence the probability of FN results and are a drawback of this study. Similar diagnosis with FNAB was not specified in many types of research, having an influence on the appropriate analysis of the comparability of data. Data from other relevant studies that demonstrate the diagnostic accuracy of US in contrast to other diagnostic imaging modalities might also be provided to emphasize its significance. To clearly distinguish between a benign and a malignant nodule, specific information about a patient’s case history, physical examination and pathological testing can help to improve the diagnostic accuracy rate of USG in predicting thyroid cancer.

### Conclusions

Ultrasound is a widespread diagnostic investigation tool since it is easy to use, inexpensive and efficient, even though FNAB has considerably reduced the mortality rate owing to its complex surgical technique and high cost. It is a noninvasive, nonionizing radiation approach for

nodule identification in patients of all ages and an efficient diagnostic method to decrease the difficulties associated with FNAB.

### ORCID iDs

Wanlu Nie  <https://orcid.org/0000-0003-4565-7631>

Lili Zhu  <https://orcid.org/0000-0002-6734-4647>

Ping Yan  <https://orcid.org/0000-0002-3533-9413>

Jie Sun  <https://orcid.org/0000-0003-0644-3657>

### References

- Chaturvedi R, Kumar A, Balasubramanian B, Sreehari S. A retrospective study correlating ultrasound based Thyroid Imaging Reporting and Data System (TIRADS) with Bethesda system for thyroid cytopathology in thyroid nodule risk stratification. *NEMJ*. 2021;2(2):121–128. doi:10.2174/025068820366621011152307
- Chen H, Ye J, Song J, You Y, Chen W, Liu Y. Comparison of different ultrasound classification systems of thyroid nodules for identifying malignant potential: A cross-sectional study. *Clinics (Sao Paulo)*. 2021;76:e2126. doi:10.6061/clinics/2021/e2126
- Hahn SY, Shin JH, Oh YL, Park KW. Ultrasound-guided core needle biopsy techniques for intermediate or low suspicion thyroid nodules: Which method is effective for diagnosis? *Korean J Radiol*. 2019;20(10):1454–1461. doi:10.3348/kjr.2018.0841
- Al-Salam S, Sharma C, Abu Sa'a MT, et al. Ultrasound-guided fine needle aspiration cytology and ultrasound examination of thyroid nodules in the UAE: A comparison. *PLoS One*. 2021;16(4):e0247807. doi:10.1371/journal.pone.0247807
- Kim SC, Kim JH, Choi SH, et al. Off-site evaluation of three-dimensional ultrasound for the diagnosis of thyroid nodules: Comparison with two-dimensional ultrasound. *Eur Radiol*. 2016;26(10):3353–3360. doi:10.1007/s00330-015-4193-2
- Xie C, Cox P, Taylor N, LaPorte S. Ultrasonography of thyroid nodules: A pictorial review. *Insights Imaging*. 2016;7(1):77–86. doi:10.1007/s13244-015-0446-5
- Tessler FN, Middleton WD, Grant EG, et al. ACR Thyroid Imaging, Reporting and Data System (TI-RADS): White paper of the ACR TI-RADS committee. *J Am Coll Radiol*. 2017;14(5):587–595. doi:10.1016/j.jacr.2017.01.046
- Nam SJ, Kwak JY, Moon HJ, Yoon JH, Kim EK, Koo JS. Large ( $\geq 3$ cm) thyroid nodules with benign cytology: Can Thyroid Imaging Reporting and Data System (TIRADS) help predict false-negative cytology? *PLoS One*. 2017;12(10):e0186242. doi:10.1371/journal.pone.0186242
- Russ G, Bonnema SJ, Erdogan MF, Durante C, Ngu R, Leenhardt L. European Thyroid Association guidelines for ultrasound malignancy risk stratification of thyroid nodules in adults: The EU-TIRADS. *Eur Thyroid J*. 2017;6(5):225–237. doi:10.1159/000478927
- Trimboli P, Durante C. Ultrasound risk stratification systems for thyroid nodule: Between lights and shadows, we are moving towards a new era. *Endocrine*. 2020;69(1):1–4. doi:10.1007/s12020-020-02196-6
- Colakoglu B, Yildirim D, Alis D, et al. Elastography in distinguishing benign from malignant thyroid nodules. *J Clin Imaging Sci*. 2016;6:51. doi:10.4103/2156-7514.197074
- Arpana, Panta OB, Gurung G, Pradhan S. Ultrasound findings in thyroid nodules: A radio-cytopathologic correlation. *J Med Ultrasound*. 2018;26(2):90–93. doi:10.4103/JMU.JMU\_7\_17
- Al-Ghanimi IA, Al-Sharydah AM, Al-Mulhim S, et al. Diagnostic accuracy of ultrasonography in classifying thyroid nodules compared with fine-needle aspiration. *Saudi J Med Med Sci*. 2020;8(1):25–31. doi:10.4103/sjmm.sjmm\_126\_18
- Smith-Bindman R, Lebda P, Feldstein VA, et al. Risk of thyroid cancer based on thyroid ultrasound imaging characteristics: Results of a population-based study. *JAMA Intern Med*. 2013;173(19):1788–1796. doi:10.1001/jamainternmed.2013.9245
- Liu T, Guo Q, Lian C, et al. Automated detection and classification of thyroid nodules in ultrasound images using clinical-knowledge-guided convolutional neural networks. *Med Image Anal*. 2019;58:101555. doi:10.1016/j.media.2019.101555
- Luo W, Zhang Y, Yuan J, et al. Differential diagnosis of thyroid nodules through a combination of multiple ultrasonography techniques: A decision-tree model. *Exp Ther Med*. 2020;19(6):3675–3683. doi:10.3892/etm.2020.8621
- Kwak JY, Han KH, Yoon JH, et al. Thyroid imaging reporting and data system for US features of nodules: A step in establishing better stratification of cancer risk. *Radiology*. 2011;260(3):892–899. doi:10.1148/radiol.11110206
- Srinivas MN, Amogh VN, Gautam MS, et al. A prospective study to evaluate the reliability of thyroid imaging reporting and data system in differentiation between benign and malignant thyroid lesions. *J Clin Imaging Sci*. 2016;6:5. doi:10.4103/2156-7514.177551
- Mohanty J, Sanket, Mishra P. Role of ACR-TIRADS in risk stratification of thyroid nodules. *Int J Res Med Sci*. 2019;7(4):1039–1043. doi:10.18203/2320-6012.ijrms20191076
- Nabahati M, Moazezi Z, Fartookzadeh S, Mehraeen R, Ghaemian N, Sharbatdaran M. The comparison of accuracy of ultrasonographic features versus ultrasound-guided fine-needle aspiration cytology in diagnosis of malignant thyroid nodules. *J Ultrasound*. 2019;22(3):315–321. doi:10.1007/s40477-019-00377-2
- Ghani FA, Nurismah MI, Husyairi H, Shahrun Niza AS, Radhika S. Reliability of the ultrasound classification system of thyroid nodules in predicting malignancy. *Med J Malaysia*. 2018;73(5):263–271. PMID:30350802.
- Ram N, Hafeez S, Qamar S, et al. Diagnostic validity of ultrasonography in thyroid nodules. *J Pak Med Assoc*. 2015;65(8):875–878. PMID:26228335.
- Wettasinghe MC, Rosairo S, Ratnatunga N, Wickramasinghe ND. Diagnostic accuracy of ultrasound characteristics in the identification of malignant thyroid nodules. *BMC Res Notes*. 2019;12(1):193. doi:10.1186/s13104-019-4235-y
- Azizi G, Faust K, Ogden L, et al. 3-D ultrasound and thyroid cancer diagnosis: A prospective study. *Ultrasound Med Biol*. 2021;47(5):1299–1309. doi:10.1016/j.ultrasmedbio.2021.01.010
- Zayadeen AR, Abu-Yousef M, Berbaum K. Retrospective evaluation of ultrasound features of thyroid nodules to assess malignancy risk: A step toward TIRADS. *AJR Am J Roentgenol*. 2016;207(3):460–469. doi:10.2214/AJR.15.15121
- Richie AJ, Mellonie P. Accuracy of thyroid imaging and reporting data systems in risk stratification of thyroid nodules: A retrospective observational study. *Int J Anat Radio Surg*. 2021;10(1):58–61. doi:10.7860/IJARS/2021/47306:2627
- Latif MA, El Rakhawy MM, Saleh MF. Diagnostic accuracy of B-mode ultrasound, ultrasound elastography and diffusion weighted MRI in differentiation of thyroid nodules (prospective study). *Egypt J Radiol Nucl Med*. 2021;52:256. doi:10.1186/s43055-021-00640-9
- Jiang D, Zang Y, Jiang D, Zhang X, Zhao C. Value of rapid on-site evaluation for ultrasound-guided thyroid fine needle aspiration. *J Int Med Res*. 2019;47(2):626–634. doi:10.1177/0300060518807060

# Oral cancer awareness among patients at 3 university hospitals in Poland and Germany: A survey research

Hanna Gerber<sup>1,A–F</sup>, Tomasz Gedrange<sup>2,A,B,F</sup>, Piotr Szymor<sup>3,B,C</sup>, Anna Leszczyszyn<sup>4,B,C</sup>, Marcin Kubiak<sup>1,A–F</sup>, Monika Rutkowska<sup>5,D,E</sup>, Michał Sarul<sup>6,D,E</sup>, Sylwia Hnitecka<sup>1,C–F</sup>

<sup>1</sup> Department of Maxillofacial Surgery, Wrocław Medical University, Poland

<sup>2</sup> Department of Orthodontics, Technische Universität Dresden, Germany

<sup>3</sup> Maxillofacial Department, Medical University of Lodz, Poland

<sup>4</sup> Dental Outpatient Clinic, 4<sup>th</sup> Military Hospital, Wrocław, Poland

<sup>5</sup> Department of Maxillofacial Surgery, 4<sup>th</sup> Military Hospital, Wrocław, Poland

<sup>6</sup> Department of Maxillofacial Orthopaedics and Orthodontics, Wrocław Medical University, Poland

A – research concept and design; B – collection and/or assembly of data; C – data analysis and interpretation;

D – writing the article; E – critical revision of the article; F – final approval of the article

Advances in Clinical and Experimental Medicine, ISSN 1899–5276 (print), ISSN 2451–2680 (online)

*Adv Clin Exp Med.* 2022;31(6):607–613

## Address for correspondence

Sylwia Hnitecka

E-mail: sylwia.hnitecka@gmail.com

## Funding sources

None declared

## Conflict of interest

None declared

Received on May 18, 2021

Reviewed on November 1, 2021

Accepted on February 7, 2022

Published online on February 23, 2022

## Cite as

Gerber H, Gedrange T, Szymor P, et al. Oral cancer awareness among patients at 3 university hospitals in Poland and Germany: A survey research. *Adv Clin Exp Med.* 2022;31(6):607–613. doi:10.17219/acem/146455

## DOI

10.17219/acem/146455

## Copyright

Copyright by Author(s)

This is an article distributed under the terms of the Creative Commons Attribution 3.0 Unported (CC BY 3.0) (<https://creativecommons.org/licenses/by/3.0/>)

## Abstract

**Background.** The epidemic of cancer (including oral cancer) is a growing public health and economic problem in the European societies. A high percentage of patients who come for the appropriate treatment are in the late stages of advancement, often with nodal and/or distant metastases. The literature on the public oral cancer awareness in Poland and Germany is limited.

**Objectives.** To investigate the levels of public awareness about the early symptoms and risk factors of oral cancer, and to analyze the findings in the context of the socioeconomic profiles of the subjects.

**Materials and methods.** The survey consisted of a 20-item questionnaire divided into 4 sections: socioeconomic and demographic factors, the awareness of oral cancer, symptoms of oral cancer, and its risk factors. It was distributed to 465 adult patients in Poland (Wrocław and Łódź) and Germany (Dresden).

**Results.** The response rate was 97.6%. Most of the respondents (65.4%) had heard of oral cancer. The sources of information were mainly the traditional mass media and the Internet, with only 23.8% of the respondents indicating doctors as a source of information about oral cancer. What is worrying, only about 1/5 of the participants in each of the 3 centers had an oral cancer examination last year. The awareness of oral cancer correlated positively with the age of the respondents and negatively with the size of the place of residence. Education level had no significant impact on declared knowledge.

**Conclusions.** The results of this survey do not only show unsatisfactory levels of patients' awareness of the risk factors and symptoms of oral cancer but also emphasize the need to improve the level of healthcare concerning this disease, including screening programs.

**Key words:** oncology, awareness, head and neck, oral cancer

## Background

The silent epidemic of cancer is a growing public health and economic problem in European societies, while oral cancer has been well recognized as part of this problem. As many as 377,713 people were diagnosed with oral and lip cancer in 2020 in the world, according to GLOBOCAN 2020.<sup>1</sup> Around 7300 German and more than 4200 Polish citizens were newly diagnosed with oral and lip cancer in 2020, with 2320 (Germany) and 2051 (Poland) people dying of these cancers over that period.<sup>2,3</sup> Oral and lip cancer are the 17<sup>th</sup> most common malignancy in Germany (1.2%), and the 15<sup>th</sup> most common one in Poland (2.1%). Most of the patients were diagnosed with oral cancer at the age of 50 or older and the 5-year survival rate was about 50–60% both for men and women, which is comparatively lower than rates for most digestive tract cancers, as oral cancer is usually diagnosed at its advanced stages.<sup>4–6</sup> A worryingly high percentage of patients who come for the appropriate treatment are in the late stages of advancement, often with nodal and/or distant metastases.<sup>6</sup> Such advanced cancers usually require aggressive surgical treatment that leads to aesthetic and functional defects of the face and the oral cavity, which significantly decreases patients' quality of life.<sup>6–9</sup> Unfortunately, sometimes, cancer advancement along with patients' general conditions make only palliative therapy possible.<sup>6</sup>

Therefore, the early diagnosis could further improve the survival rate.<sup>10</sup> It has been shown that both patients and healthcare professionals are responsible for delays in the implementation of the appropriate treatment.<sup>6,11</sup> Given the constant advances in medicine regarding the diagnosis and treatment of various diseases, including malignancies, the key question becomes what exactly causes the delayed diagnosis of cancer (which contributes to high mortality) and how it can be improved.

The literature on the public oral cancer awareness in Poland and Germany is limited. Recent studies showed that one of the reasons for advanced-stage diagnosis is the low level of public awareness about oral cancer, its risk factors and symptoms.<sup>7,10,12–14</sup>

## Objectives

This study was designed to investigate the levels of public awareness about the early symptoms and risk factors of oral cancer, and to analyze the findings in the context of the socioeconomic profiles of the subjects.

## Materials and methods

### Questionnaire

A self-designed validated questionnaire was used. The questionnaire was a shortened version of the original one

by Yellowitz et al.,<sup>14</sup> and it was translated into German and Polish in a standardized way. The survey comprised of a 20-item questionnaire divided into 4 sections: 1. Socioeconomic and demographic factors (5 items: age, gender, education level, family status, and place of residence); 2. The awareness of oral cancer (4 items); 3. The symptoms of oral cancer (5 items); 4. The risk factors of oral cancer (6 items).

### Study population

The questionnaire was distributed to 465 selected adult patients at the Departments of Maxillofacial Surgery in Wrocław (Poland), Łódź (Poland) and Dresden (Germany) from January to October 2013, and in January 2021. The cities were chosen as the research sites due to numerous similarities: population, infrastructure, and comparable educational and economic profiles. Randomly selected adult patients already diagnosed with oral cancer who were receiving the treatment, along with the patients visiting the Departments for the first time with potentially cancerous lesions, were included in the study. The questionnaire was distributed in the waiting rooms of the Departments. Prospective respondents had been assured of their anonymity and the confidentiality of the survey.

### Statistical analyses

The analyses were performed using the statistical package STATISTICA v. 13.3 (TIBCO Software Inc., Palo Alto, USA). Each categorical variable is presented as numbers and percentages. The comparisons were performed with the  $\chi^2$  test. The value of  $p < 0.050$  was considered statistically significant. Due to the dichotomous nature of the dependent variables (answers to the questionnaire questions), a logistic regression analysis was performed. The independent (describing) variables were sociodemographic characteristics of the patients. Logistic regression coefficients were estimated using the maximum likelihood method. Dependent variables (explained, e.g., having knowledge) are dichotomous variables; therefore, to assess the probability of their occurrence depending on the level of independent variables, uni- and multivariate logistic regressions were used.

### Ethics statement

The research was conducted in 3 cities (Wrocław, Łódź and Dresden). All data was collected, kept and analyzed in Wrocław (Maxillofacial Department of Wrocław Medical University). The study was officially approved by Wrocław Medical University (Bioethics Committee of Wrocław Medical University, approval No. KB 760/2012). The research was conducted in accordance with the Declaration of Helsinki of 1975, as revised in 2008.



## Results

The response rate was 97.6% (454 out of 465 respondents completed the questionnaire). In 9 cases, the respondents wrote additional notes unrelated to the study, and some answers were omitted in 11 cases. Nonetheless, all of the questionnaires were taken into consideration. The reliability of the questionnaire was rated as acceptable (Cronbach’s alpha 0.72).

The age of the participants ranged from 18 to 95 years, and the men to women ratio was 161:293. There were no statistically significant differences between the compared centers in the gender structure ( $p = 0.230$ ). The majority of respondents had completed secondary education (55.9%). The detailed demographics of the study population are presented in Table 1.

Most of the respondents (65.4%) had heard of oral cancer, but the levels of self-declared awareness were significantly lower in the Polish population than in the German one (50% in Wrocław and 50% in Łódź compared to 100% in Dresden) (Fig. 1). The sources of information were mainly the traditional mass media (similar values in 3 centers) and the Internet. The knowledge about oral cancer was obtained less frequently from the Internet by patients in Dresden than patients in Wrocław (35.7% compared to 53.3%;  $p < 0.001$ ) and Łódź (35.7% compared to 65.7%;  $p = 0.002$ ). Only 23.8%

of the respondents indicated doctors as a source of information about oral cancer. The majority of the respondents would consult with general practitioners and dentists, if concerned.

The information about neoplasms was less frequently reported by patients aged 19–39 than patients over the age of 65 (54.8% compared to 70.0%;  $p = 0.034$ ), and in the age of 40–65 (54.8% compared to 78.7%;  $p < 0.001$ ). However, the knowledge about oral cancer is more often obtained from the Internet by patients aged 19–39 than patients over the age of 65 (57.8% compared to 30.2%;  $p < 0.001$ ), and in patients aged 40–65 (57.8% compared to 43.1%;  $p = 0.015$ ). The older the patients, the less frequently they use the Internet to obtain the information about oral cancer. Using Internet for this purpose correlates positively with education ( $r = 0.159$ ,  $df = 322$ ,  $p = 0.04$ ). People with higher education more often gathered the knowledge from the Internet.

About 20% of the participants in each of the 3 centers had an oral cancer examination last year (Table 2, Fig. 2).

The perception of most signs and symptoms in the studied groups was similar (Table 3). A lump in the oral cavity, on the tongue or lips would worry less often patients in Dresden than patients in Wrocław (44.3% compared to 68.0%;  $p < 0.001$ ) and Łódź (44.3% compared to 61.4%;  $p = 0.020$ ).

The features most frequently identified as oral cancer risk factors were: tobacco smoking (84.4%), alcohol (69.8%) and prior viral infection (for example human papillomavirus (HPV)) (39.2%). According to the inhabitants of Wrocław,

Table 1. Basic statistics of demographic data of the studied patients and the results of comparisons ( $\chi^2$  test)

Demographic data	Wrocław n = 244	Łódź n = 70	Dresden n = 140	p-value
	n	n	n	
Age				
19–39 years	153	30	47	$\chi^2 = 42.6$ $df = 4$ <b>&lt;0.001</b>
40–65 years	56	33	75	
≥66 years	35	7	18	
Sex				
Women	163	39	91	$\chi^2 = 2.94$ $df = 2$ 0.230
Men	81	31	49	
Education level				
Primary	20	9	38	$\chi^2 = 32.2$ $df = 4$ <b>&lt;0.001</b>
Secondary	159	36	59	
Tertiary	65	25	43	
Family status				
Single	143	24	56	$\chi^2 = 38.0$ $df = 6$ <b>&lt;0.001</b>
Married	77	34	79	
Divorced	14	5	5	
Widow(-er)	10	7	0	
Place of residence				
Village	60	10	75	$\chi^2 = 110$ $df = 4$ <b>&lt;0.001</b>
County town	76	10	59	
Voivodeship city	108	50	6	

df – degrees of freedom. Values in bold are statistically significant.

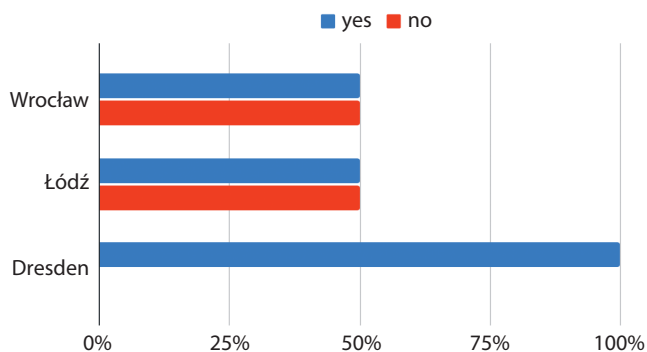


Fig. 1. Insufficient knowledge about cancer among the general population

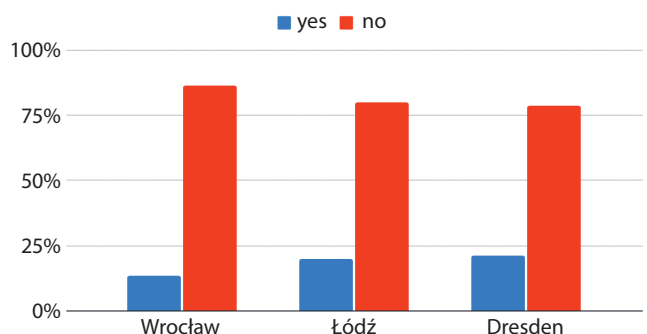


Fig. 2. Low percentage of oral cavity cancer routine check-up

**Table 2.** The number (n) and proportion (%) of patients in respective subgroups regarding responses to the questionnaire on knowledge about oral cancer and the results of comparisons

Question	Wrocław		Łódź		Dresden		$\chi^2$	p-value
	n = 244		n = 70		n = 140			
	n	%	n	%	n	%		
1. Do you have information about cancers of the mouth, tongue or lip?								
Yes	122	50.0	35	50.0	140	100.0	107	<b>&lt;0.001</b>
No	122	50.0	35	50.0	0	0.0		
2. What sources do you have the information from?								
a. TV, radio, newspapers	61	40.7	19	54.3	78	55.7	7.07	<b>0.029</b>
b. Internet	80	53.3	23	65.7	50	35.7	14.5	<b>&lt;0.001</b>
c. Doctor	47	31.3	16	45.7	45	32.1	2.78	0.250
d. Friends	32	21.3	3	8.6	54	38.6	17.8	<b>&lt;0.001</b>
3. If something disturbed you in your mouth, which doctor would you go to?								
a. General practitioner	120	49.6	25	37.3	69	49.3	3.38	0.184
b. Dentist	112	46.3	46	68.7	79	56.4	11.6	<b>0.003</b>
c. ENT	56	23.1	10	14.9	28	20.0	2.25	0.325
d. Other	9	3.7	4	6.0	1	0.7	4.77	0.092
4. Have you had an oral cavity cancer check-up in the last 12 months?								
No	211	86.5	56	80.0	110	78.6	4.49	0.106
Yes	33	13.5	14	20.0	30	21.4	–	

ENT – ear, nose, and throat doctor. For all  $\chi^2$  tests, the number of degrees of freedom is 2. Values in bold are statistically significant.

**Table 3.** Number (n) and proportion (%) of patients in subgroups who differed by study site and questionnaire responses to disturbing symptoms and comparison results

Question	Wrocław n = 244		Łódź n = 70		Dresden n = 140		$\chi^2$	p-value
	n	%	n	%	n	%		
5. Which of the symptoms in the mouth would concern you?								
a. White or red plaques in the mouth, on the tongue or on lips	109	44.7	32	45.7	68	48.6	0.55	0.760
b. Non-healing wounds in the mouth, on the tongue or on lips	148	60.7	48	68.6	80	57.1	2.56	0.278
c. Difficulty chewing or swallowing	112	45.9	37	52.9	58	41.4	2.48	0.290
d. A lump in the mouth, on the tongue or on lips	166	68.0	43	61.4	62	44.3	21.0	<b>&lt;0.001</b>
e. Oral cavity pain	127	52.0	41	58.6	60	42.9	5.32	0.070
f. Numbness of the tongue or other parts of the mouth	130	53.3	30	42.9	62	44.3	4.09	0.130

For all  $\chi^2$  tests, the number of degrees of freedom is 2. Values in bold are statistically significant.

alcohol consumption may have an impact on the development of oral cancer less often, as compared with the inhabitants of Dresden (56.6% compared to 88.6%;  $p < 0.001$ ). Age influences cancer less often, according to the inhabitants of Wrocław, when compared with the inhabitants of Dresden (28.7% compared to 44.3%;  $p = 0.002$ ) and Łódź (28.7% compared to 41.4%;  $p = 0.044$ ). The infection with viruses, e.g., HPV, may have an influence on the development of cancer in the oral cavity more often, according to the patients in Wrocław, compared with the patients in Łódź and Dresden (45.5% compared to 25.7%;  $p = 0.003$  and 35.0%;  $p = 0.045$ , respectively; Table 4). Patients with higher education more often believed that the analyzed factors could affect the development of cancer in the oral cavity than patients with primary and secondary education.

Statistically significant differences were observed for all factors, except for alcohol consumption, diet and nutrition.

The estimated values of the logistic regression coefficients of the analyzed features with the survey responses are presented in supplementary material (<https://doi.org/10.5281/zenodo.6078355>).

The knowledge of oral cancer positively correlated ( $r = 0.200$ , degrees of freedom (df) = 453,  $p < 0.001$ ) with the patients' age (the older the patient, the bigger the knowledge) and negatively ( $r = 0.137$ ,  $p = 0.004$ ) with the place of residence (the more inhabitants of a given place, the less the knowledge).

Interestingly, the education level has no significant impact on declared knowledge ( $r = 0.015$ , df = 453,  $p = 0.938$ ). On the other hand, people with higher education name

**Table 4.** Number (n) and proportion (%) of patients in subgroups that differed by study site and survey responses to the causes of cancer and comparison results

Question	Wrocław n = 244		Łódź n = 70		Dresden n = 140		$\chi^2$	p-value
	n	%	n	%	n	%		
6. Which of the following factors, in your opinion, may affect the development of cancer in the oral cavity?								
a. Tobacco use	204	83.6	55	78.6	124	88.6	3.76	0.152
b. Alcohol consumption	138	56.6	55	78.6	124	88.6	46.3	<b>&lt;0.001</b>
c. Age	70	28.7	29	41.4	62	44.3	10.7	<b>0.005</b>
d. Viral infection, i.e., HPV	111	45.5	18	25.7	49	35.0	10.4	<b>0.005</b>
e. Overexposure to sunlight	88	36.1	33	47.1	69	49.3	7.34	<b>0.025</b>
f. Nutrition, diet	58	23.8	17	24.3	28	20.0	0.84	0.657

HPV – human papillomavirus. For all  $\chi^2$  tests, the number of degrees of freedom is 2. Values in bold are statistically significant.

the symptoms and risk factors of oral cancer correctly more often than patients with primary and secondary education only.

Acquiring the information about oral cancer from the Internet correlates negatively with age ( $r = -0.580$ ), and positively with the size of the place of residence ( $r = 0.465$ ) and the level of education ( $r = 0.607$ ).

More people aged over 65 than younger ones attended oral cancer examinations last year. The very low interest rate (less than 20%) is alarming.

It is important that the explanatory ability of the models is poor, as reflected by a very low Nagelkerke's R<sup>2</sup>. A weak but statistically significant correlation was observed between the independent (explanatory) variables, i.e., education, age and place of residence. The dependent variable (described) values of the odds ratios (ORs) and their 95% confidence intervals (95% CIs) were estimated using multivariate logistic regression.

## Discussion

The study was conducted to assess the awareness of the risk factors and early signs of oral cancer among patients at 3 maxillofacial surgery departments in Poland and Germany, and analyze the findings in the context of the socioeconomic profile of the subjects. To the authors' knowledge, this is the first German-Polish study of this type. Relatively little attention has been paid to the level of public awareness of this type of cancer, taking into account both patients and healthcare providers.

Over 65% of the respondents in our study had ever heard about oral cancer, which is comparable to the studies from different countries.<sup>15–17</sup> The sources of the information were, similarly to the other studies, mainly television, radio and newspapers, but the role of the Internet is gaining significance.<sup>18–20</sup> The fact that less than a quarter of respondents mentioned doctors as a source of information about oral cancer is alarming. The other studies, however, showed even lower rates.<sup>19,20</sup> Also, the study concluded

that less than 20% of the participants had an oral cancer examination last year, which may be related to the low levels of awareness.<sup>21,22</sup>

It is important to point out that non-medical sources of information increase the level of basic knowledge about cancer and contribute to raising awareness. On the other hand, however, they may turn out to be insufficient for patients without medical education and knowledge.

Grant et al. researched young oral cancer patients in the aspect of symptom recognition and delays in seeking professional help. Actually, most of the participants had some awareness of this disease before noticing the initial symptoms (mainly from the television). However, what is interesting, in some cases, prior knowledge was neither instrumental for patients to suspect they may have oral malignancy nor did it prompt them to visit a doctor. The patients, ignoring the seriousness of the symptoms, undertook self-treatment. A very important conclusion of the authors was that the relationship between having awareness and knowing the symptoms might be disturbing for the patients and persuade them to visit a healthcare professional.<sup>18</sup>

Therefore, it turns out that healthcare professionals play an essential role in terms of increasing the awareness and early detection of the disease. In our research, when asked "If something worrisome would appear in your oral cavity, where would you go for a consultation?", the patients indicated not only a dentist but also a general practitioner (GP), otolaryngologist and other healthcare professionals.

People, depending on the disturbing symptoms they notice within the oral cavity, seek advice from doctors of various specializations.<sup>6</sup> It means that oncological vigilance against oral cancer is necessary not only among dentists but also among all doctors.

In terms of the main risk factors of oral cancer, the vast majority (84.3%) of the respondents indicated tobacco, similarly to data from other studies.<sup>19,20,23</sup> Alcohol consumption was recognized as a risk factor by less than 70% of subjects. Some researchers showed even lower results: 55% for tobacco<sup>24</sup> and 33.8% for alcohol.<sup>23</sup> Since

the synergistic effect of both of these risk factors is little known to the public, it is very important to inform more people about its role in the oral cancer pathogenesis. Also, a relatively high percentage (39.2%) of the respondents described infections as an oral cancer risk factor, compared to lower such rates (about 25%) in other studies.<sup>23</sup> A significantly lower percentage of patients indicated diet and malnutrition, as well as ultraviolet (UV) and sunlight exposure as risk factors. Therefore, intending to persuade the population to eliminate modifiable risk factors for cancer development, it is crucial to make people aware of all the factors that predispose them to the disease.

The study showed few associations between the level of awareness of oral cancer and socioeconomic factors. The self-declared awareness of oral cancer correlated positively with age and no significant differences were found in terms of gender. This is consistent with some studies,<sup>17</sup> while other ones showed deficits in older patients and male respondents.<sup>23</sup> An important observation was that the awareness of risk factors and early signs of the disease correlates positively with the level of education, as shown in previous studies.<sup>20,23</sup>

The survey was designed to assess oral cancer awareness among patients seeking advice in maxillofacial surgery departments in 3 selected cities. However, its results do not only show unsatisfactory levels of patients' awareness of the risk factors and symptoms of oral cancer, but also emphasize the need to improve the level of healthcare concerning this disease. It has been shown that to a large extent, people's knowledge comes from the sources of mass media, which positively indicates the advisability of running pro-health campaigns. On the other hand, the patients' knowledge is basic and not sufficient to significantly reduce the causes that delay the implementation of the appropriate treatment. Also, it has been shown that oral cancer screening is not commonly performed. Relatively often, the first (and often early) symptom of malignancy is detected accidentally or during a check-up for another reason; therefore, the improvement in the scope of more frequent screening tests is crucial.<sup>6</sup> This also applies to medical students. Other authors pointed out that the undergraduate students lacked knowledge on the identification and detection of oral cancer, and they were not examining patients' oral mucosae routinely. Also, many students had insufficient information on risk factors and associated oral cancer lesions.<sup>25,26</sup>

It is worth noting that the very low values of Nagelkerke's R2 statistics prove that the ability to explain logistic models is poor.

## Limitations









The limitation of our results is a questionnaire assessing patient awareness and taking into account the suggested answers. Patients, having a choice of the proposed variants (possibility of multiple choice), even without any

knowledge, marked random answers. Open questions, without the option of selecting particular variants, would be more credible. It would be advisable to do such research and compare it with the results presented in this study.

## Conclusion

This study emphasizes the need for public oral cancer preventive programs and public awareness campaigns. Educational efforts of healthcare professionals (especially general practitioners and dentists) should be intensified too. Therefore, it is advisable to conduct the following research among groups of doctors and medical students, and find effective ideas to increase the level of awareness. Similarly, it is important to conduct such research on the pre-malignant disorders, in the aspect of early prevention.

## ORCID iDs

Hanna Gerber  <https://orcid.org/0000-0002-0954-3955>  
 Tomasz Gedrange  <https://orcid.org/0000-0002-3551-6467>  
 Piotr Szymor  <https://orcid.org/0000-0002-6768-5812>  
 Anna Leszczyszyn  <https://orcid.org/0000-0001-7853-2814>  
 Marcin Kubiak  <https://orcid.org/0000-0003-4886-3369>  
 Monika Rutkowska  <https://orcid.org/0000-0003-0243-7751>  
 Michał Sarul  <https://orcid.org/0000-0002-2518-0007>  
 Sylwia Hnitecka  <https://orcid.org/0000-0002-1171-9817>

## References

1. World Health Organization (WHO). Globocan 2020. Lip, oral cavity. <https://gco.iarc.fr/today/data/factsheets/cancers/1-Lip-oral-cavity-fact-sheet.pdf>. Accessed October 11, 2021.
2. World Health Organization (WHO). Globocan 2020. Poland. <https://gco.iarc.fr/today/data/factsheets/populations/616-poland-fact-sheets.pdf>. Accessed October 11, 2021.
3. World Health Organization (WHO). Globocan 2020. Germany. <https://gco.iarc.fr/today/data/factsheets/populations/276-germany-fact-sheets.pdf>. Accessed October 12, 2021.
4. Centre for Oncology – Institute, Polish National Cancer Registry. Cancer in Poland in 2014. Warsaw: Centre for Oncology – Institute, 2016 [http://onkologia.org.pl/wp-content/uploads/Nowotwory\\_2016.pdf](http://onkologia.org.pl/wp-content/uploads/Nowotwory_2016.pdf). Accessed November 20, 2021.
5. Villa A, Kreimer AR, Pasi M, et al. Oral cancer knowledge: A survey administered to patients in dental departments at large Italian hospitals. *J Cancer Educ.* 2011;26(3):505–509. doi:10.1007/s13187-010-0189-4
6. Rutkowska M, Hnitecka S, Nahajowski M, Dominiak M, Gerber H. Oral cancer: The first symptoms and reasons for delaying correct diagnosis and appropriate treatment. *Adv Clin Exp Med.* 2020;29(6):735–743. doi:10.17219/acem/116753
7. Warnakulasuriya KA, Harris CK, Scarrott DM, et al. An alarming lack of public awareness towards oral cancer. *Br Dent J.* 1999;187(6):319–322. doi:10.1038/sj.bdj.4800269
8. Valdez JA, Brennan MT. Impact of oral cancer on quality of life. *Dent Clin North Am.* 2018;62(1):143–154. doi:10.1016/j.cden.2017.09.001
9. Becker ST, Menzebach M, Kuchler T, Hertrampf K, Wenz HJ, Wiltfang J. Quality of life in oral cancer patients: Effects of mandible resection and socio-cultural aspects. *J Craniomaxillofac Surg.* 2012;40(1):24–27. doi:10.1016/j.jcms.2011.01.021
10. Horowitz AM, Moon HS, Goodman HS, Yellowitz JA. Maryland adults' knowledge of oral cancer and having oral cancer examinations. *J Public Health Dent.* 1998;58(4):281–287. doi:10.1111/j.1752-7325.1998.tb03010.x
11. Esmalbeigi F, Hadji M, Harirchi I, Omranipour R, vand Rajabpour M, Zendehehdel K. Factors affecting professional delay in diagnosis and treatment of oral cancer in Iran. *Arch Iran Med.* 2014;17(4):253–257. PMID:24724601.

12. Patton LL, Agans R, Elter JR, Southerland JH, Strauss RP, Kalsbeek WD. Oral cancer knowledge and examination experiences among North Carolina adults. *J Public Health Dent.* 2004;64(3):173–180. doi:10.1111/j.1752-7325.2004.tb02748.x
13. Hertrampf K, Wenz HJ, Koller M, Wiltfang J. Public awareness about prevention and early detection of oral cancer: A population-based study in Northern Germany. *J Craniomaxillofac Surg.* 2012;40(3):e82–e86. doi:10.1016/j.jcms.2011.04.007
14. Yellowitz JA, Horowitz AM, Goodman HS, Canto MT, Farooq NS. Knowledge, opinions and practices of general dentists regarding oral cancer: A pilot survey. *J Am Dent Assoc.* 1998;129(5):579–583. doi:10.14219/jada.archive.1998.0275
15. Tomar SL, Logan HL. Florida adults' oral cancer knowledge and examination experiences. *J Public Health Dent.* 2005;65(4):221–230. doi:10.1111/j.1752-7325.2005.tb03022.x
16. West R, Alkhatib MN, McNeill A, Bedi R. Awareness of mouth cancer in Great Britain. *Br Dent J.* 2006;200(3):167–169. doi:10.1038/sj.bdj.4813197
17. Kawecki MM, Nedeva IR, Iloya J, Macfarlane TV. Mouth cancer awareness in general population: Results from Grampian region of Scotland, United Kingdom. *J Oral Maxillofac Res.* 2019;10(2):e3. doi:10.5037/jomr.2019.10203
18. Grant E, Silver K, Bauld L, Day R, Warnakulasuriya S. The experiences of young oral cancer patients in Scotland: Symptom recognition and delays in seeking professional help. *Br Dent J.* 2010;208(10):465–471. doi:10.1038/sj.bdj.2010.450
19. Babiker TM, Osman KA, Mohamed SA, Mohamed MA, Almahdi HM. Oral cancer awareness among dental patients in Omdurman, Sudan: A cross-sectional study. *BMC Oral Health.* 2017;17(1):69. doi:10.1186/s12903-017-0351-z
20. Al-Maweri SA, Al-Soneidar WA, Dhaifullah E, Halboub ES, Tarakji B. Oral cancer: Awareness and knowledge among dental patients in Riyadh. *J Cancer Educ.* 2017;32(2):308–313. doi:10.1007/s13187-015-0924-y
21. Horowitz AM, Nourjah PA. Factors associated with having oral cancer examinations among US adults 40 years of age or older. *J Public Health Dent.* 1996;56(6):331–335. doi:10.1111/j.1752-7325.1996.tb02460.x
22. Stahl S, Meskin LH, Brown LJ. The American Dental Association's oral cancer campaign: The impact on consumers and dentists. *J Am Dent Assoc.* 2004;135(9):1261–1267. doi:10.14219/jada.archive.2004.0401
23. Hassona Y, Scully C, Abu Ghosh M, Khoury Z, Jarrar S, Sawair F. Mouth cancer awareness and beliefs among dental patients. *Int Dent J.* 2015;65(1):15–21. doi:10.1111/idj.12140
24. Luryi AL, Yarbrough WG, Niccolai LM, et al. Public awareness of head and neck cancers: A cross-sectional survey. *JAMA Otolaryngol Head Neck Surg.* 2014;140(7):639–646. doi:10.1001/jamaoto.2014.867
25. Carter LM, Ogden GR. Oral cancer awareness of undergraduate medical and dental students. *BMC Med Educ.* 2007;7:44. doi:10.1186/1472-6920-7-44
26. Keser G, Pekiner FN. Assessing oral cancer awareness among dental students. *J Cancer Educ.* 2019;34(3):512–518. doi:10.1007/s13187-018-1332-x



# Incidence and survival of ocular melanoma in National Cancer Registry of Poland in 2010–2017

Michał Szymon Nowak<sup>1,2,A,C,D,F</sup>, Bożena Romanowska-Dixon<sup>3,C,E,F</sup>,  
Iwona Grabska-Liberek<sup>4,C,F</sup>, Michał Żurek<sup>5,6,A,B,D,F</sup>

<sup>1</sup> Provisus Eye Clinic, Częstochowa, Poland

<sup>2</sup> Institut of Optics and Optometry, University of Social Sciences, Łódź, Poland

<sup>3</sup> Department of Ophthalmology and Ophthalmic Oncology, Jagiellonian University Medical Collegium, Kraków, Poland

<sup>4</sup> Department of Ophthalmology, Center of Postgraduate Medical Education, Warszawa, Poland

<sup>5</sup> Department of Analyses and Strategies, Ministry of Health, Warszawa, Poland

<sup>6</sup> Doctoral School, Medical University of Warsaw, Poland

A – research concept and design; B – collection and/or assembly of data; C – data analysis and interpretation;

D – writing the article; E – critical revision of the article; F – final approval of the article

Advances in Clinical and Experimental Medicine, ISSN 1899–5276 (print), ISSN 2451–2680 (online)

*Adv Clin Exp Med.* 2022;31(6):615–621

## Address for correspondence

Michał Szymon Nowak

E-mail: michaelnovak@interia.pl

## Funding sources

The present study was a part of the Polish Ministry of Health project “Maps of Healthcare Needs – Database of Systemic and Implementation Analyses” and was co-financed by the European Union funds through the European Social Fund under the Knowledge, Education and Development Operational Program (EU grant No. POWR 05.02.00-00-0149/15-01).

## Conflict of interest

None declared

Received on December 6, 2021

Reviewed on December 29, 2021

Accepted on February 10, 2022

Published online on March 29, 2022

## Cite as

Nowak MS, Romanowska-Dixon B, Grabska-Liberek I, Żurek M. Incidence and survival of ocular melanoma in National Cancer Registry of Poland in 2010–2017.

*Adv Clin Exp Med.* 2022;31(6):615–621.

doi:10.17219/acem/146581

## DOI

10.17219/acem/146581

## Copyright

Copyright by Author(s)

This is an article distributed under the terms of the Creative Commons Attribution 3.0 Unported (CC BY 3.0) (<https://creativecommons.org/licenses/by/3.0/>)

## Abstract

**Background.** Oncology trends are based on data coming from different countries and ocular melanoma is the most common primary eye cancer in adults.

**Objectives.** To investigate the incidence and characteristics of ocular melanoma in the overall population of Poland.

**Materials and methods.** The retrospective survey of both the National Cancer Registry (NCR) and National Health Fund (NHF) databases was performed to identify all ocular melanoma cases in Poland in 2010–2017.

**Results.** The mean incidence of ocular melanoma was 8.76/1,000,000 person-years; the lowest incidence was observed in the 19–29 age group (1.17/1,000,000 person-years) and the highest in the group over 70 (22.88/1,000,000 person-years). There were no statistically significant trends in the incidence rates over the study period. The overall incidences of uveal, eyelid and conjunctival melanoma were 6.67/1,000,000, 0.47/1,000,000 and 0.28/1,000,000 person-years, respectively. The 5-year overall survival (OS) was 60.76%; the higher risk of death was associated with male sex (hazard ratio (HR) = 1.2959), older age at diagnosis (HR = 1.0379), chemotherapy treatment (HR = 1.6774), metastasis (HR = 1.5716), loco-regional hyperplasia (HR = 1.5936), and systemic tumor spread (HR = 3.9872), compared to the carcinoma in situ. The risk of death was reduced by radiotherapy treatment (HR = 0.6645).

**Conclusions.** The incidence rate of ocular melanoma in Poland is in the middle of the range worldwide, and the 5-year OS is relatively low.

**Key words:** radiotherapy, patient survival, ocular melanoma

## Background

Ocular melanoma is the most common primary eye cancer in adults arising from melanocytes located in the conjunctival membrane and uveal tract of the eye, which accounts for 3.7% of all melanoma cases. Among ocular melanomas, 83% arise from the uvea, 5% from the conjunctiva and 10% from other sites in the eye. Uveal melanoma is the most common primary intraocular cancer in adults.<sup>1–5</sup> The incidence of ocular melanoma varies across ethnicities and regions worldwide, with the highest rates in Northern Europe and Australia and the lowest rates in Asian, Hispanic and black populations (i.e., the incidence of uveal melanoma ranges from 0.31 in Black and 0.38 in Asian populations to 11.7/1,000,000 person-years in Northern Europe). However, the incidence rate of uveal melanoma remained stable over the recent decades, while conjunctival melanoma showed an increase in the incidence rate among white men and individuals over 60.<sup>1,4,6–10</sup> The occurrence rate of ocular melanoma is positively correlated with older age, with a peak around the age of 70. However, the mean age of the ocular melanoma diagnosis also varies in different populations, i.e., in Asia, as it affects younger individuals than in Europe or the USA, where it usually presents around the age of 60. The anterior uveal melanoma is also more common in young patients. It represents more than 20% of all uveal melanomas in the age group under 20 compared to 4% and 2% in patients aged 20–60 and over 60, respectively.<sup>1,3,6</sup> Other risk factors associated with ocular melanoma include sex, Caucasian origin, light skin and iris pigmentation, genetic predisposition (BAP1 mutation), environmental factors, and certain dermatological conditions like dysplastic nevus syndrome or nevus of Ota.<sup>11–14</sup> Despite the fact that the treatment of ocular melanoma has evolved with a therapeutic shift to eye-conserving treatment options, it is estimated that still more than 50% of patients develop metastases within 25 years from the initial diagnosis. Poor prognosis indicators include older age at diagnosis, large tumor diameter, anterior location, extraocular extension, histopathological type, and cytogenetic abnormalities.<sup>3,8,15–19</sup> Although the local data from Poland concerning conjunctival and uveal melanomas were analyzed by the RARECAREnet and the European Cancer Registry (EUROCARE) working groups,<sup>4,7,20</sup> data from the entire population of Poland are lacking.

## Objectives

The present study aims to analyze the incidence and characteristics of ocular melanoma in the overall population of Poland in 2010–2017, and to report the patient survival and coexisting risk factors.

## Materials and methods

### Data sources, disease codes and definitions

The present study was a part of the project “Maps of Healthcare Needs – Database of Systemic and Implementation Analyses” coordinated by the Polish Ministry of Health and co-financed by the European Union funds through the European Social Fund under the Knowledge, Education and Development Operational Program (EU grant No. POWR 05.02.00-00-0149/15-01).<sup>21–24</sup> The study design was a retrospective and nationwide survey concerning patients with ocular melanoma diagnosed between January 1, 2010 and December 31, 2017. Patients were identified in the National Cancer Registry (NCR) using personal identification number (PESEL), the 10<sup>th</sup> revision of the International Statistical Classification of Diseases and Related Health Problems (ICD-10), and the 3<sup>rd</sup> edition of the International Classification of Diseases for Oncology (ICD-O-3) codes. The ICD-10 codes defining ocular neoplasms are C43.1 and C69 with extensions. Ocular melanomas were found in this group of patients using ICD-O-3 codes 872–877 with extensions. Therefore, all patients with both the ICD-10 and ICD-O-3 codes (as mentioned above) were included in the study group. The analysis of the study group also included demographic data from the National Health Fund (NHF) database, such as patient sex, age at diagnosis and area code. As both the NCR and the NHF databases cover the entire population of Poland, we believe that all ocular melanoma cases diagnosed in Poland between 2010 and 2017 were included in the statistical analysis. In addition, population data for Poland and patient death records were obtained from Statistics Poland.<sup>25–27</sup>

### Data analyses

In the 1<sup>st</sup> part of the study, the descriptive statistics and demographic characteristics of the study group and the incidence analysis of ocular melanoma were performed for each year of the study period, separately. Then, the analysis of patients diagnosed with ocular melanoma in 2010–2014 with 5 years of follow-up was carried out, allowing the performance of survival analysis. The 1-year and 5-year overall survival (OS) rates were calculated. The Cox proportional hazards model was applied, and hazard ratios (HRs) with a 95% confidence interval (95% CI) were computed. A value of  $p < 0.05$  was considered statistically significant. The Kaplan–Meier curve was employed to present the 5-year survival. Many different factors were considered in the survival analysis, including patient sex, age at the time of diagnosis, place of residence, and treatment method. Data on the general treatment schedule were available in the NCR database; these data concern surgical treatment, radiotherapy, chemotherapy, and other therapies. Additionally, detailed therapies were identified using



the ICD-9 codes according to the ICD-9-CM Volume 3 classification (a subset of the International Statistical Classification of Diseases and Related Health Problems (ICD)-9-CM) and obtained from the NHF database of medical services. They were matched with the study group from NCR. The ICD-9 codes, namely 16.31, 16.39, 16.41, 16.42, 16.49, 16.51, and 16.52, were used to identify surgical treatment by enucleation, and ICD-9 codes 14.26, 14.27 and 92.4 with extensions were applied to identify radiotherapy by plaque brachytherapy. Other therapies indicated in the NCR database included laser therapy and targeted therapy. Other clinical factors obtained from the NCR database were also taken into account, including metastases or advancement stages. Tumor growth advancement was divided into 4 categories: in situ, local, loco-regional, and systemic. The reference group was the tumor in situ. The R statistical software v. 3.6.2 (R Foundation for Statistical Computing, Vienna, Austria) was used for all analyses. The demographic characteristics of patients are presented with the mean and standard deviation (SD).

Since our study did not require ethics committee approval, it adhered to the tenets of the Declaration of Helsinki for research involving human subjects (socio-demographic data, including age, sex and place of residence, were recorded anonymously). Furthermore, the study protocol was approved by the Polish Ministry of Health, which is entitled by the laws of the Republic of Poland to process the NHF data. The informed consent was waived.

## Results

In total, 2143 patients with ocular melanoma were identified in Poland between January 1, 2010 and December 31, 2017. The incidence rates for each age group in the study period are presented in Table 1 and Fig. 1. The mean incidence of ocular melanoma was 8.76/1,000,000 person-years (95% CI: [6.94; 10.58]). The incidence of ocular melanoma increased with age: the lowest incidence was observed in patients aged 19–29 (1.17/1,000,000 person-years) and the highest in patients over

**Table 1.** Age-standardized incidence of ocular melanoma among Polish adults from 2010 to 2017 by age group

Variable	2010	2011	2012	2013	2014	2015	2016	2017	All
Number of people aged 19–29 years (in thousands)	6117.1	6015.0	5854.2	5651.8	5451.4	5243.7	5062.3	4890.1	44,285.7
Number of melanoma cases	9	11	8	4	6	6	2	6	52
Incidence/1,000,000 person-years	1.47	1.83	1.37	0.71	1.10	1.14	0.39	1.23	1.17
Percentage of women [%]	33.33	45.45	50.00	25.00	50.00	83.33	0.00	83.33	50.00
Number of people aged 30–39 years (in thousands)	5895.1	6005.6	6123.5	6239.5	6314.5	6348.3	6330.6	6290.1	49,547.1
Number of melanoma cases	15	12	14	12	14	15	15	12	109
Incidence/1,000,000 person-years	2.54	2	2.29	1.92	2.22	2.36	2.37	1.91	2.2
Percentage of women [%]	40.00	66.67	64.29	83.33	28.57	46.67	60.00	41.67	53.21
Number of people aged 40–49 years (in thousands)	4847.2	4822.2	4838.4	4879.8	4956.0	5064.6	5202.4	5341.5	39,952.2
Number of melanoma cases	28	29	33	10	17	19	22	37	195
Incidence/1,000,000 person-years	5.78	6.01	6.82	2.05	3.43	3.75	4.23	6.93	4.88
Percentage of women [%]	46.43	68.97	48.48	70.00	76.47	57.89	40.91	43.24	53.85
Number of people aged 50–59 years (in thousands)	5847.7	5765.5	5656.6	5536.1	5406.3	5245.3	5089.3	4928.3	43,475.2
Number of melanoma cases	63	47	49	44	42	50	61	81	437
Incidence/1,000,000 person-years	10.77	8.15	8.66	7.95	7.77	9.53	11.99	16.44	10.05
Percentage of women [%]	58.73	55.32	44.90	50.00	59.52	52.00	55.74	58.02	54.69
Number of people aged 60–69 years (in thousands)	3712.0	3,931.3	4,171.2	4,409.8	4,642.8	4,888.3	5,024.7	5,127.3	35,907.4
Number of melanoma cases	68	82	77	51	53	96	88	115	630
Incidence/1,000,000 person-years	18.32	20.86	18.46	11.57	11.42	19.64	17.51	22.43	17.55
Percentage of women [%]	41.18	40.24	57.14	54.90	41.51	57.29	45.45	51.30	49.05
Number of people aged ≥70 years (in thousands)	3830.6	3865.3	3874.0	3882.9	3905.0	3914.7	4030.5	4166.8	31,469.2
Number of melanoma cases	78	80	94	68	74	85	101	140	720
Incidence/1,000,000 person-years	20.36	20.7	24.26	17.51	18.95	21.71	25.06	33.6	22.88
Percentage of women [%]	53.26	54.41	51.27	58.20	52.91	55.35	52.60	52.43	57.08
Total number of people in all above age groups combined (in thousands)	30,249.8	30,404.7	30,518.0	30,599.9	30,675.9	30,705.0	30,739.9	30,743.6	244,636.8
Number of melanoma cases	261	261	275	189	206	271	289	391	2143
Incidence/1,000,000 person-years	8.63	8.58	9.01	6.18	6.71	8.83	9.40	12.72	8.76
Percentage of women [%]	53.26	54.41	51.27	58.20	52.91	55.35	52.60	52.43	53.57

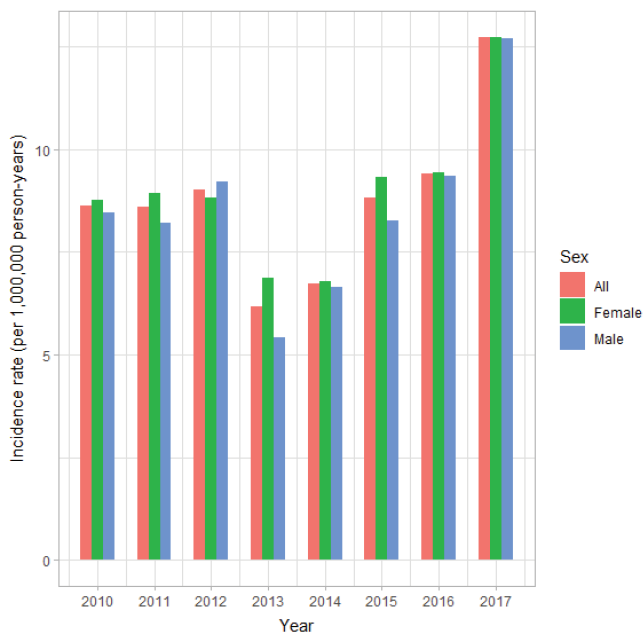


Fig. 1. Incidence of ocular melanoma in Poland according to standard annual analysis during 2010–2017

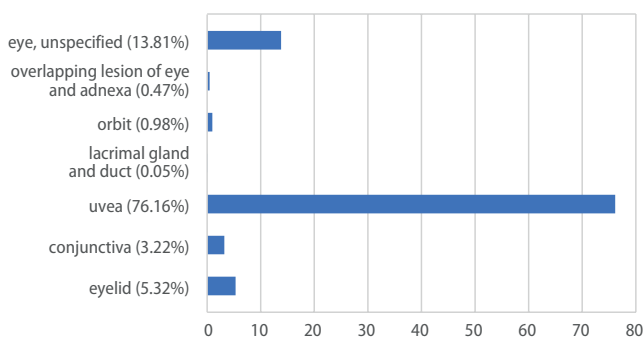


Fig. 2. Localization of ocular melanoma among Polish adults from 2010 to 2017

70 (22.88/1,000,000 person-years). The number of ocular melanoma diagnoses by anatomical localization is presented in Fig. 2. The uveal melanoma (iris, ciliary body and choroid localizations) was the most common and was diagnosed in 1632 (76.16%) patients. Eyelid melanoma was the 2<sup>nd</sup> most common and was diagnosed in 114 (5.32%) patients. The 3<sup>rd</sup>

most common was conjunctival melanoma, which was diagnosed in 69 (3.22%) patients. The other melanomas were localized in orbit (21 patients (0.98%)), overlapping lesion of eye and adnexa (10 patients (0.47%)) and lacrimal gland and duct (1 patient (0.05%)). At the same time, unspecified ocular melanoma was diagnosed in 296 (13.81%) patients. The overall incidences of uveal, eyelid and conjunctival melanoma were 6.67/1,000,000, 0.47/1,000,000 and 0.28/1,000,000 person-years, respectively.

The demographic characteristics of patients with ocular melanoma in Poland are presented in Fig. 1 and Table 1,2. The mean age at the time of diagnosis was  $62.73 \pm 14.43$  years, and there was a slight increase in the mean age of diagnosis over the study period. The majority of patients were female (53.57%), and the proportion of women in each analyzed year was more than half. In addition, the vast majority of patients (65%) were urban residents. The overall ocular melanoma incidence rate was also higher in women (8.96/1,000,000 person-years) than in men (8.54/1,000,000 person-years).

The OS analysis included 1192 patients diagnosed in 2010–2014. One hundred patients (8.39%) died within 1 year and 507 patients (39.24%) died within 5 years from ocular melanoma diagnosis. The 1-year and 5-year OS rates were 91.61% and 60.76%, respectively. Among statistically significant variables, a higher risk of death within 5 years was associated with male sex (HR = 1.2959; 95% CI: [1.086; 1.547]), older age at diagnosis (HR = 1.0379; 95% CI: [1.03; 1.046]), chemotherapy treatment (HR = 1.6774; 95% CI: [1.317; 2.136]), metastasis (HR = 1.5716; 95% CI: [1.056; 2.340]), loco-regional hyperplasia (HR = 1.5936; 95% CI: [1.111; 2.286]), and systemic tumor spread (HR = 3.9872; 95% CI: [3.021; 5.263]) compared to the carcinoma in situ. The risk of death was statistically reduced by radiotherapy treatment (HR = 0.6645; 95% CI: [0.529; 0.835]). However, place of residence, surgery treatment and local tumor growth (compared to the tumor in situ) were not associated with the mortality rate. All results of survival analysis are presented in Table 3. The Kaplan–Meier curve shows the patient survival (Fig. 3). The results of the test for the proportional hazards assumption are presented in Table 4.

Table 2. Demographic characteristics of patients with ocular melanoma among Polish adults from 2010 to 2017

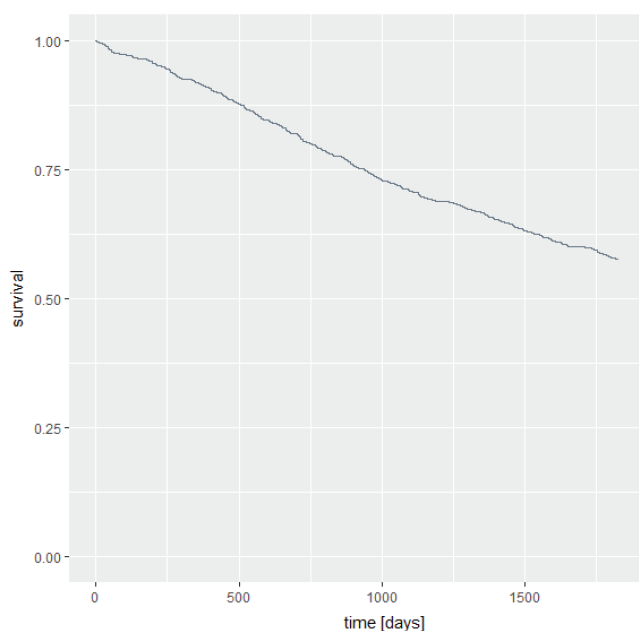
Variable	2010	2011	2012	2013	2014	2015	2016	2017	All
Age [years], mean $\pm$ SE	60.72 $\pm$ 14.88	60.68 $\pm$ 14.83	62.17 $\pm$ 14.39	63.47 $\pm$ 14.26	62.59 $\pm$ 15.53	63.46 $\pm$ 14.09	63.92 $\pm$ 14.10	64.18 $\pm$ 13.61	62.73 $\pm$ 14.43
Women, n (%)	139 (53.26)	142 (54.41)	141 (51.27)	110 (58.20)	109 (52.91)	150 (55.35)	152 (52.60)	205 (52.43)	1148 (53.57)
Men, n (%)	122 (46.74)	119 (45.59)	134 (48.73)	79 (41.80)	97 (47.09)	121 (44.65)	137 (47.40)	186 (47.57)	995 (46.43)
Urban residence, n (%)	163 (62.45)	181 (69.35)	167 (60.73)	122 (64.55)	121 (58.74)	175 (64.58)	196 (67.82)	268 (68.54)	1393 (65.00)
Rural residence, n (%)	98 (37.55)	80 (30.65)	108 (39.27)	67 (35.45)	85 (41.26)	96 (35.42)	93 (32.18)	123 (31.46)	750 (35.00)

SE – standard error.

**Table 3.** Results of Cox proportional hazards model of 5-year survival

Variable	B	SE	p-value	HR	2.5% HR	97.5% HR
Rural residence	−0.012038	0.092972	0.896974	0.9880	0.8234	1.1855
Male sex	0.259177	0.090260	0.004086	1.2959	1.0857	1.5466
Age	0.037241	0.003708	<0.00001	1.0379	1.0304	1.0455
Surgery	0.139545	0.111631	0.211279	1.1498	0.9238	1.4310
Chemotherapy	0.517221	0.123385	0.0000277	1.6774	1.3170	2.1362
Radiotherapy	−0.408784	0.116795	0.000465	0.6645	0.5285	0.8354
Metastasis	0.452075	0.203065	0.025997	1.5716	1.0556	2.3398
Local cancer	−0.107813	0.110736	0.330253	0.8978	0.7226	1.1154
Loco-regional cancer	0.465971	0.184095	0.011369	1.5936	1.1109	2.2860
Systemic cancer	1.383081	0.141593	<0.00001	3.9872	3.0209	5.2625

SE – standard error; HR – hazard ratio.

**Fig. 3.** Kaplan–Meier curve of ocular melanoma survival in Poland

## Discussion

This study evaluates for the first time the incidence and characteristics of ocular melanoma in the overall population of Poland. The analysis included both the age-standardized incidence of ocular melanoma (the unit of incidence is captured by 1,000,000 person-years) in 2010–2017 and the survival analysis of patients diagnosed with ocular melanoma in 2010–2014, with 5 years of follow-up. The mean incidence of ocular melanoma was 8.76/1,000,000 person-years, and the mean age at the time of diagnosis was  $62.73 \pm 14.43$  years. The overall incidences of uveal, eyelid and conjunctival melanoma were 6.67/1,000,000, 0.47/1,000,000 and 0.28/1,000,000 person-years, respectively. Our results were in the middle of the range of ocular melanoma incidence worldwide, which is much higher among Whites than Blacks and Asians.<sup>1–3</sup> Our age-standardized incidence of uveal melanoma was similar to that reported earlier

in Poland by the EURO CARE working group for the 1983–1994 period.<sup>7</sup> It was also similar to that reported in Central Europe (Slovakia, Slovenia and Switzerland), higher than that reported in South Korea, Singapore, USA, and Southern Europe (Italy and Spain) but lower than in Northern Europe (Denmark, Norway, Sweden, and Estonia), Ireland and Australia.<sup>6,7,9,11,15</sup> However, we cannot exclude the misclassification bias. The number of uveal melanoma cases might have been underestimated, while unspecified ocular melanoma might have been overestimated. Errors in using specific ICD-10 codes might have occurred at different levels (hospitals, outpatient clinics, and NCR and NHF offices). However, we believe that such errors had only minor impact on the study findings. Our age-standardized incidence of conjunctival melanoma was similar to that reported earlier in Eastern Europe by the EURO CAREnet working group for the 1995–2007 period and higher than that reported among Blacks in the USA and whole population in Southern Europe but lower than among Whites in the USA and the whole population in Northern Europe.<sup>4</sup> The north-to-south decreasing gradient in the uveal melanoma incidence in Europe might be related to the protective effect of ocular pigmentation in the southern populations with respect to higher exposure to ultraviolet light at lower latitudes. Moreover, Eastern European countries like Poland have the lowest rates of both conjunctival and skin melanomas in Europe.<sup>4,7</sup> Most of the previous studies showed an increased age-adjusted incidence rate of ocular melanoma among men,<sup>6,9,11,12,14,15,17</sup> but in other large cohort clinical studies with no age adjustment, no sex-based differences were reported.<sup>3</sup> In contrast to those studies, the incidence rate of ocular melanoma in Poland was higher in women, which might be attributable to the excess male death rate, characteristic to the Eastern European countries, which is visible in Poland.<sup>27–29</sup>

Since the Collaborative Ocular Melanoma Study (COMS) showed no survival advantage of enucleation over brachytherapy for medium-size tumors, the therapeutic shift to eye-conserving treatment options was observed worldwide.<sup>17,19</sup> However, medical management of ocular

Table 4. Results of the test for the proportional hazards assumption

Variable	$\chi^2$	Degree of freedom (df)	p-value
Rural residence	0.0754	1	0.7837
Male sex	1.2156	1	0.2702
Age	0.3953	1	0.5295
Surgery	1.182	1	0.277
Chemotherapy	1.9842	1	0.1590
Radiotherapy	0.2413	1	0.6233
Metastasis	1.3794	1	0.2402
Local cancer	0.3865	1	0.534
Loco-regional cancer	0.2574	1	0.6119
Systemic cancer	1.9519	1	0.162
Global	11.80962	10	0.212

melanoma depends on the tumor location, size, local extension, visual acuity at presentation, and systemic status. Most patients with posterior tumors are currently treated with plaque brachytherapy. Other available options include laser photocoagulation, transpupillary thermotherapy, particle beam radiotherapy, gamma knife radiosurgery, local surgical resection, and/or enucleation (with or without orbital exenteration). The current standard for anterior tumors management is a surgical treatment with adjuvant therapy, including brachytherapy. Other management methods for both anterior and posterior tumors include targeted therapy and/or chemotherapy (in case of metastases). Although more than 90% of primary tumors are managed with surgery or eye-conserving therapies, more than 50% of patients develop metastases, usually involving the liver.<sup>1,3,16,30</sup>

The OS analysis revealed that 100 patients (8.39%) died within 1 year and 507 patients (39.24%) died within 5 years from the initial diagnosis of ocular melanoma in Poland, which gives the 1-year and 5-year mortality rates of 8.39% and 39.24%, respectively. The 1-year OS was 91.61%, and the 5-year OS was 60.76%, which is comparable to the data from an epidemiological study of uveal melanoma from US Surveillance, Epidemiology and End Results Program for 2010–2015, where the 5-year OS was 61.8%. However, our mortality rate was higher than that found in the UK, Denmark, Sweden, Singapore, or Israel.<sup>2,10,14,20,31,32</sup> The Cox proportional hazards model showed that the higher risk of death within 5 years from the initial ocular melanoma diagnosis in Poland was associated with male sex, older age at diagnosis, chemotherapy treatment, metastasis, loco-regional hyperplasia, and systemic tumor spread compared to the carcinoma in situ. The risk of death was statistically reduced by radiotherapy treatment. However, chemotherapy treatment increased the risk of death in our model. It should be assumed that the treatment method depends on the carcinoma stage and chemotherapy is used in more severe stage of tumor. Our results were consistent with previously published studies that showed older age

at diagnosis, severe stage of the tumor, distant metastasis, and no radiation to be associated with the mortality risk. Those studies also revealed that beyond 15 years from diagnosis, a patient with uveal melanoma is more likely to die from other causes than uveal melanoma metastasis itself.<sup>14,31,32</sup>

## Limitations

The limitations of the present study include selection bias as there is an increasing proportion of cases without histopathological proof of diagnosis. In addition, both NHF and NCR databases do not cover the family history and genetic information of ocular melanoma patients in Poland, with disease laterality also not available for all included subjects. Therefore, we might have missed some data and the investigation of potential risk factors of mortality was not complex. However, this likely had only a minor impact on our findings. The most important strengths of the present study are the population size, nationwide recruitment, and the usefulness of its results for clinicians and health-care providers in Poland.

## Conclusions

This study found that the incidence rate of ocular melanoma in Poland is in the middle range of worldwide incidence, and the 5-year OS is relatively low. Furthermore, a higher risk of mortality from ocular melanoma in Poland is associated with male sex, older age at diagnosis, chemotherapy treatment, metastasis, loco-regional hyperplasia, and systemic tumor spread compared to carcinoma in situ.

## ORCID iDs

Michał Szymon Nowak  <https://orcid.org/0000-0001-6304-1545>  
 Bożena Romanowska-Dixon  <https://orcid.org/0000-0001-6940-5485>  
 Iwona Grabska-Liberek  <https://orcid.org/0000-0003-4190-4826>

## References

- Jovanovic P, Mihajlovic M, Djordjevic-Jocic J, Vlajkovic S, Cekic S, Stefanovic V. Ocular melanoma: An overview of the current status. *Int J Clin Exp Pathol.* 2013;6(7):1230–1244. PMID:23826405, PMCID: PMC3693189.
- Tan LLY, Hong J, Goh WL, et al. Clinical features and survival outcomes of ocular melanoma in a multi-ethnic Asian cohort. *Sci Rep.* 2020;10(1):16367. doi:10.1038/s41598-020-73534-x
- Kaliki S, Shields CL. Uveal melanoma: Relatively rare but deadly cancer. *Eye (Lond).* 2017;31(2):241–257. doi:10.1038/eye.2016.275
- Virgili G, Parravano M, Gatta G, et al; RARECAREnet Working Group. Incidence and survival of patients with conjunctival melanoma in Europe. *JAMA Ophthalmol.* 2020;138(6):601–608. doi:10.1001/jamaophthalmol.2020.0531
- Mierzwa-Dobranowska M, Romanowska-Dixon B. The impact of selected factors on early diagnosis of multiple primary cancers in patients with uveal melanoma. *Contemp Oncol (Pozn).* 2013;17(6):510–514. doi:10.5114/wo.2013.38914
- Ortega MA, Fraile-Martínez O, García-Honduvilla N, et al. Update on uveal melanoma: Translational research from biology to clinical practice (review). *Int J Oncol.* 2020;57(6):1262–1279. doi:10.3892/ijo.2020.5140

7. Virgili G, Gatta G, Ciccolallo L, et al; EUROCARE Working Group. Incidence of uveal melanoma in Europe. *Ophthalmology*. 2007;114(12):2309–2315. doi:10.1016/j.ophtha.2007.01.032
8. Burr JM, Mitry E, Rachet B, Coleman MP. Survival from uveal melanoma in England and Wales 1986 to 2001. *Ophthalmic Epidemiol*. 2007;14(1):3–8. doi:10.1080/09286580600977281
9. Park SJ, Oh CM, Kim BW, Woo SJ, Cho H, Park KH. Nationwide incidence of ocular melanoma in South Korea by using the National Cancer Registry Database (1999–2011). *Invest Ophthalmol Vis Sci*. 2015;56(8):4719–4724. doi:10.1167/iovs.15-16532
10. Frenkel S, Hendler K, Peer J. Uveal melanoma in Israel in the last two decades: Characterization, treatment and prognosis. *Isr Med Assoc J*. 2009;11(5):280–285. PMID:19637505.
11. Stang A, Parkin DM, Ferlay J, Jöckel KH. International uveal melanoma incidence trends in view of a decreasing proportion of morphological verification. *Int J Cancer*. 2005;114(1):114–123. doi:10.1002/ijc.20690
12. Nichols EE, Richmond A, Daniels AB. Disparities in uveal melanoma: Patient characteristics. *Semin Ophthalmol*. 2016;31(4):296–303. doi:10.3109/08820538.2016.1154176
13. Lucena E, Goldemberg DC, Thuler LCS, de Melo AC. Epidemiology of uveal melanoma in Brazil. *Int J Retina Vitreous*. 2020;6(1):51. doi:10.1186/s40942-020-00261-w
14. Xu Y, Lou L, Wang Y, et al. Epidemiological study of uveal melanoma from US Surveillance, Epidemiology, and End Results Program (2010–2015). *J Ophthalmol*. 2020;2020:3614039. doi:10.1155/2020/3614039
15. Baily C, O'Neill V, Dunne M, et al. Uveal melanoma in Ireland. *Ocul Oncol Pathol*. 2019;5(3):195–204. doi:10.1159/000492391
16. Nichols EE, Richmond A, Daniels AB. Tumor characteristics, genetics, management, and the risk of metastasis in uveal melanoma. *Semin Ophthalmol*. 2016;31(4):304–309. doi:10.3109/08820538.2016.1154175
17. Aronow ME, Topham AK, Singh AD. Uveal melanoma: 5-year update on incidence, treatment, and survival (SEER 1973–2013). *Ocul Oncol Pathol*. 2018;4(3):145–151. doi:10.1159/000480640
18. Mahendraraj K, Lau CS, Lee I, Chamberlain RS. Trends in incidence, survival, and management of uveal melanoma: A population-based study of 7516 patients from the Surveillance, Epidemiology, and End Results database (1973–2012). *Clin Ophthalmol*. 2016;10:2113–2119. doi:10.2147/OPTh.S113623
19. Scheffler AC, Kim RS. Recent advancements in the management of retinoblastoma and uveal melanoma. *Fac Rev*. 2021;10:51. doi:10.12703/r/10-51
20. Virgili G, Gatta G, Ciccolallo L, et al; EUROCARE Working Group. Survival in patients with uveal melanoma in Europe. *Arch Ophthalmol*. 2008;126(10):1413–1418. doi:10.1001/archophth.126.10.1413
21. Nowak MS, Grabska-Liberek I, Michalska-Małecka K, et al. Incidence and characteristics of cataract surgery in Poland during 2010–2015. *Int J Environ Res Public Health*. 2018;15(3):435. doi:10.3390/ijerph15030435
22. Nowak MS, Grzybowski A, Michalska-Małecka K, et al. Incidence and characteristics of endophthalmitis after cataract surgery in Poland during 2010–2015. *Int J Environ Res Public Health*. 2019;16(12):2188. doi:10.3390/ijerph16122188
23. Koziół M, Nowak MS, Udziela M, Piątkiewicz P, Grabska-Liberek I, Szaflik JP. First nation-wide study of diabetic retinopathy in Poland in the years 2013–2017. *Acta Diabetol*. 2020;57(10):1255–1264. doi:10.1007/s00592-020-01540-6
24. Nowak MS, Romanowska-Dixon B, Grabska-Liberek I, Żurek M. Incidence and characteristics of retinoblastoma in Poland: The first nationwide study 2010–2017. *Int J Environ Res Public Health*. 2021;18(12):6539. doi:10.3390/ijerph18126539
25. The National Cancer Registry Data. <http://onkologia.org.pl>. Accessed July 16, 2021.
26. The National Health Fund Data. <http://www.nfz.gov.pl>. Accessed July 16, 2021.
27. Statistics Poland Data. <http://www.stat.gov.pl>. Accessed July 16, 2021.
28. Nowak MS, Śmigiełski J. The prevalence and causes of visual impairment and blindness among older adults in the city of Lodz, Poland. *Medicine (Baltimore)*. 2015;94(5):e505. Erratum in: *Medicine (Baltimore)*. 2015;94(7):1. doi:10.1097/MD.0000000000000505
29. Nowak MS, Jurowski P, Gos R, Śmigiełski J. Ocular findings among young men: A 12-year prevalence study of military service in Poland. *Acta Ophthalmol*. 2010;88(5):535–540. doi:10.1111/j.1755-3768.2008.01476.x
30. Chattopadhyay C, Kim DW, Gombos DS, et al. Uveal melanoma: From diagnosis to treatment and the science in between. *Cancer*. 2016;122(15):2299–2312. doi:10.1002/cncr.29727
31. Rajeshuni N, Zubair T, Ludwig CA, Moshfeghi DM, Mruthyunjaya P. Evaluation of racial, ethnic, and socioeconomic associations with treatment and survival in uveal melanoma, 2004–2014. *JAMA Ophthalmol*. 2020;138(8):876–884. doi:10.1001/jamaophthalmol.2020.2254
32. Radivoyevitch T, Zabor EC, Singh AD. Uveal melanoma: Long-term survival. *PLoS One*. 2021;16(5):e0250939. doi:10.1371/journal.pone.0250939



# The influence of mosapride on gut microbiota of carbon tetrachloride-induced cirrhosis rats based on 16S rRNA gene sequencing

Dongya Chen<sup>1,A,D,F</sup>, Jingfang Xiong<sup>2,B,D,F</sup>, Hui Feng<sup>1,B,D,F</sup>, Yihui Liu<sup>1,B,D,F</sup>, Jianjun Xu<sup>1,C,D,F</sup>, Hong Xu<sup>1,D-F</sup>

<sup>1</sup> Department of Gastroenterology and Hepatology, Zhejiang Integrated Traditional Chinese and Western Medicine Hospital, Hangzhou, China

<sup>2</sup> Department of Geriatrics, Zhejiang Integrated Traditional Chinese and Western Medicine Hospital, Hangzhou, China

A – research concept and design; B – collection and/or assembly of data; C – data analysis and interpretation; D – writing the article; E – critical revision of the article; F – final approval of the article

Advances in Clinical and Experimental Medicine, ISSN 1899–5276 (print), ISSN 2451–2680 (online)

Adv Clin Exp Med. 2022;31(6):623–633

## Address for correspondence

Hong Xu

E-mail: hongxuhzrc@aliyun.com

## Funding sources

This study was supported by Medical Science and Technology Project of Zhejiang Province (grant No. 2018KY602), Hangzhou Agriculture and Social Developmental Research Program (grant No. 20180533B74) and Scientific Research Fund for TCM in Zhejiang Province (grant No. 2019ZB093).

## Conflict of interest

None declared

Received on August 13, 2021

Reviewed on December 10, 2021

Accepted on February 1, 2022

Published online on March 11, 2022

## Cite as

Chen D, Xiong J, Feng H, Liu Y, Xu J, Xu H. The influence of mosapride on gut microbiota of carbon tetrachloride-induced cirrhosis rats based on 16S rRNA gene sequencing. *Adv Clin Exp Med*. 2022;31(6):623–633. doi:10.17219/acem/146320

## DOI

10.17219/acem/146320

## Copyright

Copyright by Author(s)

This is an article distributed under the terms of the Creative Commons Attribution 3.0 Unported (CC BY 3.0) (<https://creativecommons.org/licenses/by/3.0/>)

## Abstract

**Background.** Mosapride significantly improves intestinal motility in liver cirrhosis, ultimately leading to the reduction in plasma endotoxin levels and bacterial translocation.

**Objectives.** To investigate the effects of mosapride on intestinal microecology in cirrhotic rats and its potential mechanisms.

**Materials and methods.** Forty-five healthy male Sprague–Dawley rats that were pathogen-free (weight 200–220 g) were randomly divided into a control group (n = 15), model group (n = 15) and mosapride group (n = 15). Then, the pathological changes in the liver and intestine were determined through tissue staining and using transmission electron microscope (TEM). Bacterial translocation was examined. High throughput 16S rRNA sequencing was performed to determine the changes of gut microbiota in each group.

**Results.** Compared with the model group, mosapride treatment induced no attenuation in hepatic morphology and pathology changes. The TEM indicated no differences in intestinal structure in both groups. There was a significant decline in the rate of gut microbiota translocation in the mosapride group compared with the model group. There were intestinal microbiota changes in the mosapride group compared with that of the model group, including Bacteroidetes, Prevotellaceae, *Alloprevotella*, *Ruminiclostridium*, Negativicutes, Selenomonadales, Veillonellaceae, *Anaerovibrio*, Campylobacteriales, Epsilonbacteraeota, *Helicobacter*, *Oscillibacter*, Verrucomicrobiales, *Akkermansia*, *Intestinimonas*, *Eubacterium*, Clostridiaceae, *Clostridium*, *Bacteroides*, *Tyzzarella*, Actinobacteria, and Bifidobacteriales. Among these bacteria, *Alloprevotella* showed a strong correlation with the other bacteria.

**Conclusions.** Taken together, we concluded that mosapride may reduce intestinal bacterial translocation through regulating the gut microbiota in rats with hepatic cirrhosis.

**Key words:** liver cirrhosis, mosapride, bacterial translocation, gut microbiota, 16S rRNA

## Background

Liver cirrhosis, the end-stage of the development of various chronic liver diseases, is characterized by the progressive replacement of functional hepatic architecture with nonfunctional fibrotic tissues.<sup>1</sup> Patients with cirrhosis are prone to endotoxemia, spontaneous bacterial peritonitis and other bacterial infections.<sup>2</sup> Severe complications, including hepatic encephalopathy, hepatopulmonary syndrome and liver failure, may be triggered or aggravated by infection.<sup>3–5</sup> Bacterial translocation (BT) from the intestinal lumen to extraintestinal sites is the initial and key step in the pathogenesis of infection in cirrhosis.<sup>6</sup>

Gut microbiota disorder and increased intestinal permeability are 2 important causes of BT.<sup>7,8</sup> Intestinal bacterial overgrowth (IBO) has been reported in both cirrhotic patients and experimental animal models of cirrhosis.<sup>9,10</sup> Cirrhosis with BT displayed increased intestinal permeability, which may be caused by intestinal mucosal peroxidation and the impairment of the intestinal epithelial barrier.<sup>7,8</sup>

Mosapride, serving as an agonist of 5-hydroxytryptamine<sub>4</sub> (5-HT<sub>4</sub>) receptors, has been commonly utilized as a prokinetic element for treating gastrointestinal dysfunction.<sup>11</sup> It has been reported to be effective in enhancing gastric emptying and increasing intestinal frequency, together with improving gastric mucosal injury.<sup>12</sup> Our previous study showed that mosapride significantly increased intestinal motility, effectively preventing the translocation of bacteria and reducing plasma endotoxin level in carbon tetrachloride (CCl<sub>4</sub>)-induced cirrhotic rats.<sup>13</sup> However, we could not identify which genus of bacteria was involved in the improvement of endotoxin-mediated mosapride.

## Objectives

In this study, we aimed to investigate gut microbiota changes after the administration of mosapride in rats with liver cirrhosis.

## Materials and methods

### Animals

This study was approved by the Committee of Animal Research and Ethics of Zhejiang Integrated Traditional Chinese and Western Medicine Hospital, Hangzhou, China (approval No. IACUC-20190128-04). All experimental procedures on animals were in accordance with the Guide for the Care and Use of Laboratory Animals.<sup>14</sup> Forty-five healthy male Sprague–Dawley rats, weighing 200–220 g, were used for the following experiments. Rats were acclimatized to laboratory conditions for 1 week prior to the experiment. All rats were housed under specific

pathogen-free conditions where temperature (25 ± 1°C) and humidity (55 ± 5%) were controlled. Rats were fed ad libitum with free access to water and food under a 12-hour light-dark cycle.

## Induction of liver cirrhosis and mosapride treatment

Cirrhosis was induced with subcutaneous injection of CCl<sub>4</sub>. Animals were randomly divided into the control group (n = 15), model group (n = 15) and mosapride group (n = 15). The CCl<sub>4</sub> (Sigma-Aldrich, St. Louis, USA) was dissolved in the olive oil at a dilution rate of 2:3 (v/v). The animals were administered subcutaneously with CCl<sub>4</sub> at an initial dose of 5 mL/kg, and then 3 mL/kg twice every week for 12 weeks. During this period, animals in the mosapride group were additionally treated by gavage with mosapride (Dainippon Sumitomo Pharmaceutical Co., Ltd., Osaka, Japan), at a daily dose of 3 mg/kg, using an orogastric feeding tube. In the control group, animals received the same volume of olive oil subcutaneously and normal saline intragastrically.

## Liver and intestine histological analysis

Liver and terminal ileum specimens were fixed in 4% paraformaldehyde, followed by dehydration and paraffin embedding. The tissues were cut into sections of 4 µm in thickness and stained with hematoxylin and eosin (H&E). The Image-Pro plus v. 5.0 software (Media Cybernetics, Inc., Rockville, USA) was utilized to measure the height and the width of the villi, and the thickness of the mucosa. Picosirius red (Polysciences, Warrington, USA) staining was performed to evaluate hepatic collagen deposition. Five randomly selected fields were obtained for each rat liver. The area of fibrosis was analyzed according to the following formula: Picosirius red-positive area/(total area – vascular lumen area) × 100%.<sup>15</sup>

## Ultrastructure analysis of the intestine

Intestinal tissues were obtained at a position that was about 15–20 cm from the ileocecal junction. Tissues were fixed using glutaraldehyde and osmic acid. Tissues were dehydrated using a series of increasing concentrations of acetone, cleared in toluene and embedded with resin. Tissues were cut with an ultramicrotome (Leica, Wetzlar, Germany) and 70 nm-thick ultrathin sections were obtained. The sections were stained with lead citrate and uranyl acetate. Microvillus and organelles were observed under the transmission electron microscope (TEM) (FEI, Eindhoven, the Netherlands), the images were captured with SIS Mega View III CCD camera and visualized using AnalySIS software (SIS, Münster, Germany).



## Determination of plasma endotoxin level

Plasma endotoxin was detected using Pyrochrome® chromogenic endotoxin testing kit (Associates of Cape Cod, Falmouth, USA), according to the manufacturer's instructions. A standard curve was plotted with endotoxin standard (*Escherichia coli* O113:H10). Pyrochrome lyophilized powder was gently dissolved in 3.2 mL of the reconstitution buffer. Appropriately, 50 µL of plasma sample was mixed with 50 µL of reconstitution buffer in 96-well plates, and incubated at 37°C for 12 min. The reaction was terminated by adding 25 µL of acetic acid (1:1). The samples were examined at the optical density of 405 nm.

## Bacterial translocation assessment

All the procedures were performed under strict sterile conditions to avoid contamination. Animals were anesthetized, shaved and subjected to laparotomy. Mesenteric lymph nodes (MLNs) obtained from the ileocecal junction and mesenteric roots, liver and spleen tissues were homogenized in phosphate-buffered saline (PBS; 0.1 mL per 0.1 g). Then, 100 µL of homogenates were transferred to a blood plate medium and incubated for 48 h at a constant temperature of 37°C. The BT was defined as the positive culture of enteric bacteria in the MLNs, liver or spleen, regardless of the species.

## High throughput 16S rRNA sequencing

Fresh fecal samples from the ileum were collected before the sacrifice, and immediately transferred into liquid nitrogen container for temporary storage. Fecal genomic DNA was extracted using QIAamp DNA Stool Mini Kit (Qiagen, Hilden, Germany). The polymerase chain reaction (PCR) amplification was conducted to amplify V3 and V4 regions of 16S rRNA based on specific primers of 338F-806R (5'-ACTCCTACGGGAGGCAGCAG-3'; 5'-GGACTACHVGGGTWTCTAAT-3'). Purified PCR products for V3 and V4 regions in 16S rRNA were subject to the high-throughput sequencing, using the Illumina MiSeq device (Illumina, San Diego, USA). Quantitative Insights Into Microbial Ecology (QIIME 2; <http://qiime.org>) platform was used to study the effects of mosapride treatment on the microbiome in cirrhotic rats.<sup>16</sup> The DADA2 was used to remove noise signals.<sup>17</sup>

## Statistical analyses

GraphPad Prism v. 6.0 software (GraphPad Software, San Diego, USA) was used for the data analysis. Measurement data were presented as the median and quartiles (1<sup>st</sup> and 3<sup>rd</sup> quartile (Q1, Q3)). Statistical significance was ascertained using nonparametric Mann–Whitney test. The value of  $p < 0.05$  was considered statistically significant.

Community composition and clustering analysis were presented using stacked bar charts and a heat map. Alpha diversity was evaluated by calculating Chao1, Good's coverage, operational taxonomic units (OTUs), and Shannon's and Simpson's indices with the script from QIIME 2.<sup>16</sup> The Kruskal–Wallis test was used to test the differences in alpha diversities among the groups. The Chao1 index for abundance data was used to estimate species richness, which is suitable for the estimation of the number of shared species in multiple assemblages.<sup>18,19</sup> The Good's coverage assessed sampling depth coverage.<sup>20</sup> The OTUs represent the number of different features. The Shannon's diversity index was used to measure the diversity of species in a community.<sup>21</sup> The Simpson's index shows the representativeness of a species.<sup>22</sup> The beta diversity was used to measure the similarity in the bacterial composition between the different groups. Unweighted UniFrac distances were used for evaluating beta diversity with principal coordinates analysis (PCoA).<sup>23</sup> The analysis of similarities (ANOSIM) was used to calculate the p-values for beta diversity.<sup>24</sup> Linear discriminant analysis effect size (LEfSe) was used for high-dimensional class comparisons.<sup>25</sup> The Bugbase algorithm was used to predict bacterial phenotype associated with cirrhosis.<sup>26</sup>

## Results

### Mosapride did not alleviate liver injury in cirrhotic rats

Three rats in the model group and 2 rats in the mosapride group died at the end of the 12-week experiment. The CCl<sub>4</sub> significantly increased the level of alanine aminotransferase (ALT) ( $p = 0.0022$ ), aspartate aminotransferase (AST) ( $p = 0.0022$ ) and total bilirubin (TBIL) ( $p = 0.0022$ ) (all p-values were calculated using Mann–Whitney test). Serum albumin (ALB) was significantly decreased by CCl<sub>4</sub> ( $p = 0.0022$ ; Mann–Whitney test) (Fig. 1A). The H&E and Picrosirius red staining indicated that the normal liver structure was severely destroyed with significant fibrous septa and cirrhotic nodules in the model group (Fig. 1B,C). The quantification of Picrosirius red staining showed that the fibrotic area was 0.70 (0.52, 1.15) in the control group, 27.42 (22.33, 30.16) in the model group, and 27.32 (23.21, 29.87) in the mosapride group (Fig. 1D). The CCl<sub>4</sub> significantly induced fibrosis in the model group compared to the control group ( $p < 0.0001$ ; Mann–Whitney test), while no significant difference was observed between model and mosapride groups ( $p = 0.9502$ ; Mann–Whitney test).

### Mosapride reduced plasma endotoxin level and BT

As shown in Fig. 2A, the plasma endotoxin level in the model group was significantly increased compared to the control group: 0.02 (0.01, 0.04) EU/mL (control)

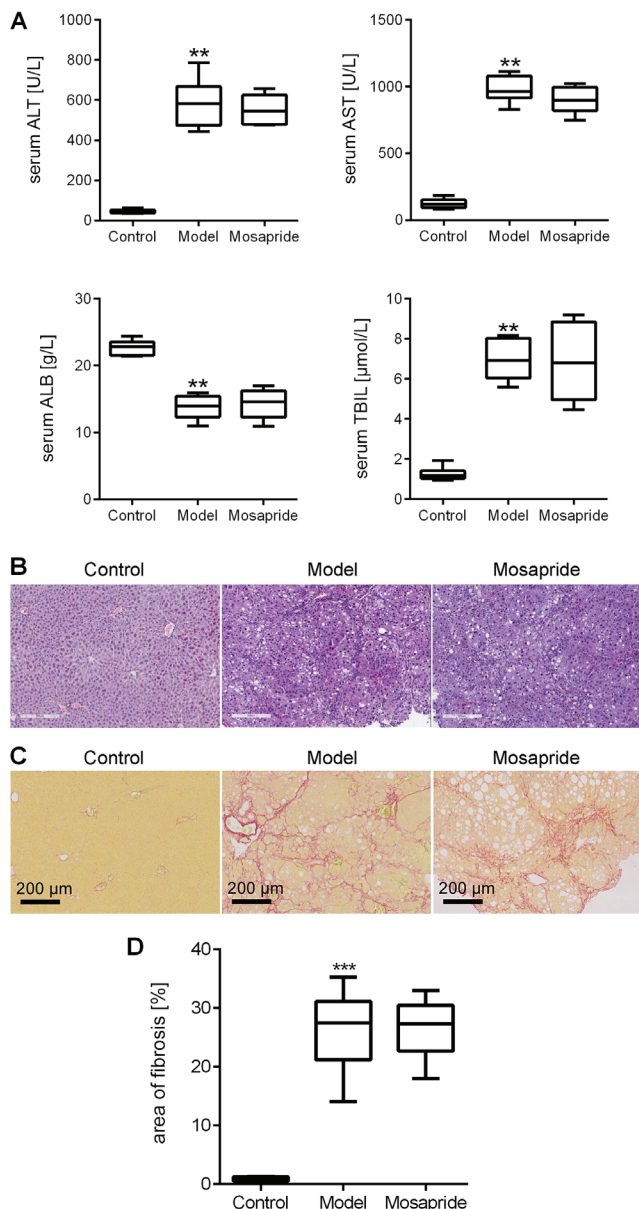


**Fig. 1.** Mosapride does not improve biochemical parameters and alleviate hepatic histological damages in carbon tetrachloride ( $\text{CCl}_4$ )-induced cirrhotic rats. **A.** Serum concentrations of alanine aminotransferase (ALT), aspartate aminotransferase (AST), albumin (ALB), and total bilirubin (TBIL) in the control group ( $n = 15$ ), model group ( $n = 12$ ) and mosapride group ( $n = 13$ ). \*\* $p < 0.01$  compared to control; **B.** Hematoxylin and eosin (H&E) staining. Scale bar: 200  $\mu\text{m}$ ; **C.** Picrosirius red staining. Scale bar: 200  $\mu\text{m}$ ; **D.** Quantitative analysis of liver fibrosis. The fibrotic area was expressed according to the following formula: Picrosirius red-positive area/(total area – vascular lumen area)  $\times$  100%. \*\*\* $p < 0.001$  compared to control

compared to 0.37 (0.14, 0.41) EU/mL in the model group ( $p < 0.0001$ ; Mann–Whitney test). The plasma endotoxin level in the mosapride group was 0.18 (0.11, 0.22) EU/mL, which was significantly decreased compared to the model group ( $p = 0.0223$ ; Mann–Whitney test).

The BT was detected in 10 out of 12 rats (83.3%) in the model group, whereas its occurrence was nil in the control group ( $p < 0.0001$ ; Fisher's exact test). The incidence of BT was significantly lower in the mosapride group (5 out of 13, 38.5%) than in the model group ( $p < 0.0001$ ; Fisher's exact test)

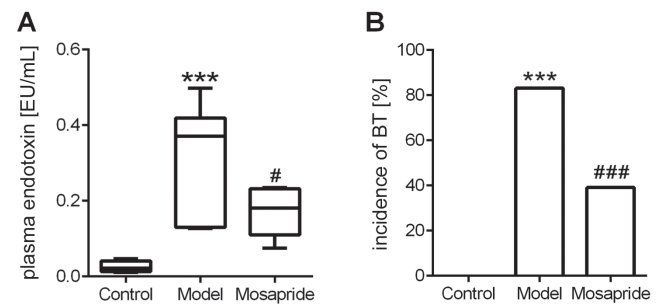


**Fig. 2.** Mosapride reduces plasma endotoxin and bacterial translocation (BT) in carbon tetrachloride ( $\text{CCl}_4$ )-induced cirrhotic rats. **A.** The plasma endotoxin levels in the control group ( $n = 14$ ), the model group ( $n = 12$ ) and the mosapride group ( $n = 13$ ). \*\*\* $p < 0.001$  compared to the control group, # $p < 0.05$  compared to the model group; **B.** The incidences of BT in the control group ( $n = 15$ ), the model group ( $n = 12$ ) and the mosapride group ( $n = 13$ ). The BT was defined as the positive culture of enteric bacteria in the mesenteric lymph nodes (MLNs), liver or spleen, regardless of the species. \*\*\* $p < 0.001$  compared to the control group, ### $p < 0.001$  compared to the model group (Fisher's exact test)

(Fig. 2B). Table 1 shows the bacteria and the sites where bacteria were isolated. *Escherichia coli* from MLNs and liver tissues were counted.

## Mosapride did not improve intestinal mucosa damage

As illustrated in Fig. 3A, the ileum tissues of the control rats displayed a normal intact architecture of intestinal mucosa without hyperemia, edema or inflammatory cell infiltration. The villi were well arranged, smooth and intact. In the model and mosapride groups, the mucosa was destroyed with atrophic and shorter villi. As presented in Fig. 3B, the villi height and width, as well as the thickness of mucosa in the model group were significantly

**Table 1.** Translocating bacteria and the sites where bacteria were isolated

Groups	No.	MLNs	Liver	Spleen
Model	1	<i>E. coli</i>	<i>E. coli</i>	<i>E. coli</i>
	2	<i>E. coli</i>	–	–
	3	<i>E. coli</i>	–	–
	4	<i>E. coli</i>	<i>E. coli</i>	<i>E. coli</i>
	5	<i>E. coli</i>	–	–
	6	<i>E. coli</i>	–	–
	7	<i>E. coli</i>	<i>E. coli</i>	<i>E. coli</i>
	8	<i>E. coli</i>	–	–
	9	<i>E. coli</i>	–	–
	10	<i>E. coli</i>	–	–
Mosapride	1	<i>E. coli</i>	–	–
	2	<i>E. coli</i>	–	–
	3	–	<i>E. coli</i>	–
	4	<i>E. coli</i>	–	–
	5	–	<i>E. coli</i>	–

MLNs – mesenteric lymph nodes; *E. coli* – *Escherichia coli*.

decreased compared to the control group ( $p < 0.0001$ ,  $p = 0.0417$  and  $p < 0.0001$ , respectively; Mann–Whitney test). There were no differences in the villi height, villi width and thickness of mucosa between the model group and the mosapride group ( $p = 0.5601$ ,  $p = 0.9155$  and  $p = 0.7135$ , respectively; Mann–Whitney test). Representative images of intestinal ultrastructural changes were shown in Fig. 3C. The epithelial cells in the control group were tightly arranged with neatly arranged surface microvilli. The paracellular spaces were narrow and the tight junctions of the epithelial cells in the control group were intact and clear. By contrast, the tight junctions were discontinuous and the paracellular spaces were widen in both, the model group and the mosapride group.

### Effects of mosapride on the abundance of intestinal bacteria at the phylum and genus levels

We analyzed the abundance of intestinal bacteria among 3 groups at the phylum and genus levels, and the results are shown in Fig. 4A,B. In the control group, Bacteroidetes were the most abundant, followed by Firmicutes and Proteobacteria. In the model group, Firmicutes were the most abundant, followed by Bacteroidetes and Epsilonbacteraeota. In the mosapride group, the top 3 abundant bacteria were Firmicutes, Bacteroidetes and Proteobacteria. Figure 4C,D showed the clustering analysis of intestinal bacteria in the heat map. In the model group, there was

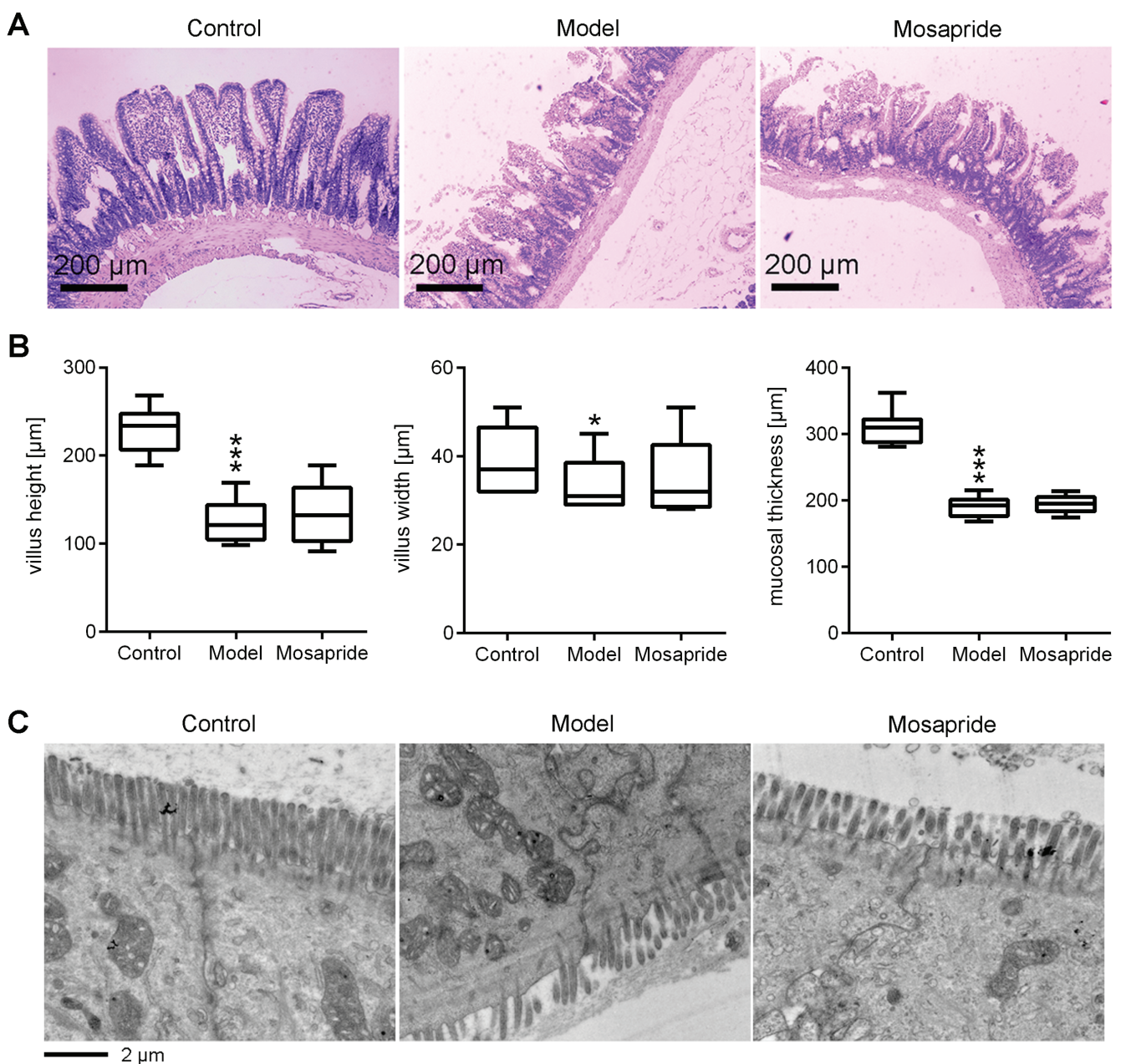


Fig. 3. Mosapride does not improve intestinal mucosal damage. A. Hematoxylin–eosin staining images show histological alterations of ileum tissues. Scale bar: 200 µm; B. Quantitative morphometry of the villi height, villi width and the thickness of the mucosa; C. Transmission electron microscopy of ileum tissues

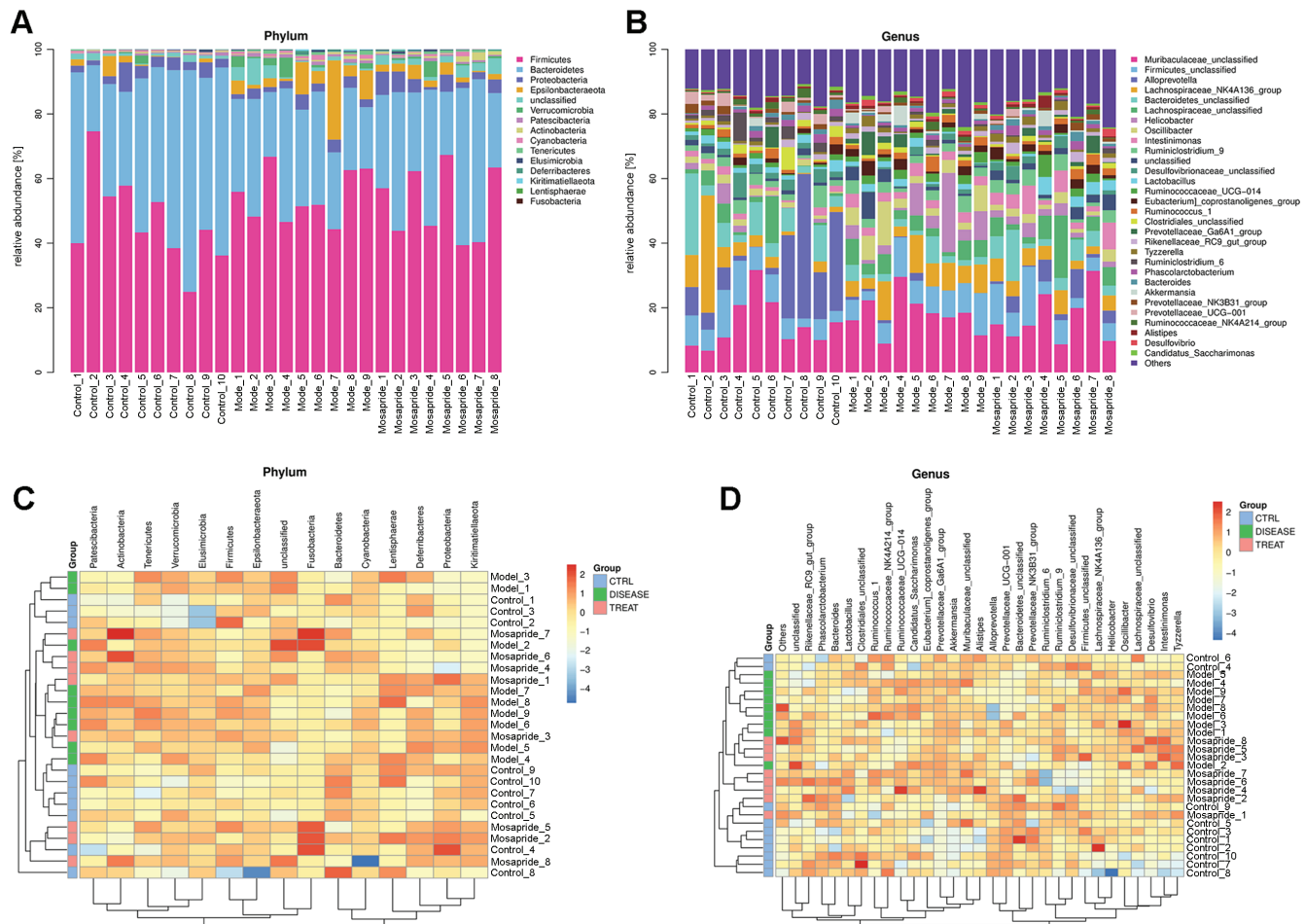


Fig. 4. Bacterial abundance and clustering analysis in control, model and mosapride rats. Stacked bars of top 30 bacteria at phylum level (A) and genus level (B). Heat map of top 30 bacteria at phylum level (C) and genus level (D). Cirrhosis was induced using carbon tetrachloride (CCl<sub>4</sub>) (0.3–0.5 mL/100 g) for 12 weeks. Meanwhile, rats in the mosapride group were daily treated with mosapride (3 mg/kg body weight)

a decrease of Prevotellaceae, Bacteroidetes, *Alloprevotella*, Desulfovibrionaceae, Phascolarctobacterium, *Eubacterium*, Clostridiales, and *Ruminiclostridium* when compared to the control group, which showed an increase after the administration of mosapride. In contrast, Firmicutes, *Prevotella*, *Oscillibacter*, *Helicobacter*, Candidatus, Muribaculaceae, and *Akkermansia* were increased in the model group, and they decreased after the administration of mosapride. The levels of Lachnospiraceae, *Intestinimonas* and *Tyzzereella* showed an increase in the model group compared to the control group, and a further increase after mosapride administration.

### Effect of mosapride on bacterial diversity in cirrhotic rats

The alpha diversity analysis was carried out to determine the bacterial diversity at the genus level among the 3 groups. The violin plot showed no statistical differences in alpha diversity among the control, model and mosapride groups based on Chao1 ( $p = 0.99$ ), Good's coverage ( $p = 0.57$ ), OTUs ( $p = 0.99$ ), Shannon's index ( $p = 0.13$ ), and Simpson's index ( $p = 0.087$ ) (all  $p$ -values were calculated using

Kruskal–Wallis test) (Fig. 5A and Supplementary Information, File 2). This indicated that there was no statistical difference in alpha diversity of gut microbiota among the control group, the model group or the mosapride group. Unweighted UniFrac-based PCoA was conducted to evaluate beta diversity of the gut microbiota among the 3 groups. The PCoA plot showed that the constitution of the gut microbiota in the treatment group was significantly different compared with that of the control group and the model group, respectively ( $p = 0.001$ ; ANOSIM) (Fig. 5B). The unweighted UniFrac distance matrix was shown in Supplementary Information (File 3). Figure 5C showed the number of common and unique species between control and model groups or between model and mosapride groups. The specific genus was listed in Supplementary Information (File 4).

### LefSe analysis of gut microbiota in cirrhotic rats after mosapride treatment

The LefSe analysis was conducted to identify bacteria that may be involved in the pathological changes of the lesions. The LefSe cladogram showed the bacteria that played the most important roles in each group. As shown

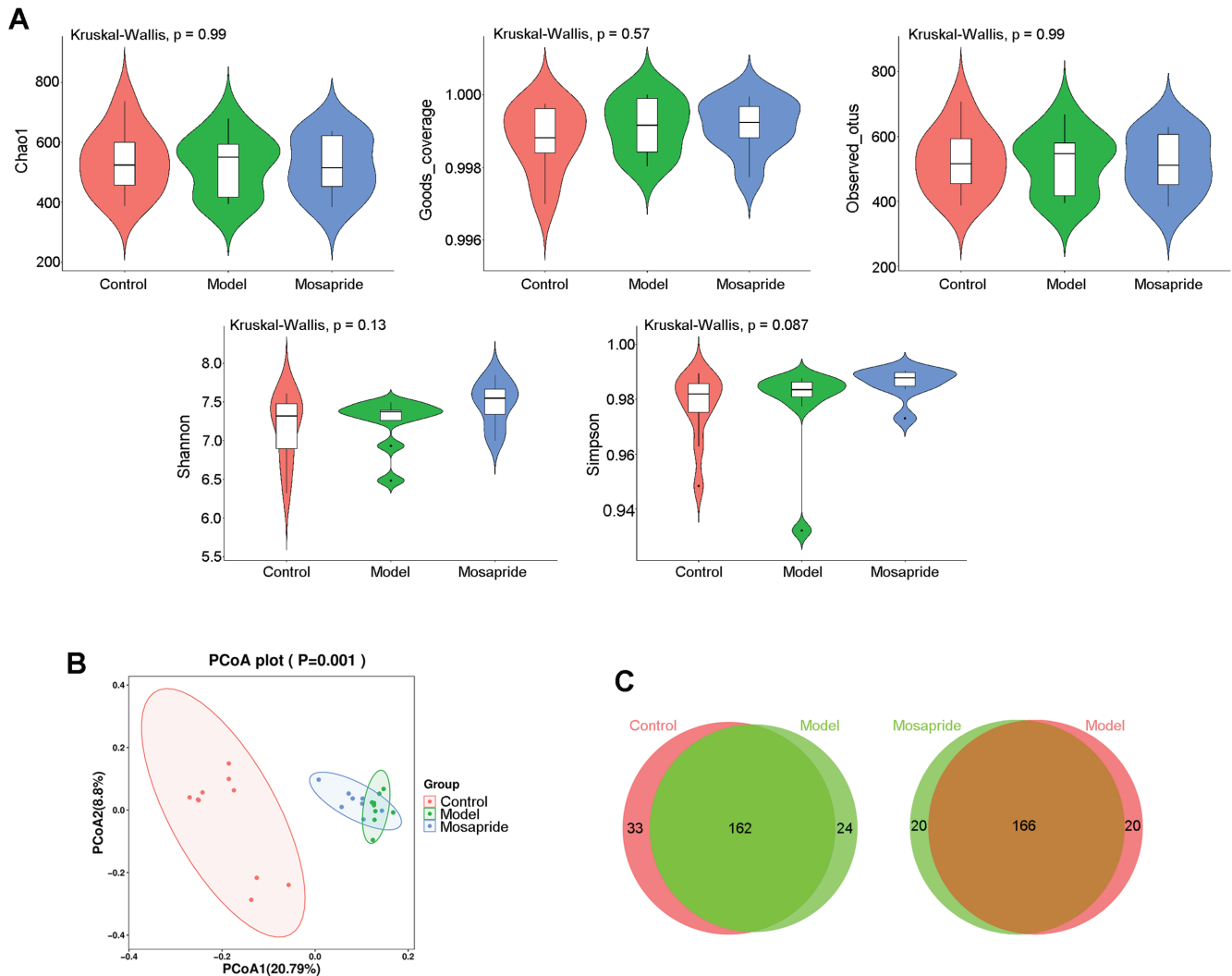


**Fig. 5.** Effects of mosapride on bacterial diversity in rats with liver cirrhosis. Alpha diversity at the genus level was evaluated using Chao1, Good’s coverage, operational taxonomic units (OTUs), and Shannon’s and Simpson’s indices (A). Beta diversity was analyzed using principal coordinates analysis (PCoA) (B). Venn diagram of different bacteria between control and model rats or between mosapride and model rats (C). Cirrhosis was induced with carbon tetrachloride (CCl<sub>4</sub>) (0.3–0.5 mL/100 g) for 12 weeks. Meanwhile, rats in the mosapride group were daily treated with mosapride (3 mg/kg body weight)

in Fig. 6, 14 dominant bacteria were found in the control group, 32 dominant communities in the model group and 20 dominant communities in the mosapride group. In the control group, the crucial genera included Bacteroidetes, Prevotellaceae, *Alloprevotella*, *Ruminiclostridium*, Negativicutes, Selenomonadales, Veillonellaceae, and *Anaerovibrio*. In the model group, the closely related bacteria included Campylobacterales, Epsilonbacteraeota, *Helicobacter*, *Oscillibacter*, *Prevotellaceae\_Ga6A1\_group*, Verrucomicrobiales, and *Akkermansia*. In the mosapride group, the bacteria included *Intestinimonas*, *Eubacterium*, Clostridiaceae, *Clostridium*, *Bacteroidaceae*, *Bacteroides*, *Tyzzarella*, Actinobacteria, and Bifidobacteriales.

### Prediction of bacterial phenotype associated with cirrhosis

Biologically interpretable phenotypes were predicted to investigate the association of cirrhosis and microbiota.

Figures 7A–I showed that the differential microbiota may not be associated with aerobiosis ( $p = 0.0591$ ; Kruskal–Wallis), and that it contains mobile elements ( $p = 0.1697$ ; Kruskal–Wallis), Gram-negative phenotype ( $p = 0.3011$ ; Kruskal–Wallis) and Gram-positive phenotype ( $p = 0.3011$ ; Kruskal–Wallis). Cirrhosis-related phenotypes of bacteria included anaerobiosis ( $p = 0.0084$ ; Kruskal–Wallis), facultative anaerobiosis ( $p = 0.0124$ ; Kruskal–Wallis), formed biofilms ( $p = 0.0161$ ; Kruskal–Wallis), potential pathogenicity ( $p = 0.0461$ ; Kruskal–Wallis), and stress tolerance ( $p = 0.0405$ ; Kruskal–Wallis). This finding may have implications for understanding the relationship between different microbial phenotypes and cirrhosis.

### Discussion

In this study, we investigated the efficiency of mosapride in hepatic cirrhosis by illustrating the pathological changes and the intestinal microbiota changes after

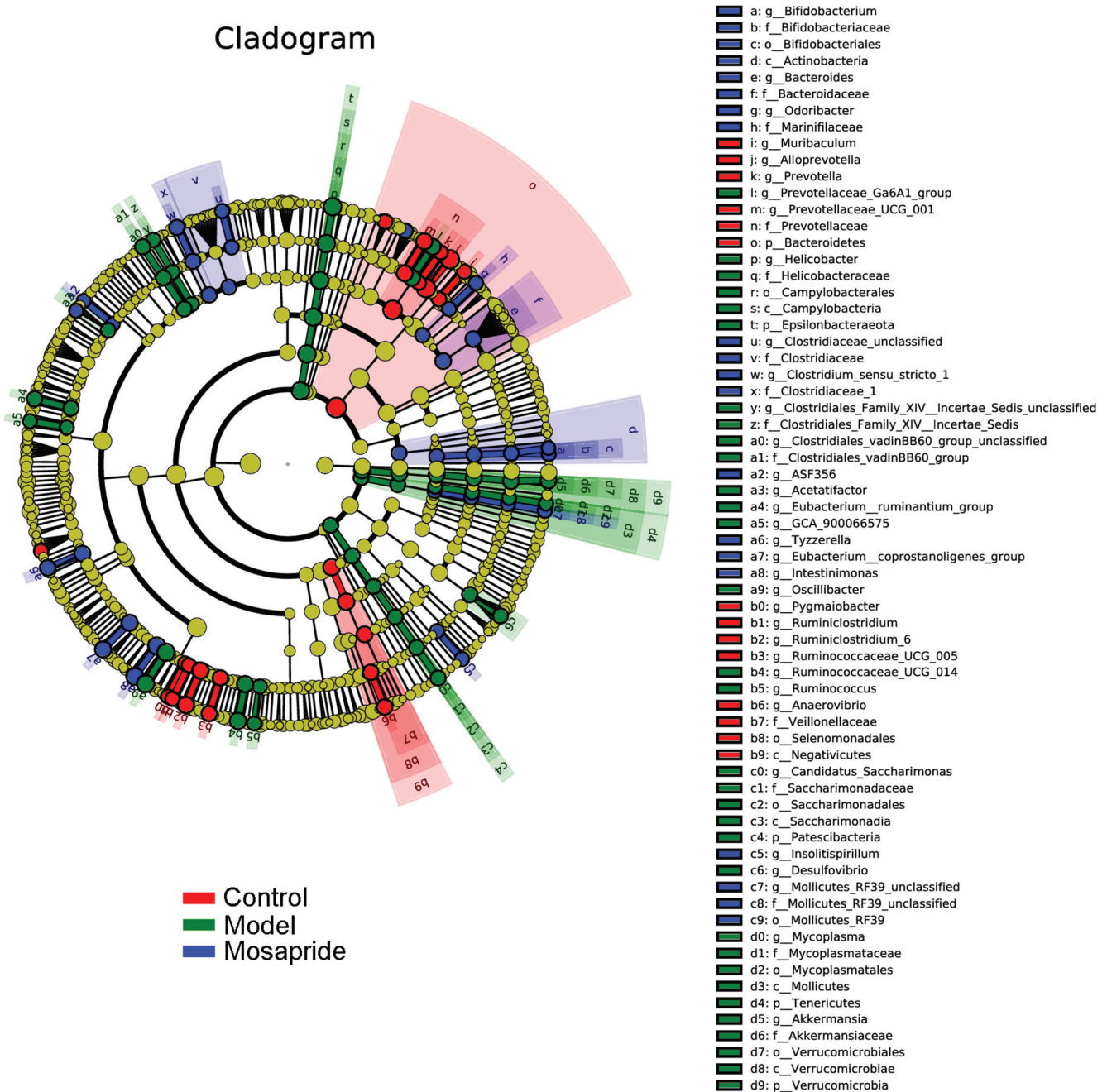


**Fig. 6.** Linear discriminant analysis effect size (LEfSe) cladogram indicated the differentially abundant taxa among the control, model and mosapride groups. The taxonomic cladogram was gained based on LEfSe analysis of 165 sequences for the control group (red), model group (green) and mosapride group (blue). Cirrhosis was induced using carbon tetrachloride (CCl<sub>4</sub>) (0.3–0.5 mL/100 g) for 12 weeks. Meanwhile, rats in the mosapride group were daily treated with mosapride (3 mg/kg body weight)

the administration of mosapride. In addition, we tried to discover the potential cause of the improvement of liver condition after the administration of mosapride. In our previous study, mosapride mediated bacterial translocation and endotoxin levels in rats. Besides, the attempts have been made to screen for potential bacteria involved in the translocation that may lead to increased permeability of the intestinal wall in vivo. Our data showed that mosapride could improve gut microbiota translocation, which then resulted in gut microbiota changes that may be associated with the pathogenesis of hepatic cirrhosis in rats.

Mosapride has been commonly utilized for treating liver diseases as it induces no significant adverse events.<sup>13</sup> For instance, in nonalcoholic steatohepatitis mice, mosapride citrate could improve hepatic histological damage and colonic inflammation.<sup>27</sup> Our previous studies have shown that mosapride could significantly reduce plasma endotoxin concentrations and reduce the incidence of bacterial translocation in cirrhosis.<sup>13</sup> Additionally, mosapride did not improve hepatic and intestinal injuries. In this study, we tried to validate that mosapride did not change the hepatic morphology of rats. However, to some extent, it could

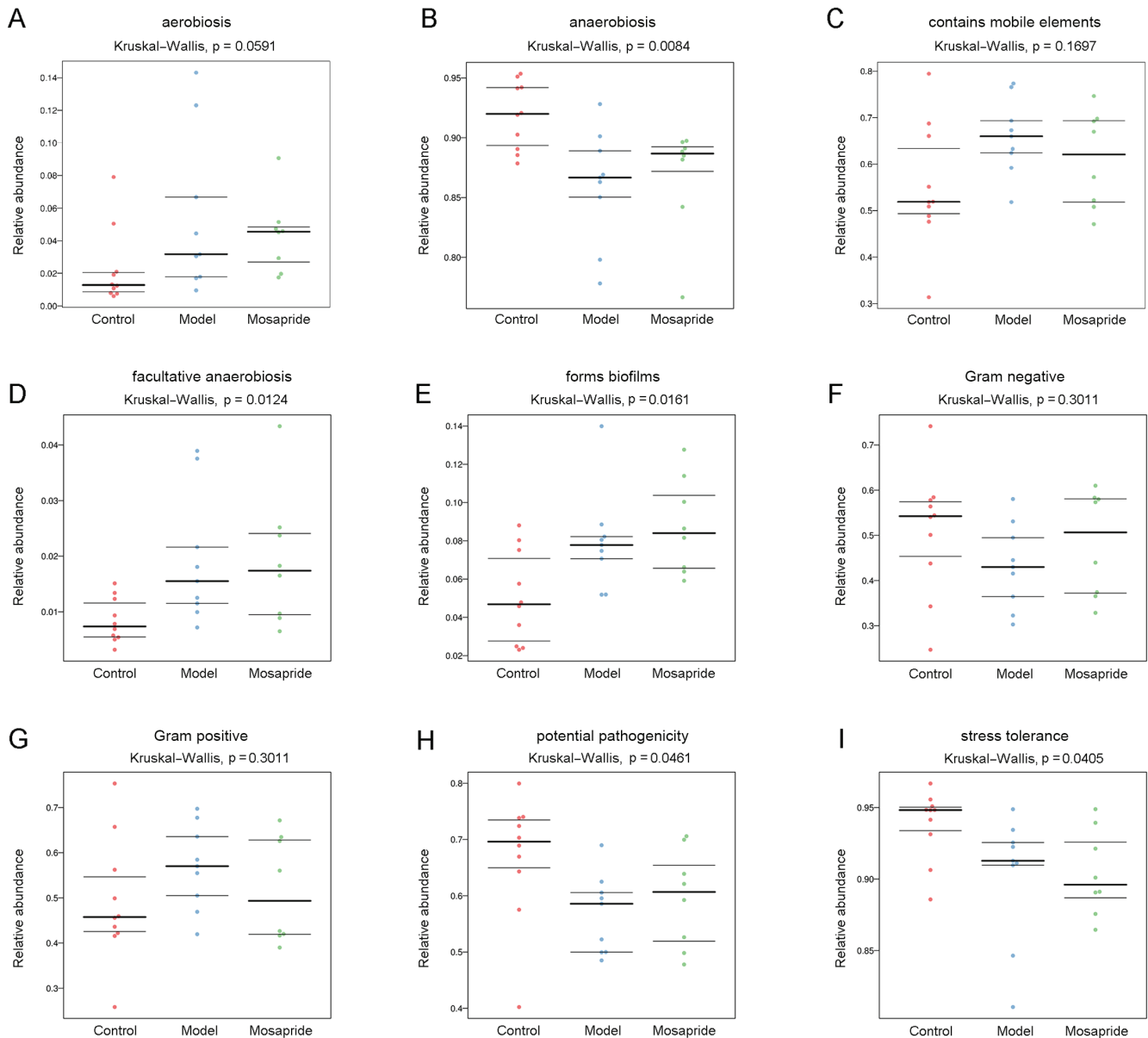


**Fig. 7.** Prediction of bacterial phenotype related to cirrhosis. Bugbase algorithm was used to predict the bacterial phenotype of aerobiosis (A), anaerobiosis (B), mobile elements contained (C), facultative anaerobiosis (D), biofilms (E), Gram-negative (F), Gram-positive (G), potential pathogenicity (H), and stress tolerance (I). Cirrhosis was induced by carbon tetrachloride (CCl<sub>4</sub>) (0.3–0.5 mL/100 g) for 12 weeks. Meanwhile, rats in the mosapride group were treated daily with mosapride (3 mg/kg body weight)

attenuate intestinal injuries. This was not similar with our previous findings. Compared with the model group, there was a significant attenuation in intestinal mucosa injury after the mosapride treatment. Additionally, after the mosapride treatment, villus showed shortening together with partial rupture and distortion. There were no differences in the width of the villus on intestinal mucosa. Compared with the control group, there was a significant decline in villus width, mucosal thickness and intestinal wall thickness in the model group. In view of this, we investigated the potential mechanism that intestinal mucosa damage may associate with the change of intestinal microbiota.

In LEfSe analysis, we screened several bacteria that were associated with the pathological changes of intestinal

injury, including Bacteroidetes, Prevotellaceae, *Alloprevotella*, *Ruminiclostridium*, Negativicutes, Selenomonadales, Veillonellaceae, *Anaerovibrio*, Campylobacterales, Epsilonbacteraeota, *Helicobacter*, *Oscillibacter*, Verrucomicrobiales, *Akkermansia*, *Intestinimonas*, *Eubacterium*, *Tyzzebella*, Clostridiaceae, *Clostridium*, Vacteroidaceae, *Bacteroides*, *Tyzzerella*, Actinobacteria, and Bifidobacteriales. The *Oscillibacter* genus has been reported to be associated with atrial fibrillation,<sup>28</sup> stroke and transient ischemic attack,<sup>29</sup> and human infection.<sup>30</sup> However, no previous studies reported the roles of *Oscillibacter* genus in hepatic diseases. For *Alloprevotella*, genus has been reported to be less abundant in rheumatoid arthritis patients.<sup>31</sup> In patients with chronic kidney disease,

*Alloprevotella* were enriched in the fecal samples.<sup>32</sup> A study focusing on screening of pathogens for oral cavity squamous cell cancer (OC-SCC) reported the enrichment of *Alloprevotella*.<sup>33</sup> Similarly, *Alloprevotella* were abundant in patients with oral cancer.<sup>34</sup> For *Bacteroides*, a beneficial gut Bacteroides-folate-liver pathway was demonstrated to regulate lipid metabolism.<sup>35</sup> *Ruminiclostridium* has been closely involved in the obesity and metabolic dysfunction.<sup>36</sup> *Anaerovibrio* are the key microbiota signature after quercetin treatment.<sup>37</sup> Besides, they were considered to play a certain role in the evolution of gut microbiota following acute human immunodeficiency virus type 1 (HIV-1) infection.<sup>38</sup> Prevotellaceae alternation was proposed to be involved in the protection of the central nervous system (CNS) autoimmunity and oral cancer.<sup>34,39</sup> The human gut bacteria *Akkermansia* are newly investigated to be associated with many healthy problems<sup>40</sup> and their regional distribution is associated with metabolic syndromes.<sup>41</sup> However, their roles in the pathogenesis of hepatic cirrhosis are not well defined. In this study, our data showed that the mosapride treatment would lead to significant changes in the gut microbiota in hepatic cirrhosis rats. In the future, further studies are required to investigate the exact roles of these microbiota.

After screening gut microbiota, the prediction of bacterial phenotypes was conducted. Mosapride may change bacterial phenotypes related with cirrhosis, and these phenotypes included anaerobiosis, facultative anaerobiosis, biofilm formation, potential pathogenicity, and stress tolerance. However, little is known about the exact roles of microbiota in the pathogenesis of liver diseases. In the future, more studies are required to investigate the correlation between bacterial phenotypes and the pathogenesis of hepatic cirrhosis.

## Limitations

There are some limitations to our study. In this study, we could not find out which bacteria are the direct causes for the attenuation of intestinal lesions mediated by mosapride. As there are so many signaling pathways involved in the intestinal lesion and repairment, we could not illustrate the exact pathway affected by the intestinal microbiota after mosapride treatment. Besides, the sample size is another limitation in this study. We will focus on these limitations in our subsequent studies.

## Conclusions

Our data showed that mosapride could modulate the gut microbiota changes and trigger the decrease of gut microbiota translation and attenuation of endotoxin concentrations. This may help to illustrate the pathogenesis of hepatic cirrhosis in rats.

## Data availability statement

The original contributions presented in the study are included in the Supplementary Information containing:

File 1: Bacterial abundance and clustering analysis in control, model and mosapride rats.

File 2: Alpha diversity at the genus level was evaluated using Chao1, Good's coverage, OTUs, Shannon's, and Simpson's indices.

File 3: The unweighted UniFrac distance matrix was used for evaluating beta diversity with principal coordinates analysis.

File 4: Abundance of the detected bacteria between control and model rats or between mosapride and model rats.

Further inquiries can be directed to the corresponding author. The Supplementary Information is available online at <https://doi.org/10.5281/zenodo.6021342>.

## ORCID iDs

Dongya Chen  <https://orcid.org/0000-0001-8548-9869>  
 Jingfang Xiong  <https://orcid.org/0000-0002-6156-8287>  
 Hui Feng  <https://orcid.org/0000-0001-7805-2167>  
 Yihui Liu  <https://orcid.org/0000-0003-0399-0807>  
 Jianjun Xu  <https://orcid.org/0000-0002-7638-3015>  
 Hong Xu  <https://orcid.org/0000-0002-9767-1761>

## References

- Parola M, Pinzani M. Liver fibrosis: Pathophysiology, pathogenetic targets and clinical issues. *Mol Aspects Med.* 2019;65:37–55. doi:10.1016/j.mam.2018.09.002
- Piano S, Singh V, Caraceni P, et al. Epidemiology and effects of bacterial infections in patients with cirrhosis worldwide. *Gastroenterology.* 2019;156(5):1368–1380.e10. doi:10.1053/j.gastro.2018.12.005
- Yuan LT, Chuah SK, Yang SC, et al. Multiple bacterial infections increase the risk of hepatic encephalopathy in patients with cirrhosis. *PLoS One.* 2018;13(5):e0197127. doi:10.1371/journal.pone.0197127
- Suk KT, Kim MY, Jeong SW, Jang JY, Jang YO, Baik SK. Impact of bacterial translocation on hepatopulmonary syndrome: A prospective observational study. *Dig Dis Sci.* 2018;63(1):248–256. doi:10.1007/s10620-017-4868-4
- Mücke MM, Rummyantseva T, Mücke VT, et al. Bacterial infection-triggered acute-on-chronic liver failure is associated with increased mortality. *Liver Int.* 2018;38(4):645–653. doi:10.1111/liv.13568
- Fine RL, Manfredo Vieira S, Gilmore MS, Krieger MA. Mechanisms and consequences of gut commensal translocation in chronic diseases. *Gut Microbes.* 2020;11(2):217–230. doi:10.1080/19490976.2019.1629236
- Ponziani FR, Zocco MA, Cerrito L, Gasbarrini A, Pompili M. Bacterial translocation in patients with liver cirrhosis: Physiology, clinical consequences, and practical implications. *Expert Rev Gastroenterol Hepatol.* 2018;12(7):641–656. doi:10.1080/17474124.2018.1481747
- Muñoz L, Borrero MJ, Úbeda M, et al. Intestinal immune dysregulation driven by dysbiosis promotes barrier disruption and bacterial translocation in rats with cirrhosis. *Hepatology.* 2019;70(3):925–938. doi:10.1002/hep.30349
- Ghosh G, Jesudian AB. Small intestinal bacterial overgrowth in patients with cirrhosis. *J Clin Exp Hepatol.* 2019;9(2):257–267. doi:10.1016/j.jceh.2018.08.006
- Sánchez E, Casafont F, Guerra A, de Benito I, Pons-Romero F. Role of intestinal bacterial overgrowth and intestinal motility in bacterial translocation in experimental cirrhosis. *Rev Esp Enferm Dig.* 2005;97(11):805–814. doi:10.4321/s1130-01082005001100005
- Aoki K, Kamiyama H, Masuda K, Togashi Y, Terauchi Y. Mosapride citrate, a 5-HT<sub>4</sub> receptor agonist, increased the plasma active and total glucagon-like peptide-1 levels in non-diabetic men. *Endocr J.* 2013;60(4):493–499. PMID:23257734.



12. Endo J, Nomura M, Morishita S, et al. Influence of mosapride citrate on gastric motility and autonomic nervous function: Evaluation by spectral analyses of heart rate and blood pressure variabilities, and by electrogastrography. *J Gastroenterol*. 2002;37(11):888–895. doi:10.1007/s005350200150
13. Xu H, Xiong J, Xu J, et al. Mosapride stabilizes intestinal microbiota to reduce bacterial translocation and endotoxemia in CCl(4)-induced cirrhotic rats. *Dig Dis Sci*. 2017;62(10):2801–2811. doi:10.1007/s10620-017-4704-x
14. Institute of Laboratory Animal Research; Committee on Care, Use of Laboratory Animals. *Guide for the Care and Use of Laboratory Animals*. Bethesda, USA: US Department of Health and Human Services, Public Health Service, National Institutes of Health; 1986.
15. Dong A, Mueller P, Yang F, Yang L, Morris A, Smyth SS. Direct thrombin inhibition with dabigatran attenuates pressure overload-induced cardiac fibrosis and dysfunction in mice. *Thromb Res*. 2017;159:58–64. doi:10.1016/j.thromres.2017.09.016
16. Bolyen E, Rideout JR, Dillon MR, et al. Reproducible, interactive, scalable and extensible microbiome data science using QIIME 2. *Nat Biotechnol*. 2019;37(8):852–857. doi:10.1038/s41587-019-0209-9
17. Callahan BJ, McMurdie PJ, Rosen MJ, Han AW, Johnson AJ, Holmes SP. DADA2: High-resolution sample inference from Illumina amplicon data. *Nat Methods*. 2016;13(7):581–583. doi:10.1038/nmeth.3869
18. Chao A. Nonparametric estimation of the number of classes in a population. *Scand J Statist*. 1984;265–270. <http://www.jstor.org/stable/4615964>. Accessed August 4, 2021.
19. Pan HY, Chao A, Foissner W. A nonparametric lower bound for the number of species shared by multiple communities. *J Agric Biol Environ Stat*. 2009;14(4):452–468. doi:10.1198/jabes.2009.07113
20. Good IJ. The population frequencies of species and the estimation of population parameters. *Biometrika*. 1953;40(3–4):237–264. doi:10.2307/2333344
21. Spellerberg IF, Fedor PJ. A tribute to Claude Shannon (1916–2001) and a plea for more rigorous use of species richness, species diversity and the ‘Shannon–Wiener’ index. *Glob Ecol Biogeogr*. 2003;12(3):177–179. doi:10.1046/j.1466-822X.2003.00015.x
22. Simpson EH. Measurement of diversity. *Nature*. 1949;163(4148):688. doi:10.1038/163688a0
23. Lozupone C, Knight R. UniFrac: A new phylogenetic method for comparing microbial communities. *Appl Environ Microbiol*. 2005;71(12):8228–8235. doi:10.1128/aem.71.12.8228-8235.2005
24. Clarke KR. Non-parametric multivariate analyses of changes in community structure. *Austral Ecol*. 1993;18(1):117–143. doi:10.1111/j.1442-9993.1993.tb00438.x
25. Segata N, Izard J, Waldron L, et al. Metagenomic biomarker discovery and explanation. *Genome Biol*. 2011;12(6):R60. doi:10.1186/gb-2011-12-6-r60
26. Ward T, Larson J, Meulemans J, et al. BugBase predicts organism-level microbiome phenotypes. *BioRxiv*. 2017:133462. doi:10.1101/133462
27. Okubo H, Nakatsu Y, Sakoda H, et al. Mosapride citrate improves nonalcoholic steatohepatitis with increased fecal lactic acid bacteria and plasma glucagon-like peptide-1 level in a rodent model. *Am J Physiol Gastrointest Liver Physiol*. 2015;308(2):G151–G158. doi:10.1152/ajpgi.00198.2014
28. Zuo K, Li J, Li K, et al. Disordered gut microbiota and alterations in metabolic patterns are associated with atrial fibrillation. *Gigascience*. 2019;8(6):giz058. doi:10.1093/gigascience/giz058
29. Yin J, Liao SX, He Y, et al. Dysbiosis of gut microbiota with reduced trimethylamine-n-oxide level in patients with large-artery atherosclerotic stroke or transient ischemic attack. *J Am Heart Assoc*. 2015;4(11):e002699. doi:10.1161/jaha.115.002699
30. Sydenham TV, Arpi M, Klein K, Justesen US. Four cases of bacteremia caused by *Oscillibacter ruminantium*, a newly described species. *J Clin Microbiol*. 2014;52(4):1304–1307. doi:10.1128/jcm.03128-13
31. Sun Y, Chen Q, Lin P, et al. Characteristics of gut microbiota in patients with rheumatoid arthritis in Shanghai, China. *Front Cell Infect Microbiol*. 2019;9:369. doi:10.3389/fcimb.2019.00369
32. Li F, Wang M, Wang J, Li R, Zhang Y. Alterations to the gut microbiota and their correlation with inflammatory factors in chronic kidney disease. *Front Cell Infect Microbiol*. 2019;9:206. doi:10.3389/fcimb.2019.00206
33. Ganly I, Yang L, Giese RA, et al. Periodontal pathogens are a risk factor of oral cavity squamous cell carcinoma, independent of tobacco and alcohol and human papillomavirus. *Int J Cancer*. 2019;145(3):775–784. doi:10.1002/ijc.32152
34. Zhang L, Liu Y, Zheng HJ, Zhang CP. The oral microbiota may have influence on oral cancer. *Front Cell Infect Microbiol*. 2020;9:476. doi:10.3389/fcimb.2019.00476
35. Qiao S, Bao L, Wang K, et al. Activation of a specific gut bacteroides-foolate-liver axis benefits for the alleviation of nonalcoholic hepatic steatosis. *Cell Rep*. 2020;32(6):108005. doi:10.1016/j.celrep.2020.108005
36. Liu J, Hao W, He Z, et al. Beneficial effects of tea water extracts on the body weight and gut microbiota in C57BL/6J mice fed with a high-fat diet. *Food Funct*. 2019;10(5):2847–2860. doi:10.1039/c8fo02051e
37. Wu DN, Guan L, Jiang YX, et al. Microbiome and metabonomics study of quercetin for the treatment of atherosclerosis. *Cardiovasc Diagn Ther*. 2019;9(6):545–560. doi:10.21037/cdt.2019.12.04
38. Rocafort M, Noguera-Julian M, Rivera J, et al. Evolution of the gut microbiome following acute HIV-1 infection. *Microbiome*. 2019;7(1):73. doi:10.1186/s40168-019-0687-5
39. Cignarella F, Cantoni C, Ghezzi L, et al. Intermittent fasting confers protection in CNS autoimmunity by altering the gut microbiota. *Cell Metab*. 2018;27(6):1222–1235.e6. doi:10.1016/j.cmet.2018.05.006
40. Derrien M, Belzer C, de Vos WM. *Akkermansia muciniphila* and its role in regulating host functions. *Microb Pathog*. 2017;106:171–181. doi:10.1016/j.micpath.2016.02.005
41. Everard A, Belzer C, Geurts L, et al. Cross-talk between *Akkermansia muciniphila* and intestinal epithelium controls diet-induced obesity. *Proc Natl Acad Sci U S A*. 2013;110(22):9066–9071. doi:10.1073/pnas.1219451110



# Improving tear ferning patterns collected from goats and camels after adding various electrolyte solutions

Raied Fagehi<sup>A,C-F</sup>, Gamal A. El-Hiti<sup>A,C-F</sup>, Abdulaziz Alanazi<sup>A,B</sup>, Mohammed A. Aldawood<sup>A,B</sup>, Ali Abusharha<sup>A,F</sup>, Mana A. Alanazi<sup>A,F</sup>, Ali M. Masmali<sup>A,E,F</sup>, Turki Almubrad<sup>A,E,F</sup>

Optometry Department, College of Applied Medical Sciences, King Saud University, Riyadh, Saudi Arabia

A – research concept and design; B – collection and/or assembly of data; C – data analysis and interpretation; D – writing the article; E – critical revision of the article; F – final approval of the article

Advances in Clinical and Experimental Medicine, ISSN 1899–5276 (print), ISSN 2451–2680 (online)

Adv Clin Exp Med. 2022;31(6):635–642

## Address for correspondence

Raied Fagehi  
E-mail: rfagehi@ksu.edu.sa

## Funding sources

Researchers Supporting Project No. RSP-2021/404,  
King Saud University, Riyadh, Saudi Arabia.

## Conflict of interest

None declared

Received on August 19, 2021  
Reviewed on December 31, 2021  
Accepted on February 3, 2022

Published online on February 23, 2022

## Abstract

**Background.** Good quality of tear film is essential for healthy vision in both animals and humans. Therefore, improving the quality of tears through the addition of electrolytes is important.

**Objectives.** To assess the effect of adding various electrolyte solutions on tear ferning (TF) patterns collected from goats and camels.

**Materials and methods.** Tear samples (20  $\mu$ L) were collected from 5 goats (2 males and 3 females; 3.4  $\pm$ 1.6 years) and 5 camels (2 males and 3 females; 4.0  $\pm$ 1.1 years) using microcapillary tubes. A tear sample (0.5  $\mu$ L) from each animal was mixed with various volumes (0.5–5  $\mu$ L) of each electrolyte solution to produce homogenous mixtures. A sample (1  $\mu$ L) of each mixture was dried on a microscopic glass at 22°C with a humidity  $\leq$ 40%. The obtained TF pattern was observed, graded and compared with those obtained for the corresponding pure tear samples. The effect of dilution using purified water on the TF patterns of animals was also tested.

**Results.** The TF grades of animals were generally enhanced when mixed with electrolyte solutions. Specifically, the TF grade for tears collected from a goat was improved from 1.4 to 0.7 and to 0.8 when magnesium chloride hexahydrate and calcium chloride were added, respectively. Similarly, the TF grade for tears collected from a camel was improved from 1.8 to 0.9 and to 1.1, when calcium chloride and sodium dihydrogen phosphate solutions were added, respectively.

**Conclusions.** The TF grades of tears collected from both goats and camels were improved after adding electrolyte solutions, and they were most remarkably improved when divalent electrolyte solutions were added, followed by the hydrogenated electrolyte.

**Key words:** animals, electrolytes, tears, tear film, tear ferning

## Cite as

Fagehi R, El-Hiti GA, Alanazi A, et al. Improving tear ferning patterns collected from goats and camels after adding various electrolyte solutions. *Adv Clin Exp Med.* 2022;31(6):635–642. doi:10.17219/acem/146390

## DOI

10.17219/acem/146390

## Copyright

Copyright by Author(s)  
This is an article distributed under the terms of the Creative Commons Attribution 3.0 Unported (CC BY 3.0) (<https://creativecommons.org/licenses/by/3.0/>)

## Background

The stability of the tear film is critical for a healthy ocular system. Tear film lubricates the eye surface, transports oxygen and nutrients to the cornea, and washes away foreign bodies and waste.<sup>1</sup> It protects the ocular surface against infections, high temperature and chemicals, facilitates eyelid movement, and makes the reflection of the corneal surface smooth.<sup>1</sup> The tear film structure is very complex, but can be simplified as a three-layer model.<sup>2</sup> However, a different model structure has been suggested for the tear film. It includes a mixture of inner aqueous phase containing hydrophilic mucins, electrolytes and large molecules, such as enzymes and lipids as the outermost layer.<sup>3,4</sup> Mucins mix well with aqueous contents and spread over the ocular surface. Both the main and accessory lacrimal glands are responsible for producing aqueous contents of tear film.<sup>4</sup> Notably, meibomian glands produce lipids.<sup>5</sup> In animals, the conjunctiva accessory lacrimal glands produce tears.<sup>6</sup> The disturbance in lacrimal and meibomian glands functions induces tear film abnormality and dry eye disorder.<sup>7</sup>

The ocular tear film can be examined using several tests, in which each test determines a specific parameter. Tear volume can be measured using the phenol red thread test, while the Schirmer's test measures tear production.<sup>8</sup> When the tear evaporates, the breakup and thinning of tear film occur.<sup>9</sup> Therefore, tear breakup time measurement provides valuable information about tear film stability. The tear osmolarity test detects the equilibrium between tear evaporation, absorption, drainage, and production.<sup>10</sup> Osmolality is mainly controlled by the electrolyte concentration in the aqueous contents of tear film.<sup>11</sup> Tear lipid stability can be assessed by measuring the tear evaporation rate. Dry eye, discomfort and tear thinning are associated with excessive tear evaporation rate.<sup>12</sup> The tear ferning (TF) test has been used as a simple and low-cost tool to detect dry eye.<sup>13,14</sup> Capillary tubes are commonly used to collect tear samples with a low coefficient of variation.<sup>15</sup> Tears produce ferns when dried and their shapes are independent of sex, race and duration of day.<sup>16–18</sup> Dry eye tears have a shortage of ferns with large spaces between the branches.<sup>14</sup> The TF test has good specificity and sensitivity and has been used with other tests to assess the quality of tears in both animals and humans.<sup>19–27</sup>

Goats and camels have big eyes and are considered good animal models for surgical interventions.<sup>28,29</sup> Therefore, this study investigated the effect of adding electrolyte solutions on the TF patterns of tears collected from goats and camels. Recently, it has been reported that TF patterns of artificial tears have been improved when mixed with electrolyte and large molecule solutions.<sup>30</sup>

## Objectives

To assess the effect of adding various electrolyte solutions on the TF patterns of tears collected from both goats and camels.

## Materials and methods

### Animals

The animals were randomly selected from a farm 120 km east of Riyadh, Saudi Arabia. The animals were healthy, without ocular disorders or diseases. The tear samples were collected from the lower meniscus of the right eye of 5 goats (2 males and 3 females;  $3.4 \pm 1.6$  years) and 5 camels (2 males and 3 females;  $4.0 \pm 1.1$  years) in the same environment by the same examiner. During the tear collection, no lacrimation instruments or anesthetics were used. The tears were stored in Eppendorf tubes in a cooled container and were transported immediately to the clinic. The study was ethically approved before tear collection. The study was approved by the Institutional Review Board of King Saud University Riyadh, Saudi Arabia (approval No. 131-3637).

### Electrolyte solutions

The salts were obtained from Avonchem Limited (Macclesfield, UK). Solutions of sodium chloride (NaCl; 680 mg/mL), potassium chloride (KCl; 140 mg/100 mL), calcium chloride (CaCl<sub>2</sub>; 5 mg/100 mL), magnesium chloride hexahydrate (MgCl<sub>2</sub>·6H<sub>2</sub>O; 12 mg/100 mL), and sodium hydrogen phosphate (NaH<sub>2</sub>PO<sub>4</sub>; 9.4 mg/100 mL) were prepared in double-distilled water (100 mL). The mixtures were stirred for 5 min using a Stuart magnetic stirrer (Cole-Parmer, St Neots, UK) to produce a solution of each electrolyte. The concentration of electrolytes was the same as in the basic tear solution.<sup>31</sup>

### TF test

Microcapillary tubes (50 µL) obtained from Merck (Darmstadt, Germany) were used to collect the tear samples (20 µL) from the right eyes of the animals. A tear sample (1 L) of each animal was transferred over a microscopic slide to dry at normal environmental conditions (22°C with humidity ≤40%). The formed TF patterns were observed using an Olympus DP72 digital microscope (Olympus Key Med Limited, Southend-On-Sea, UK) at ×20 magnification. The produced ferns were graded based on the 5-point grading scale in 0.1 increments.<sup>19</sup> A tear sample (0.5 µL) from each animal was thoroughly mixed with different volumes of each electrolyte (0.5–5 µL). A tear sample (1 µL) of each mixture was dried over a glass slide and the produced ferns were graded and compared with those of the corresponding pure tears collected from each animal.

For comparison, a tear sample from each sheep (0.5  $\mu$ L) was diluted with double-distilled water (0.5  $\mu$ L) and the TF patterns were recorded for each mixture. The TF grades of diluted tears were the same as those of pure animal tears before the dilution. Three independent examiners graded the TF patterns. The 2<sup>nd</sup> and 3<sup>rd</sup> examiner were blinded to avoid bias. In many cases, the scores from the examiners were exactly the same and in other cases, the variation was less than  $\pm 0.05$ . An average TF grade was recorded and rounded to the nearest decimal place. The standard deviation (SD) has not been recorded since it was negligible in all cases (less than  $\pm 0.05$ ). The TF patterns were graded in 0.1 increments.<sup>19</sup> No statistical tests were used to test the significance of the differences between the tear ferning grades (TFG) before and after the addition of the electrolyte solutions, mainly due to the small sample size.

## Results

The age and sex of goats (n = 5; 2 males and 3 females; 3.4  $\pm$  1.6 years) and camels (n = 5; 2 males and 3 females; 4.0  $\pm$  1.1 years) from whom the tear samples (20  $\mu$ L) were collected are shown in Table 1.

Table 2 shows the TF grades for tears collected from goats and their homogenous mixtures with different

Table 1. The age and sex of goats and camels from whom tear samples were collected

Tear sample	Age [years]	Sex
G1	6	female
G2	3	male
G3	4	female
G4	1	female
G5	3	male
C1	3	female
C2	4	female
C3	6	female
C4	3	male
C5	4	male

G1 – 1<sup>st</sup> goat tear sample; G2 – 2<sup>nd</sup> goat tear sample; G3 – 3<sup>rd</sup> goat tear sample; G4 – 4<sup>th</sup> goat tear sample; G5 – 5<sup>th</sup> goat tear sample; C1 – 1<sup>st</sup> camel tear sample; C2 – 2<sup>nd</sup> camel tear sample; C3 – 3<sup>rd</sup> camel tear sample; C4 – 4<sup>th</sup> camel tear sample; C5 – 5<sup>th</sup> camel tear sample.

volumes of electrolyte solutions (goat tear samples to electrolyte solutions = 1:1, 1:2, 1:4, 1:6, 1:8, and 1:10), based on the 5-point grading scale in 0.1 increments. Examples of the TF images of tears collected from the 3<sup>rd</sup> and 4<sup>th</sup> goat, and those obtained from their homogenous mixtures with some electrolyte solutions, which lead to the most improvements, are shown in Fig. 1 and Fig. 2, respectively.

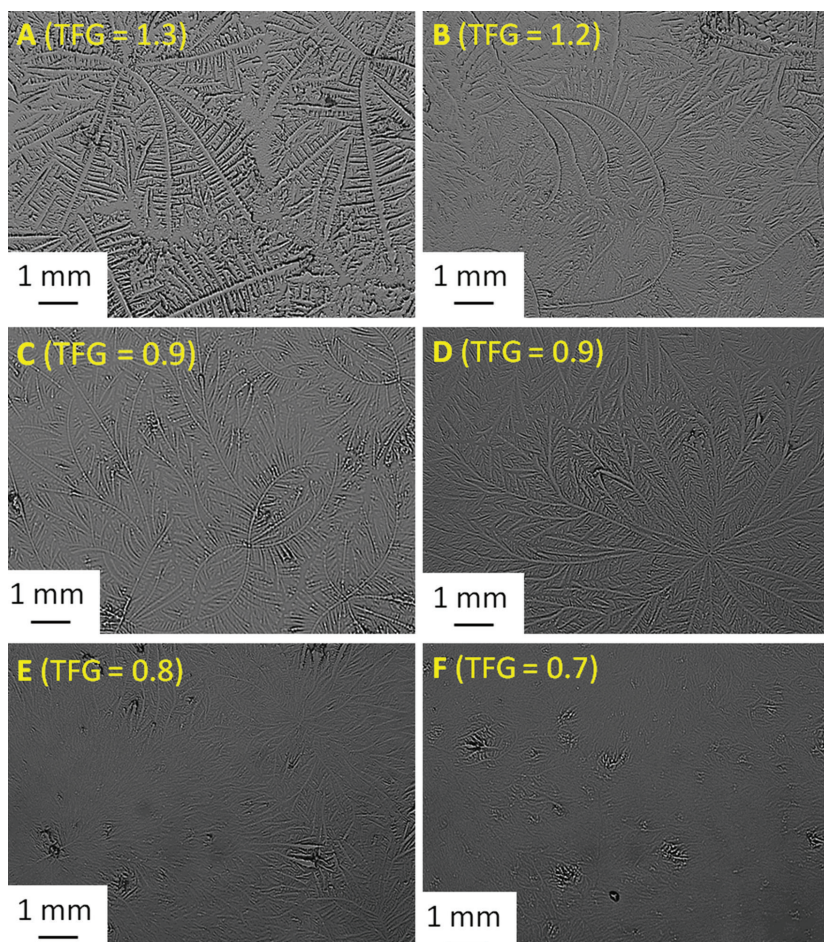


Fig. 1. The tear ferning (TF) patterns of A. pure G3; B. G3:NaCl (1:1); C. G3:KCl (1:4); D. G3:CaCl<sub>2</sub> (1:1); E. G3:MgCl<sub>2</sub>·6H<sub>2</sub>O (1:8); and F. G3:NaH<sub>2</sub>PO<sub>4</sub> (1:8)

G3 – 3<sup>rd</sup> goat tear sample; TFG – tear ferning grade.

**Table 2.** Tear ferning (TF) grades of goat tears and those obtained from their corresponding mixtures with electrolyte solutions

Electrolyte	Ratio <sup>a</sup>	Tear sample				
–	–	0.8	1.5	1.3	1.2	1.4
NaCl	1:1	1.5	1.6	1.2	1.4	1.6
	1:2	1.4	1.6	1.3	1.2	1.3
	1:4	1.3	1.6	1.2	1.1	1.4
	1:6	1.4	1.6	1.2	1.2	1.5
	1:8	1.4	1.7	1.3	1.2	1.5
	1:10	1.4	1.7	1.3	1.2	1.3
KCl	1:1	1.5	1.5	1.2	1.4	1.4
	1:2	1.5	1.5	1.2	0.9	1.1
	1:4	1.5	1.4	0.9	0.9	1.1
	1:6	1.4	1.4	1.1	0.8	1.3
	1:8	1.4	1.4	1.1	0.5	1.2
	1:10	1.4	1.4	1.1	0.9	1.1
CaCl <sub>2</sub>	1:1	1.3	1.3	0.9	0.8	1.3
	1:2	1.2	1.3	0.9	1.1	1.2
	1:4	1.2	1.3	0.9	0.4	0.9
	1:6	1.2	1.3	0.9	0.9	0.8
	1:8	1.2	1.3	1.0	0.7	0.8
	1:10	1.2	0.8	1.0	0.8	0.8
MgCl <sub>2</sub> .6H <sub>2</sub> O	1:1	1.3	1.2	1.1	0.6	1.3
	1:2	1.3	1.2	1.2	1.2	1.1
	1:4	1.2	1.2	0.9	1.1	1.1
	1:6	1.1	1.1	1.1	1.1	1.1
	1:8	1.1	1.2	0.8	1.1	0.7
	1:10	1.1	1.2	1.2	1.1	0.7
NaH <sub>2</sub> PO <sub>4</sub>	1:1	1.4	1.3	1.1	1.1	1.0
	1:2	1.3	1.3	0.8	1.1	1.1
	1:4	1.2	1.3	0.8	1.1	1.1
	1:6	1.1	1.2	0.8	0.7	1.1
	1:8	1.1	1.2	0.7	0.6	0.9
	1:10	0.6	1.2	0.8	0.9	0.9

<sup>a</sup> – the volume ratio between tear sample and electrolyte solution. The TF grade was rounded to the nearest one decimal place.

The TF grades for the diluted animal tear samples using double-distilled water were the same as those recorded before the dilution. Such result eliminates the effect of water used to prepare the salt solution on the TF patterns of animal tear samples.

The TF grades of tears collected from goats (1.5–0.8) were improved after adding electrolyte solutions, and were mostly improved when the CaCl<sub>2</sub> solution was added. For example, the TF grade of tears collected from the 4<sup>th</sup> goat (G4) was improved from 1.2 to 0.4 when CaCl<sub>2</sub> solution (G4 tears to CaCl<sub>2</sub> ratio = 1:4) was added. Similarly, adding KCl solution (G4 tears to KCl ratio = 1:8) improved the TF grade of G4 to 0.5. Additionally, the TF grade of G4 was improved to 0.6 after either MgCl<sub>2</sub>.6H<sub>2</sub>O (G4 tears to MgCl<sub>2</sub>.6H<sub>2</sub>O ratio = 1:1) or NaH<sub>2</sub>PO<sub>4</sub> solution (G4 tears to NaH<sub>2</sub>PO<sub>4</sub> ratio = 1:8) was added. Limited

or no improvement was observed when the NaCl solution was used, regardless of its proportion within the mixtures. Adding divalent (CaCl<sub>2</sub> and MgCl<sub>2</sub>.6H<sub>2</sub>O) and hydrogenated (NaH<sub>2</sub>PO<sub>4</sub>) electrolyte solutions provided a better improvement in TF grades of goat tear samples compared with monovalent electrolytes (NaCl and KCl).

Table 3 shows the TF grades for pure tears collected from 5 camels and those obtained from the corresponding homogenous mixtures with different volumes of electrolyte solutions (camel tear samples to electrolyte solutions = 1:1, 1:2; 1:4, 1:6, 1:8, and 1:10) in 0.1 increments. Figure 3 shows TF images of tears collected from one of the camels (C3), and those obtained from their homogenous mixtures with some electrolyte solutions. The mean ±SD for the TF grades for both goats and camels after the addition of electrolytes are shown in Table 2,3, respectively.

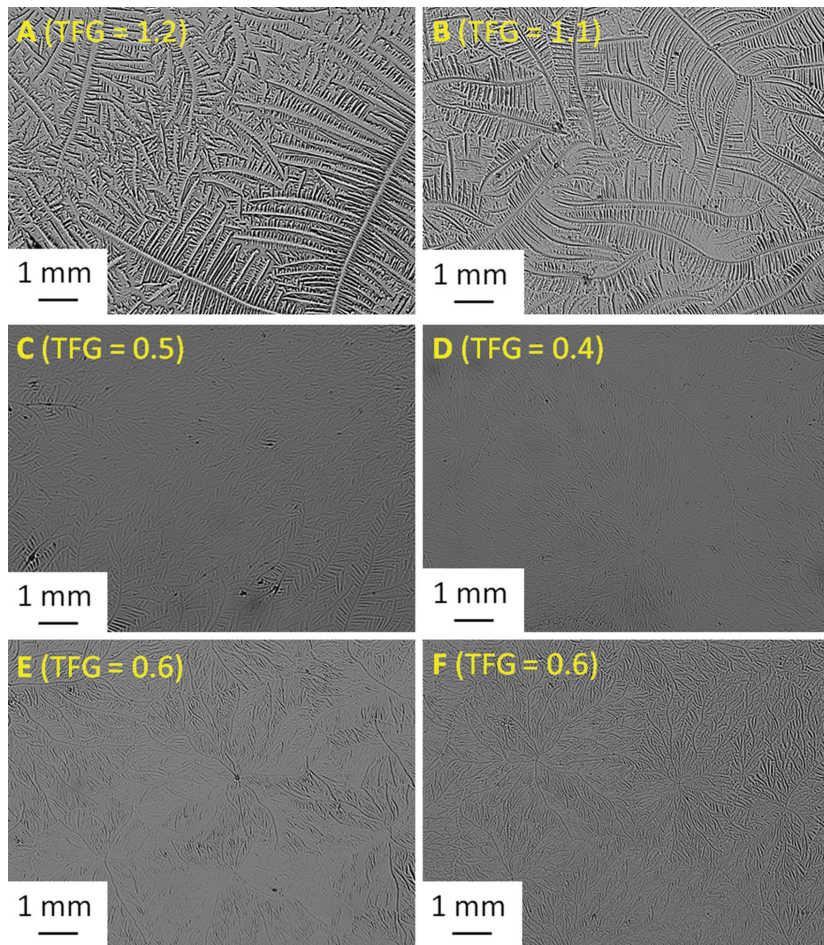


Fig. 2. The tear ferning (TF) patterns of A. pure G4; B. G4:NaCl (1:4); C. G4:KCl (1:8); D. G4:CaCl<sub>2</sub> (1:4); E. G4:MgCl<sub>2</sub>·6H<sub>2</sub>O (1:1); and F. G4:NaH<sub>2</sub>PO<sub>4</sub> (1:8) G4 – 4<sup>th</sup> goat tear sample; TFG – tear ferning grade.

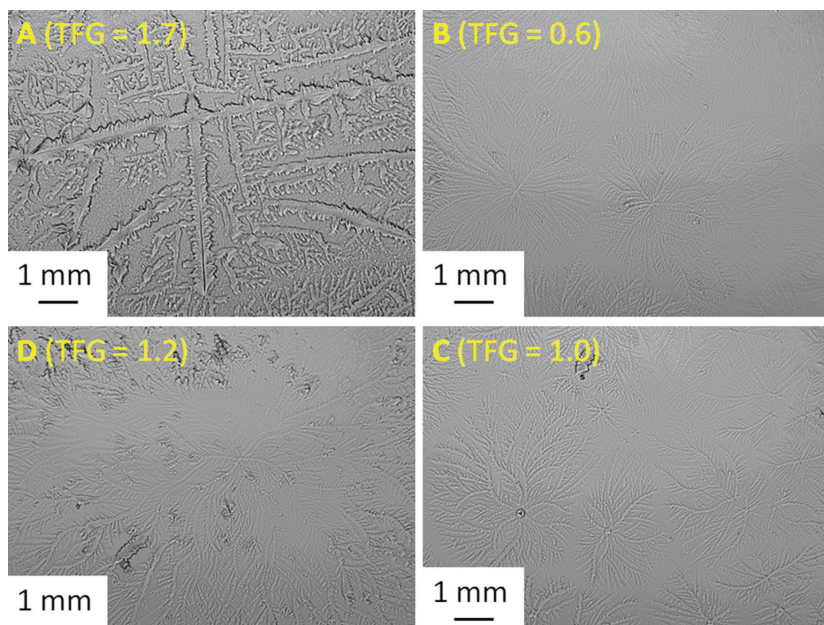


Fig. 3. The tear ferning (TF) patterns of A. pure C3; B. C3:CaCl<sub>2</sub> (1:4); C. C3:MgCl<sub>2</sub>·6H<sub>2</sub>O (1:2); and D. C3:NaH<sub>2</sub>PO<sub>4</sub> (1:2) C3 – 3<sup>rd</sup> camel tear sample; TFG – tear ferning grade.

The TF grade improvements of tears collected from camels when mixed with electrolyte solutions were limited in all cases. However, the TF grade of tears collected from one of the camels (C3) was improved from 1.7 to 0.6–0.7 when CaCl<sub>2</sub> was added, regardless of its proportion

in the mixtures. Similarly, the TF grade of the same camel was improved to 0.9 when NaH<sub>2</sub>PO<sub>4</sub> (tears to electrolyte ratio = 1:1) was added to camel tears. The effect of the addition of different proportions of various electrolyte solutions on the TFG of the tears collected from the 3<sup>rd</sup> goat

**Table 3.** Tear ferning (TF) grades of camel tears and those obtained from their corresponding mixture with electrolyte solutions

Electrolyte	Ratio <sup>a</sup>	Tear sample				
–	–	1.8	1.9	1.7	1.8	1.9
NaCl	1:1	1.6	1.4	1.6	1.6	1.4
	1:2	1.7	1.4	1.5	1.4	1.4
	1:4	1.7	1.3	1.6	1.4	1.4
	1:6	1.6	1.3	1.7	1.5	1.5
	1:8	1.6	1.5	1.7	1.5	1.5
	1:10	1.7	1.5	1.7	1.5	1.6
KCl	1:1	1.4	1.4	1.3	1.3	1.3
	1:2	1.5	1.3	1.4	1.4	1.3
	1:4	1.5	1.5	1.4	1.4	1.4
	1:6	1.6	1.6	1.5	1.5	1.4
	1:8	1.6	1.6	1.5	1.6	1.5
	1:10	1.6	1.7	1.5	1.6	1.6
CaCl <sub>2</sub>	1:1	1.7	1.3	0.7	1.2	1.2
	1:2	1.4	1.2	0.6	1.5	1.1
	1:4	1.5	1.4	0.6	1.2	1.4
	1:6	1.3	1.2	0.7	1.1	1.3
	1:8	1.3	1.2	0.7	1.1	1.4
	1:10	1.4	1.2	0.7	1.1	1.4
MgCl <sub>2</sub> ·6H <sub>2</sub> O	1:1	1.4	1.6	1.2	1.5	1.3
	1:2	1.5	1.7	1.2	1.5	1.5
	1:4	1.4	1.6	1.2	1.4	1.5
	1:6	1.8	1.6	1.6	1.6	1.6
	1:8	1.6	1.6	1.5	1.4	1.5
	1:10	1.7	1.7	1.5	1.4	1.4
NaH <sub>2</sub> PO <sub>4</sub>	1:1	1.4	1.5	0.9	1.5	1.2
	1:2	1.6	1.6	1.0	1.5	1.3
	1:4	1.4	1.5	1.4	1.3	1.4
	1:6	1.3	1.4	1.3	1.2	1.3
	1:8	1.4	1.3	1.2	1.2	1.4
	1:10	1.4	1.3	1.2	1.2	1.4

<sup>a</sup> – the volume ratio between tear sample and electrolyte solution. The TF grade was rounded to the nearest one decimal place.

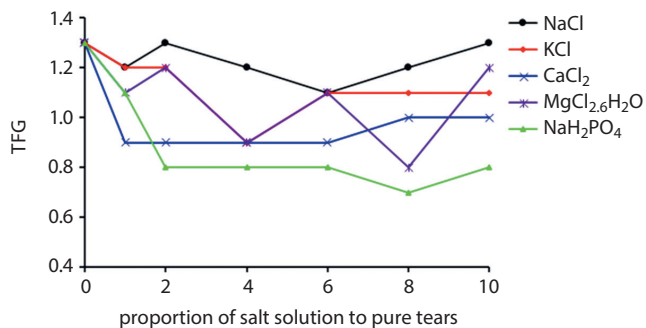


**Fig. 4.** Effect of various electrolyte solutions on the tear ferning grade (TFG) of the tears collected from the 3<sup>rd</sup> goat (G3)

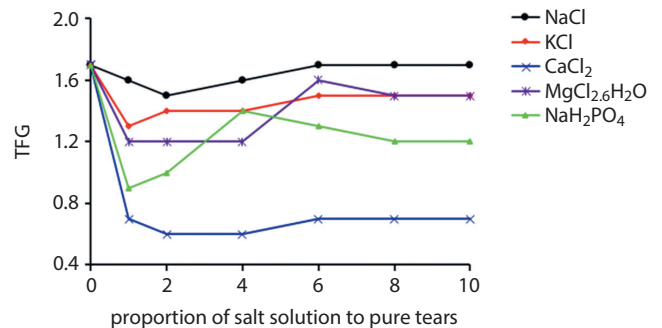


**Fig. 5.** Effect of various electrolyte solutions on the tear ferning grade (TFG) of the tears collected from the 3<sup>rd</sup> camel (C3)

(G3) and the 3<sup>rd</sup> camel (C3) are shown in Fig. 4 and Fig. 5, respectively. Clearly, NaH<sub>2</sub>PO<sub>4</sub> solution led to the highest improvement in TF patterns of tears collected from

the 3<sup>rd</sup> goat. At the same time, the addition of CaCl<sub>2</sub> solution led to the most noticeable improvement in TF patterns of the tears collected from the 3<sup>rd</sup> camel.



## Discussion

This study showed that adding different volumes of several electrolyte solutions to tear samples collected from goats and camels improved their TF grades. The TF grades most remarkably improved when a solution of  $\text{CaCl}_2$ ,  $\text{NaH}_2\text{PO}_4$  or  $\text{MgCl}_2 \cdot 6\text{H}_2\text{O}$  was used. While relatively low proportions of  $\text{CaCl}_2$  solution improved TF grades of goats, large volumes of  $\text{NaH}_2\text{PO}_4$  solution were required to improve these grades. The  $\text{NaCl}$  and  $\text{KCl}$  solutions did not improve TF grades of tears collected from camels, since the high levels of ions ( $\text{Na}^+$ ,  $\text{K}^+$  and  $\text{Cl}^-$ ) could upset the balance between electrolytes and large molecule concentrations in the camel tears.

Tear ferns are formed due to the interactions between electrolytes, specifically  $\text{Na}^+$  and  $\text{Cl}^-$  ions, with macromolecules (mucins and proteins) within tear film.<sup>32</sup> The ratio between monovalent (e.g.,  $\text{Na}^+$  and  $\text{K}^+$ ) and divalent (e.g.,  $\text{Ca}^{+2}$  and  $\text{Mn}^{+2}$ ) cations controls fern formation.<sup>33</sup> Notably, the TF patterns of tears collected from camels outperformed the corresponding ones for Refresh Plus eye drops.<sup>27</sup> The scanning electron microscope revealed that the tears collected from camels have perfect tertiary and quaternary divisions.<sup>27</sup> The ions such as  $\text{K}^+$  and  $\text{Cl}^-$  are responsible for fern formation and were more prevalent in tears collected from camels compared with human tears and Refresh Plus eye drops.<sup>27</sup> Presumably, these anions help maintain healthy TF patterns in camels.<sup>27</sup> Also, the balance between  $\text{Na}^+$ ,  $\text{K}^+$  and  $\text{Cl}^-$  affected the fern formation rather than each individual ion concentration.<sup>33</sup> Both proteins and mucins facilitate fern formation, but are uninvolved in the fern structure.<sup>33,34</sup> Adding electrolyte and large molecule solutions improved the TF grades of artificial tears.<sup>30</sup>

Animals and humans have different types of protein in their tears.<sup>35</sup> In animals, season and sex can influence tear production.<sup>36,37</sup> This study showed no difference among TF grades in tears collected from both goats and camels, and those obtained from their corresponding homogeneous mixtures with electrolyte solutions.

Very recently, the improvement of TF patterns of sheep tears has been achieved through the addition of electrolyte solutions. The divalent electrolytes led to a noticeable improvement in TF patterns of sheep tears followed by sodium dihydrogen phosphate. The use of various concentrations of sodium chloride led to no improvement in TF patterns when added to sheep tears.<sup>38</sup> The TF patterns depend on the type and concentration of electrolyte in tears.<sup>39</sup> Salts are essential to adjust the osmolarity of tears, improve the secretion of tears, and suppress tear evaporation.<sup>40</sup> However, it is not clear why divalent electrolytes improve the TF patterns of tears obtained from both goats and camels compared with monovalent salts. The concentration of monovalent electrolytes used in this study was much higher (140–680 mg in 100 mL water) compared with that used for divalent salts (5–12 mg in 100 mL water), as in the basic tear solution.<sup>31</sup> Such high concentrations

of salts ( $\text{NaCl}$  and  $\text{KCl}$ ) could lead to hyperosmolality and as a result, high TF grades. To confirm this hypothesis, further research is needed to test the effect of a low concentration of monovalent electrolytes on the TF patterns of natural tears (in animals and humans).

The mean difference and 95% limits of agreement for TF grades of normal eye tears for different day durations were  $0.1 \pm 0.4$ .<sup>17</sup> The TF grade mean difference for tears collected from goats and camels and those obtained from their corresponding mixtures with electrolyte solutions was minute ( $\pm 0.1$ ). The scores recorded by 2 examiners were exactly the same in many cases and the changes in TF grades were minute (less than  $\pm 0.05$ ) in other cases, particularly for camel tears. The correlations between TF grades and the scores from other dry eye tests in healthy and dry eye subjects are generally weak.<sup>17,23,41</sup> Nevertheless, the TF test is repeatable and reliable to detect dry eye.<sup>41–43</sup>



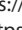
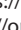
## Limitations

The current study has some limitations, which can be addressed in related future research. First, the sample size for both goats ( $n = 5$ ) and camels ( $n = 5$ ) was small. Second, the animals involved in the study had healthy eyes. No animal with a dry eye was involved in the study (the TF grades of tears were less than 2). We anticipated that the effect of electrolytes solution will improve the TF patterns of tears collected from dry eyes even better than those recorded for normal eye tears. However, such prediction needs to be investigated. Third, the effect of other electrolytes in different concentrations needs to be tested. Fourth, the animals have been recruited from a single farm that represents a specific location in Saudi Arabia. Fifth, no statistical tests were used to test the significance of the differences between the TFG before and after the addition of the electrolyte solutions, mainly due to the small sample size.

## Conclusions

The TF grades of tears collected from both goats and camels were improved after adding the electrolyte solutions, and were most improved when divalent electrolytes (calcium chloride and magnesium chloride hexahydrate) were added, followed by the hydrogenated electrolyte (sodium dihydrogen phosphate).

### ORCID iDs

Raied Fagehi  <https://orcid.org/0000-0002-6255-4549>  
 Gamal A. El-Hiti  <https://orcid.org/0000-0001-6675-3126>  
 Abdulaziz Alanazi  <https://orcid.org/0000-0003-0249-7623>  
 Mohammed A. Aldawood  <https://orcid.org/0000-0003-4668-2548>  
 Ali Abusharha  <https://orcid.org/0000-0001-7097-0852>  
 Mana A. Alanazi  <https://orcid.org/0000-0003-3599-6242>  
 Ali M. Masmali  <https://orcid.org/0000-0001-5992-6332>  
 Turki Almubrad  <https://orcid.org/0000-0001-9806-8254>

## References

- Willcox MDP, Argüeso P, Georgiev GA, et al. TFOS DEWS II tear film report. *Ocul Surf*. 2017;15(3):366–403. doi:10.1016/j.jtos.2017.03.006
- Wolff E. The muco-cutaneous junction of the lid margin and the distribution of the tear fluid. *Trans Ophthalmol Soc UK*. 1946;66:291–308.
- Lemp MA. Advances in understanding and managing dry eye disease. *Am J Ophthalmol*. 2008;146(3):350–356. doi:10.1016/j.ajo.2008.05.016
- Rolando M, Zierhut M. The ocular surface and tear film and their dysfunction in dry eye disease. *Surv Ophthalmol*. 2001;45(Suppl 2):S203–S210. doi:10.1016/s0039-6257(00)00203-4
- Peters E, Colby K. Chapter 3: The tear film. In: Tasman W, Jaeger EA, eds. *Foundation Volume 2: Physiology of the Eye and Visual System*. Philadelphia, USA: Lippincott Williams & Wilkins; 2013.
- Maitchouk DY, Beuerman RW, Ohta T, Stern M, Varnell RJ. Tear production after unilateral removal of the main lacrimal gland in squirrel monkeys. *Arch Ophthalmol*. 2000;118(2):246–252. doi:10.1001/archophth.118.2.246
- Phadattare SP, Momin M, Nighojkar P, Askarkar S, Singh KK. A comprehensive review on dry eye disease: Diagnosis, medical management, recent developments, and future challenges. *Adv Pharm*. 2015;2015:704946. doi:10.1155/2015/704946
- Masmali A, Alqahtani TA, Alharbi A, El-Hiti GA. Comparative study of repeatability of phenol red thread test versus Schirmer test in normal adults in Saudi Arabia. *Eye Contact Lens*. 2014;40(3):127–131. doi:10.1097/ICL.0000000000000025
- King-Smith PE, Ramamoorthy P, Braun RJ, Nichols JJ. Tear film images and breakup analyzed using fluorescent quenching. *Invest Ophthalmol Vis Sci*. 2013;54(9):6003–6011. doi:10.1167/iovs.13-12628
- Tomlinson A, Khanal S. Assessment of tear film dynamics: Quantification approach. *Ocul Surf*. 2005;3(2):81–95. doi:10.1016/s1542-0124(12)70157-x
- Stahl U, Willcox M, Stapleton F. Osmolality and tear film dynamics. *Clin Exp Optom*. 2012;95(1):3–11. doi:10.1111/j.1444-0938.2011.00634.x
- Khanal S, Tomlinson A, McFadyen A, Diaper C, Ramaesh K. Dry eye diagnosis. *Invest Ophthalmol Vis Sci*. 2008;49(4):1407–1414. doi:10.1167/iovs.07-0635
- Rolando M. Tear mucus ferning test in normal and keratoconjunctivitis sicca eyes. *Chib Int J Ophthalmol*. 1984;2(4):32–41.
- Masmali MA, Murphy PJ, Purslow C. Development of a new grading scale for tear ferning. *Cont Lens Anterior Eye*. 2014;37(3):178–184. doi:10.1016/j.clae.2013.09.011
- Norn M. Quantitative tear ferning: Methodologic and experimental investigations. *Acta Ophthalmol (Copenh)*. 1988;66(2):201–205. doi:10.1111/j.1755-3768.1988.tb04012.x
- Norn M. Quantitative tear ferning: Clinical investigations. *Acta Ophthalmol (Copenh)*. 1994;72(3):369–372. doi:10.1111/j.1755-3768.1994.tb02775.x
- Masmali A, Al-Bahlal JM, El-Hiti GA, et al. Repeatability and diurnal variation of tear ferning test. *Eye Contact Lens*. 2015;41(5):262–267. doi:10.1097/ICL.0000000000000116
- Sharanjeet K, Ho CY, Mutalib HA, Ghazali AR. The relationship between tear ferning patterns and non-invasive tear break-up time in normal Asian population. *J Optom*. 2016;9:175–181. doi:10.1016/j.optom.2015.10.004
- Masmali AM, Al-Qhtani S, Al-Gasham TM, El-Hiti GA, Purslow C, Murphy PJ. Application of a new grading scale for tear ferning in non-dry eye and dry eye subjects. *Cont Lens Anterior Eye*. 2015;38(1):39–43. doi:10.1016/j.clae.2014.09.007
- Masmali AM, Alanazi SA, Alotaibi AG, Fagehi R, Abusharaha A, El-Hiti GA. The acute effect of a single dose of green tea on the quality and quantity of tears in normal eye subjects. *Clin Ophthalmol*. 2019;13:605–610. doi:10.2147/OPHT.S201127
- Masmali AM, Alanazi SA, Almagren B, El-Hiti GA. Assessment of the tear film in normal eye subjects after consumption of a single dose of hot peppermint drink. *Clin Optom (Auckl)*. 2019;11:39–45. doi:10.2147/OPTO.S206904
- Masmali AM, Maeni YA, El-Hiti GA, Murphy PJ, Almubrad T. Investigation of ocular tear ferning in controlled and uncontrolled diabetic subjects. *Eye Contact Lens*. 2018;44(Suppl 2):S70–S75. doi:10.1097/ICL.0000000000000419
- Masmali AM, Al-Shehri A, Alanazi SA, Abusharaha A, Fagehi R, El-Hiti GA. Assessment of tear film quality among smokers using tear ferning patterns. *J Ophthalmol*. 2016;2016:8154315. doi:10.1155/2016/8154315
- Coassin M, Lambiase A, Costa N, et al. Efficacy of topical nerve growth factor treatment in dogs affected by dry eye. *Graefes Arch Clin Exp Ophthalmol*. 2005;243(2):151–155. doi:10.1007/s00417-004-0955-2
- Silva LR, Gouveia AF, Fátima CJT, et al. Tear ferning test in horses and its correlation with ocular surface evaluation. *Vet Ophthalmol*. 2016;19(2):117–123. doi:10.1111/vop.12268
- Oriá AP, Raposo ACS, Araújo NLLC, Lima FB, Masmali MA. Tear ferning test in healthy dogs. *Vet Ophthalmol*. 2018;21(4):391–398. doi:10.1111/vop.12524
- Masmali AM, Fagehi RA, El-Naggar AH, Almubrad TM, Akhtar S. Structure and microanalysis of tear film ferning of camel tears, human tears, and Refresh Plus. *Mol Vis*. 2018;24:305–314. PMID:29692599.
- Martini L, Fini M, Giavaresi G, Giardino R. Sheep model in orthopedic research: A literature review. *Comp Med*. 2001;51(4):292–299. PMID:11924786.
- Greene CA, Misra SL, Lee H, et al. The sheep cornea: Structural and clinical characteristics. *Curr Eye Res*. 2018;43(12):1432–1438. doi:10.1080/02713683.2018.1510970
- Masmali AM. Improvement of ferning patterns of lubricant eye drops mixed with various electrolytes and carboxymethylcellulose. *Cont Lens Anterior Eye*. 2019;42(6):633–639. doi:10.1016/j.clae.2019.04.010
- Bachman WG, Wilson G. Essential ions for maintenance of the corneal epithelial surface. *Invest Ophthalmol Vis Sci*. 1985;26(11):1484–1488. PMID:2414247.
- Golding TR, Brennan NA. The basis of tear ferning. *Clin Exp Optom*. 1989;72(4):102–112. doi:10.1111/j.1444-0938.1989.tb03069.x
- Kogbe O, Liotet S, Tiffany J. Factors responsible for tear ferning. *Cornea*. 1991;10(5):433–444. doi:10.1097/00003226-199109000-00013
- Pearce EI, Tomlinson A. Spatial location studies on the chemical composition of human tear ferns. *Ophthalmic Physiol Opt*. 2000;20(4):306–313. PMID:10962696.
- Evangelista M, Koverech A, Messano M, Pescosolido N. Comparison of three lubricant eye drop solutions in dry eye patients. *Optom Vis Sci*. 2011;88(12):1439–1444. doi:10.1097/OPX.0b013e3182348c28
- Dedousi A, Karatzia MA, Katsoulos PD. Reference values of Schirmer tear test in sheep and the effect of season on the test results. *Acta Vet Hung*. 2019;67(4):553–560. doi:10.1556/004.2019.054
- İşler CT, Altuğ ME, Kilic S. Evaluation of tear fluid secretion and intraocular pressure in normal merinos sheep and Saanen goats. *Rev Med Vet*. 2013;164(5):278–282. [https://www.researchgate.net/publication/287613168\\_Evaluation\\_of\\_Tear\\_fluid\\_secretion\\_and\\_Intraocular\\_Pressure\\_in\\_normal\\_Merinos\\_Sheep\\_and\\_Saanen\\_Goats](https://www.researchgate.net/publication/287613168_Evaluation_of_Tear_fluid_secretion_and_Intraocular_Pressure_in_normal_Merinos_Sheep_and_Saanen_Goats). Accessed on July 20, 2021.
- Fagehi R, El-Hiti GA, Alqarni BM, Alanazi MA, Masmali AM, Almubrad T. Improvement in tear ferning patterns of sheep tears after addition of various electrolyte solutions. *Front Med (Lausanne)*. 2021; 8:721969. doi:10.3389/fmed.2021.721969
- Masmali MA, Purslow C, Murphy PJ. The tear ferning test: A simple clinical technique to evaluate the ocular tear film. *Clin Exp Optom*. 2014;97(5):399–406. doi:10.1111/cxo.12160
- Okanobo A, Chauhan SK, Dastjerdi M, Kodati S, Dana R. Efficacy of topical blockade of interleukin-1 in experimental dry eye disease. *Am J Ophthalmol*. 2012;154(1):63–71. doi:10.1016/j.ajo.2012.01.034
- Alanazi SA, Alomran AA, Abusharaha A, et al. An assessment of the ocular tear film in patients with thyroid disorders. *Clin Ophthalmol*. 2019;13:1019–1026. doi:10.2147/OPHT.S210044
- Alanazi SA, El-Hiti GA, Al-Baloud AA, et al. Effects of short-term oral vitamin A supplementation on the ocular tear film in patients with dry eye. *Clin Ophthalmol*. 2019;13:599–604. doi:10.2147/OPHT.S198349
- Alanazi SA, Alfaifi AS, Abusharaha A, et al. Effect of short-term oral vitamin D3 supplementation on tear film in dry eye subjects. *Int J Ophthalmol Vis Sci*. 2019;4(3):51–57. doi:10.11648/j.ijovs.20190403.13

# Effects of Galp and alarin peptides on HPA axis gene expression and adrenal function: In vivo experiments

Marianna Tyczewska<sup>A–F</sup>, Marta Szyszka<sup>B,C,F</sup>, Karol Jopek<sup>B,C,F</sup>, Marcin Ruciński<sup>A,E,F</sup>

Department of Histology and Embryology, Poznan University of Medical Sciences, Poland

A – research concept and design; B – collection and/or assembly of data; C – data analysis and interpretation; D – writing the article; E – critical revision of the article; F – final approval of the article

Advances in Clinical and Experimental Medicine, ISSN 1899–5276 (print), ISSN 2451–2680 (online)

*Adv Clin Exp Med.* 2022;31(6):643–654

## Address for correspondence

Marianna Tyczewska  
E-mail: maritycz@ump.edu.pl

## Funding sources

The study was supported by grant No. 2015/17/D/NZ4/02294 from the National Science Centre, Poland.

## Conflict of interest

None declared

Received on August 25, 2021  
Reviewed on November 7, 2021  
Accepted on February 17, 2022

Published online on March 11, 2022

## Cite as

Tyczewska M, Szyszka M, Jopek K, Ruciński M. Effects of Galp and alarin peptides on HPA axis gene expression and adrenal function: In vivo experiments. *Adv Clin Exp Med.* 2022;31(6):643–654. doi:10.17219/acem/146775

## DOI

10.17219/acem/146775

## Copyright

Copyright by Author(s)  
This is an article distributed under the terms of the Creative Commons Attribution 3.0 Unported (CC BY 3.0) (<https://creativecommons.org/licenses/by/3.0/>)

## Abstract

**Background.** Many experimental data indicate interactions between peptides involved in the control of food intake, energy homeostasis and adrenocortical hormone release. Glucocorticoids stimulate or inhibit the secretion of orexigenic and anorexigenic peptides, which in turn are involved in the regulation of adrenal growth, structure and function. Galanin-like peptide (Galp) and alarin (Ala) are involved in the regulation of food intake. *Galp* and *Ala* mRNAs have already been shown to be present in the arcuate nucleus (ARC) of the hypothalamus in both rats and mice.

**Objectives.** To investigate the expression of *Ala*, *Galp* and their receptors in the hypothalamus and pituitary and adrenal glands of the rat hypothalamic–pituitary–adrenal (HPA) axis after intraperitoneal administration of peptides *in vivo*.

**Materials and methods.** Experimental *in vivo* models were used: acute and long-term exposure to peptides.

**Results.** The expression of *Galp*, *Ala*, their receptors, and steroidogenesis enzymes was analyzed using quantitative real-time polymerase chain reaction (qRT-PCR). Statistically significant expression changes were found in the hypothalamus and pituitary after 1-hour exposure to the peptides, such as a decrease in corticotropin-releasing hormone (*CRH*) expression after *Ala*, *Galp* and adrenocorticotropin hormone (ACTH) administration, and a decrease in the expression of receptors for galanin (*Gal*) (*Galr1* and *Galr2*). In the pituitary, there was a statistically significant increase in the expression of *Ala*, *Galr1*, *Galr2*, and *Galr3* receptors 1 h after *Galp* administration. In the adrenal glands, only a statistically significant decrease in *Galr2* expression was observed after 1 h of *Ala* 0.5 administration. The mRNA expression of steroidogenesis enzymes also changed: for example, the expression of cholesterol desmolase increased 24 h after *Ala* peptide administration.

**Conclusions.** The results indicate that the peptides tested under *in vivo* conditions can alter the expression of the peptides tested, as well as of *Galp*, *Ala* and *Gal* receptors and steroidogenesis enzymes – *Cyp11a1* (cholesterol desmolase), *Cyp11b1* (11 $\beta$ -hydroxylase) and *Cyp11b2* (aldosterone synthase).

**Key words:** adrenal gland, HPA axis, *Galp*, alarin (*Ala*), *in vivo* experiments

## Background

Adrenal glands are known to be involved in the maintenance of energy homeostasis in the body. There are 2 principal mechanisms of energy homeostasis regulation, central and peripheral, which involve many different hypothalamic peptides, such as neuropeptide Y (NPY), orexins (Ox), proopiomelanocortin (POMC), ghrelin (Ghrel), and cerebelin (Cer), that are directly or indirectly involved in food intake. Numerous experimental data have provided evidence of interactions between peptides involved in the control of food intake, energy homeostasis and steroidogenic hormones released by the adrenal glands.<sup>1–3</sup> It is well known that glucocorticoids stimulate NPY and inhibit corticotropin-releasing hormone (CRH) or POMC secretion.<sup>4–6</sup> On the other hand, numerous orexigenic and anorexigenic peptides are involved in the regulation of growth, structure and function of the adrenal gland, such as galanin (Gal), which is the “parental” peptide of a family that also includes galanin-like peptide (Galp) and alarin (Ala). As it is known, *Gal* mRNA and Gal receptors are expressed in rat adrenocortical cells.<sup>7–10</sup> Gal is known to be involved in the control of energy homeostasis and plays an important role in the regulation of adrenocortical hormone secretion.<sup>7</sup> Moreover, Gal stimulates cortisol secretion from human adrenocortical cells, acting through galanin receptor type 1 (Galr1), and stimulates the release of corticosterone and cyclic-AMP from dispersed inner rat adrenocortical cells.<sup>7,9–12</sup>

More than 20 years ago, Galp was first isolated from the porcine hypothalamus as an endogenous ligand of galanin receptor type 2 (Galr2).<sup>13</sup> Later study provided evidence that Galp interacts also with other galanin receptor isoforms (Galr1 and Galr3).<sup>14</sup> *Galp* mRNA was identified in different species, including rat, mouse and human.<sup>13,15,16</sup> Immunohistochemical studies demonstrated that around 85% of arcuate nucleus Galp-positive neurons (ARC-Galp) also express leptin receptors. There are already reports in the literature regarding the involvement of the Galp peptide in the regulation of body homeostasis.<sup>17–20</sup>

Another member of the Gal family – Ala, a 25-amino acids peptide – arises as a splice variant of the *Galp* gene.<sup>21,22</sup> This variant results from the exclusion of exon 3. Therefore, the N-terminal end of both *Galp* and *Ala* precursors is the same – it comprises the same signal sequence and proteolytic cleavage site. Alarin peptide was isolated from mouse brain and thymus.<sup>22</sup> Alarin-like immunoreactivity was observed in the locus coeruleus (LC) and the ARC of rats and mice. Both regions are involved in feeding behavior and homeostatic control. Alarin was identified as an orexigenic compound involved in the regulation of reproductive hormones secretion, an effect mediated through hypothalamic gonadotropin releasing hormone 1 (Gnrh1), but also in the regulation of feeding behavior in male rats and stimulation of NPY release from hypothalamic explants.<sup>23,24</sup>

Based on previous reports on the involvement of Galp and Ala peptides in homeostatic maintenance processes, and considering the role of Gal in adrenal cell function, the hypothalamic–pituitary–adrenal (HPA) axis and Gal involvement in the regulation of energy homeostasis, there is still a lack of data on the involvement of both Galp and Ala in the regulation of adrenal hormone secretion, and the interaction of the HPA axis.<sup>25</sup> Previous quantitative polymerase chain reaction (qPCR) studies have demonstrated Gal receptor mRNA expression in rat adrenal glands (mainly *Galr2* and *Galr3*).<sup>8</sup> Since the HPA axis and adrenal function are closely linked to stress regulation and maintenance of energy homeostasis, it would be interesting to determine whether Galp and/or Ala, like Gal, affect HPA axis gene expression or adrenal function.

## Objectives

The aim of the study was to investigate the expression of *Ala*, *Galp* and their receptors in hypothalamus, pituitary gland and adrenal gland of the HPA axis of the rat after in vivo intraperitoneal (ip.) peptides administration.

## Materials and methods

### Animals, reagents and experimental design

Adult male Wistar rats (final body weight 100–150 g) from the Laboratory Animal Breeding Center, Poznan Science and Technology Park of Adam Mickiewicz University Foundation, Poznań, Poland (the specific-pathogen-free (SPF) category), were used. The total number of animals used was 144 (104 in the acute exposition group and 40 in the prolonged exposition group). This study was carried out in accordance with the recommendations of the Directive 2010/63/EU of the European Parliament and of the Council of 22 September, 2010 on the protection of animals used for scientific purposes, as stated in the Polish law (Act of January 15, 2015 on the Protection of Animals Used for Scientific or Educational Purposes). The study protocol was approved by the Ethics Committee for Animal Studies of the Department of Animal Physiology, Biochemistry and Biostructure, Poznań University of Life Sciences (resolution No. 11/2015). Animals of both experimental groups were maintained in constant, strictly defined conditions, i.e., at a temperature of 22°C ± 2°C and air humidity 55–60%, in a daily cycle of 12 h of light (12-hour continuum)/12 h of dark (12-hour continuum), in a room where the air exchange was at the level of 15 exchanges/h, with free access to standard pellets and tap water. Galp and Ala peptides were obtained from Phoenix Pharmaceuticals, Inc. (cat. No. 026-52 and 026-33, respectively; Phoenix, USA).

In order to determine the effect of both peptides (Galp and Ala) on HPA axis genes expression, 2 experimental *in vivo* models were used: acute and prolonged exposition to peptides. During the surgical operation, both control and experimental groups of animals were under standard ketamine and xylazine anesthesia (100 mg/kg of ketamine *ip.* and 10 mg/kg of xylazine *ip.*). All experiments were performed between 9 AM and 12 AM. All possible efforts have been undertaken to minimize the number of animals and their suffering.

### One-hour and 24-hour exposure to the peptides

The experimental model consisted of *ip.* peptides administration. Animals were initially injected *ip.* daily for 2 weeks with 0.2 mL of 0.9% saline to prepare for the experiment. Next, they were given an *ip.* injection of tested substances and peptides. After the exposition time (1 h – the acute exposition group, or 24 h – the prolonged exposition group), the animals were decapitated. The trunk blood was collected in the presence of ethylenediaminetetraacetic acid (EDTA; 1 mg/mL), and plasma was separated and stored at  $-20^{\circ}\text{C}$  until biochemical assays were performed. Hypothalami, pituitary glands and adrenal glands were collected to an RNAlater (Sigma-Aldrich, St. Louis, USA) and stored in  $-80^{\circ}\text{C}$  for further qRT-PCR analysis.

Each experimental group consisted of 8 animals and there were 13 groups (7 groups in the 1 h experiment and 6 groups in the 24 h experiment, 104 animals in total), as follows: 0,9% NaCl  $\times$  2 (negative control), 60% acetonitrile in water with dimethyl sulfoxide (DMSO)  $\times$  1 (Galp negative control), Galp (1.5 nmol)  $\times$  2, Galp (0.5 nmol)  $\times$  2, Ala (1.5 nmol)  $\times$  2, Ala (0.5 nmol)  $\times$  2, and ACTH ( $10^{-7}$ )  $\times$  2 (adrenocorticotrophic hormone, positive control). Since the Galp peptide was dissolved in 30  $\mu\text{L}$  of 60% acetonitrile in water with DMSO, and it is known that DMSO affects the expression of genes, additional negative control by means of Galp solvent was used.<sup>27</sup> Alarin peptide was dissolved in 0.9% saline. Peptide concentrations were established based on earlier experimental data and the team members' experience.<sup>26,27</sup>

### Two-day exposure to peptides

The experimental model consisted of subcutaneous (*sc.*) mini osmotic pumps (ALZET 2001; Durect Corp., Cupertino, USA). Animals were first administered daily for 2 weeks with a *sc.* injection of 0.2 mL of 0.9% saline to prepare them for the experiment. Next, they underwent a surgical operation during which mini osmotic pumps were inset under the skin of ridge. Pumps were loaded with test substances (Galp and Ala) and control substances (NaCl, DMSO and ACTH) at 0.5 nmol/100 g body weight/0.5  $\mu\text{L}$ . The secretion of examined substances was 2.2 nmol/day. After the exposition time (2 days) animals were decapitated. The trunk blood was collected in the presence of EDTA (1 mg/mL), and plasma was separated and stored at  $-20^{\circ}\text{C}$

until biochemical assays were performed (cf. the ELISA experiments). Hypothalami, pituitary glands and adrenal glands were collected to RNAlater and stored in  $-80^{\circ}\text{C}$  for further qRT-PCR analysis. There were 5 groups with 8 animals in each group. As noted above, since Galp peptide was dissolved in 30  $\mu\text{L}$  of 60% acetonitrile in water with DMSO, additional negative control by means of Galp solvent was used. Alarin peptide was dissolved in 0.9% saline.

### RNA isolation

Total RNA was extracted from the obtained tissue (hypothalami, pituitary glands and adrenal glands) using GeneMATRIX Universal RNA Purification Kit (cat. No. E3598-02; EURx Ltd., Gdańsk, Poland). First, tissues were mechanically shredded with a homogenizer. Then, samples were centrifuged for 3 min at maximum speed (13,000  $\times$  g). The supernatant was collected and 350  $\mu\text{L}$  of 70% of ethanol were added to every sample. The mixture was transferred to pure mini-columns and centrifuged for 1 min at 11,000  $\times$  g. Subsequently, 3 consecutive steps consisted in adding the appropriate rinsing buffer concentration to all samples. Each time, samples were centrifuged for 1 min at 11,000  $\times$  g. In the final stage, the mini-columns were placed in clean tubes and 30  $\mu\text{L}$  of water were added. The amount of total RNA was determined using optical density (OD) at 260 nm, and its purity was estimated by 260/280 nm absorption ratio (higher than 1.8) (NanoDrop Spectrophotometer; Thermo Fisher Scientific, Waltham, USA). Samples were stored at  $-80^{\circ}\text{C}$  for further qRT-PCR analysis.

### Reverse transcription PCR (RT-PCR)

Reverse transcription was performed using Transcriptor High Fidelity cDNA Synthesis Kit (cat. No. 05081963001; Roche, Basel, Switzerland) at  $42^{\circ}\text{C}$  for 60 min (Thermocycler UNO II; Biometra; Analytik Jena GmbH, Jena, Germany). The primers were designed using Primer 3 software (Whitehead Institute for Biomedical Research, Cambridge, USA; Table 1). The primers were purchased from the Laboratory of DNA Sequencing and Oligonucleotide Synthesis, Institute of Biochemistry and Biophysics, Polish Academy of Sciences, Warszawa, Poland.

### qRT-PCR analysis

Expression levels of selected genes (Table 1) were performed by means of qRT-PCR (7900HT Fast Real-Time PCR System; Applied Biosystems, Waltham, USA). Using the primers presented in Table 1, the SYBR-Green detection system was applied according to the specific protocol. Every 25  $\mu\text{L}$  reaction mixture contained: 2  $\mu\text{L}$  of template cDNA, 1  $\mu\text{L}$  of every gene-specific primer (0.3  $\mu\text{M}$ ), 12.5  $\mu\text{L}$  of 2 $\times$  Maxima SYBR Green/ROX qPCR Master mix (Thermo Fisher Scientific), and 8.5  $\mu\text{L}$  of RNase-free water. The qRT-PCR program included: 10-minute initial

**Table 1.** Conventional qRT-PCR analyses of *CRH*. Oligonucleotide sequences for sense (S) and antisense (A) primers are shown. Hypoxanthine phosphorybosyl transferase (*Hprt*) was the reference gene

cDNA	Genbank accession number	Primer	Primer sequence (5'-3')	Position	PCR product size (bp)
<i>CRH</i>	NM_031019.1	S A	GTACCTCGCAGAACAACAGT CTTCACCCATGCGGATCAGA	113–132 340–359	247
<i>POMC</i>	NM_139326.2	S A	TCACCACGGAAAGCAACCTG CATGACGTACTCCGGGGAT	231–250 339–358	128
<i>Ala</i>	NM_022633.1	S A	TGCTCACAGGGGACGAGGA CCGGAACATTCTGTCCAC	200–218 429–447	248
<i>Alarin</i>	NM_022633.1	S A	ACAGTCTCCACCTTTCC CATTGACCTTTTGGTCATCCTTGG	205–233 314–337	133
<i>Galr1</i>	NM_012958.3	S A	TTCATCGGGACAGCAACCA GCCAAATACCACAACGACCA	755–774 974–994	239
<i>Galr2</i>	NM_019172.5	S A	CATCCTGTGCTGCGTGCC CTAGCCCCAGATGAGCCC	251–269 468–487	236
<i>Galr3</i>	NM_019173.1	S A	AGGACTGAGGAAGATGGCTGA ATTGCCACCATGCCCAAC	13–34 112–131	118
<i>Cyp11a1</i>	NM_017286	S A	GATGACCTATTCGGCTTTGC GTTGGCCTGGATGTTCTTG	592–611 930–948	357
<i>Cyp11b1</i>	NM_012537	S A	AGAGTATCTCCCGCATCG GCCAGTCTGCCCATTTAG	311–329 394–412	102
<i>Cyp11b2</i>	NM_012538.2	S A	TGGCAGCACTAATAACTCAGG AAAAGCCACCAACAGGGTAG	875–895 1131–1150	276
<i>Hprt</i>	NM_012583	S A	CAGTCAACGGGGACATAAAAG ATTTGGGGCTGTACTGCTTGA	391–412 515–536	146

qRT-PCR – quantitative real-time polymerase chain reaction; *CRH* – corticotropin-releasing hormone; *POMC* – proopiomelanocortin; *Ala* – alarin; *Galp* – galanin-like peptide; *Galr1* – galanin receptor type 1; *Galr2* – galanin receptor type 2; *Galr3* – galanin receptor type 3; *Cyp11a1* – cholesterol desmolase; *Cyp11b1* – 11 $\beta$ -hydroxylase; *Cyp11b2* – aldosterone synthase.

denaturation step to activate the Taq DNA Polymerase (95°C), followed by a 3-step amplification program: 1) denaturation at 95°C for 15 s; 2) annealing at 60°C for 30 s; and 3) extension at 72°C for 30 s. The specificity of reaction products was checked by determination of melting points (0.1°C/s transition rate).

## ELISA – hormones level detection

Plasma was separated using centrifuge and the blood serum was stored at –20°C for enzyme-linked immunosorbent assay (ELISA) analysis. Galarin, Ala, ACTH, corticosterone, and aldosterone concentration were determined with the ELISA method performed in adherence to specific protocols. Galarin ELISA kit was obtained from MyBioSource, Inc. (Rat Galanin-like peptide (GALP) ELISA Kit, cat. No. MBS7216341; San Diego, USA). Alarin and ACTH ELISA kits were obtained from Phoenix Pharmaceuticals, Inc. (cat. No. EK-026-33 and cat. No. EK-001-21, respectively). Corticosterone and aldosterone ELISA kits were obtained from Demeditec Diagnostics GmbH (cat. No. DEV9922 and cat. No. DE5298, respectively; Kiel, Germany).

## Statistical analyses

Statistical analyses of the data were performed using the Kruskal–Wallis test and Dunn's post hoc test. Data

are presented as medians, 1<sup>st</sup> and 3<sup>rd</sup> quartiles (boxes) and ranges (whiskers – minimum and maximum without outliers).

## Results

### qRT-PCR analysis

The expression analysis of *Galp*, *Ala*, *Galr1*, *Galr2*, and *Galr3*, *CRH*, and proopiomelanocortin genes was performed by means of qRT-PCR. In addition, the expression of *Cyp11a1* (cholesterol desmolase), *Cyp11b1* (11 $\beta$ -hydroxylase) and *Cyp11b2* (aldosterone synthase) as steroidogenic enzymes in the adrenal glands was determined. The qRT-PCR graphs of 3 experiments were presented in Fig. 1–5.

### One-hour, 24-hour and 2-day exposure to the peptides in hypothalamus

Statistically significant changes of genes expression were observed mostly in hypothalamus and pituitary gland after 1 h of exposition to peptides (Fig. 1,3).

In hypothalamus, after both doses of Ala peptide administration, the decrease of expression of mRNA *Galp*, *Ala* and their receptors was noted, compared with control and/or ACTH. Expression changes were visible especially after

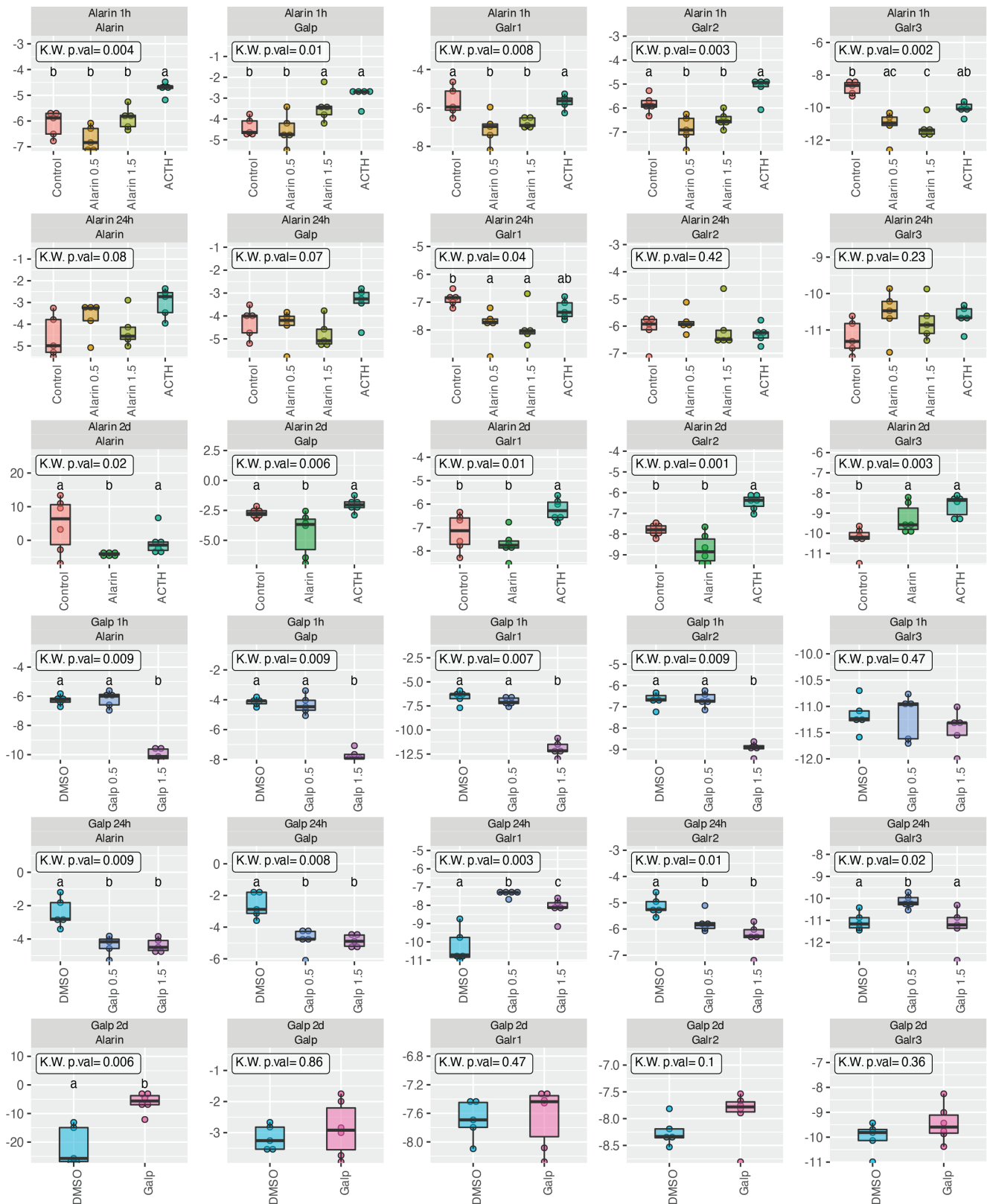


**Fig. 1.** Relative mRNA expression of the galanin-like peptide (*Galp*), alarin (*Ala*) and mRNA receptors in the hypothalamus after the administration of the peptides (*Galp/Ala*, 1 h, 24 h and 2 days). Quantitative real-time polymerase chain reaction (qRT-PCR) was performed to determine the mRNA expression levels. Data points were presented as medians, 1<sup>st</sup> and 3<sup>rd</sup> quartiles (boxes) and ranges (whiskers – minimal and maximal values without outliers). Statistical analysis of the data was performed using the Kruskal–Wallis test and Dunn’s post hoc test. Different letters in the graphs indicate significant differences between specific groups. Outliers were also presented on the graphs. Statistical differences detected with post hoc test were indicated with letters, where different letters correspond to statistical significance ( $p < 0.05$ ) between groups.

ACTH – adrenocorticotrophic hormone; DMSO – dimethyl sulfoxide; Galr – galanin receptor.



**Fig. 2.** Relative mRNA expression of the galanin-like peptide (*Galp*), alarin (*Ala*) and mRNA receptors in the pituitary gland after the administration of the peptides (Galp/Ala, 1 h, 24 h and 2 days). Quantitative real-time polymerase chain reaction (qRT-PCR) was performed to determine the mRNA expression levels. Data points were presented as medians, 1<sup>st</sup> and 3<sup>rd</sup> quartiles (boxes) and ranges (whiskers – minimal and maximal values without outliers). Statistical analysis of the data was performed using the Kruskal–Wallis test and Dunn’s post hoc test. Different letters in the graphs indicate significant differences between specific groups. Outliers were also presented on the graphs. Statistical differences detected with post hoc test were indicated with letters, where different letters correspond to statistical significance ( $p < 0.05$ ) between groups.

ACTH – adrenocorticotrophic hormone; DMSO – dimethyl sulfoxide; Galp – galanin receptor.



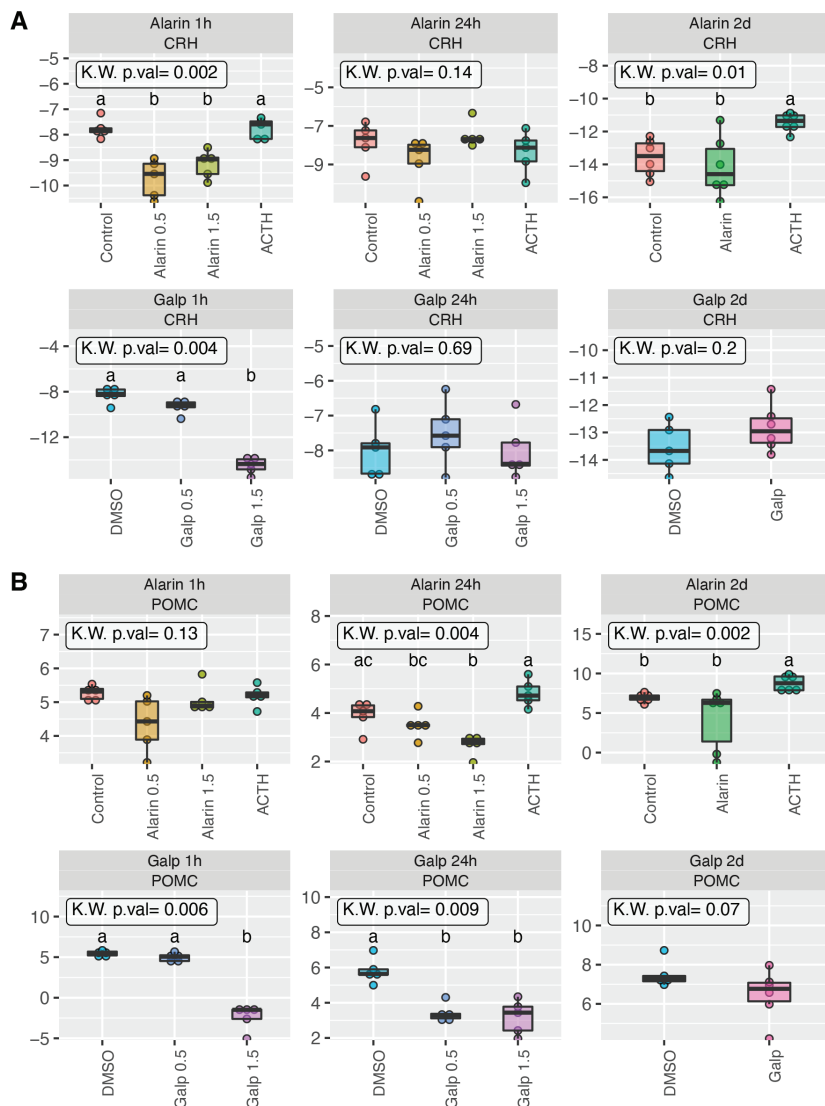


**Fig. 3.** Relative mRNA expression of the corticotropin-releasing hormone (*CRH*) and proopiomelanocortin (*POMC*) mRNAs after the administration of the peptides (galanin-like peptide (*Galp*)/alarin (*Ala*), 1 h, 24 h and 2 days). Quantitative real-time polymerase chain reaction (qRT-PCR) was performed to determine the mRNA expression levels. Data points were presented as medians, 1<sup>st</sup> and 3<sup>rd</sup> quartiles (boxes) and ranges (whiskers – minimal and maximal values without outliers). Statistical analysis of the data was performed using the Kruskal–Wallis test and Dunn’s post hoc test. Different letters in the graphs indicate significant differences between specific groups. Outliers were also presented on the graphs. Statistical differences detected with post hoc test were indicated with letters, where different letters correspond to statistical significance ( $p < 0.05$ ) between groups.

ACTH – adrenocorticotrophic hormone; DMSO – dimethyl sulfoxide.

1 h and 2 days of the peptide administration. However, after 24 h of *Ala* administration, the decrease of expression of *Galr1* mRNA and the increase of expression of *Galr3* mRNA was also noted (Fig. 1).

On the other hand, there was a significant decrease in mRNA expression of *Galp*, *Ala*, *Galr1*, and *Galr2* 1 h after *Galp* 1.5 nmol peptide administration (Fig. 1). In contrast, a decrease in mRNA expression of only *Galp*, *Ala* and *Galr2* was observed after 24 h of *Galp* administration (both doses), whereas *Galr1* and *Galr3* mRNAs showed an increase in their expression.

After 2 days of experiment, there was a statistically significant increase in mRNA expression of *Ala* only (Fig. 1). After ACTH administration, there was an increase in the expression of most of the mRNAs tested, especially 1 h and 2 days after peptide administration compared to control and test peptides groups (Fig. 1). In the hypothalamus, under the influence of both *Ala* and *Galp*, there was also a decrease in *CRH* expression 1 h after the peptide administration (Fig. 2A).

### One-hour, 24-hour and 2-day exposure to the peptides in the pituitary gland

In the pituitary gland, a decrease in the expression of *Galr2* and *Galr3* mRNAs was observed 1 h after the administration of *Ala* peptide at a dose of 1.5 nmol, while at the same time, after the administration of *Galp* at a dose of 1.5 nmol, there was an increase in the expression of all tested mRNAs (Fig. 3).

In contrast, after 24 h of the experiment, a decrease in *Galp* and *Ala* mRNA expression was noted after the administration of *Ala* peptide (both doses), and after the administration of *Galp* peptide (both doses), a decrease in expression of all mRNAs tested was observed.

Two days after the administration of the *Ala* peptide, there was an increase in the expression of *Ala* mRNA only, while 2 days after administration of *Galp* peptide, there was a statistically significant decrease in *Galp* mRNA only (Fig. 3).

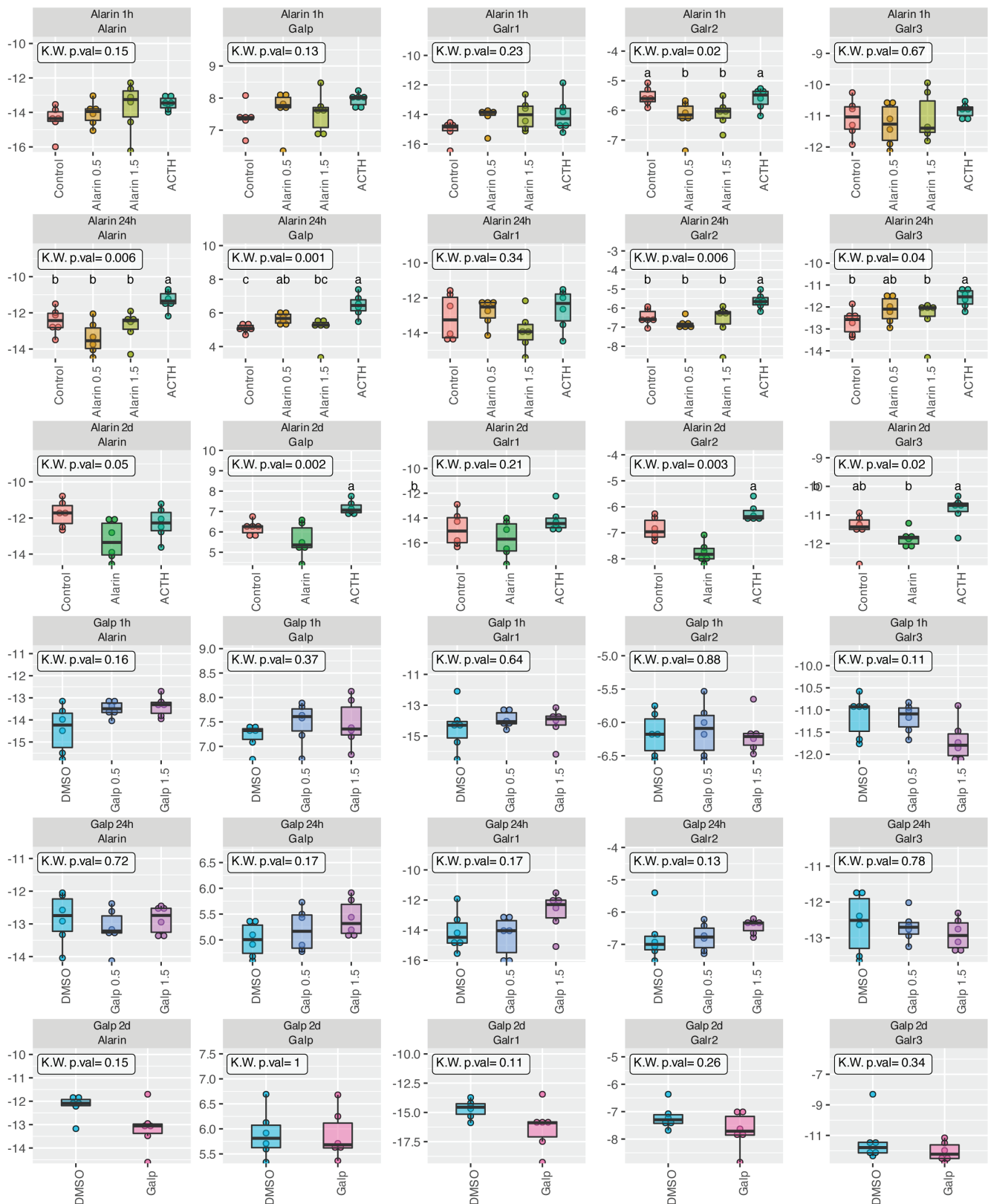


**Fig. 4.** Relative mRNA expression of the galanin-like peptide (*Galp*), alarin (*Ala*) and receptors mRNAs in the adrenal gland after the administration of the peptides (Galp/Ala, 1 h, 24 h and 2 days). Quantitative real-time polymerase chain reaction (qRT-PCR) was performed to determine the mRNA expression levels. Data points were presented as medians, 1<sup>st</sup> and 3<sup>rd</sup> quartiles (boxes) and ranges (whiskers – minimal and maximal values without outliers). Statistical analysis of the data was performed using the Kruskal–Wallis test and Dunn’s post hoc test. Different letters in the graphs indicate significant differences between specific groups. Outliers were also presented on the graphs. Statistical differences detected with post hoc test were indicated with letters, where different letters correspond to statistical significance ( $p < 0.05$ ) between groups.

ACTH – adrenocorticotrophic hormone; DMSO – dimethyl sulfoxide; Galr – galanin receptor.

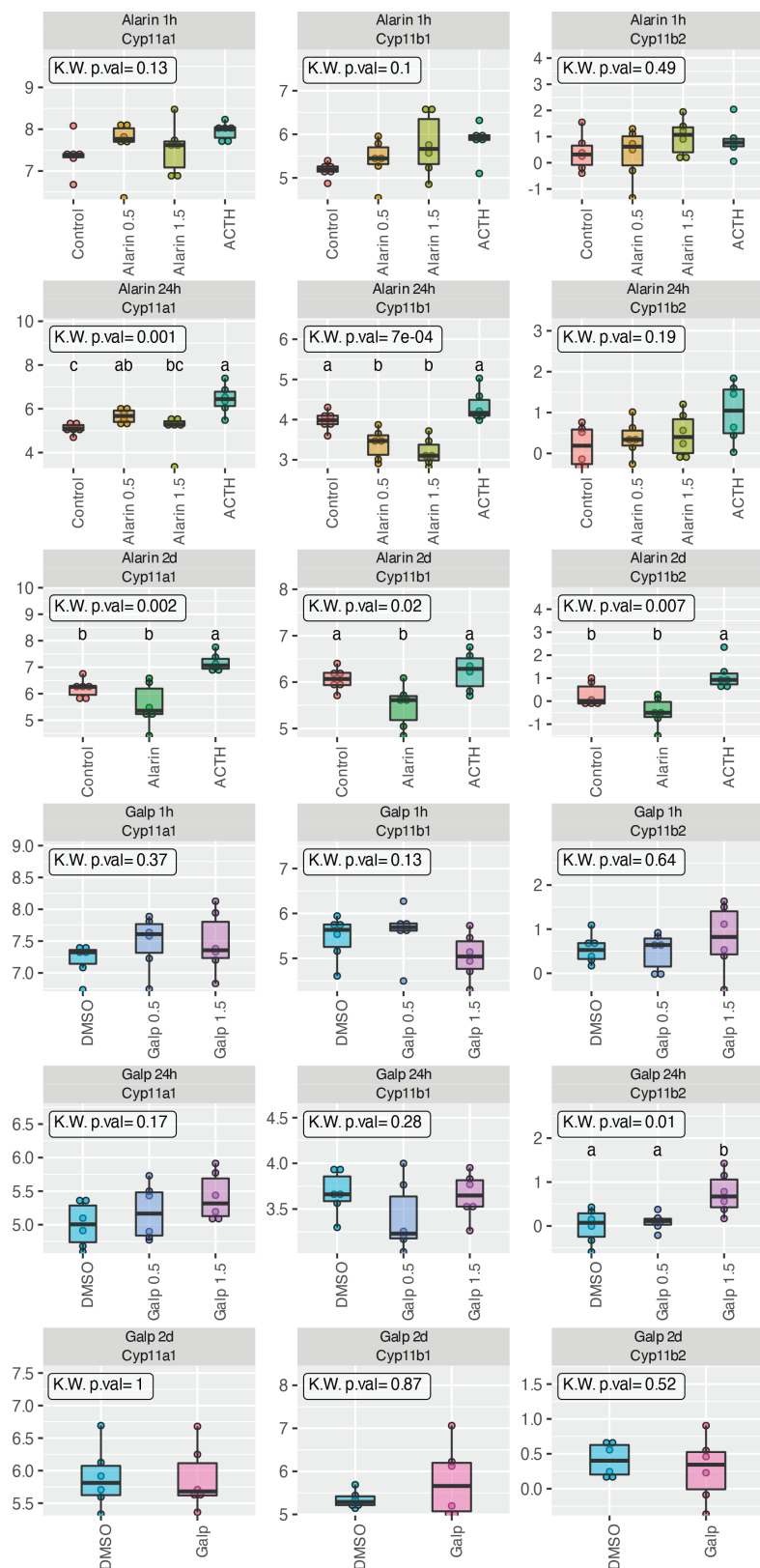


**Fig. 5.** Relative mRNA expression of the *Cyp11a1*, *Cyp11b1* and *Cyp11b2* mRNAs in the adrenal gland after the administration of the peptides (galanin-like peptide (Galp)/alarin (Ala), 1 h, 24 h and 2 days). Quantitative real-time polymerase chain reaction (qRT-PCR) was performed to determine the mRNA expression levels. Data points were presented as medians, 1<sup>st</sup> and 3<sup>rd</sup> quartiles (boxes) and ranges (whiskers – minimal and maximal values without outliers). Statistical analysis of the data was performed using the Kruskal–Wallis test and Dunn’s post hoc test. Different letters in the graphs indicate significant differences between specific groups. Outliers were also presented on the graphs. Statistical differences detected with post hoc test were indicated with letters, where different letters correspond to statistical significance ( $p < 0.05$ ) between groups.

ACTH – adrenocorticotrophic hormone; DMSO – dimethyl sulfoxide; Cyp11a1 – cholesterol desmolase; Cyp11b1 – 11 $\beta$ -hydroxylase; Cyp11b2 – aldosterone synthase.

### One-hour, 24-hour and 2-day exposure to the peptides in the adrenal gland

Changes in single mRNA expression were also noted in the adrenal glands, mainly under the influence of the Ala peptide (Fig. 4). One hour after the administration of the Ala peptide (both doses), a statistically significant decrease in the expression of receptor 2 mRNA was observed, whereas after 24 h, an increase in the expression was noted for *Galp* and *Galr3* mRNA (only under the influence of 0.5 nmol Ala).

A statistically significant decrease in the expression was also noted for *Galr2* and *Galr3* mRNA under the influence of Ala peptide 2 days after its administration.

Slight changes in expression were also noted for *Cyp11a1*, *Cyp11b1* and *Cyp11b2* mRNAs (Fig. 5). Under the influence of Ala peptide, statistically significant expression changes were observed for *Cyp11a1* and *Cyp11b1* mRNAs, visible especially after 24 h and 2 days of the experiment, compared to control and ACTH.

When exposed to Galp peptide (at a dose of 1.5 nmol), there was an increase in the expression of aldosterone synthase mRNA, only 24 h after the peptide administration. No other changes in the expression of the tested steroidogenesis enzymes under the influence of Galp were noted.

### ELISA

After in vivo experiments, blood levels of several hormones were determined: ACTH, corticosterone, aldosterone, and the Galp and Ala peptides themselves. It was

For *POMC* mRNA expression in the pituitary gland, a statistically significant decrease in its expression was noted 1 h after the Galp administration at a 1.5 nmol dose and 24 h after both Ala and Galp peptide administration (both doses) (Fig. 2B).

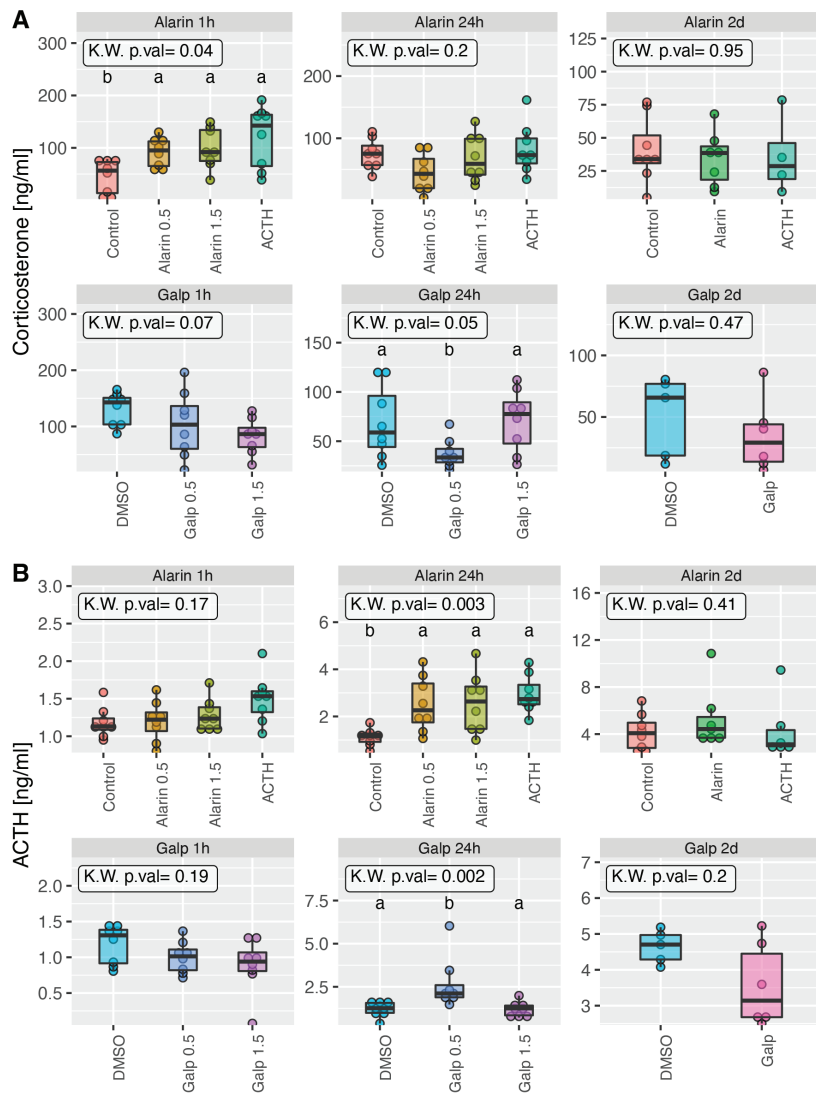


**Fig. 6.** Level of corticosterone and ACTH in blood after peptides administration (galanin-like peptide (Galp)/alarin (Ala), 1 h, 24 h and 2 days). The analysis was performed with enzyme-linked immunosorbent assay (ELISA). Data points were presented as medians, 1<sup>st</sup> and 3<sup>rd</sup> quartiles (boxes) and ranges (whiskers – minimal and maximal values without outliers). Statistical analysis of the data was performed using the Kruskal–Wallis test and Dunn's post hoc test. Different letters in the graphs indicate significant differences between specific groups

ACTH – adrenocorticotropic hormone; DMSO – dimethyl sulfoxide.

found that ip. administration of the Ala peptide at both doses (0.5 nmol and 1.5 nmol) led to a significant increase in blood ACTH concentration 24 h after peptide administration. A significant increase in blood ACTH concentration was also observed 24 h after the administration of Galp peptide at a dose of 0.5 nmol (Fig. 6). There was also a significant increase in blood corticosterone concentration after the administration of Ala peptide, but only 1 h after administration. In contrast, the administration of Galp peptide at 1.5 nmol and 0.5 nmol led to a decrease in corticosterone levels in the blood of rats at 1 h and 24 h after the administration, respectively (Fig. 6).

No effect of peptides on blood levels of either aldosterone, Galp or Ala has been demonstrated (data not shown).

## Discussion

According to the available literature, little is known about the involvement of Galp and Ala in the regulation of adrenocortical hormone secretion and the interaction of HPA axis organs. In rat brain, *Galp* mRNA and protein have been detected in cell bodies located exclusively in the ARC of the hypothalamus and the medial ganglion.<sup>16,28–30</sup> It is well known that galanin, the main peptide of the Gal peptide family, is involved in the control of energy homeostasis. It plays an important role in the regulation of adrenal hormone secretion.<sup>11,12,31</sup> As previously reported, Galp infusion has been shown to stimulate luteinizing hormone (LH) secretion in adult ovariectomized mice given estradiol. This effect was abolished by pretreatment with a gonadotropin-releasing hormone 1 (Gnrh1) antagonist.<sup>32</sup> Furthermore, central administration of Galp increased serum LH levels in male diabetic rats.<sup>33</sup> On the other hand, Boughton et al. found that acute intracerebroventricular (icv.) administration of Ala stimulates food intake and increases circulating LH levels in male rats.<sup>23</sup>

Our study, as well as several others, demonstrated the effects of Galp and Ala peptides on the expression of enzymes involved in steroidogenesis. Both Galp and Ala were shown to affect the expression of HPA axis mRNAs, including *CRH*, *POMC*, cholesterol desmolase, 11 $\beta$ -hydroxylase, and aldosterone synthase. As shown above, *CRH* expression was strongly down-regulated in the hypothalamus after both doses of Ala (0.5 nmol and 1.5 nmol) and Galp (1.5 nmol), especially after 1 h of ip. exposure to the peptides. These results appear to confirm those previously obtained by Wang et al., according to whom icv. administration of 1.0 nmol Ala to the mouse brain resulted in a reduction of *CRH* mRNA levels in the hypothalamus.<sup>34</sup> In this context, the decrease in *POMC* mRNA expression that we noted 24 h after administration of the tested peptides is also significant. The decrease in *POMC* expression coincides with a decrease in mRNA expression of steroidogenesis enzymes in adrenal gland took place mainly under the influence of the Ala and ACTH peptides, especially after 24 h and prolonged exposure to the peptides. It can be observed that both Ala and Galp peptides affect the expression of major HPA mRNAs such as *CRH* and *POMC*, whereas for enzymes, changes in their mRNA expression are primarily

appear to confirm those previously obtained by Wang et al., according to whom icv. administration of 1.0 nmol Ala to the mouse brain resulted in a reduction of *CRH* mRNA levels in the hypothalamus.<sup>34</sup> In this context, the decrease in *POMC* mRNA expression that we noted 24 h after administration of the tested peptides is also significant. The decrease in *POMC* expression coincides with a decrease in mRNA expression of steroidogenesis enzymes in adrenal gland took place mainly under the influence of the Ala and ACTH peptides, especially after 24 h and prolonged exposure to the peptides. It can be observed that both Ala and Galp peptides affect the expression of major HPA mRNAs such as *CRH* and *POMC*, whereas for enzymes, changes in their mRNA expression are primarily

seen under the influence of the Ala peptide, suggesting that it may have a more important function in regulating HPA axis function.

In 2005, Onaka et al. presented evidence that icv. injection of Galp significantly increased plasma ACTH concentrations.<sup>35</sup> Similarly, our results showed an increase in blood ACTH levels after 24-hour ip. administration of Ala (both doses) and Galp (0.5 nmol dose only). In contrast, Wang et al. showed that an icv. injection of 1.0 nmol Ala resulted in a decrease in blood levels of CRH, ACTH and corticosterone.<sup>34</sup> In our experiment, there was an increase in blood corticosterone levels 1 h after exposure to Ala (both doses). However, 24-hour ip. administration of both Ala and Galp reduced plasma corticosterone levels, but the result was significant only with Galp peptide administration. The effect of both Galp and Ala peptide was short-lived, as no changes in blood hormone concentrations were observed after longer (2-day) experiments. Equally important, neither Galp nor Ala caused statistically significant changes in blood aldosterone concentrations.

It would seem interesting to establish whether the peptides studied affect their own expression in HPA organs, and also whether and to what extent they affect the expression of their own receptors, the expression of which is known to have been recorded in all 3 organs of the HPA.<sup>7,8</sup> It has been clearly shown that both peptides influence the mRNA expression of Galp, Ala peptides and their receptors. However, it is primarily the Galp peptide that modulates their expression, especially in the hypothalamus and pituitary gland, where it decreases the expression of the mRNAs studied in a statistically significant manner. In the adrenal glands, where the mRNA expression of these peptides was already at a very low level, the mRNA expression of the Galp–Ala system was mainly influenced by the Ala peptide.

## Limitations of the study

A limitation of the present study is the small size of the experimental groups, but these are standard group sizes in our in vivo animal experiments. Furthermore, the animal analyses were carried out according to the 3R principle (replacement, reduction, refinement) of animal studies to make them more humane. Thus, the present experiments were designed in such a way as to not involve too many animals. The experimental protocol could be strengthened by additional doses of administered peptides, e.g., a dose of 1.0 nmol or 2.0 nmol could be added, or the number of time intervals could be increased to test the effect of the tested peptides additionally after a longer time after injection (2 h or 6 h). However, such changes would also involve increasing the number of experimental animals, which could raise the objections from the local ethics committee.

## Conclusions

There is evidence in the scientific literature for a link between both Galp and Ala peptides in the regulation of food intake, hormone release and control of metabolic processes.<sup>14,19,23–25,31,36–38</sup> However, there is little data on the effects of the studied peptides on the blood levels of adrenal hormones and on the mRNA expression of steroidogenesis enzymes within the organs of the HPA axis, which makes it very difficult to discuss the results of the studies of interest. So far, our results coincide, at least in part, with literature data. Unfortunately, it is hard to find pure relationships between the action of the 2 peptides. However, it seems that the Galp peptide is the one that has a greater effect on mRNA expression of the Galp–Ala system in the hypothalamus and pituitary gland, while the Ala peptide affects mRNA expression of steroidogenesis enzymes in the adrenal glands and hormone levels in the blood. A number of further studies, e.g., adrenal cell culture and an analysis of signaling pathways in adrenocortical cells, are required to determine exactly how the Ala peptide is involved in adrenal gland function.


## Additional data


Additional material showing the exact statistical analysis data has been deposited at <https://zenodo.org/> (<https://doi.org/10.5281/zenodo.6145227>). The calculations are presented in separate files – as appropriate to the figures presented in the manuscript.


We generated the graphs in R, where it turned out that the ggplot2 library inserts minimum and maximum values into the boxplots as whiskers, ignoring the outliers (<https://r-coder.com/boxplot-r/>). A data point considered as outlier is greater than  $Q3 + 1.5 \cdot IQR \cdot IQR$  (right outlier), or is less than  $Q1 - 1.5 \cdot IQR \cdot IQR$  (left outlier), but we still left such points on the graphs.

## ORCID iDs

Marianna Tyczewska  <https://orcid.org/0000-0003-0623-9496>

Marta Szyszka  <https://orcid.org/0000-0003-0150-3665>

Karol Jopek  <https://orcid.org/0000-0002-7399-0303>

Marcin Ruciński  <https://orcid.org/0000-0002-2525-5777>

## References

1. Mazzocchi G, Malendowicz LK, Rebuffat P, Nussdorfer GG. Effects of galanin on the secretory activity of the rat adrenal cortex: In vivo and in vitro studies. *Res Exp Med (Berl)*. 1992;192(6):373–381. doi:10.1007/BF02576294
2. Malendowicz LK, Nussdorfer GG, Nowak KW, Mazzocchi G. The possible involvement of galanin in the modulation of the function of rat pituitary–adrenocortical axis under basal and stressful conditions. *Endocr Res*. 1994;20(3):307–317. doi:10.1080/07435809409035866
3. Ruciński M, Ziółkowska A, Szyszka M, Malendowicz LK. Cerebellin and des-cerebellin exert ACTH-like effects on corticosterone secretion and the intracellular signaling pathway gene expression in cultured rat adrenocortical cells: DNA microarray and QPCR studies. *Int J Mol Med*. 2009;23(4):539–546. doi:10.3892/ijmm\_00000162

4. Jones PM, O'Halloran DJ, Ghatei MA, Domin J, Bloom SR. The influence of adrenal hormone status on neuroendocrine peptides in the rat anterior pituitary gland. *J Endocrinol.* 1990;127(3):437–444. doi:10.1677/joe.0.1270437
5. White BD, Dean RG, Martin RJ. Adrenalectomy decreases neuropeptide Y mRNA levels in the arcuate nucleus. *Brain Res Bull.* 1990;25(5):711–715. doi:10.1016/0361-9230(90)90047-4
6. Neri G, Andreis PG, Nussdorfer GG. Effects of neuropeptide-Y and substance-P on the secretory activity of dispersed zona-glomerulosa cells of rat adrenal gland. *Neuropeptides.* 1990;17(3):121–125. doi:10.1016/0143-4179(90)90074-9
7. Tortorella C, Neri G, Nussdorfer GG. Galanin in the regulation of the hypothalamic–pituitary–adrenal axis (Review). *Int J Mol Med.* 2007;19(4):639–647. doi:10.3892/ijmm.19.4.639
8. Tyczewska M, Milecka P, Szyszka M, et al. Expression profile of Galp, alarin and their receptors in rat adrenal gland. *Adv Clin Exp Med.* 2019;28(6):737–746. doi:10.17219/acem/95039
9. Belloni AS, Malendowicz LK, Ruciński M, Guidolin D, Nussdorfer GG. Galanin stimulates cortisol secretion from human adrenocortical cells through the activation of galanin receptor subtype 1 coupled to the adenylate cyclase-dependent signaling cascade. *Int J Mol Med.* 2007;20(6):859–864. doi:10.3892/ijmm.20.6.859
10. Andreis PG, Malendowicz LK, Rebuffat P, Spinazzi R, Ziólkowska A, Nussdorfer GG. Galanin enhances corticosterone secretion from dispersed rat adrenocortical cells through the activation of GAL-R1 and GAL-R2 receptors coupled to the adenylate cyclase-dependent signaling cascade. *Int J Mol Med.* 2007;19(1):149–155. doi:10.3892/ijmm.19.1.149
11. Lawrence CB, Baudoin FM, Luckman SM. Centrally administered galanin-like peptide modifies food intake in the rat: A comparison with galanin. *J Neuroendocrinol.* 2002;14(11):853–860. doi:10.1046/j.1365-2826.2002.00846.x
12. Leibowitz SF. Regulation and effects of hypothalamic galanin: Relation to dietary fat, alcohol ingestion, circulating lipids and energy homeostasis. *Neuropeptides.* 2005;39(3):327–332. doi:10.1016/j.npep.2004.12.022
13. Ohtaki T, Kumano S, Ishibashi Y, et al. Isolation and cDNA cloning of a novel galanin-like peptide (GALP) from porcine hypothalamus. *J Biol Chem.* 1999;274(52):37041–37045. doi:10.1074/jbc.274.52.37041
14. Lang R, Berger A, Santic R, et al. Pharmacological and functional characterization of galanin-like peptide fragments as potent galanin receptor agonists. *Neuropeptides.* 2005;39(3):179–184. doi:10.1016/j.npep.2004.12.015
15. Juréus A, Cunningham MJ, Li D, et al. Distribution and regulation of galanin-like peptide (GALP) in the hypothalamus of the mouse. *Endocrinology.* 2001;142(12):5140–5144. doi:10.1210/endo.142.12.8542
16. Takatsu Y, Matsumoto H, Ohtaki T, et al. Distribution of galanin-like peptide in the rat brain. *Endocrinology.* 2001;142(4):1626–1634. doi:10.1210/endo.142.4.8089
17. Cunningham MJ, Krasnow SM, Gevers EF, et al. Regulation of galanin-like peptide gene expression by pituitary hormones and their downstream targets. *J Neuroendocrinol.* 2004;16(1):10–18. doi:10.1111/j.1365-2826.2004.01118.x
18. Lawrence C, Fraley GS. Galanin-like peptide (GALP) is a hypothalamic regulator of energy homeostasis and reproduction. *Front Neuroendocrinol.* 2011;32(1):1–9. doi:10.1016/j.yfrne.2010.06.001
19. Kageyama H, Takenoya F, Kita T, Hori T, Guan JL, Shioda S. Galanin-like peptide in the brain: Effects on feeding, energy metabolism and reproduction. *Regul Pept.* 2005;126(1–2):21–26. doi:10.1016/j.regpep.2004.08.029
20. Shiba K, Kageyama H, Takenoya F, Shioda S. Galanin-like peptide and the regulation of feeding behavior and energy metabolism. *FEBS J.* 2010;277(24):5006–5013. doi:10.1111/j.1742-4658.2010.07933.x
21. Lang R, Gundlach AL, Kofler B. The galanin peptide family: Receptor pharmacology, pleiotropic biological actions, and implications in health and disease. *Pharmacol Ther.* 2007;115(2):177–207. doi:10.1016/j.pharmthera.2007.05.009
22. Santic R, Fenninger K, Graf K, et al. Gangliocytes in neuroblastic tumors express alarin, a novel peptide derived by differential splicing of the galanin-like peptide gene. *J Mol Neurosci.* 2006;29(2):145–152. doi:10.1385/JMN:29:2:145
23. Boughton CK, Patterson M, Bewick GA, et al. Alarin stimulates food intake and gonadotrophin release in male rats. *Br J Pharmacol.* 2010;161(3):601–613. doi:10.1111/j.1476-5381.2010.00893.x
24. Van Der Kolk N, Madison FN, Mohr M, Eberhard N, Kofler B, Fraley GS. Alarin stimulates food intake in male rats and LH secretion in castrated male rats. *Neuropeptides.* 2010;44(4):333–340. doi:10.1016/j.npep.2010.04.001
25. Mikó A, Füredi N, Tenk J, et al. Acute central effects of alarin on the regulation on energy homeostasis. *Neuropeptides.* 2017;64:117–122. doi:10.1016/j.npep.2016.09.001
26. Jopek K, Tyczewska M, Ramanjaneya M, et al. Effect of ACTH and hCG on the expression of gonadotropin-inducible ovarian transcription factor 1 (*Giot1*) gene in the rat adrenal gland. *Int J Mol Sci.* 2018;19(8):2285. doi:10.3390/ijms19082285
27. Ruciński M, Trejter M, Ziólkowska A, Tyczewska M, Malendowicz LK. Ghrelin and obestatin inhibit enucleation-induced adrenocortical proliferation in the rat. *Int J Mol Med.* 2010;25(5):793–800. doi:10.3892/ijmm\_00000406
28. Juréus A, Cunningham MJ, McClain ME, Clifton DK, Steiner RA. Galanin-like peptide (GALP) is a target for regulation by leptin in the hypothalamus of the rat. *Endocrinology.* 2000;141(7):2703–2706. doi:10.1210/endo.141.7.7669
29. Kerr NC, Holmes FE, Wynick D. Galanin-like peptide (GALP) is expressed in rat hypothalamus and pituitary, but not in DRG. *Neuroreport.* 2000;11(17):3909–3913. doi:10.1097/00001756-200011270-00060
30. Larm JA, Gundlach AL. Galanin-like peptide (GALP) mRNA expression is restricted to arcuate nucleus of hypothalamus in adult male rat brain. *Neuroendocrinology.* 2000;72(2):67–71. doi:10.1159/000054573
31. Man PS, Lawrence CB. The effects of galanin-like peptide on energy balance, body temperature and brain activity in the mouse and rat are independent of the GALR2/3 receptor. *J Neuroendocrinology.* 2008;20(1):128–137. doi:10.1111/j.1365-2826.2007.01625.x
32. Kauffmann AS, Buenzle J, Fraley GS, Rissman EF. Effects of galanin-like peptide (GALP) on locomotion, reproduction and body weight in female and male mice. *Horm Behav.* 2005;48(2):141–151. doi:10.1016/j.jybeh.2005.01.010
33. Stoyanovitch AG, Johnson MA, Clifton DK, Steiner RA, Fraley GS. Galanin-like peptide rescues reproductive function in the diabetic rat. *Diabetes.* 2005;54(8):2471–2476. doi:10.2337/diabetes.54.8.2471
34. Wang M, Chen Q, Li M, et al. Alarin-induced antidepressant-like effects and their relationship with hypothalamus–pituitary–adrenal axis activity and brain derived neurotrophic factor levels in mice. *Peptides.* 2014;56:163–172. doi:10.1016/j.peptides.2014.04.009
35. Onaka T, Kuramochi M, Saito J, Ueta Y, Yada T. Galanin-like peptide stimulates vasopressin, oxytocin and adrenocorticotrophic hormone release in rats. *Neuroreport.* 2005;16(3):243–247. doi:10.1097/00001756-200502280-00008
36. Crown A, Clifton DK, Steiner RA. Neuropeptide signaling in the integration of metabolism and reproduction. *Neuroendocrinology.* 2007;86(3):175–182. doi:10.1159/000109095
37. Gundlach AL. Galanin/GALP and galanin receptors: Role in central control of feeding, body weight/obesity and reproduction? *Eur J Pharmacol.* 2002;440(2–3):255–268. doi:10.1016/s0014-2999(02)01433-4
38. Lawrence CB. Galanin-like peptide modulates energy balance by affecting inflammatory mediators? *Physiol Behav.* 2009;97(5):515–519. doi:10.1016/j.physbeh.2009.02.041

# MicroRNA-139-5p negatively regulates NME1 expression in hepatocellular carcinoma cells

Jun Yang<sup>1,B,C,E,F</sup>, De Zhi Li<sup>2,B,D,F</sup>, Yu Pang<sup>3,B,D,F</sup>, Tao Zhou<sup>2,B,D,F</sup>, Jia Sun<sup>2,4,B,D,F</sup>, Xian Yi Cheng<sup>3,B,D,F</sup>, Wei V. Zheng<sup>2,A,E,F</sup>

<sup>1</sup> Department of Radiology, Peking University Shenzhen Hospital, China

<sup>2</sup> Intervention and Cell Therapy Center, Peking University Shenzhen Hospital, China

<sup>3</sup> Department of Minimally Invasive Intervention, Peking University Shenzhen Hospital, China

<sup>4</sup> Shenzhen Beike Biotechnology Research Institute, China

A – research concept and design; B – collection and/or assembly of data; C – data analysis and interpretation;

D – writing the article; E – critical revision of the article; F – final approval of the article

Advances in Clinical and Experimental Medicine, ISSN 1899–5276 (print), ISSN 2451–2680 (online)

*Adv Clin Exp Med.* 2022;31(6):655–670

## Address for correspondence

Wei V. Zheng

E-mail: zhengw2013@yeah.net

## Funding sources

This work was supported by grants from the Sanming Project of Medicine in Shenzhen (grant No. SZSM201612071), the Cell Technology Center and Transformation Base, Innovation Center of Guangdong-Hong Kong-Macao Greater Bay Area, Ministry of Science and Technology of China (grant No. YCZYPT [2018]03-1), and Shenzhen Key Discipline of Stem Cell Clinical Research, the Key Medical Disciplines Construction Funding in Shenzhen (grant No. SZXK078).

## Conflict of interest

None declared

Received on November 16, 2021

Reviewed on January 20, 2022

Accepted on February 10, 2022

Published online on April 19, 2022

## Cite as

Yang J, Li DZ, Pang Y, et al. MicroRNA-139-5p negatively regulates NME1 expression in hepatocellular carcinoma cells.

*Adv Clin Exp Med.* 2022;31(6):655–670.

doi:10.17219/acem/146579

## DOI

10.17219/acem/146579

## Copyright

Copyright by Author(s)

This is an article distributed under the terms of the Creative Commons Attribution 3.0 Unported (CC BY 3.0)

(<https://creativecommons.org/licenses/by/3.0/>)

## Abstract

**Background.** High expression of NME1 is associated with hepatocellular carcinoma (HCC) progression and poor prognosis. However, there are few reports on the association between NME1 and microRNAs (miRNAs) in HCC progression.

**Objectives.** To explore miRNAs that regulate NME1 expression in HCC.

**Materials and methods.** Data from the Cancer Genome Atlas (TCGA), Human Protein Atlas (HPA), TargetScan, starBase, and mirDIP were used to analyze the expression pattern of NME1 in HCC tissues, the relationship between NME1 level and the progression of HCC or patient prognosis, miRNAs targeting NME1, and the biological processes that may be regulated by NME1. The regulation of miRNAs to NME1 was assessed using the dual-luciferase reporter assay, quantitative reverse transcription polymerase chain reaction (qRT-PCR) and western blotting. The cell cycle and cell proliferation were detected using propidium iodide (PI) staining and EdU assay, respectively.

**Results.** Highly expressed NME1 in HCC was associated with HCC progression and prognosis. The miR-139-5p and miR-335-5p were weakly expressed in HCC samples and negatively correlated with NME1. The down-regulation of miR-139-5p in HCC patients resulted in worse overall survival (OS) and disease-free interval (DFI); however, the level of miR-335-5p was not significantly correlated with OS and DFI in patients with HCC. In vitro experiments verified that the level of miR-139-5p was lower and NME1 expression was higher in HCC cell lines compared to L-02. Moreover, miR-139-5p negatively regulates the expression of NME1 in HCC cell lines. The NME1 may regulate cell cycle, DNA replication, oxidative phosphorylation, and the pentose phosphate pathway. The miR-139-5p inhibited cell proliferation by negatively regulating NME1 expression.

**Conclusions.** The upregulation of NME1 in HCC indicates a poor prognosis. The NME1 is negatively regulated by miR-139-5p to inhibit cell proliferation.

**Key words:** microRNA, hepatocellular carcinoma, bioinformatics analysis, NME1

## Background

Hepatocellular carcinoma (HCC) has become the second deadliest cancer-related factor globally.<sup>1</sup> The occurrence of liver cancer depends on the complex interaction between genetic susceptibility factors, environmental factors, carcinogens, and viral exposure.<sup>2</sup> Importantly, recent studies suggest that some single nucleotide polymorphisms (SNPs) are associated with HCC development and clinical outcomes.<sup>3,4</sup>

The *NME1*, also known as *NDPK-A* and *NM23-H1*, is located on chromosome 17q21.<sup>5,6</sup> The *NME1* contains an arginine–glycine–asparagine (RGD) sequence, which is a ligand that exists in a variety of adhesive protein molecules that specifically bind to integrin receptors, participate in the polymerization of cytoskeleton protein microfilaments, and maintain cell stability and directional cell migration.<sup>7–9</sup> Moreover, *NME1* functions as a histidine kinase, nucleoside-diphosphate kinase and 3'-5' exonuclease, and plays an essential role in cellular proliferation, embryonic development, differentiation, and transcriptional regulation.<sup>7,10,11</sup> The expression of the *NME1* mRNA is reduced in cells with high metastatic ability.<sup>4</sup> Many reports have demonstrated that *NME1* plays an essential role in the growth and metastasis of various cancers such as breast cancer, non-small cell lung cancer and ovarian cancer.<sup>4,12–14</sup>

MicroRNAs (miRNAs) are common noncoding small molecular RNAs. The miRNAs bind to the 3' untranslated region (UTR) of targeting mRNAs to regulate the translation and degradation of mRNAs, thus participating in gene expression, ontogenesis and disease occurrence.<sup>8,15,16</sup> In breast cancer cells, *NME1* is regulated by miR-146a and it promotes cell growth and invasion.<sup>8</sup> In colorectal cancer cells, increased miR-28-3p downregulates the level of *NME1*, inhibiting cell growth and metastasis.<sup>17</sup> Furthermore, 1 study showed that the upregulated *NME1* in HCC tissues contribute to the advancing progression and poor prognosis of patients with HCC.<sup>18</sup> However, there are few studies about the regulation of miRNA on *NME1* in HCC.

## Objectives

In this study, we aimed to investigate the relationship between miRNAs and *NME1*, and uncover the effect of miRNAs/*NME1* axis on the progression of HCC.

## Materials and methods

### Data from the Cancer Genome Atlas database

The mRNA-seq, miRNA-seq and clinical data of Cancer Genome Atlas-Liver Hepatocellular Carcinoma (TCGA-LIHC) were obtained from the University of California,

Santa Cruz (UCSC) Xena website (<https://tcga.xenahubs.net>) and Genomic Data Commons (GDC) website (<https://portal.gdc.cancer.gov/>). The data contained 369 samples of HCC tissues and 50 samples of adjacent normal tissues. Out of the 369 HCC samples, 339 with follow-up information were included in the discovery dataset. With respect to the HCC stage, 170 out of 339 samples were in stage I, 84 out of 339 were in stage II, 81 out of 339 were in stage III, and 4 out of 339 were in stage IV (Table 1).

### Data from the Human Protein Atlas database

To compare the difference in protein levels of *NME1* between normal liver tissues and HCC tissues, we obtained data on immunohistochemistry (IHC) staining that detected *NME1*, from the Human Protein Atlas (HPA) database (<https://www.proteinatlas.org/>). According to the previous description,<sup>19</sup> the protein expression score was defined as not detected for samples with <25% stained cells and negative or weak staining intensity; the protein expression score was defined as low for samples with 25–75% stained cells and weak staining intensity, or with <25% stained cells and moderate staining intensity; the protein expression score was defined as medium for samples with 25–75% stained cells or >75% stained cells and moderate staining intensity, or with <25% stained cells and intense staining; the protein expression score was defined as high for samples with 25–75% or >75% stained cells and strong staining intensity.

### Prediction of miRNAs targeting NME1

We used TargetHumanScan ([http://www.targetscan.org/vert\\_80/](http://www.targetscan.org/vert_80/)), starBase (<https://starbase.sysu.edu.cn/>) and mirDIP (<http://ophid.utoronto.ca/mirDIP/>) databases to screen the miRNAs targeting *NME1*. The miRNAs downregulated (log<sub>2</sub> multiple change <0) in TCGA-LIHC were also screened out. Based on the aforementioned screening, the Venn diagram was drawn, using TBtools v. 1.082 (<https://github.com/CJ-Chen/TBtools/releases>). Two miRNAs at the intersection of the Venn diagram were used for further study.

### Cell culture

The L-02 cells are normal hepatocytes. The Hep3B cells are HCC cells and contain an integrated hepatitis B virus (HBV) genome. The Huh-7 is derived from liver tissue from a Japanese man with highly differentiated HCC and does not contain the HBV genome. The HepG2 is derived from the hepatic tissue of a 15-year-old American male who has hepatoblastoma, and does not contain HBV genome. The Hep3B, Huh7 and HepG2 are representatives of HCC and carry high-risk metastatic property. The SMMC-7721 is derived from a Chinese man. The L-02, Hep3B, HepG2,



**Table 1.** Correlation between clinicopathological variables and NME1 mRNA expression level in hepatocellular carcinoma (HCC)

Variables	NME1 expression			p-value <sup>a</sup>
	total	high	low	
	(n = 339)	(n = 105)	(n = 234)	
Age [years]				
<65	208 (61.4%)	68 (64.8%)	140 (59.8%)	0.458
≥65	131 (38.6%)	37 (35.2%)	94 (40.2%)	
Gender				
Male	231 (68.1%)	79 (75.2%)	152 (65.0%)	0.0797
Female	108 (31.9%)	26 (24.8%)	82 (35.0%)	
Family history of cancer				
No	196 (57.8%)	67 (63.8%)	129 (55.1%)	0.301
Yes	98 (28.9%)	25 (23.8%)	73 (31.2%)	
Unknown	45 (13.3%)	13 (12.4%)	32 (13.7%)	
TNM stage				
I	170 (50.1%)	43 (41.0%)	127 (54.3%)	0.138
II	84 (24.8%)	30 (28.6%)	54 (23.1%)	
III	81 (23.9%)	30 (28.6%)	51 (21.8%)	
IV	4 (1.2%)	2 (1.9%)	2 (0.9%)	
Histologic grade				
G1–G2	212 (62.5%)	56 (53.3%)	156 (66.7%)	<b>0.0315</b>
G3–G4	125 (36.9%)	49 (46.7%)	76 (32.5%)	
Unknown	2 (0.6%)	0 (0%)	2 (0.9%)	
Ishak score				
0–4	124 (36.6%)	42 (40.0%)	82 (35.0%)	0.237
5–6	74 (21.8%)	17 (16.2%)	57 (24.4%)	
Unknown	141 (41.6%)	46 (43.8%)	95 (40.6%)	
Child–Pugh grade				
A	207 (61.1%)	71 (67.6%)	136 (58.1%)	0.247
B–C	21 (6.2%)	5 (4.8%)	16 (6.8%)	
Unknown	111 (32.7%)	29 (27.6%)	82 (35.0%)	
Vascular invasion				
None	193 (56.9%)	49 (46.7%)	144 (61.5%)	<b>0.0166</b>
Micro	84 (24.8%)	27 (25.7%)	57 (24.4%)	
Macro	14 (4.1%)	6 (5.7%)	8 (3.4%)	
Unknown	48 (14.2%)	23 (21.9%)	25 (10.7%)	
Alpha fetoprotein				
Negative	143 (42.2%)	40 (38.1%)	103 (44.0%)	0.593
Positive	120 (35.4%)	40 (38.1%)	80 (34.2%)	
Unknown	76 (22.4%)	25 (23.8%)	51 (21.8%)	
Residual tumor				
R0	301 (88.8%)	93 (88.6%)	208 (88.9%)	0.656
R1–R2	12 (3.5%)	5 (4.8%)	7 (3.0%)	
Unknown	26 (7.7%)	7 (6.7%)	19 (8.1%)	
Living status				
Alive	224 (66.1%)	59 (56.2%)	165 (70.5%)	<b>0.0142</b>
Dead	115 (33.9%)	46 (43.8%)	69 (29.5%)	
Disease status				
No	163 (48.1%)	45 (42.9%)	118 (50.4%)	0.405
Yes	132 (38.9%)	46 (43.8%)	86 (36.8%)	
Unknown	44 (13.0%)	14 (13.3%)	30 (12.8%)	

<sup>a</sup>  $\chi^2$  test. Values in bold are statistically significant.

SMMC-7721, and Huh7 (cat. No. IM-H289, IM-H367, IM-H038, IM-H047, and IM-H040, respectively; Immocell, Xiamen, China) were maintained in Dulbecco's modified Eagle medium (DMEM; cat. No. D0819; Sigma-Aldrich, St. Louis, USA) with 10% fetal bovine serum (FBS; cat. No. 12483020; Gibco, Detroit, USA), 100 U/mL penicillin, and 100 U/mL streptomycin (cat. No. 15070063; Gibco) at 37°C.

## Plasmids and mimic

The 3' UTR of *NME1* gene was amplified from genomic DNA of Hep3B cells using polymerase chain reaction (PCR). The primers were shown in Table 2. The *NME1* 3' UTR fragment was cloned into the pmirGLO Vector (Antihela, Xiamen, China) downstream to the firefly luciferase reporter gene. Mutant *NME1* 3' UTR (3' UTR MUT) was

generated from the wide-type *NME1* 3' UTR (3' UTR WT) using the Mut Express II Fast Mutagenesis Kit V2 (cat. No. C214-1; Vazyme, Nanjing, China).

The plv-CMV-mcs-PGK-puro vector (Antihela) was used to overexpress NME1, named NME1 OE plasmid. The blank vector was used as a negative control. The primers for the construction of NME1 OE plasmid were shown in Table 2.

The mimic NC (ID: miR1N0000001-1-5), miR-139-5p mimic (ID: miR10000250-1-5), inhibitor NC (miR2N0000001-1-5), and miR-139-5p inhibitor (ID: miR20000250-1-5), whose sequences are shown in Table 3, were purchased from RiboBio (Guangzhou, China).

### Dual-luciferase reporter assay

The Hep3B and Huh7 cells ( $3 \times 10^5$ /well) were seeded into the 24-well plates. Twelve hours later, the cells were co-transfected with 200 pmol/well mimic NC or miR-139-5p mimic, and 1 µg/well 3' UTR WT or MUT plasmid using Lipofectamine 2000 (cat. No. 11668027; Invitrogen, Carlsbad, USA). After a 24-hour transfection, the luciferase activities of Hep3B and Huh7 cells were detected using The Dual-Luciferase<sup>®</sup> Reporter Assays System (cat. No. E1910; Promega, Madison, USA). The firefly luciferase activities were calibrated to Renilla luciferase activities. Each detection was performed in triplicate.

### Transfection

The Hep3B and Huh7 cells ( $2 \times 10^6$ /well) were seeded into the 6-well plates. Twelve hours later, 800 pmol/well miR-139-5p mimic, miR-139-5p inhibitor or corresponding negative control was co-transfected into Hep3B and Huh7 cells with or without 4 µg of Vector or NME1 OE plasmid using Lipofectamine 2000. After the incubation for 24–48 h, Hep3B and Huh7 cells were harvested and

subjected to the analyses of quantitative reverse transcription polymerase chain reaction (qRT-PCR), western blotting, cell cycle, and cell proliferation.

### qRT-PCR

After treatment, the total RNA was extracted from Huh7 and Hep3B cells using Total RNA Extraction Reagent (cat. No. R401-01; Vazyme, Nanjing, China.). The cDNA of NEM1 was synthesized from 1 µg of total RNA using HiScript II One Step RT-PCR Kit (cat. No. P611-01; Vazyme). The transcription reaction of miR-139-5p was performed using 1 µg of total RNA with the miRNA 1st Strand cDNA Synthesis Kit (cat. No. MR101-01; Vazyme). The qPCR was performed using an iQ5 real-time PCR detection system (Bio-Rad Laboratories, Hercules, USA) with a ChamQ Universal SYBR<sup>®</sup> qPCR Master Mix kit (cat. No. Q311-02, Vazyme). The thermocycling conditions were: 96°C for 5 min, followed by 42 cycles at 96°C for 25 s, 58°C for 30 s and 72°C for 25 s. Expression levels were measured using the  $2^{-\Delta\Delta Ct}$  method and normalized to those of U6 or 18s rRNA. The primers for reverse transcription and qPCR are shown in Table 4.

### Western blotting

After treatment, the total protein was extracted from Huh7 and Hep3B cells using RIPA lysis solution. Subsequently, the BCA protein concentration determination kit (cat. No. P0012S; Beyotime, Shanghai, China) was used to quantify total protein. Samples (12 µg/lane) were loaded for electrophoresis on 10% denaturing sodium dodecyl sulfate-polyacrylamide gel electrophoresis (SDS-PAGE) gels. Western blotting was performed as previously described.<sup>20</sup> The following primary antibodies were used: anti-NME1 (cat. No. 11086-2-AP, 1:500; Proteintech, Wuhan, China) and anti-GAPDH (cat. No. 10494-1-AP, 1:5000;

Table 2. The primers for plasmid construction

Name	Sequence 5'-3'
3' UTR WT-F	GCTCGCTAGCCTCGAGCTGTAGGAAATCTAGTTATTTACAG
3' UTR WT-R	ATGCCTGCAGGTCGACTGTATGTGAGACCTCAAATAAATC
3' UTR MUT-F	GCTCGCTAGCCTCGAGGAAATCTAGTTATTACAGGAACCTC
NME1-F	GCGTGCGGCTGCCACCATGGCCAACCTGTGAGCGTAC
NME1-R	TCTAGGGATCCGGGCCCTCATTATCATAGATCCAGTTC

F – forward primer; R – reverse primer; UTR – untranslated region; 3' UTR WT – wide-type *NME1* 3' UTR; 3' UTR MUT – mutant *NME1* 3' UTR.

Table 3. The sequences of miR-139-5p mimic and inhibitor

Name	Sequence 5'-3'
mimic NC	UCUACAGUGCACGUGUCUCCAGU
miR-139-5p mimic	UCUACAGUGCACGUGUCUCCAGU
inhibitor NC	CAGUACUUUUGUGUAGUACAA
miR-139-5p inhibitor	ACUGGAGACACGUGCACUGUAGA

**Table 4.** The primers for quantitative reverse transcription polymerase chain reaction (qRT-PCR)

Name	Sequence 5'-3'
miR-139-5p RT	GTCGTATCCAGTGCAGGGTCCGAGGTATTCGCACTGGATACGACACTGGA
miR-139-5p-QF	CGCGTCTACAGTGCACGTGTC
miR-139-5p-QR	AGTGCAGGGTCCGAGGTATT
U6-QF	CTCGCTTCGGCAGCACA
U6-QR	AACGCTTCACGAATTTGCGT
NME1-QF	ACCATCCGTGGAGACTTCTGCA
NME1-QR	ACCAGTTCCTCAGGGTGAACC
18s rRNA-QF	ACCCGTTGAACCCATTCGTGA
18s rRNA-QR	GCCTCACTAAACCATCCAATCGG

QF – forward primer for (qRT-PCR); QR – reverse primer for qRT-PCR; RT – reverse transcription.

Proteintech). The secondary antibody was horseradish peroxidase (HRP)-conjugated goat anti-rabbit IgG (cat. No. SA00001-2, 1:2000; Proteintech). The quantification by densitometry was performed using ImageJ 1.52v (National Institutes of Health, Bethesda, USA). The *GAPDH* was used as an internal control.

## Cell cycle assay

After transfection for 48 h, Huh7 and Hep3B cells were fixed using 70% ethanol at  $-20^{\circ}\text{C}$  for 6 h. The fixed cells were then treated with 0.5% Triton X-100 and 15  $\mu\text{g}/\text{mL}$  RNase at  $37^{\circ}\text{C}$  for 30 min. Subsequently, the fixed cells were stained with 15  $\mu\text{g}/\text{mL}$  propidium iodide (PI) at  $28^{\circ}\text{C}$  for 30 min. After staining, the cells were subjected to a flow cytometer NovoCyte 1300 (ACEA Biosciences Inc., Hangzhou, China) for analysis.

## Cell proliferation assay

After a 24-hour transfection, Huh7 and Hep3B cells were seeded in wells of 96-well plates. Twenty-four hours later, the proliferation of cells was detected using Cell-Light EdU Apollo 488 In Vitro Kit (cat. No. C10310-3; RiboBio) according to the manufacturer's instructions. The nucleus was stained using 10  $\mu\text{g}/\text{mL}$  4',6-diamidino-2-phenylindole (cat. No. C1002, DAPI; Beyotime). Images were photographed using a fluorescent microscope (MOTIC, Hong Kong, China). The ImageJ software was used to count cell number.

## Statistical analyses

The edgeR package v. 3.30.3 (<http://www.bioconductor.org/packages/release/bioc/html/edgeR.html>) in R was used to: analyze the divergent levels of NME1 mRNA, miR-335-5p and miR-139-5p between normal liver tissues and HCC tissues; and analyze the correlation of NME1 mRNA level with clinicopathological variables, miR-335-5p level and miR-139-5p level. Receiver operating characteristic (ROC) curve was used to judge the diagnostic value

of NME1 in HCC, and the area under the curve (AUC) was calculated using ROCR package v. 1.0-11 (<http://ipatys.github.io/ROCR/>). The Kaplan–Meier survival curves were plotted using the R survival package v. 3.1-12 (<https://github.com/therneau/survival>). Gene set enrichment analysis (GSEA) was executed using GSEA software v. 4.0.0 (<http://www.gsea-msigdb.org/>). The proportionality of hazard function was checked based on the Schoenfeld residuals. The IBM SPSS software v. 21.0. (IBM Corp., Armonk, USA) was used to perform statistical analysis of our experimental data. Data are presented as mean  $\pm$  standard deviation (SD). The Shapiro–Wilk test was performed to determine whether the data follow a normal distribution. The Levene's test was used to ensure the homogeneity of variance. The Mann–Whitney test was performed to compare the difference between the 2 groups of non-parametric data. The Kruskal–Wallis one-way analysis of variance (ANOVA) followed by Dunn's multiple comparison test were used for 3 or more groups of nonparametric data. The survival curves were calculated using the Kaplan–Meier method, and the significance was determined using the log-rank test. The Student's t-test was performed to compare the difference between 2 groups of parametric data. The ANOVA followed by the Tukey's post hoc test was used for multiple comparisons among 3 or more groups of parametric data. The value of  $p < 0.0500$  was considered statistically significant.

## Results

### NME1 is highly expressed in HCC tissues

Gene Expression Profiling Interactive Analysis (GEPIA) was used to review the mRNA levels of NME1 in different carcinomas and corresponding normal tissues adjacent to cancer. In most healthy organs of the human body, the mRNA level of NME1 was particularly low (Fig. 1A). The NME1 mRNA levels in HCC tissues ( $n = 369$ ) from TCGA were significantly higher than those in the healthy liver ( $n = 50$ ) (Fig. 1B,  $p < 0.0001$ ). The ROC curve also

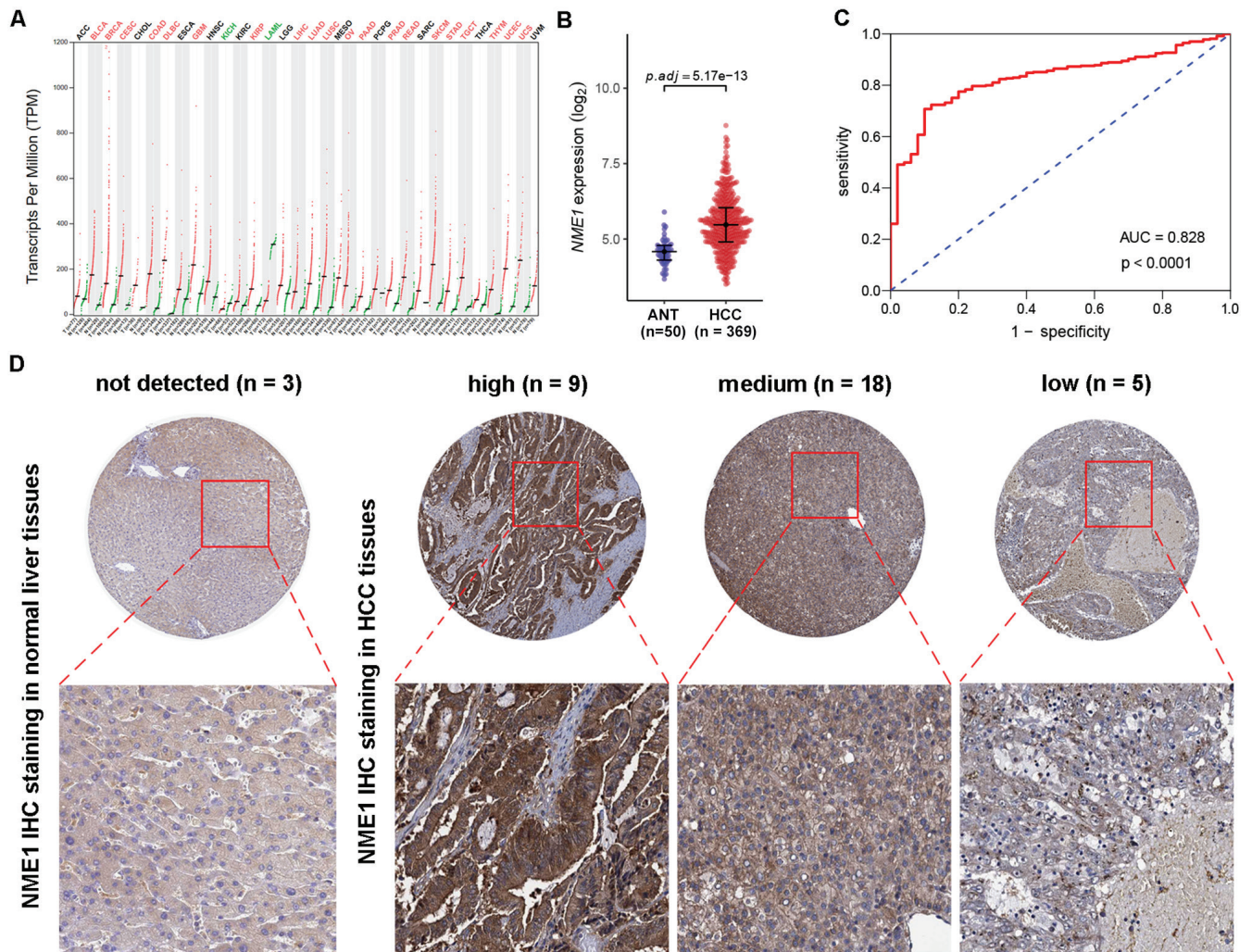


**Fig. 1.** The expression of NME1 is upregulated in hepatocellular carcinoma (HCC). **A.** mRNA levels of NME1 in different tumor tissues and normal tissues (ANT) from Gene Expression Profiling Interactive Analysis (GEPIA); **B.** The difference of NME1 mRNA level between HCC tissues ( $n = 369$ ) and ANT ( $n = 50$ ) from the Cancer Genome Atlas (TCGA); **C.** The receiver operating characteristic (ROC) curve was used to verify the diagnostic value of NME1 upregulation for HCC; **D.** Immunohistochemistry images of NME1 in normal liver tissues and HCC tissues from Human Protein Atlas (HPA). The Mann–Whitney test was used to analyze the data (A,B)

AUC – area under the curve; IHC – immunohistochemistry.

confirmed that elevated NME1 was valuable for the diagnosis of HCC (Fig. 1C,  $AUC = 0.828$ ,  $p < 0.0001$ ). Moreover, immunohistochemical staining data from the HPA database were downloaded to study the protein level of NME1 in HCC tissues and normal liver tissues. The NME1 staining was the weakest in normal liver tissues, and was high (9/32), moderate (18/32), or low (5/32) in the cytoplasm of a high proportion of HCC tissues (Fig. 1D). These data indicated that NME1 is highly expressed in HCC tissues.

### NME1 overexpression is correlated with HCC progression

Next, we divided patients from TCGA into different subgroups and compared the mRNA levels of NME1. Patients with alpha-fetoprotein positivity ( $n = 120$ ) had higher NME1 transcriptional expression than patients who were alpha-fetoprotein-negative ( $n = 143$ ) (Fig. 2A,  $p < 0.0100$ ).

The NME1 transcription levels were higher in patients with histologic grade 3 HCC ( $n = 113$ ) than in patients with histologic grade 1 ( $n = 46$ ,  $p < 0.0500$ ) or grade 2 ( $n = 166$ ,  $p < 0.0500$ ) HCC (Fig. 2B). There was no significance in the relationship between increased NME1 expression and Child–Pugh grade in HCC patients (Fig. 2C,  $n = 228$ ,  $p > 0.0500$ ). The NME1 mRNA level in deceased patients with HCC ( $n = 224$ ) was higher than that in living HCC patients ( $n = 115$ ) (Fig. 2D,  $p < 0.0100$ ). The NME1 mRNA level in patients with HCC TNM stage II ( $n = 84$ ,  $p < 0.0500$ ) or III ( $n = 81$ ,  $p < 0.0100$ ) was higher than of patients with HCC TNM stage I ( $n = 170$ ) (Fig. 2E). The NME1 expression was higher in HCC tissue with microvascular infiltration ( $n = 84$ ) than in HCC tissue without vascular infiltration ( $n = 193$ ,  $p < 0.0100$ ) (Fig. 2F). The correlation of NME1 mRNA level with clinicopathological variables was summarized in Table 1. These findings indicate that elevated NME1 is associated with HCC progression.

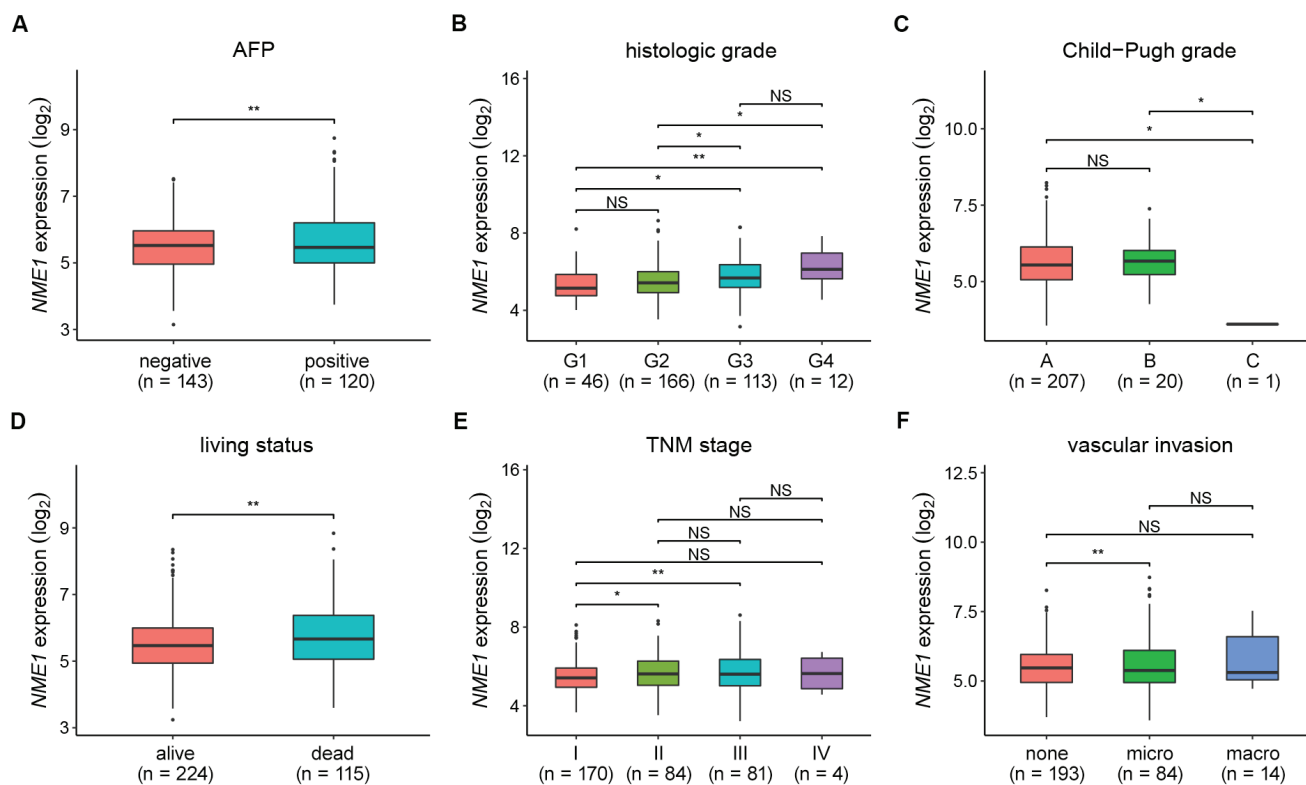


Fig. 2. The NME1 overexpression is correlated with hepatocellular carcinoma (HCC) progression. Patients from the Cancer Genome Atlas (TCGA) were grouped according to serum alpha fetoprotein (AFP) expression levels (A), histological grade (B), Child–Pugh grade (C), living status (D), TNM stages (E), and vascular invasion (F), and NME1 mRNA levels in different groups were analyzed. The Mann–Whitney test was used to analyze the data (A–F)

NS – no significance; \* $p < 0.0500$ ; \*\* $p < 0.0100$ .

### Kaplan–Meier curve and nomogram verify the prognostic value of NME1 in HCC

Analyzing the Kaplan–Meier curve drawn using data from TCGA, we found that high NME1 mRNA level was significantly correlated with poor overall survival (OS) ( $n = 339$ ,  $p = 0.0067$ ) and disease-free interval (DFI) ( $n = 295$ ,  $p = 0.0120$ ) (Fig. 3A,B). Moreover, among patients with TNM stage III or IV HCC, the OS of patients with high NME1 transcription levels was poorer than that of those with low NME1 transcription levels ( $n = 85$ ,  $p = 0.0420$ ). The relationship between DFI of patients with TNM stage III or IV of HCC and NME1 transcription levels was not significant ( $n = 68$ ,  $p = 0.0610$ ) (Fig. 3C,D). In general, high NME1 mRNA level was associated with poor OS or DFI. The following nomogram and the calibration curve confirmed that the predicted survival probabilities were in excellent agreement with the actual observed survival probabilities (1-, 3-, and 5-year OS and DFI) (Fig. 4). Together, the level of NME1 mRNA is valuable to evaluate the prognosis of HCC.

### miR-139-5p negatively regulates NME1

The Venn diagram showed that miR-139-5p and miR-335-5p may target to the 3' UTR of NEM1 (Fig. 5A, Supplementary Table 1 available at <https://doi.org/10.5281/>

zenodo.6131676). The TCGA-LIHC data showed that the levels of hsa-miR-139-5p ( $p < 0.0001$ ) and hsa-miR-335-5p ( $p < 0.0001$ ) in HCC tissues were lower than those in normal adjacent tissues, and were negatively correlated with the mRNA level of NME1 (Fig. 5B–E). Moreover, the Kaplan–Meier curve showed that HCC patients with lower miR-139-5p level had poorer OS ( $n = 367$ ,  $p < 0.0001$ ) and DFI ( $n = 314$ ,  $p < 0.0001$ ), while there was no significance in the correlation of miR-335-5p levels with OS ( $n = 364$ ,  $p = 0.2280$ ) or DFI ( $n = 314$ ,  $p = 0.0610$ ) in HCC patients (Fig. 5F–I). These data suggested that miR-139-5p may interact with NME1 3' UTR. Next, we performed in vitro experiments to verify this hypothesis. As shown in Fig. 6A, the overexpression of miR-139-3p decreased the luciferase activity in Hep3B and Huh7 cells, which was abolished by the mutation of 3' UTR of NME1. These results suggested that miR-139-5p targets NME1. The expression levels of miR-139-5p and NME1 in HCC cell lines (SMMC-7721, Huh7, HepG2, and Hep3B) and normal liver cell line (L-02) were detected. The results showed that the expression levels of miR-139-5p and NME1 in HCC cell lines were higher than those in L-02 (Fig. 6B–D,  $n = 3$ , all  $p < 0.0500$ ). Moreover, Hep3B and Huh7 cells had the highest NME1 level and the lowest miR-139-5p level. Therefore, these 2 cells were chosen for in vitro experiments. In addition, the miR-139-5p overexpression elevated the levels of miR-139-5p in HCC cells (Hep3B:  $1.015 \pm 0.2227$  fold compared to  $6.007 \pm 0.8823$  fold;

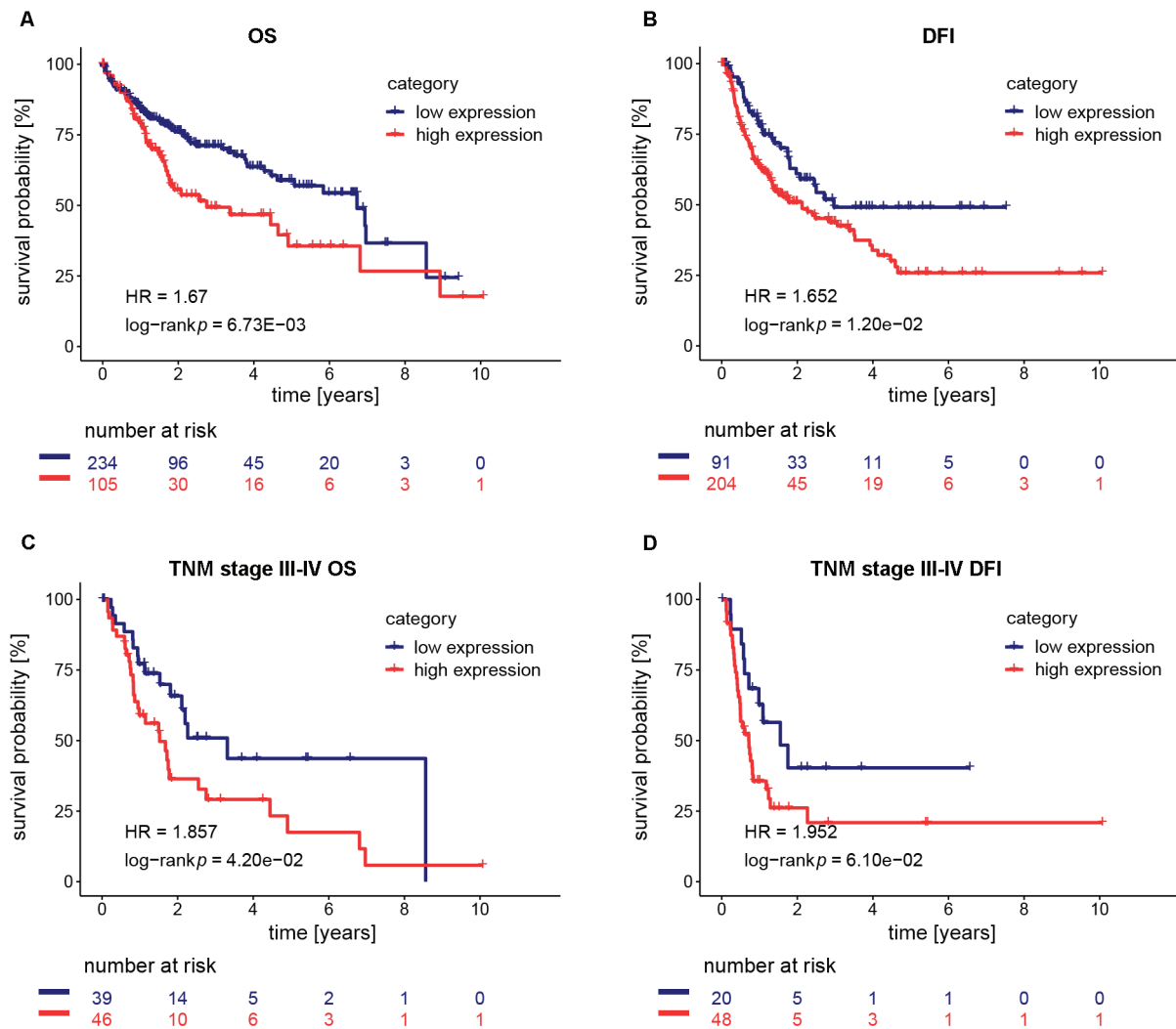


**Fig. 3.** Association between NME1 mRNA level and overall survival (OS) or disease-free interval (DFI). A,B. The Kaplan–Meier curve was used to analyze the correlation between NME1 mRNA levels and OS (A) or DFI (B) in patients with hepatocellular carcinoma (HCC); C,D. Analysis of OS (C) and DFI (D) based on mRNA levels of NME1 in patients with TNM stage III or IV of HCC. The log-rank test was used for statistical analysis (A–D)

HR – hazard ratio.

Huh7:  $1.009 \pm 0.1712$  fold compared to  $8.326 \pm 0.5093$  fold,  $n = 3$ , all  $p < 0.0010$ ), and reduced the mRNA (Hep3B:  $1.001 \pm 0.0453$  fold compared to  $0.6030 \pm 0.0430$  fold; Huh7:  $1.000 \pm 0.0187$  fold compared to  $0.4484 \pm 0.0271$  fold,  $n = 3$ , all  $p < 0.0010$ ) and protein (Hep3B:  $1.000 \pm 0.0251$  fold compared to  $0.4055 \pm 0.0047$  fold; Huh7:  $1.000 \pm 0.183$  fold compared to  $0.380 \pm 0.020$  fold,  $n = 3$ , all  $p < 0.0001$ ) levels of NME1 (Fig. 6E,F). In contrast, miR-139-5p inhibitor did not change the level of miR-139-5p in HCC cells (Hep3B:  $1.008 \pm 0.1567$  fold compared to  $1.143 \pm 0.1705$  fold; Huh7:  $1.029 \pm 0.3149$  fold compared to  $1.349 \pm 0.1209$  fold,  $n = 3$ , all  $p > 0.0500$ ), but enhanced the mRNA (Hep3B:  $1.000 \pm 0.0313$  fold compared to  $5.917 \pm 0.5942$  fold; Huh7:  $1.001 \pm 0.0527$  fold compared to  $6.160 \pm 0.1128$  fold,  $n = 3$ , all  $p < 0.0010$ ) and protein (Hep3B:  $1.000 \pm 0.0102$  fold compared to  $1.314 \pm 0.0391$  fold; Huh7:  $1.000 \pm 0.103$  fold compared to  $1.960 \pm 0.095$  fold,  $n = 3$ , all  $p < 0.0010$ ) levels of NME1 (Fig. 6E,F). Overall, miR-139-5p targets NME1 and downregulates its expression.

## NME1 is associated with cell cycle, DNA replication, oxidative phosphorylation, and pentose phosphate pathways

To investigate the biological processes that may be regulated by NME1, we analyzed the genes co-expressed with NME1 using GSEA. These genes were found to be enriched in the gene sets for cell cycle, DNA replication, oxidative phosphorylation, and pentose phosphate pathways (Fig. 7). Genes related to these biological processes and co-expressed with NME1 are listed in Fig. 7.

## miR-139-5p suppresses cellular proliferation by downregulating NME1

To confirm the conclusion of bioinformatics analysis, we investigated the effect of miR-139-5p/NME1 axis on cellular proliferation, using in vitro experiments. First, we overexpressed miR-139-5p or NME1 by transfection

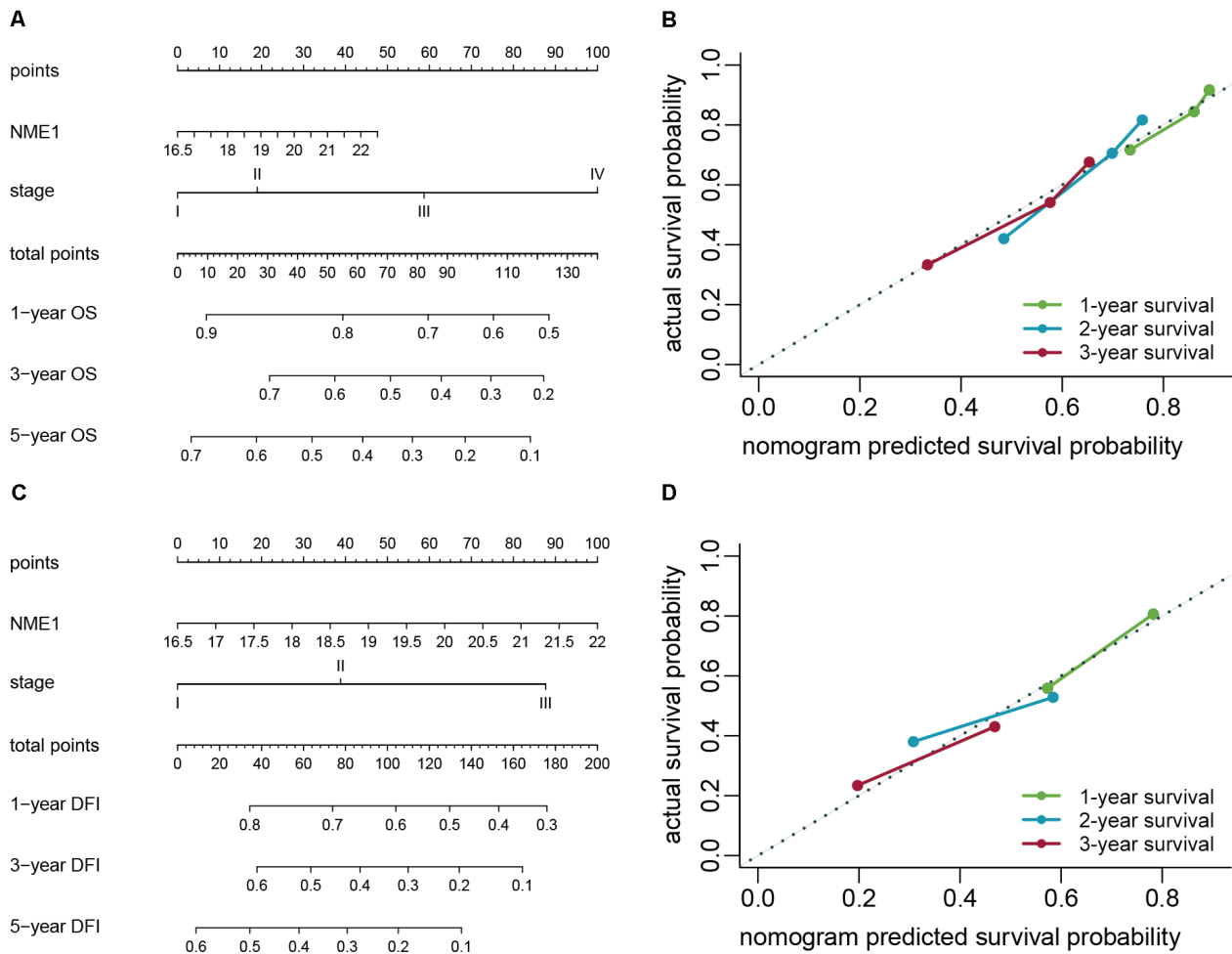


Fig. 4. Prognostic value of NME1 in hepatocellular carcinoma (HCC). A,B. Based on the expression level of NME1 and TNM stage, a prognostic nomogram (A) of HCC patients and a nomogram calibration curve (B) for predicting overall survival (OS) were plotted; C,D. Based on NME1 and TNM stage, a nomogram (C) and calibration curve (D) for patients with HCC for predicting disease-free interval (DFI) were plotted

with miR-139-5p mimic and NME1 OE plasmid, respectively. As shown in Fig. 8A, miR-139-5p mimic elevated the miR-139-5p level in Hep3B and Huh7 cells (n = 3, all p < 0.0001), and the NME1 OE plasmid had no significant effect on the level of miR-139-5p (n = 3, all p > 0.0500). Moreover, miR-139-5p mimic significantly decreased the mRNA (Fig. 8B, n = 3, all p < 0.0500) and protein (Fig. 8C, n = 3, all p < 0.0500) levels of NME1. In addition, the NME1 overexpression significantly rescued the miR-139-5p mimic-induced reduction in NME1 levels (Fig. 8B,C, n = 3, all p < 0.0500).

Next, the EdU assay was performed to determine the cell proliferation. As shown in Fig. 9A, the miR-139-5p mimic reduced the percentage of EdU<sup>+</sup> cells (Hep3B: 77.0 ± 2.7% compared to 48.4 ± 5.5%; Huh7: 54.6 ± 2.8% compared to 33.1 ± 2.1%, n = 3, all p < 0.0100), indicating that miR-139-5p suppressed the cellular proliferation. Moreover, the NME1 overexpression relieved the inhibitory effect of miR-139-5p on cell proliferation (Hep3B: 49.3 ± 4.1% compared to 62.0 ± 3.8%; Huh7: 31.9 ± 2.6% compared to 45.25 ± 2.6%, n = 3, all p < 0.0100) (Fig. 9A). In addition, the miR-139-5p overexpression caused a cell-cycle arrest

at G<sub>0</sub>/G<sub>1</sub> phase (Hep3B: 33.8 ± 1.6% compared to 51.5 ± 1.7%; Huh7: 40.4 ± 3.4% compared to 56.1 ± 0.5%, n = 3, all p < 0.0100), while NME1 overexpression alleviated the arrest induced by miR-139-5p (Hep3B: 51.7 ± 2.3% compared to 42.9 ± 2.0%; Huh7: 55.2 ± 0.7% compared to 47.6 ± 1.1%, n = 3, all p < 0.0100) (Fig. 9B).

Taken together, miR-139-5p inhibits cell growth by downregulating NME1 expression.

## Discussion

The NME1 is a highly conserved multifunctional protein. Previous studies have shown that elevating NME1 levels inhibits the migration of various tumor cells, such as melanoma, breast cancer and prostate cancer.<sup>18,21,22</sup> One study showed that the polymorphisms in the *NME1* gene are significantly associated with an increased susceptibility to gynecological cancer, decreased sensitivity to gastric cancer, increased susceptibility to non-small cell lung cancer, and reduced risk of cervical cancer.<sup>4</sup> Furthermore, reducing the expression of NME1 protein promotes the growth and

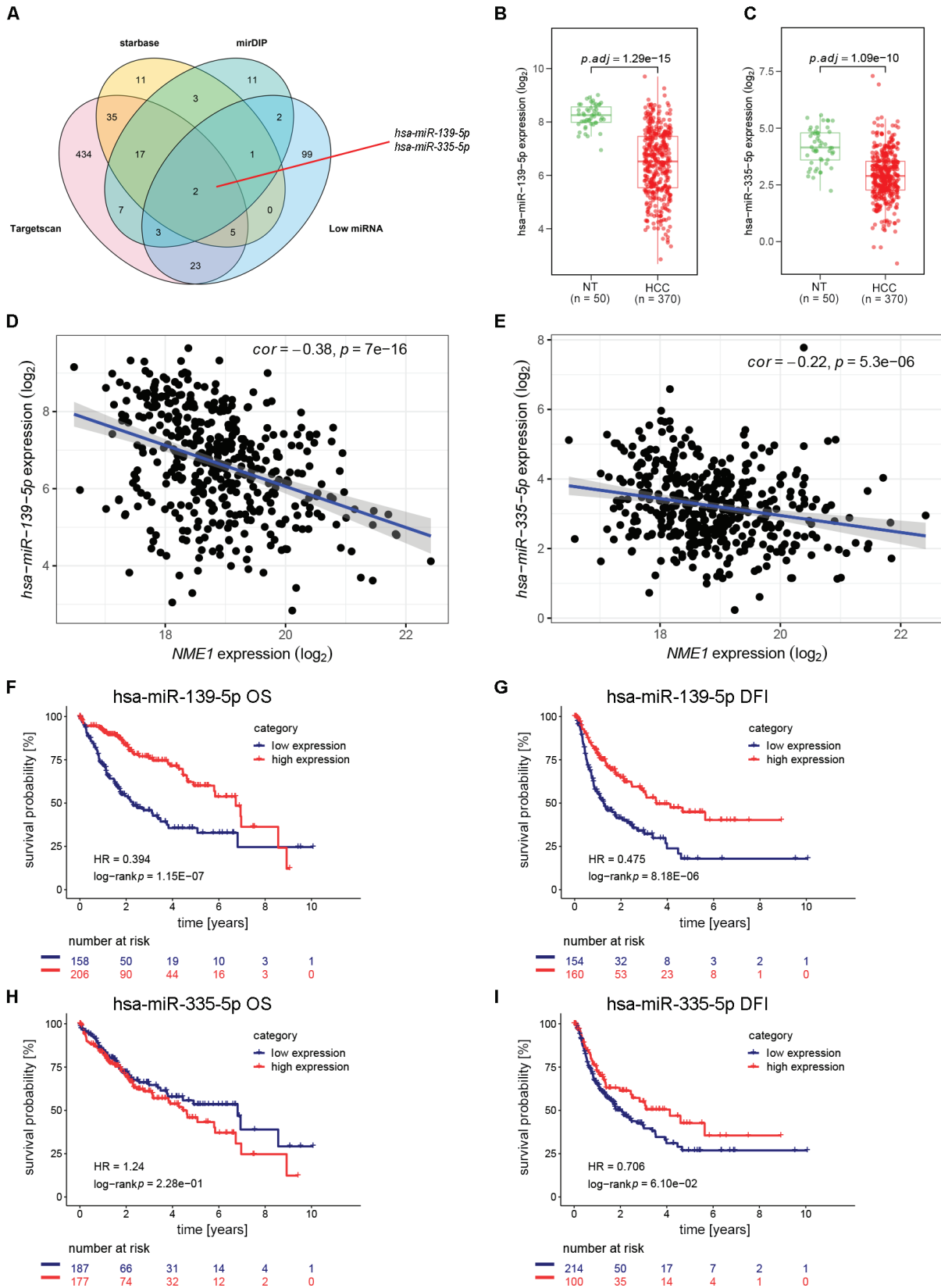


**Fig. 5.** The miR-139-5p and miR-335-5p are negatively correlated with NME1. A. Venn diagram; B,C. Comparison of miR-139-5p (B) or miR-335-5p (C) levels in hepatocellular carcinoma (HCC) tissues (n = 370) samples and normal tissues (NT) (n = 50) in the Cancer Genome Atlas liver hepatocellular carcinoma (TCGA-LIHC); D,E. The NME1 mRNA level was negatively correlated with hsa-miR-139-5p level (D) or hsa-miR-335-5p level (E); F-I. The Kaplan–Meier analysis showing the correlation of hsa-miR-139-5p level with overall survival (OS) (F) or disease-free interval (DFI) (G), and of hsa-miR-335-5p level with OS (H) or DFI (I). The Mann–Whitney test (B,C) and the log-rank test (F–I) were used for statistical analysis. Linearity curves and Kaplan–Meier curves were drawn based on the data from the TCGA

HR – hazard ratio.



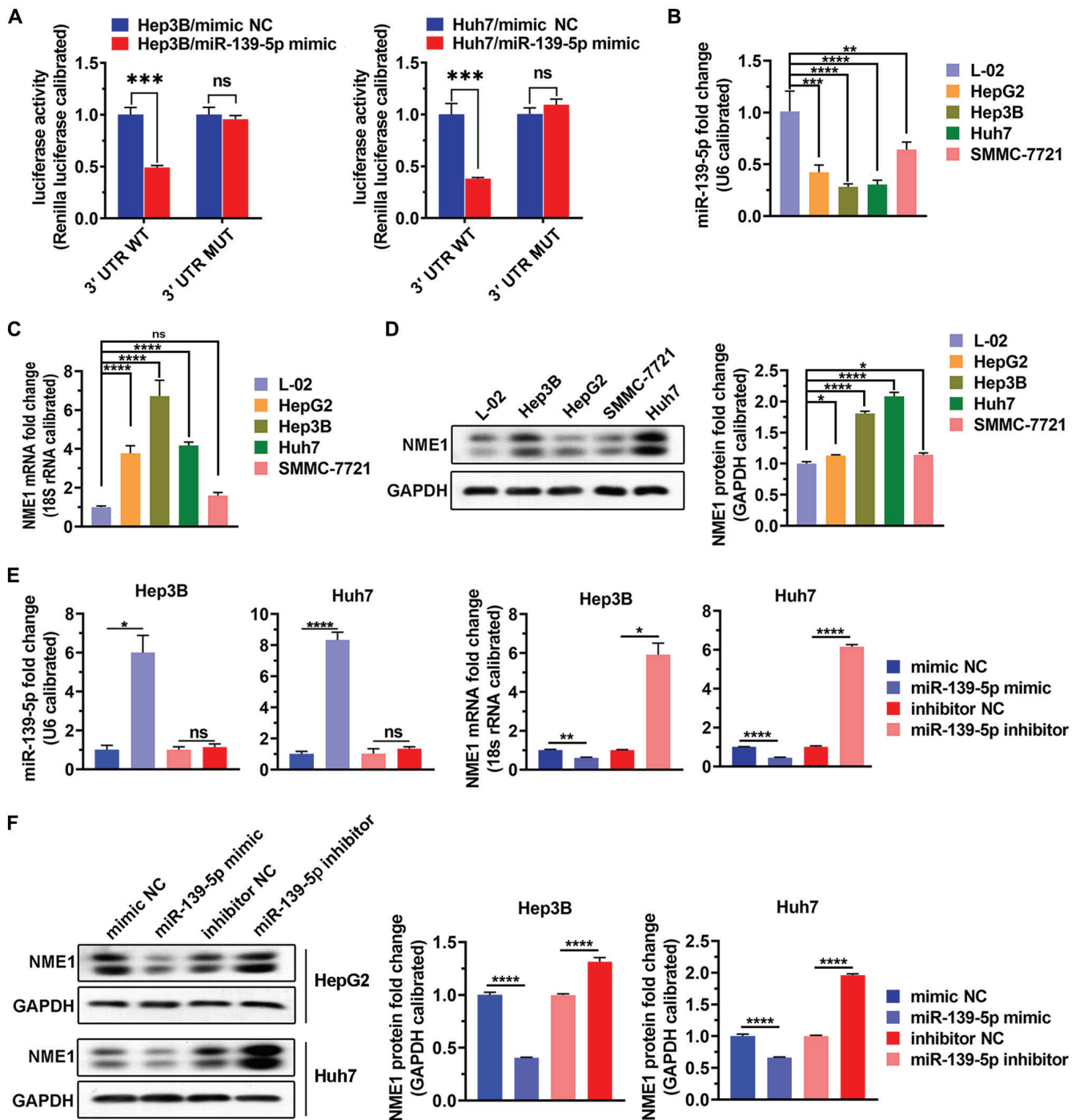


Fig. 6. The miR-139-5p suppresses the expression of NME1. A. A dual-luciferase reporter system was used to analyze the correlation between miR-139-5p and the 3' UTR of NME1; B. The miR-139-5p levels in cell lines were detected using quantitative reverse transcription polymerase chain reaction (qRT-PCR); C. The NME1 expression levels in cell lines were detected using qRT-PCR; D. Western blotting showing the NME1 protein level in cell lines; E. The NME1 mRNA levels were detected after transfection with miR-139-5p mimic and miR-139-5p inhibitor, respectively; F. The NME1 protein levels were detected after transfection with miR-139-5p mimic and miR-139-5p inhibitor, respectively. Data are presented as mean ± standard deviation (SD) of 3 biological replicates. Data were analyzed using Student's t-test (A,E,F) and analysis of variance (ANOVA), followed by Tukey's post hoc test (B–D)

UTR – untranslated region; 3' UTR WT – wide-type *NME1* 3' UTR; 3' UTR MUT – mutant *NME1* 3' UTR; ns – no significance; \* $p < 0.0500$ ; \*\* $p < 0.0100$ ; \*\*\* $p < 0.0010$ ; \*\*\*\* $p < 0.0001$ .

lymph node metastasis of human breast cancer. However, enhancing the expression of NME1 reduces survival rates in patients with neuroblastoma. Increasing expression of NME1 in gastric cancer promotes distant metastasis of gastric cancer and reduces the 2-year disease-free

survival rate of patients.<sup>23,24</sup> Bioinformatic analyses showed that NME1 levels in HCC tissues were higher than those in hepatitis, cirrhosis or normal liver tissues.<sup>18</sup> The NME1 is highly expressed in colorectal cancer tissues and is tightly associated with the metastatic potential of colorectal

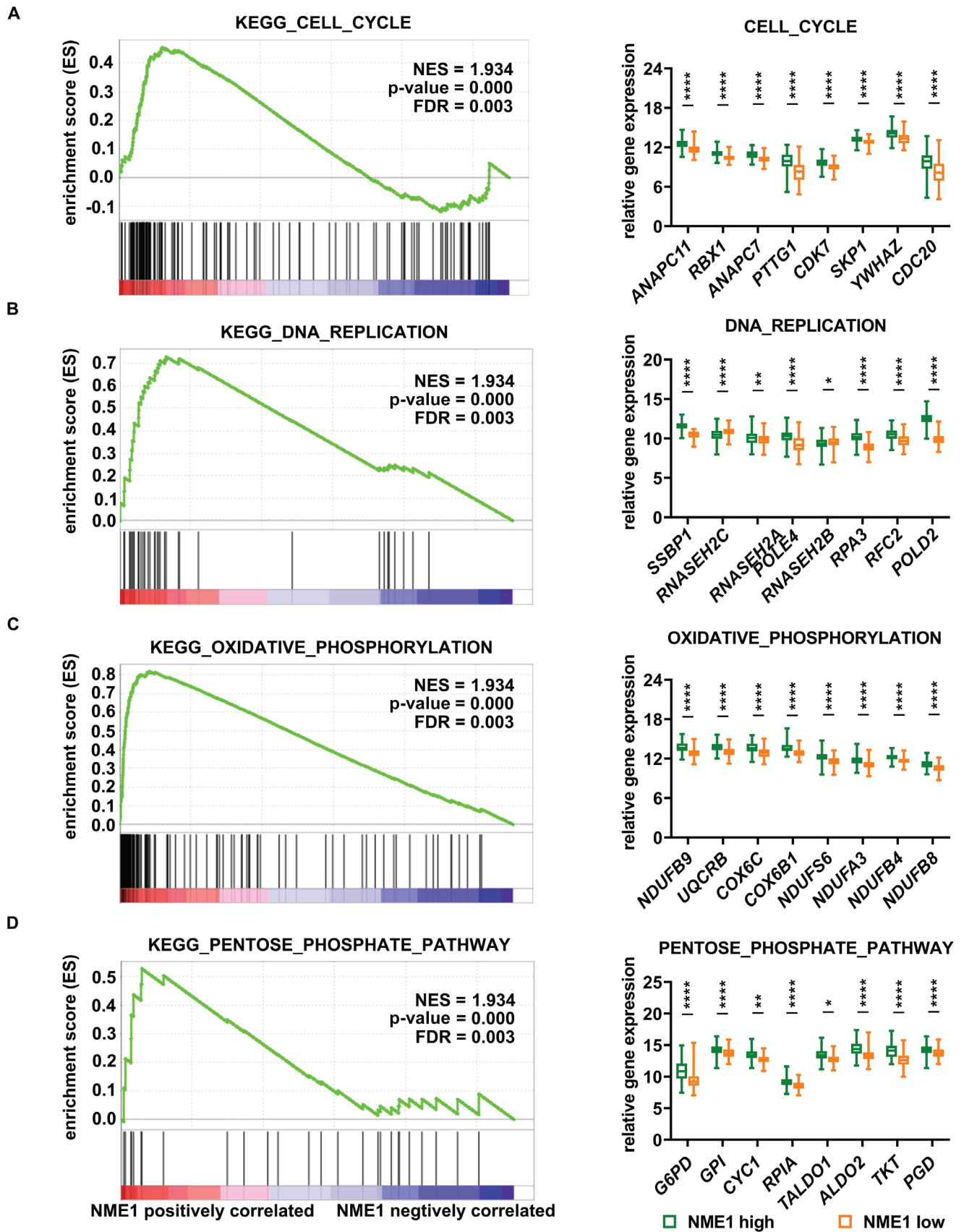


Fig. 7. Gene set enrichment analysis (GSEA) of potential biological functions of upregulated NME1 in hepatocellular carcinoma (HCC). A–D. The correlation between NME1 expression level and the cell cycle (A), DNA replication (B), oxidative phosphorylation (C) or pentose phosphate pathways (D), and the relationship between NME1 expression level and the expression of genes related to the 3 biological processes. The Mann–Whitney test was used to analyze the data (A–D)

KEGG – Kyoto Encyclopedia of Genes and Genomes; NES – normalized enrichment score; FDR – false discovery rate. \* $p < 0.05$ ; \*\* $p < 0.01$ ; \*\*\*\* $p < 0.0001$ .

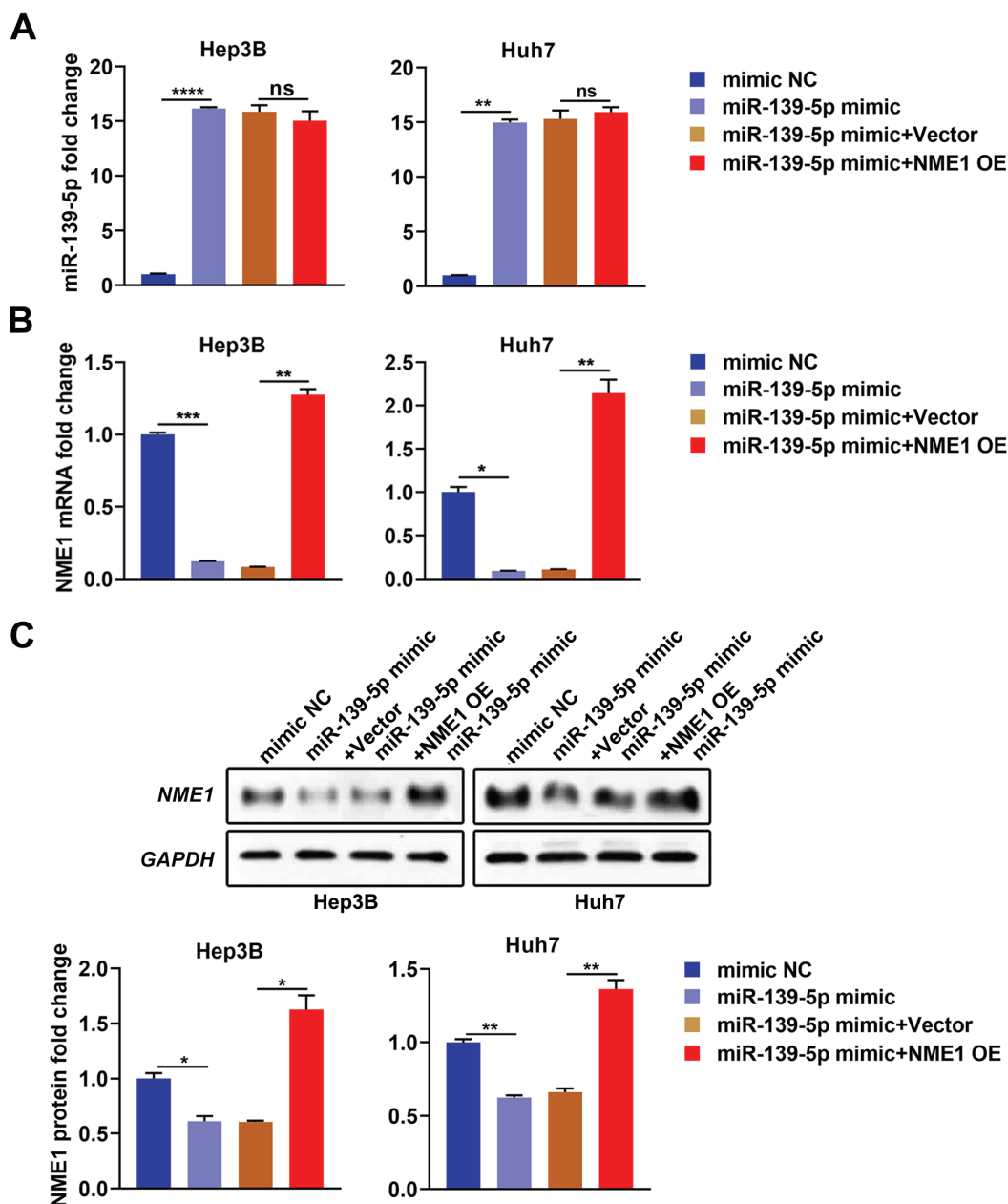


Fig. 8. The miR-139-5p inhibits cell proliferation by downregulating NME1. After miR-139-5p mimic was transfected alone or co-transfected with overexpressing NME1 (NME1 OE) plasmid into Hep3B and Huh7 cells, the levels of miR-139-5p (A), NME1 mRNA (B) and NME1 protein (C) were detected. Data are presented as mean ± standard deviation (SD) of 3 biological replicates and analyzed using Student's t-test

ns – no significance; \*p < 0.05; \*\*p < 0.01; \*\*\*p < 0.001; \*\*\*\*p < 0.0001.

cancer. The NEM1 is considered a prognostic factor for colorectal cancer.<sup>18,25</sup> Our study revealed that NME1 was upregulated in HCC, and the level of NME1 was significantly correlated with the clinicopathological characteristics and prognosis. These findings indicated that NME1 has different functions in different tumors.

Mature miRNAs binds to the 3' UTR of targeting mRNA, resulting in the degradation of mRNAs or suppression of mRNA translation.<sup>26,27</sup> Studies have shown that a single miRNA may participates in various pathophysiological processes, including cell proliferation, cell apoptosis, cell differentiation, and organ development by regulating

multiple potential targets, thereby promoting or inhibiting the progression of human cancer.<sup>26,28–30</sup> The miR-139-5p, located on chromosome 11q13.4, inhibits the occurrence of esophageal cancer by regulating vascular endothelial growth factor receptor (VEGFR) signaling pathway,<sup>26,31,32</sup> suppressing the growth and migration of osteosarcoma cells by regulating DNMT1,<sup>33</sup> promoting the invasiveness of adrenocortical carcinoma by targeting the downstream gene of N-myc,<sup>34</sup> and inhibiting the growth, metastasis and glycolysis of gallbladder cancer cells by downregulating PKM2.<sup>35</sup> In addition, serum miR-139-5p is considered an indicator of osteosarcoma.<sup>36</sup> In non-small cell

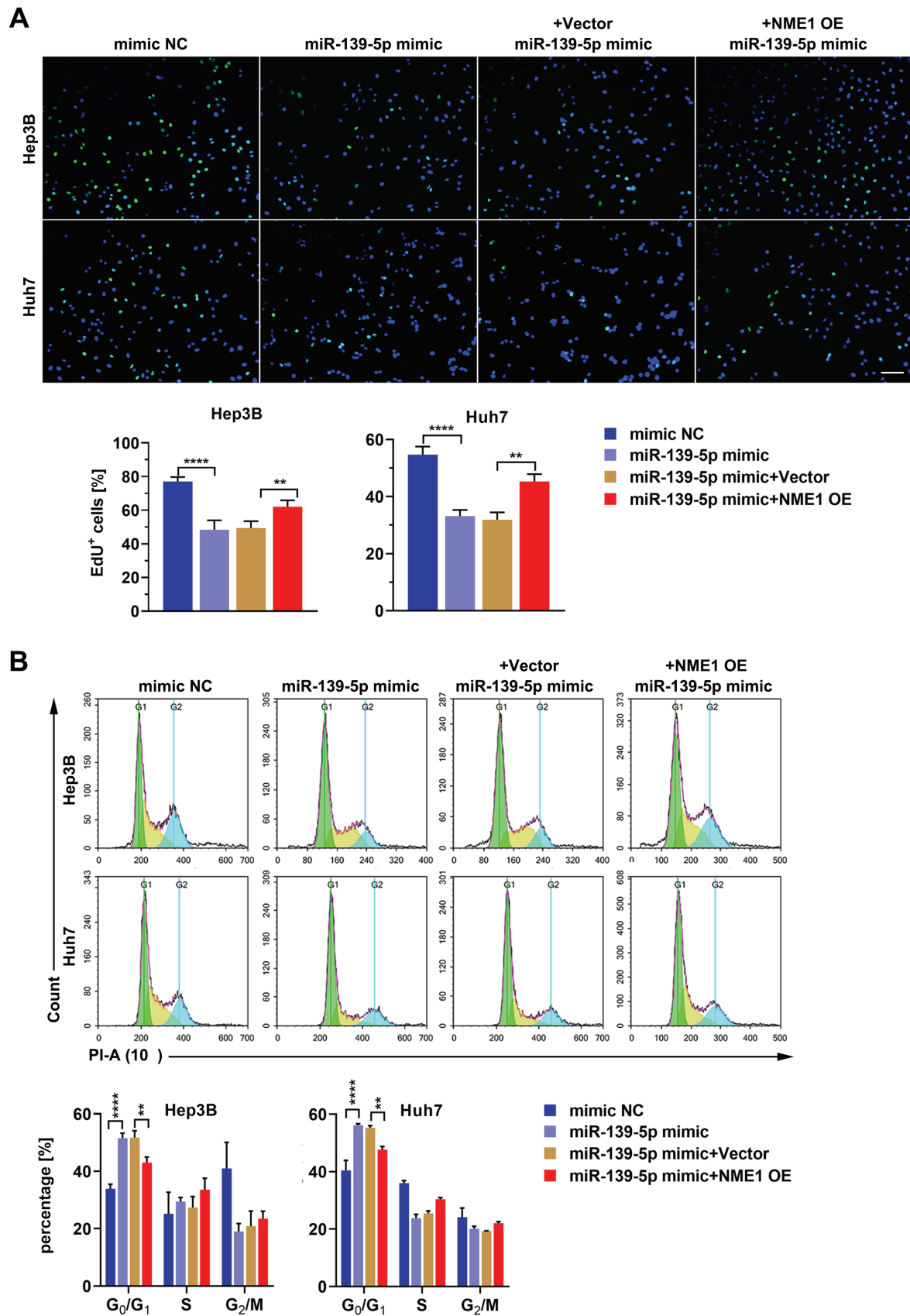


Fig. 9. The miR-139-5p inhibits cell proliferation by downregulating NME1. The cell proliferation was determined using EdU assay (A), and the cell cycle was analyzed with flow cytometry using propidium iodide (PI) staining (B). Data are presented as mean  $\pm$  standard deviation (SD) of 3 biological replicates and analyzed using Student's t-test

NME1 OE – overexpressing NME1; \*\* $p < 0.0100$ ; \*\*\* $p < 0.0010$ ; \*\*\*\* $p < 0.0001$ .

lung cancer, the lncRNA AFAP1-AS1 inhibits miR-139-5p by upregulating RRM2 to promote cell proliferation.<sup>37</sup> The miR-139-5p, which is downregulated in HCC cells, inhibits the epithelial–mesenchymal transition of HCC cells.<sup>38</sup> According to previous studies, miR-139-5p may also suppress the deterioration of HCC by targeting multiple genes, such as *ZEB1*, *ZEB2*, *TCF-4*, *XIST1*, and *c-Fos*.<sup>30,38–40</sup> Our study revealed that miR-139-5p negatively regulates the expression of NME1 in HCC cells. Our findings show that miR-139-5p may serve as a tumor suppressor in HCC.

## Limitations

It should be noted that there are also several limitations to this study. The results of our GSEA analysis indicate that NME1 is related to cell cycle, DNA replication, oxidative phosphorylation, and pentose phosphate pathways. We confirmed that miR-139-5p downregulates NME1 to induce G<sub>0</sub>/G<sub>1</sub> arrest and inhibit cellular proliferation. However, the underlying mechanism of miR-139-5p on regulating oxidative phosphorylation and pentose phosphate pathways by targeting NME1 needs to be studied further. Signaling pathways which are regulated by miR-139-5p/NME1 axis need to be determined. Moreover, we should study the effect of miR-139-5p/NME1 axis on cell apoptosis and metastasis in the next research. In addition, the antitumor activity of miR-139-5p should also be verified in vivo.

## Conclusions


The NME1 is highly expressed in HCC tissues. Higher NME1 level indicates worse OS and DFI in patients with HCC. In contrast, miR-139-5p is lowly expressed in HCC tissues. Higher NME1 level indicates better OS and DFI. Furthermore, miR-139-5p targets NME1 3' UTR and suppresses cellular proliferation by downregulating NME1 expression.

### ORCID iDs


Jun Yang  <https://orcid.org/0000-0003-3942-433X>


De Zhi Li  <https://orcid.org/0000-0002-4500-7439>

Yu Pang  <https://orcid.org/0000-0002-7457-8863>

Tao Zhou  <https://orcid.org/0000-0003-1547-0462>

Jia Sun  <https://orcid.org/0000-0002-1249-0030>

Xian Yi Cheng  <https://orcid.org/0000-0003-4265-6916>

Wei V. Zheng  <https://orcid.org/0000-0002-8942-1543>

### References

1. Ferlay J, Soerjomataram I, Dikshit R, et al. Cancer incidence and mortality worldwide: Sources, methods and major patterns in GLOBOCAN 2012. *Int J Cancer*. 2015;136(5):E359–E386. doi:10.1002/ijc.29210
2. Zucman-Rossi J, Villanueva A, Nault JC, Llovet JM. Genetic landscape and biomarkers of hepatocellular carcinoma. *Gastroenterology*. 2015;149(5):1226–1239.e1224. doi:10.1053/j.gastro.2015.05.061
3. Nahon P, Zucman-Rossi J. Single nucleotide polymorphisms and risk of hepatocellular carcinoma in cirrhosis. *J Hepatol*. 2012;57(3):663–674. doi:10.1016/j.jhep.2012.02.035
4. Shi X, Jin H, Peng M, et al. Association between NME1 polymorphisms and cancer susceptibility: A meta-analysis based on 1644 cases and 2038 controls. *Pathol Res Pract*. 2018;214(4):467–474. doi:10.1016/j.prp.2018.02.020
5. Bilitou A, Watson J, Gartner A, Ohnuma S. The NM23 family in development. *Mol Cell Biochem*. 2009;329(1–2):17–33. doi:10.1007/s11010-009-0121-6
6. Dooley S, Seib T, Engel M, et al. Isolation and characterization of the human genomic locus coding for the putative metastasis control gene *nm23-H1*. *Hum Genet*. 1994;93(1):63–66. doi:10.1007/bf00218915
7. Xue R, Peng Y, Han B, Li X, Chen Y, Pei H. Metastasis suppressor NME1 promotes non-homologous end joining of DNA double-strand breaks. *DNA Repair (Amst)*. 2019;77:27–35. doi:10.1016/j.dnarep.2019.03.003
8. Chen J, Jiang Q, Jiang XQ, et al. miR-146a promoted breast cancer proliferation and invasion by regulating NM23-H1. *J Biochem*. 2020;167(1):41–48. doi:10.1093/jb/mvz079
9. Braun S, Mauch C, Boukamp P, Werner S. Novel roles of NM23 proteins in skin homeostasis, repair and disease. *Oncogene*. 2007;26(4):532–542. doi:10.1038/sj.onc.1209822
10. Kaetzel DM, Leonard MK, Cook GS, et al. Dual functions of NME1 in suppression of cell motility and enhancement of genomic stability in melanoma. *Naunyn Schmiedebergs Arch Pharmacol*. 2015;388(2):199–206. doi:10.1007/s00210-014-1010-4
11. Puts GS, Leonard MK, Pamidimukkala NV, Snyder DE, Kaetzel DM. Nuclear functions of NME proteins. *Lab Invest*. 2018;98(2):211–218. doi:10.1038/labinvest.2017.109
12. Gao QL, Ma D, Meng L, et al. Association between *Nm23-H1* gene expression and metastasis of ovarian carcinoma. *Ai Zheng*. 2004;23(6):650–654. PMID:15191664.
13. Goncharuk VN, del-Rosario A, Kren L, et al. Co-downregulation of PTEN, KAI-1, and nm23-H1 tumor/metastasis suppressor proteins in non-small cell lung cancer. *Ann Diagn Pathol*. 2004;8(1):6–16. doi:10.1016/j.anndiagpath.2003.11.002
14. Kaetzel DM, McCorkle JR, Novak M, Yang M, Jarrett SG. Potential contributions of antimutator activity to the metastasis suppressor function of NM23-H1. *Mol Cell Biochem*. 2009;329(1–2):161–165. doi:10.1007/s11010-009-0108-3
15. Lagos-Quintana M, Rauhut R, Yalcin A, Meyer J, Lendeckel W, Tuschl T. Identification of tissue-specific microRNAs from mouse. *Curr Biol*. 2002;12(9):735–739. doi:10.1016/s0960-9822(02)00809-6
16. Bartel DP. MicroRNAs: Target recognition and regulatory functions. *Cell*. 2009;136(2):215–233. doi:10.1016/j.cell.2009.01.002
17. Almeida MI, Nicoloso MS, Zeng L, et al. Strand-specific miR-28-5p and miR-28-3p have distinct effects in colorectal cancer cells. *Gastroenterology*. 2012;142(4):886–896.e9. doi:10.1053/j.gastro.2011.12.047
18. Yang J, Lv Z, Huang J, Zhao Y, Li Y. High expression of NME1 correlates with progression and poor prognosis in patients of hepatocellular carcinoma. *Int J Clin Exp Pathol*. 2017;10(8):8561–8568. PMID:31966710.
19. Yu B, Ding Y, Liao X, Wang C, Wang B, Chen X. Overexpression of PARPBP correlates with tumor progression and poor prognosis in hepatocellular carcinoma. *Dig Dis Sci*. 2019;64(10):2878–2892. doi:10.1007/s10620-019-05608-4
20. Xu X, Zheng S. MiR-887-3p negatively regulates STARD13 and promotes pancreatic cancer progression. *Cancer Manag Res*. 2020;12:6137–6147. doi:10.2147/cmar.S260542
21. Steeg PS, Horak CE, Miller KD. Clinical-translational approaches to the Nm23-H1 metastasis suppressor. *Clin Cancer Res*. 2008;14(16):5006–5012. doi:10.1158/1078-0432.Ccr-08-0238
22. Li Y, Zhou Q, Sun Z, et al. Experimental study on molecular mechanism of *nm23-H1* gene transfection reversing the malignant phenotype of human high-metastatic large cell lung cancer cell line [in Chinese]. *Zhongguo Fei Ai Za Zhi*. 2006;9(4):307–311. doi:10.3779/j.issn.1009-3419.2006.04.01
23. Wang CS, Lin KH, Hsu YC, Hsueh S. Distant metastasis of gastric cancer is associated with elevated expression of the antimetastatic *nm23* gene. *Cancer Lett*. 1998;128(1):23–29. doi:10.1016/s0304-3835(98)00043-3
24. Müller W, Schneiders A, Hommel G, Gabbert HE. Expression of nm23 in gastric carcinoma: Association with tumor progression and poor prognosis. *Cancer*. 1998;83(12):2481–2487. doi:10.1002/(sici)1097-0142(19981215)83:12<2481::aid-cnrc11>3.0.co;2-p
25. Kapitanović S, Cacev T, Berković M, et al. nm23-H1 expression and loss of heterozygosity in colon adenocarcinoma. *J Clin Pathol*. 2004;57(12):1312–1318. doi:10.1136/jcp.2004.017954

26. Jiao W, Zhang J, Wei Y, et al. MiR-139-5p regulates VEGFR and downstream signaling pathways to inhibit the development of esophageal cancer. *Dig Liver Dis.* 2019;51(1):149–156. doi:10.1016/j.dld.2018.07.017
27. Qin C, Huang RY, Wang ZX. Potential role of miR-100 in cancer diagnosis, prognosis, and therapy. *Tumour Biol.* 2015;36(3):1403–1409. doi:10.1007/s13277-015-3267-8
28. Gu DN, Huang Q, Tian L. The molecular mechanisms and therapeutic potential of microRNA-7 in cancer. *Expert Opin Ther Targets.* 2015;19(3):415–426. doi:10.1517/14728222.2014.988708
29. Li P, Xiao Z, Luo J, Zhang Y, Lin L. MiR-139-5p, miR-940 and miR-193a-5p inhibit the growth of hepatocellular carcinoma by targeting SPOCK1. *J Cell Mol Med.* 2019;23(4):2475–2488. doi:10.1111/jcmm.14121
30. Gu W, Li X, Wang J. miR-139 regulates the proliferation and invasion of hepatocellular carcinoma through the WNT/TCF-4 pathway. *Oncol Rep.* 2014;31(1):397–404. doi:10.3892/or.2013.2831
31. Corbetta S, Vaira V, Guarnieri V, et al. Differential expression of microRNAs in human parathyroid carcinomas compared with normal parathyroid tissue. *Endocr Relat Cancer.* 2010;17(1):135–146. doi:10.1677/erc-09-0134
32. Shen K, Mao R, Ma L, et al. Post-transcriptional regulation of the tumor suppressor miR-139-5p and a network of miR-139-5p-mediated mRNA interactions in colorectal cancer. *FEBS J.* 2014;281(16):3609–3624. doi:10.1111/febs.12880
33. Shi YK, Guo YH. MiR-139-5p suppresses osteosarcoma cell growth and invasion through regulating DNMT1. *Biochem Biophys Res Commun.* 2018;503(2):459–466. doi:10.1016/j.bbrc.2018.04.124
34. Agosta C, Laugier J, Guyon L, et al. MiR-483-5p and miR-139-5p promote aggressiveness by targeting N-myc downstream-regulated gene family members in adrenocortical cancer. *Int J Cancer.* 2018;143(4):944–957. doi:10.1002/ijc.31363
35. Chen J, Yu Y, Chen X, et al. MiR-139-5p is associated with poor prognosis and regulates glycolysis by repressing PKM2 in gallbladder carcinoma. *Cell Prolif.* 2018;51(6):e12510. doi:10.1111/cpr.12510
36. Zhou L, Ma X, Yue J, et al. The diagnostic effect of serum miR-139-5p as an indicator in osteosarcoma. *Cancer Biomark.* 2018;23(4):561–567. doi:10.3233/cbm-181744
37. Huang N, Guo W, Ren K, et al. LncRNA AFAP1-AS1 suppresses miR-139-5p and promotes cell proliferation and chemotherapy resistance of non-small cell lung cancer by competitively upregulating RRM2. *Front Oncol.* 2019;9:1103. doi:10.3389/fonc.2019.01103
38. Qiu G, Lin Y, Zhang H, Wu D. miR-139-5p inhibits epithelial-mesenchymal transition, migration and invasion of hepatocellular carcinoma cells by targeting ZEB1 and ZEB2. *Biochem Biophys Res Commun.* 2015;463(3):315–321. doi:10.1016/j.bbrc.2015.05.062
39. Mo Y, Lu Y, Wang P, et al. Long non-coding RNA XIST promotes cell growth by regulating miR-139-5p/PDK1/AKT axis in hepatocellular carcinoma. *Tumour Biol.* 2017;39(2):1010428317690999. doi:10.1177/1010428317690999
40. Fan Q, He M, Deng X, et al. Derepression of c-Fos caused by microRNA-139 down-regulation contributes to the metastasis of human hepatocellular carcinoma. *Cell Biochem Funct.* 2013;31(4):319–324. doi:10.1002/cbf.2902

# miRNA profiling of human nasopharyngeal carcinoma cell lines HONE1 and CNE2 after X-ray therapy

Hui Luo<sup>1,A–D,F</sup>, Fangyan Zhong<sup>1,A–D,F</sup>, Xiang Jing<sup>2,A–D,F</sup>, Hong Lin<sup>1,A–C,F</sup>, Yong Li<sup>1,A,C,E,F</sup>

<sup>1</sup> Department of Oncology, The First Affiliated Hospital of Nanchang University, China

<sup>2</sup> Department of Oncology, Jiangxi Lushan People's Hospital, Jiujiang, China

A – research concept and design; B – collection and/or assembly of data; C – data analysis and interpretation; D – writing the article; E – critical revision of the article; F – final approval of the article

Advances in Clinical and Experimental Medicine, ISSN 1899–5276 (print), ISSN 2451–2680 (online)

Adv Clin Exp Med. 2022;31(6):671–687

## Address for correspondence

Yong Li

E-mail: liyong20210823@163.com

## Funding sources

None declared

## Conflict of interest

None declared

Received on September 3, 2021

Reviewed on October 18, 2021

Accepted on February 10, 2022

Published online on March 11, 2022

## Cite as

Luo H, Zhong F, Jing X, Lin H, Li Y. miRNA profiling of human nasopharyngeal carcinoma cell lines HONE1 and CNE2 after X-ray therapy. *Adv Clin Exp Med*. 2022;31(6):671–687. doi:10.17219/acem/146580

## DOI

10.17219/acem/146580

## Copyright

Copyright by Author(s)

This is an article distributed under the terms of the Creative Commons Attribution 3.0 Unported (CC BY 3.0) (<https://creativecommons.org/licenses/by/3.0/>)

## Abstract

**Background.** Radiotherapy is the main treatment for nasopharyngeal carcinoma. The radioresistance mechanism of cells is related to miRNAs.

**Objectives.** To investigate the miRNA profiling of HONE1 and CNE2 after X-ray therapy.

**Materials and methods.** The HONE1 and CNE2 cells were treated with X-ray at 4 Gy, 8 Gy, 16 Gy, and 20 Gy doses. The cell lines CNE2 with the best therapy effects and HONE1 with the worst therapy effects were screened out. Apoptosis and cell viability were detected with flow cytometry and Cell Counting Kit-8 (CCK-8). High-throughput sequencing was performed. A miRNA library was constructed. The miRNA annotation expression distribution, family prediction and target gene interaction, Gene Ontology and Kyoto Encyclopedia of Genes and Genomes (KEGG) pathway analysis were conducted.

**Results.** The 24-hour 20 Gy dose X-rays were selected as the optimal therapy conditions. The CNE2\_C, CNE2\_M, HONE1\_C and HONE1\_M miRNAs accounted for 26.5%, 31.7%, 21.3%, and 22.9% of the Cleandata reads count, respectively, and the contents of rRNAs accounted for 24.9%, 14.7%, 25.1%, and 25.1% of the Cleandata reads count, respectively. The miRNAs with differential expression between the HONE1 and CNE2 cell lines including hsa-miR-21-5p, hsa-let-7a-5p, hsa-miR-125a-5p, hsa-miR-26a-5p, hsa-let-7f-5p, hsa-miR-20a-5p, and hsa-miR-24a-3p. There were also differentially expressed miRNAs in HONE1\_C vs. HONE1\_M, such as hsa-miR-21-5p and hsa-let-7i-5p. The differentially expressed miRNA in CNE2\_C vs. CNE2\_M was hsa-miR-148b-3p. The Gene Ontology analysis showed that the differentially expressed miRNA interacting genes in HONE1\_M vs. CNE2\_M were mainly enriched in biological process such as negative and positive regulation of transcription from RNA polymerase II promoter, cellular component such as cytosol and molecular function such as protein binding factor. The KEGG pathway analysis revealed that the differentially expressed miRNA interacting genes in HONE1\_M vs. CNE2\_M were enriched in the cancer-related pathways, such as pathways in cancer, MAPK signaling pathway and Wnt signaling pathway.

**Conclusions.** Twelve miRNAs and 9 genes which contribute to X-ray radiation resistance were identified. Among those with differential expression between the HONE1 and CNE2 cell lines, which played a regulatory role in multiple pathways, were hsa-miR-20a-5p, hsa-let-7a-5p, hsa-let-7f-5p, hsa-let-7i-5p, hsa-miR-30e-5p, hsa-miR-148b-3p, and hsa-miR-200c-3p. The corresponding genes were *MAPK1*, *SOS1*, *TGFBR1*, *TGFBR2*, *TP53*, *CASP3*, *CCNE2*, *PTEN*, and *CDK2*.

**Key words:** HONE1, CNE2, X-ray radiation resistance, human nasopharyngeal carcinoma, miRNA profiling

## Background

Nasopharyngeal carcinoma (NPC) is a type of squamous cell carcinoma formed in nasopharyngeal tissue.<sup>1</sup> It is mainly divided into poorly differentiated squamous cell carcinoma and undifferentiated carcinoma, of which type III NPC is the most common subtype.<sup>2</sup> The NPC can be induced by long-term smoking, Epstein–Barr virus (EBV) infection and genetic factors.<sup>3,4</sup> The incidence of NPC is regional, and mainly focused in the southern part of China, Southeast Asia and Northern Africa.<sup>5,6</sup>

The main treatment for head and neck cancer is surgery. However, due to the specific anatomical structure and growth characteristics of NPC, it is not suitable for surgical treatment.<sup>7</sup> Therefore, radiotherapy is the main treatment for NPC. Radiotherapy can directly kill the cancer cells or destroy the DNA structure of the cancer cells, rendering the cancer unable to multiply indefinitely and thus achieving the purpose of treatment. However, radiotherapy has certain limitations. Due to the different cell cycle of cancer cells, the sensitivity to radiotherapy is also different. Cells in the vigorous division stage are more sensitive, and cells in the stable stage have certain resistance to radiotherapy.<sup>7</sup>

Studies have found that the radioresistance mechanism of cells is related to the regulation of apoptosis, proliferation and migration of the cancer cells by miRNAs.<sup>8,9</sup> The miRNA coding genes are located in the introns of the protein coding genes and the introns or exons of noncoding genes.<sup>10</sup> The miRNAs can be fully or partially complementary to the 3'-UTR sequence of mRNA, and inhibit mRNA expression by cutting mRNA or repressing mRNA translation.<sup>11</sup> Usually, a single miRNA can regulate multiple genes, or multiple miRNAs can regulate one gene. Radiotherapy for NPC does not guarantee curing the disease. There is a large number of people experiencing relapse who need to be treated again.<sup>12</sup> The miRNA-based therapeutic approach has the benefit of being able to target multiple effectors of pathways participating in tumor cell differentiation and proliferation concurrently. Onco-miRNAs, tumor suppressive miRNAs, metastasis promoter or suppressor miRNAs, and EBV-encoded miRNAs could be a useful therapeutic strategy for NPC. Exosomal miRNAs might also serve as useful indicators of NPC.<sup>13</sup>

Research on the resistance mechanism of cancer cells to radiotherapy plays an important role in the treatment of NPC. With the rapid development of high-throughput sequencing in recent years, we can detect the type and expression of miRNA in cancer tissue, and use bioinformatics analysis to predict miRNA-targeted regulation genes and action pathway, so as to lay the foundation for future research on the mechanism of radiotherapy resistance of NPC.

## Objectives

In this study, we investigated the miRNA profiling of HONE1 and CNE2 after X-ray therapy. We subjected

the X-ray-sensitive NPC cell line CNE2 and X-ray-resistant NPC cell line HONE1 screened in the preliminary experiment to radiotherapy, performed post-treatment miRNA high-throughput sequencing for the control and model groups, miRNA species and expression analysis, target gene prediction and regulatory pathway enrichment analysis, and compared the differences of miRNAs in the 2 types of cell lines. The findings of this study may provide a reference for future research on anti-X-ray mechanism in NPC cells.

## Materials and methods

### Experimental materials

The HONE1 cells (BNCC338405) and CNE2 cells (BNCC100088) were purchased from Bena Culture Collection (Beijing, China).

This study was conducted in strict accordance to the standard guidelines and university procedures.

### Experimental reagents and instruments

The following reagents and equipment were used: Qubit 2.0 RNA detection kit (Q32855) and Qubit 2.0 DNA detection kit (Q10212; Life Technologies Corp., Carlsbad, USA); T4 RNA Ligase 1 (0011309) and T4 RNA Ligase 2 (0511412; New England Biolabs, Ipswich, USA); M-MuLV Reverse Transcriptase (B600005; Sangon Biotech Co., Ltd., Shanghai, China); Qubit2.0 fluorometer (Q32866; Invitrogen, Waltham, USA); micro vortex mixer (WH-3; Shanghai Luxi Analysis Instrument Factory Co., Ltd., Shanghai, China); desktop high-speed low-temperature centrifuge (Thermo Scientific Sorvall Legend Micro 21R; Thermo Fisher Scientific, Waltham, USA); polymerase chain reaction (PCR) instrument (T100™ Thermal Cycler; Bio-Rad Laboratories, Inc., Hercules, USA); electrophoresis instrument (DYY-11; Beijing Liuyi Biotechnology Co., Ltd., Beijing, China); and imaging analysis of nucleic acid and protein (FR-980A; Shanghai Furi Science & Technology Co., Ltd., Shanghai, China).

### Cell culture

The cells were plated, washed twice with 1× phosphate-buffered saline (PBS) and digested with 0.25% trypsin (containing 0.02% ethylenediaminetetraacetic acid (EDTA)) for 2–3 min; then, medium was added to terminate digestion and the cells were suspended. Then, the cells were collected into a 10-mL centrifuge tube, centrifuged at 1000 rpm for 3 min and the supernatant was discarded. Culture medium was added and the cell suspension was blown evenly through a pipette. After cell counting, the above cell suspension was diluted into the appropriate cell density according to the grouping, added to the prepared culture plate and cultured in a 37°C 5% CO<sub>2</sub> incubator.



## X-ray irradiation

When the cells were inoculated to 70% confluence, the model was initiated and 2 types of cells (HONE1 and CNE2) were treated with X-rays at 4 Gy, 8 Gy, 16 Gy, and 20 Gy doses. After treatment, flow cytometry apoptosis detection and Cell Counting Kit-8 (CCK-8) detection were performed.

## Apoptosis detected with flow cytometry

Approximately  $1 \times 10^6$  to  $3 \times 10^6$  cells were collected, 1 mL of PBS was added, and then the cells were centrifuged at 1500 rpm for 3 min and washed twice. Double distilled water was used to dilute the 5× binding buffer to 1× binding buffer, and 300 μL of precooled 1× binding buffer was used to resuspend the cells. Then, 3 μL of Annexin V-APC and 5 μL of 7-AAD were added into each tube, slightly mixed, and incubated at room temperature (RT) in the dark for 10 min. Subsequently, 200 μL of precooled 1× binding buffer was added into each tube, mixed and detected using flow cytometry.

## Cell viability detected by CCK-8

After X-ray irradiation of HONE1 and CNE2 cells, 10 μL of CCK-8 detection reagent were added into each well of a 96-well plate and incubated for 2 h at 37°C. The optical density (OD) value of each well was detected at 450 nm wavelength with the microplate reader and the cell viability rate was calculated.

## Construction of miRNA library

According to the small RNA with 3'-hydroxyl group and 5'-phosphate group structural characteristics, 3' adaptor ligation, reverse transcription primer hybridization, 5' adaptor ligation, cDNA single-stranded synthesis, and library amplification were performed on 4 types of cell samples – HONE1\_Control (HONE1\_C), HONE1\_Model (HONE1\_M), CNE2\_Control (CNE2\_C) and CNE2\_Model (CNE2\_M) – using related enzyme catalytic reaction characteristics and molecular biology techniques. After quality inspection and purification, a library that satisfied the sequencing requirement of the Illumina platform (<http://www.usadellab.org/cms/?page=trimmomatic>) was finally obtained.

## Database and analysis methods

The databases used in the study included:

1. Rfam (v. 12.0, <http://rfam.xfam.org/>)

Rfam is a database of the non-coding RNA (ncRNA) family expressed by multiple sequence alignment and covariance model (CM) for homology detection and sequence alignment, and used for enrichment analysis of the miRNA family.

2. miRBase (v. 21; <http://www.mirbase.org/ftp.shtml>)

After miRNA quantification, the analysis was performed on miRBase with known miRNA family information.

3. miRDB (<http://mirdb.org/index.html>), miRTarBase 7.0 (<http://www.microrna.gr/tarbase>)

This database is used to predict miRNAs and target binding genes.

4. mirPath (<http://www.microrna.gr/miRPathv2>)

This database is used to integrate miRNA interacting genes into various regulatory pathways.

5. Gene Ontology (GO; <http://www.geneontology.org/>)

The GO database is used for enrichment analysis of gene function.

6. Kyoto Encyclopedia of Genes and Genomes (KEGG pathway; <http://www.genome.jp/kegg/pathway.html>)

This database is used to enrich and analyze the role of miRNA in various interaction pathways.

## The miRNA quality control analysis

The 3' adapter was removed from the raw data. The software used was Cutadapt (<https://cutadapt.readthedocs.io/en/stable/installation.html>). The length of reads after removing the adapter was set to be within 17–35 bp. The reads after removing the adapter were treated with Trimmomatic (v. 0.36; <http://www.usadellab.org/cms/?page=trimmomatic>).<sup>14</sup> The bases with a quality value lower than 20 at the 5' and 3' terminals were deleted; 4 consecutive bases with an average quality value of <20 and reads with length of <17 after processing were filtered out in order to obtain total reads. The reads with duplicates removed were called unique reads and the number of reads was statistically analyzed.

## Comparison of reference genomes and classification annotation

Bowtie (<http://bowtie-bio.sourceforge.net/index.shtml>) was used to compare the reads of each sample with the reference genome (mismatch was set to ≤1). The number and percentage of reads were counted, and the reads that could not be compared to the reference genome were filtered. The reads were annotated and counted in the sequence of rRNA, tRNA, snRNA, snoRNA, miRNA, and others. The reads of miRNA sequencing might contain other small RNAs. The analysis was performed using Blastn search tool (<https://blast.ncbi.nlm.nih.gov/Blast.cgi>) for reads, with rRNA, sRNA, snRNA, and snoRNA of the Rfam<sup>2</sup> database. The alignment conditions were set as follows: gapopen 0, evaluate < 0.01 and mismatch ≤ 1, and the reads on the alignment were filtered out.

## The miRNA family prediction

MicroRNA family is a group of miRNAs from the same ancestor. They usually have similar biological functions, but not necessarily conservative in primary and secondary structures.

After miRNA quantification was completed, the known miRNA family information on miRBase was used for analysis. The miRNAs that did not belong to any family were represented by “not applicable” (N/A). These miRNAs is not classified into any miRNA family; some detected miRNAs have not been studied yet, and their structures are different from the miRNA structures of the currently known families.

## The miRNA expression analysis

The expression levels of miRNAs were evaluated. By calculating reads per million (RPM), the counts were normalized to RPM value. The boxplot was constructed for the RPM of the sample to show the RPM distribution. This article mainly displayed the data analysis of the top 20 miRNAs with the highest total miRNA expressions.

## The miRNA target gene prediction

The miRTarBase ([http://www.targetscan.org/vert\\_72/](http://www.targetscan.org/vert_72/)) was used to predict the target genes that the miRNAs might bind to in the cancer gene pathway. The miRDB database was used to rescreen genes that might interact with miRNAs. TargetScan database is a predictor that produces predicted interactions, while miRTarBase and miRDB databases provide verified target genes that have binding sites with miRNAs. The miRNAs and target genes that play a role in cancer genes were screened out and the miRNA-gene interaction network was constructed using Cytoscape v. 3.8.0 (<https://cytoscape.org/>).

## Gene enrichment analysis

The mRNA-targeted binding genes were used as the target gene. The GO and KEGG pathway annotation of the species were used for enrichment analysis. By classifying, sorting and analyzing GO functional annotations, the differences in the GO annotation distribution of different target gene sets were displayed in the form of a bar graph, and the biological significance of corresponding miRNAs was explored. The software used for GO enrichment analysis was clusterProfiler (<https://www.rdocumentation.org/packages/clusterProfiler/versions/3.0.4>), and the network diagram drawing software was iGraph (<https://igraph.org/>). The KEGG pathway database collects biological pathways. Each pathway contains molecular interactions and metabolic reactions, a network diagram connecting genes and gene products. The clusterProfiler was used for KEGG pathway enrichment analysis.

## Statistical analyses

All bioinformatics statistics were performed using R software (<https://www.r-project.org>). The data obtained from the cells experiment were plotted using GraphPad Prism

v. 8.0.1 (GraphPad Software, San Diego, USA), and analyzed with IBM SPSS v. 19.0 (IBM Corp., Armonk, USA). The comparison between groups was performed using Kruskal–Wallis test. A value of  $p < 0.05$  indicated significant difference.

# Results

## Cellular X-ray therapy modeling

In the preliminary experiment, we irradiated several NPC cell lines with different doses of X-rays, established a 24-hour 20 Gy X-ray dose as the optimal therapy conditions, and screened out the NPC cell line CNE2 with the best therapy effects and NPC cell line HONE1 with the worst therapy effects. The CCK-8 and flow cytometry detection of cell viability and apoptosis were performed on these 2 cell lines. The HONE1 and CNE2 cells were irradiated with X-rays at doses of 4 Gy, 8 Gy, 16 Gy, and 20 Gy for 24 h. Compared with the control group, the cell viability rate for CNE2 at 8 Gy dose and for HONE1 at 16 Gy and 20 Gy doses decreased significantly; the apoptosis rate for CNE2 at 20 Gy dose increased significantly (Fig. 1 and Supplementary Table 1 and 2: <https://doi.org/10.5281/zenodo.6132842>). High-throughput sequencing was performed on the modeled CNE2\_C, CNE2\_M, HONE1\_C, and HONE1\_M groups.

## miRNA quality control analysis

The quality of the sequenced raw data was evaluated using FastQC (<https://www.bioinformatics.babraham.ac.uk/projects/fastqc/>), and the Rawdata reads were screened. The screening condition was set to reads, with a length of 17–35 bp, and an average base quality value >20. The Cleandata reads were obtained. After removing the duplicate data, Uniq\_reads were acquired. Compared with the number of CNE2\_C miRNA reads, the number of miRNA reads in the CNE2\_M group was significantly increased. The results are shown in Table 1.

## The miRNA annotation analysis

Blastn search tool was used to compare the reads in CNE2\_C, CNE2\_M, HONE1\_C and HONE1\_M with tRNA, snRNA, snoRNA, rRNA, mRNA, and miRNA in the Rfam database. The number and percentage of reads of the comparison were calculated, and a pie chart was built (Fig. 2). The miRNAs accounted for 26.5%, 31.7%, 21.3%, and 22.9% of the Cleandata reads count in CNE2\_C, CNE2\_M, HONE1\_C and HONE1\_M, respectively. The contents of tRNA, snRNA, snoRNA, rRNA, and mRNA are shown in Fig. 2. The contents of rRNA were relatively high, with 24.9%, 14.7%, 25.1%, and 25.1% of the Cleandata reads count, respectively.

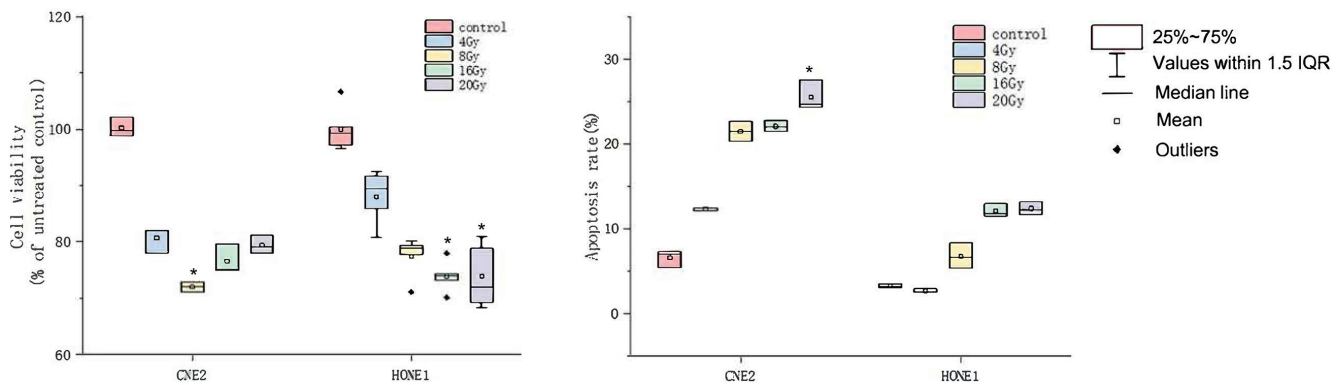


**Fig. 1.** Cell viability rate and apoptosis rate. Compared with the control group, \**p* < 0.05. The box-and-whiskers are built of the ranges without outliers (whiskers), interquartile ranges (IQR; boxes) and medians. The black quadrates represent outliers whose values were more than 1.5 IQR above the 3<sup>rd</sup> quartile or below the 1<sup>st</sup> quartile

**Table 1.** Reads statistics

Sample	CNE2_C	CNE2_M	HONE1_C	HONE1_M
Rawdata_reads_count	19433472	17093316	17680806	17887854
Cleandata_reads_count	7298449	10721464	8153171	8027142
Uniq_reads_count	752853	949023	813644	871208
miRNA_total_reads	1937301 (26.5%)	3399170 (31.7%)	1739849 (21.3%)	1845162 (22.9%)

### The miRNA expression distribution analysis

In order to show the overall expression distribution of miRNAs in each group, the RPM log<sub>10</sub> of miRNAs in each group was taken and a box plot was built, as shown in Fig. 3A. It can be seen that the median of the CNE2\_M group was lower than in the other groups, indicating that in the CNE2\_M group, there were more miRNAs with low expression levels. However, in the quality control analysis, the miRNA\_total\_reads of the CNE2\_M group was higher than of the other 3 groups, indicating that the expression levels of some miRNAs in the CNE2\_M group was abnormally high. We took the top 20 miRNAs in expression for heat map cluster analysis, as shown in Fig. 3B. The Z-cord value of RPM was used for the heat map cluster analysis. Red represented high expression and green represented low expression. It could be seen that in the CNE2\_M group, the amount of miRNAs with expressions which appeared red was higher than in the other 3 groups. The expressions of the HONE1 cells were low and appeared as green miRNAs, while most of those in the CNE2 group were relatively high and appeared red. Among them, there were significant differences in the expressions of hsa-miR-21-5p, hsa-let-7a-5p, hsa-miR-125a-5p, hsa-miR-26a-5p, hsa-let-7f-5p, hsa-miR-20a-5p, and hsa-miR-24a-3p between the HONE1 and CNE2 cell lines. There were also differentially expressed miRNAs in HONE1\_C vs. HONE1\_M, such as hsa-miR-21-5p and hsa-let-7i-5p, and in CNE2\_C vs. CNE2\_M, such as hsa-miR-148b-3p.

### The miRNA family prediction analysis

The quantified miRNAs were analyzed using the known miRNA family information in the miRBase, and miRNAs that did not belong to any family were marked as N/A. We selected the top 20 miRNAs in family total reads for family prediction analysis. As shown in Fig. 3C, these families were mir-21, mir-10, let-7, mir-24, mir-27, mir-26, mir-28, mir-30, mir-25, mir-17, mir-15, mir-205, mir-8, mir-148, mir-103, mir-365, mir-23, mir-378, and mir-181. Among them, the reads of miR-21, mir-10 and let-7 families were relatively higher than reads for other miRs.

### The miRNA target gene interaction analysis

We used miRTarBase and miRDB online software ([http://www.targetscan.org/vert\\_72/](http://www.targetscan.org/vert_72/) and <http://mirdb.org/mirdb/index.html>) to predict target genes for the top 20 miRNAs with the highest number of reads in Uniq\_reads, enriched the interacting genes in various pathways, and constructed a miRNA-gene interaction network diagram using Cytoscape v. 3.8.0 (<https://cytoscape.org/>). The cancer, transforming growth factor beta (TGF-β), p53, phosphatidylinositol 3-kinase (PI3K)-protein kinase B (Akt), mitogen-activated protein kinase (MAPK), and forkhead box O (FoxO) signaling pathways play an important role in regulating cancer cell proliferation, apoptosis and migration. The miRNAs that interact with these signaling pathways were selected and network interaction maps were built. The network interaction map for the miRNA-cancer

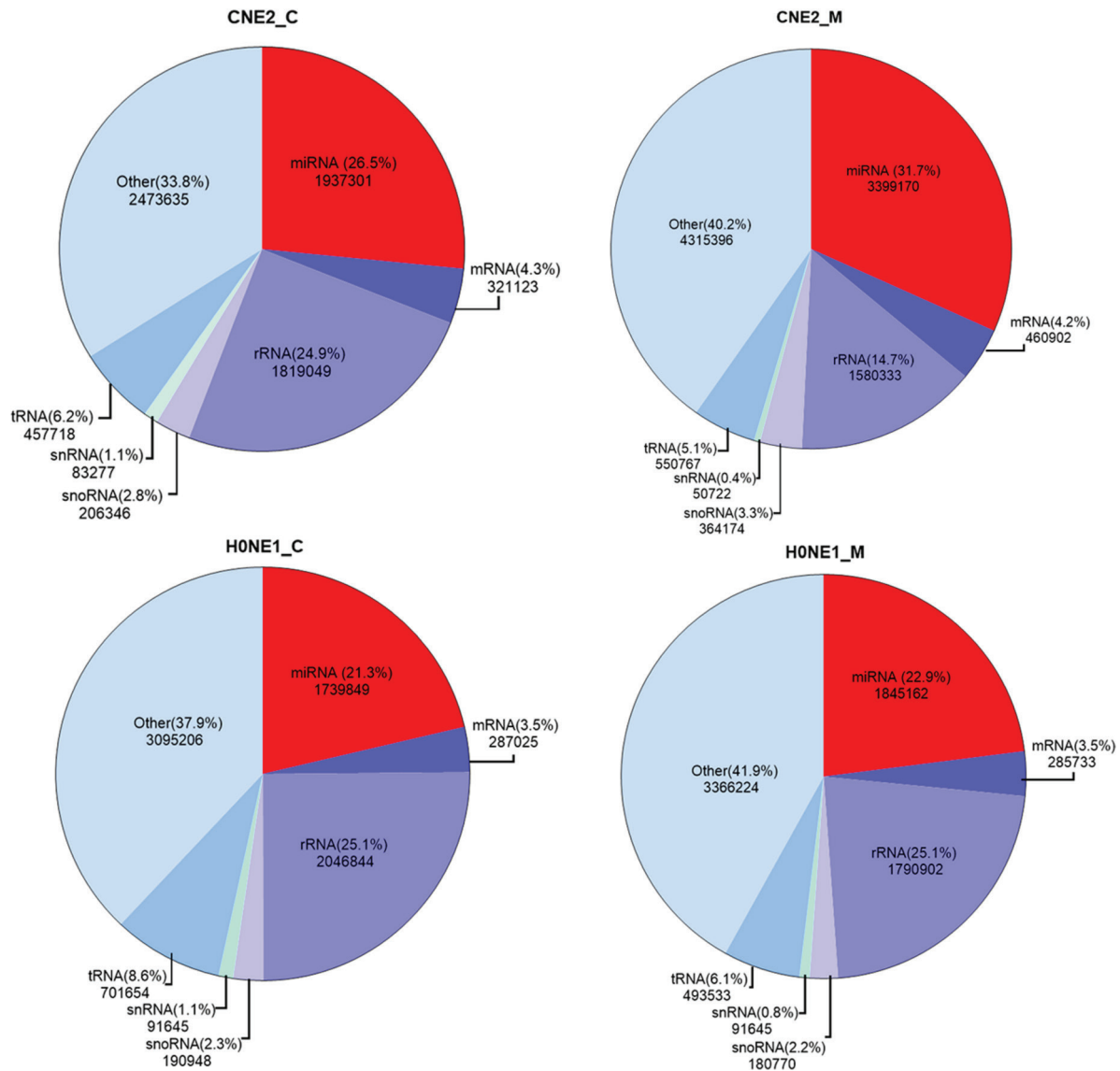


Fig. 2. RNA annotation diagram

signaling pathway was shown in Fig. 3D. The network interaction map for other pathways were presented in Fig. 4A–4E.

The gene analysis of the interactions of various pathways found that hsa-miR-17-5p and hsa-miR-20a-5p in the cancer, TGF- $\beta$ , PI3K-Akt, MAPK, and FoxO signaling pathways co-regulated MAPK1, son of sevenless homolog 1 (*SOS1*) and transforming growth factor beta receptor II (*TGF $\beta$ R2*) genes. The hsa-let-7a-5p, hsa-let-7f-5p and hsa-let-7i-5p in the cancer, TGF- $\beta$  and MAPK pathways targeted and regulated the *TGF $\beta$ R1* gene. The hsa-let-7a-5p, hsa-let-7f-5p and hsa-let-7i-5p in the cancer, MAPK and p53 signaling pathways targeted and regulated the tumor protein 53 (*TP53*) and caspase 3 (*CASP3*) genes. The hsa-miR-30e-5p, hsa-miR-92a-3p and hsa-miR-200c-3p in the cancer, p53 and PI3K-Akt signaling pathways targeted and regulated the cyclin E2 (*CCNE2*) gene. The hsa-miR-92a-3p, hsa-miR-26a-5p and hsa-miR-148b-3p in the cancer, p53

and FoxO signaling pathways targeted and regulated phosphatase and tensin homolog (*PTEN*) gene. The hsa-miR-200c-3p in the cancer, p53 and PI3K-Akt signaling pathways targeted and regulated the *CDK2* gene. The specific miRNA corresponding pathways and target genes are shown in Table 2.

### The miRNA-targeted GO and KEGG pathway enrichment analyses

Enrichment analysis was performed on HONE1\_M vs. CNE2\_M differentially expressed miRNA interacting genes. The enrichment paths of the top 10 counts were displayed in a bar graph (Fig. 5). As shown in Fig. 5, the GO analysis showed that HONE1\_M vs. CNE2\_M was mainly enriched in biological process such as negative regulation of transcription from RNA polymerase II promoter (GO:0000122), and positive regulation of transcription

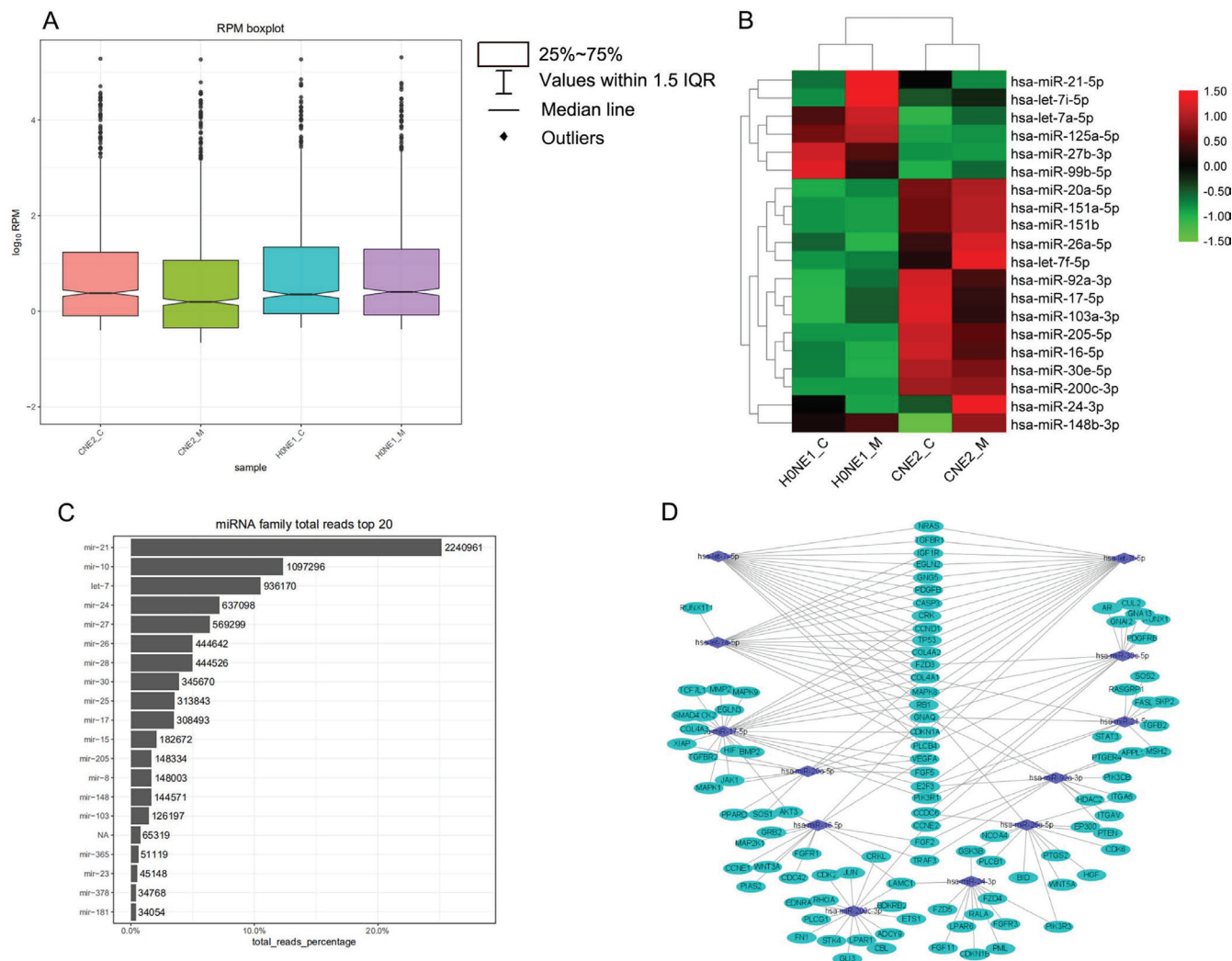


**Fig. 3.** Map of total miRNA expressions. A. Overall expression distribution of miRNAs in each group. The box-and-whiskers are built of the ranges without outliers (whiskers), interquartile ranges (IQRs) (boxes) and medians. The black quadrates represent outliers whose values were more than 1.5 IQR above the 3<sup>rd</sup> quartile or below the 1<sup>st</sup> quartile; B. Heat map cluster analysis; C. Family prediction analysis; D. Network interaction map for the miRNA-cancer signaling pathway

from RNA polymerase II promoter (GO:0045944), cellular component such as cytosol (GO:0005829), and molecular function such as protein binding (GO:0005515). In KEGG pathway enrichment analysis, the differentially expressed miRNA interacting genes in HONE1\_M vs. CNE2\_M were enriched in the cancer-related pathways, such as pathways in cancer (hsa05200), MAPK signaling pathway (hsa04010) and Wnt signaling pathway (hsa04310). The GO and KEGG pathway enrichment analyses for other groups are shown in Fig. 6–8.

## Discussion

At present, NPC is mainly treated with radiotherapy, but the treatment effect is not very satisfactory. Most people with NPC will relapse and need to undergo radiotherapy again, which cause a heavy burden to the patient and economy. In radiotherapy, some cancer cells will resist

radiation, causing reduction in the apoptosis rate of cancer cells. This resistance is related to the regulation of gene expressions in cell proliferation, apoptosis and migration by miRNA.<sup>15–17</sup> The miRNA enhances the reproductive ability of cancer cells<sup>18</sup> and increases the resistance to radiation by downregulating the apoptotic genes of cancer cells, upregulating the expression of proliferation genes or disrupting the cell cycle. There are several cancer cell lines in NPC. In our preliminary experiments, we screened out the X-ray-sensitive CNE2 and the X-ray-insensitive HONE1 cell lines. We performed high-throughput sequencing on these 2 types of irradiated cell lines and explored which miRNAs between the different cell lines regulate related genes to resist X-ray therapy.

We sorted out the data of 4 groups – CNE2\_C, CNE2\_M, HONE1\_C, and HONE1\_M – for high-throughput sequencing quality control. After screening by miRNA length and removing duplicate data, we found that the number of reads of CNE2\_C and CNE2\_M was higher

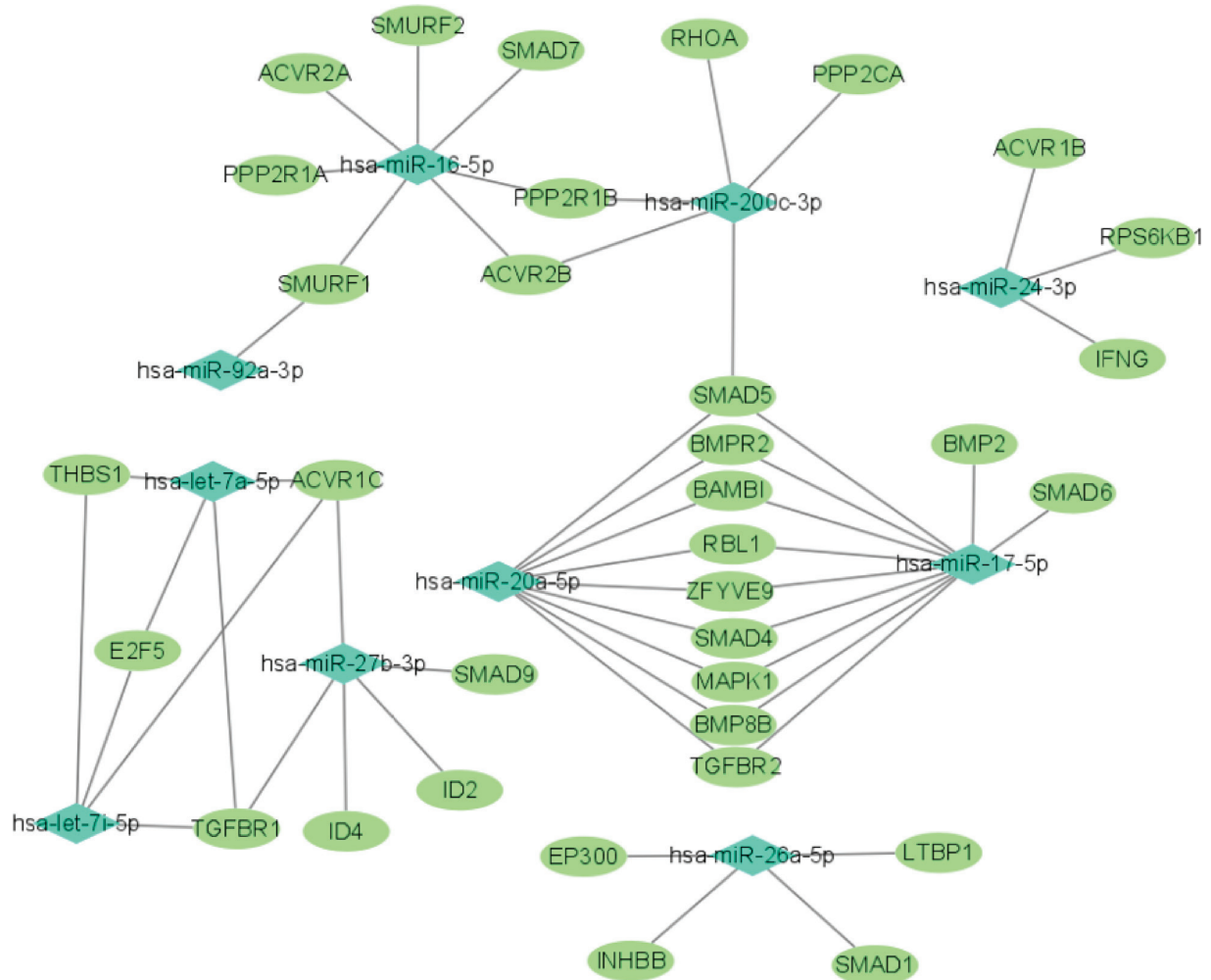


Fig. 4A. Network interaction map for other pathways. The miRNA-transforming growth factor beta (TGF- $\beta$ ) signaling pathway

Table 2. Statistics of miRNA in corresponding pathway-targeted genes

Name of targeted gene	Cancer	TGF- $\beta$	p53	PI3K-Akt	MAPK	FoxO
MAPK1	hsa-miR-17-5p hsa-miR-20a-5p	hsa-miR-17-5p hsa-miR-20a-5p	N/A	hsa-miR-17-5p hsa-miR-20a-5p	hsa-miR-17-5p hsa-miR-20a-5p	N/A
SOS1	hsa-miR-20a-5p	N/A	N/A	hsa-miR-20a-5p	hsa-miR-20a-5p	hsa-miR-20a-5p
TGFBR1	hsa-let-7f-5p hsa-let-7i-5p	hsa-let-7f-5p hsa-let-7i-5p	N/A	N/A	hsa-let-7a-5p hsa-let-7f-5p hsa-let-7i-5p	N/A
TGFBR2	hsa-miR-17-5p hsa-miR-20a-5p	hsa-miR-17-5p hsa-miR-20a-5p	N/A	N/A	hsa-miR-17-5p hsa-miR-20a-5p	hsa-miR-17-5p hsa-miR-20a-5p
TP53	hsa-let-7a-5p hsa-let-7f-5p hsa-let-7i-5p	N/A	hsa-let-7a-5p hsa-let-7f-5p hsa-let-7i-5p	N/A	hsa-let-7a-5p hsa-let-7f-5p hsa-let-7i-5p	N/A
CASP3	hsa-let-7a-5p hsa-let-7f-5p hsa-let-7i-5p	N/A	hsa-let-7a-5p hsa-let-7f-5p hsa-let-7i-5p	N/A	hsa-let-7a-5p hsa-let-7f-5p hsa-let-7i-5p	N/A
CCNE2	hsa-miR-30e-5p hsa-miR-92a-3p hsa-miR-200c-3p	N/A	hsa-miR-16-5p hsa-miR-30e-5p hsa-miR-200c-3p	hsa-miR-200c-3p	N/A	N/A
PTEN	hsa-miR-92a-3p hsa-miR-26a-5p	N/A	hsa-miR-26a-5p hsa-miR-148b-3p	N/A	N/A	hsa-miR-92a-3p hsa-miR-148b-3p
CDK2	hsa-miR-200c-3p	N/A	hsa-miR-200c-3p	hsa-miR-200c-3p	N/A	N/A

N/A – not applicable; TGF- $\beta$  – transforming growth factor beta; PI3K-Akt – phosphatidylinositol 3-kinase-protein kinase B; MAPK – mitogen-activated protein kinase; FoxO – forkhead box O.

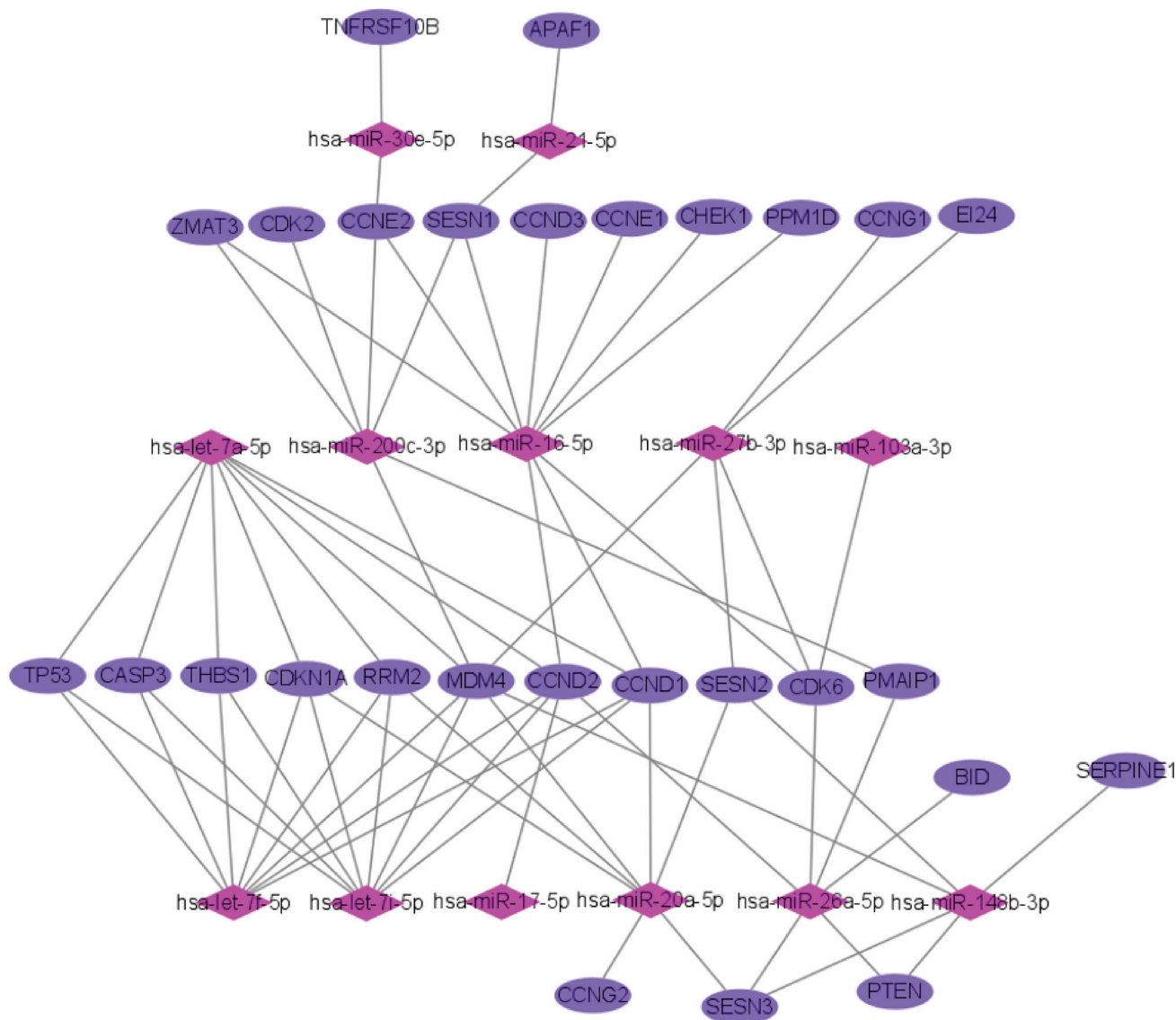


Fig. 4B. Network interaction map for other pathways. The miRNA-p53 signaling pathway

than that of HONE1\_C and HONE1\_M, and at the same time, we performed boxplot analysis and heat map analysis on the expression levels. The boxplot showed that the median value of CNE2\_M was lower than the other 3 groups. There were relatively more low expression miRNAs in CNE2\_M, but because there were outliers with relatively high number of reads, the miRNA expressions in CNE2\_M were relatively high, and the heat map cluster analysis also showed that the amount of miRNAs with high expression were relatively higher. At the same time, the sequenced RNA species were annotated, and among them, miRNA and rRNA accounted for a relatively larger proportion of the Cleandata reads count.

We conducted a detailed analysis of the top 20 miRNAs in terms of expression, predicted the miRNA family and performed cluster analysis of the miRNA expression levels. The 3 families of mir-21, mir-10 and let-7 had the highest number of miRNA reads, which was consistent with the results of the heat map analysis. In the heat map analysis,

the expression level of miRNA-21-5p in the HONE1\_M group was higher than that of the CNE2\_M and HONE1\_C groups. Flow cytometry experiments showed that the apoptosis rate of HONE1\_M was lower than that of the CNE2\_M group. It is speculated that miRNA-21-5p is related to radiation resistance and inhibition of apoptosis in HONE1\_M cells. Studies have found that miR-21 can enhance the resistance of cancer cells to radiotherapy.<sup>19</sup> The expression of miR-21 is increased in NPC tissues, downregulated the expression of B-cell lymphoma 2 (bcl2), and inhibited cell migration.<sup>20</sup> The miR-21 and miR-205 enhance the resistance of cancer cells to radiotherapy by regulating the PTEN signaling pathway.<sup>21–23</sup> The EBV infection can lead to NPC. The proto-oncogene latent membrane protein (LMP)1 of EBV can upregulate miR-21, negatively regulate the pro-apoptotic factor programmed cell death (PDCD)4 and Fas ligand (Fas-L), and increase the resistance of NPC cells to cisplatin.<sup>24</sup> The expressions of let-7i-5p and let-7a-5p of the let-7 family in the 2 groups of HONE1 were higher

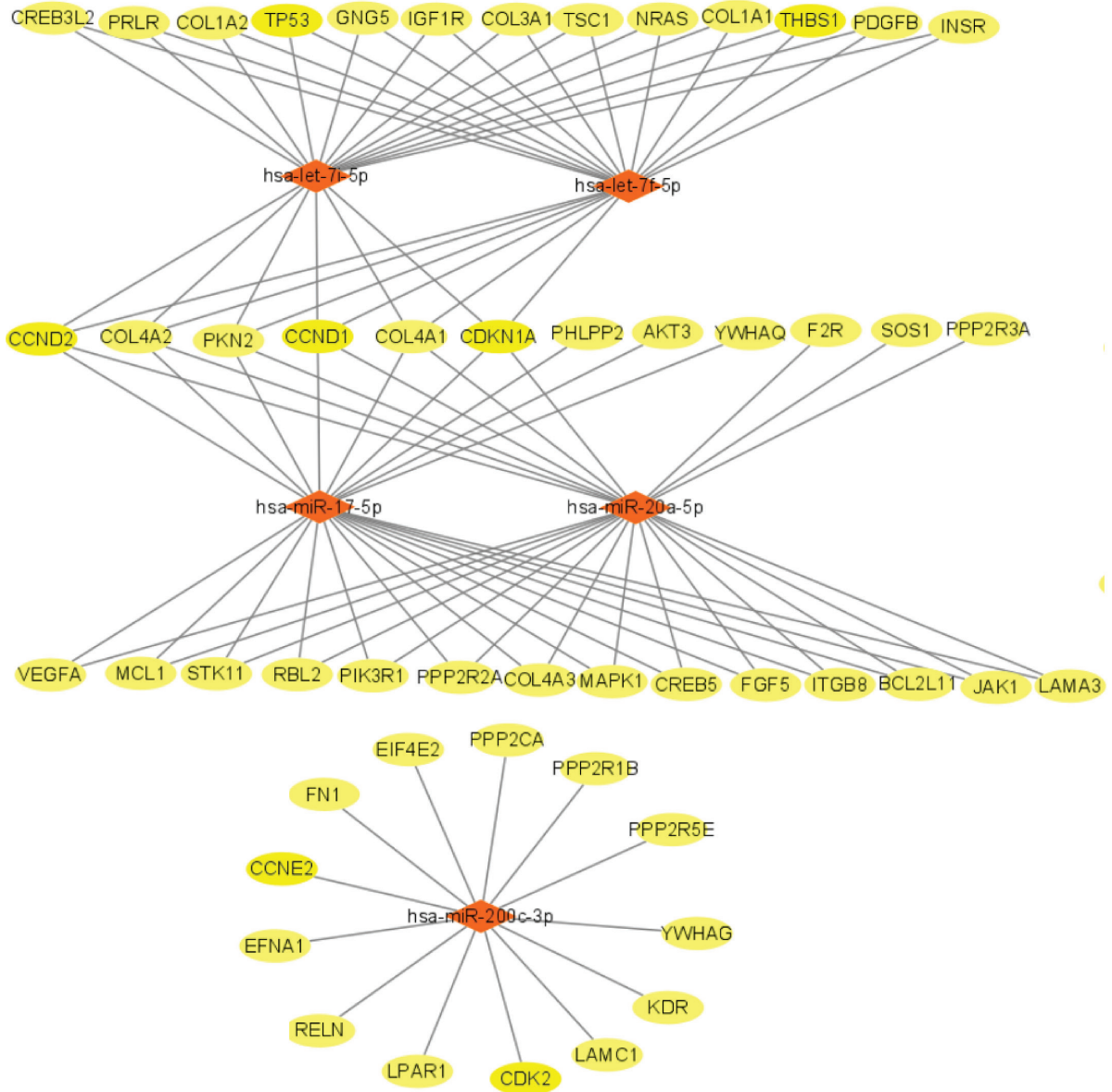


Fig. 4C. Network interaction map for other pathways. The miRNA-phosphatidylinositol 3-kinase-protein kinase B (PI3K-Akt) signaling pathway

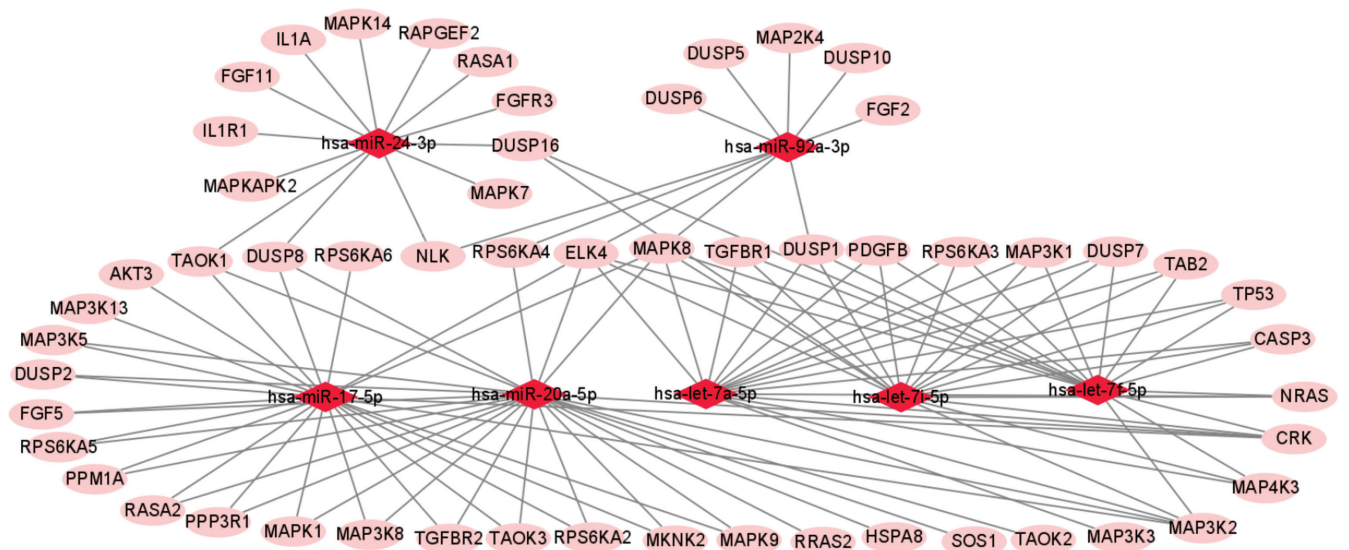


Fig. 4D. Network interaction map for other pathways. The miRNA-mitogen-activated protein kinase (MAPK) signaling pathway



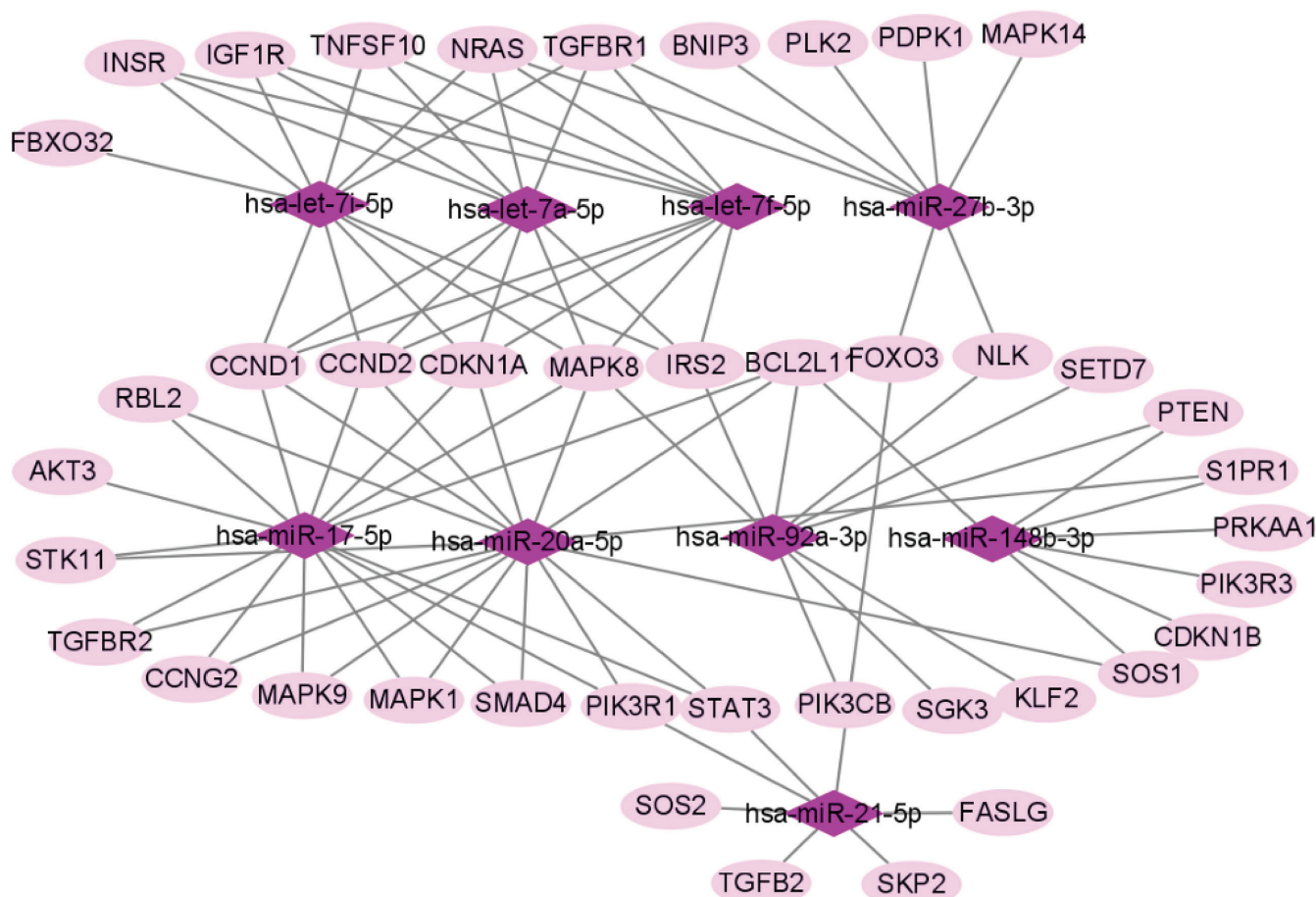


Fig. 4E. Network interaction map for other pathways. The miRNA-forkhead box O (FoxO) signaling pathway

than in the CNE2 cells. It is speculated that let-7 is related to the resistance of HONE1 to X-rays. The let-7 family is one of the best known miRNA families in cancer biology. It inhibits the proliferation of NPC cells by downregulating the expression of c-Myc.<sup>25</sup> The X-rays can enhance the expression of let-7 in NPC cells and inhibit the expression of miR-7, which may increase the radiosensitivity of NPC cells.<sup>26</sup>

In the heat map analysis, the high expression of hsa-miR-125a-5p in HONE1\_M appeared red, and the low expression in CNE2\_M appeared green. This differential expression implied that hsa-miR-125a-5p plays an important role in the resistance of cancer cells to radiotherapy. Studies have found that miR-125a-5p can increase p53 protein expression in HNE-1 cells, reduce human epidermal growth factor receptor 2 (Her2) protein expression in HNE-1 and HK-1 cells,<sup>27</sup> and promote the proliferation, migration and invasion of HONE1 cells. The expression level of miR-125a-5p in NPC patients was significantly higher than that in healthy controls.<sup>28</sup>

In the heat map analysis, the expression levels of hsa-miR-26a-5p, hsa-miR-24a-3p and hsa-miR-20a-5p in CNE2\_M were high and appeared red, while the expression levels in HONE1\_M were low and appeared green. We speculated that these 3 miRNAs are related

to the resistance of cancer cells to radiation therapy. The miR-26a has the effect of inhibiting the growth of NPC cells; miR-26a can significantly downregulate the expression of enhancer of zeste homolog 2 (EZH2),<sup>29</sup> activate p14 (ARF) and p21 (CIP1), maintain the cell cycle in the G1 phase, enhance the sensitivity of cell to radiation, and inhibit the growth and migration of cancer cells.<sup>29,30</sup> Radiation therapy damages the DNA of NPC cells. Cancer cells can repair part of the damage and inhibit apoptosis. The miR-24 can bind to Jun activation domain-binding protein 1 (Jab1) to inhibit the repair of DNA damage and increase the sensitivity of NPC cells to radiotherapy.<sup>31</sup> Some studies have found that the expression of miR-24 is decreased in patients with advanced NPC, which reduces the sensitivity to radiotherapy.<sup>31,32</sup> The miR-20a-5p can regulate the expression of neuronal PAS domain protein (NPAS)2 and Rab27B to reduce the sensitivity of NPC cells to radiotherapy.<sup>33,34</sup> In this study, the expressions of hsa-miR-26a-5p, hsa-miR-24a-3p and hsa-miR-20a-5p in the HONE1\_M group were lower than in the CNE2\_M group. We speculated that it is likely that the combined action of these 3 miRNAs co-downregulated the sensitivity of cells to X-rays in the HONE1\_M group.

We predicted the target genes of the top 20 miRNAs with the highest number of reads in Uniq\_reads, and

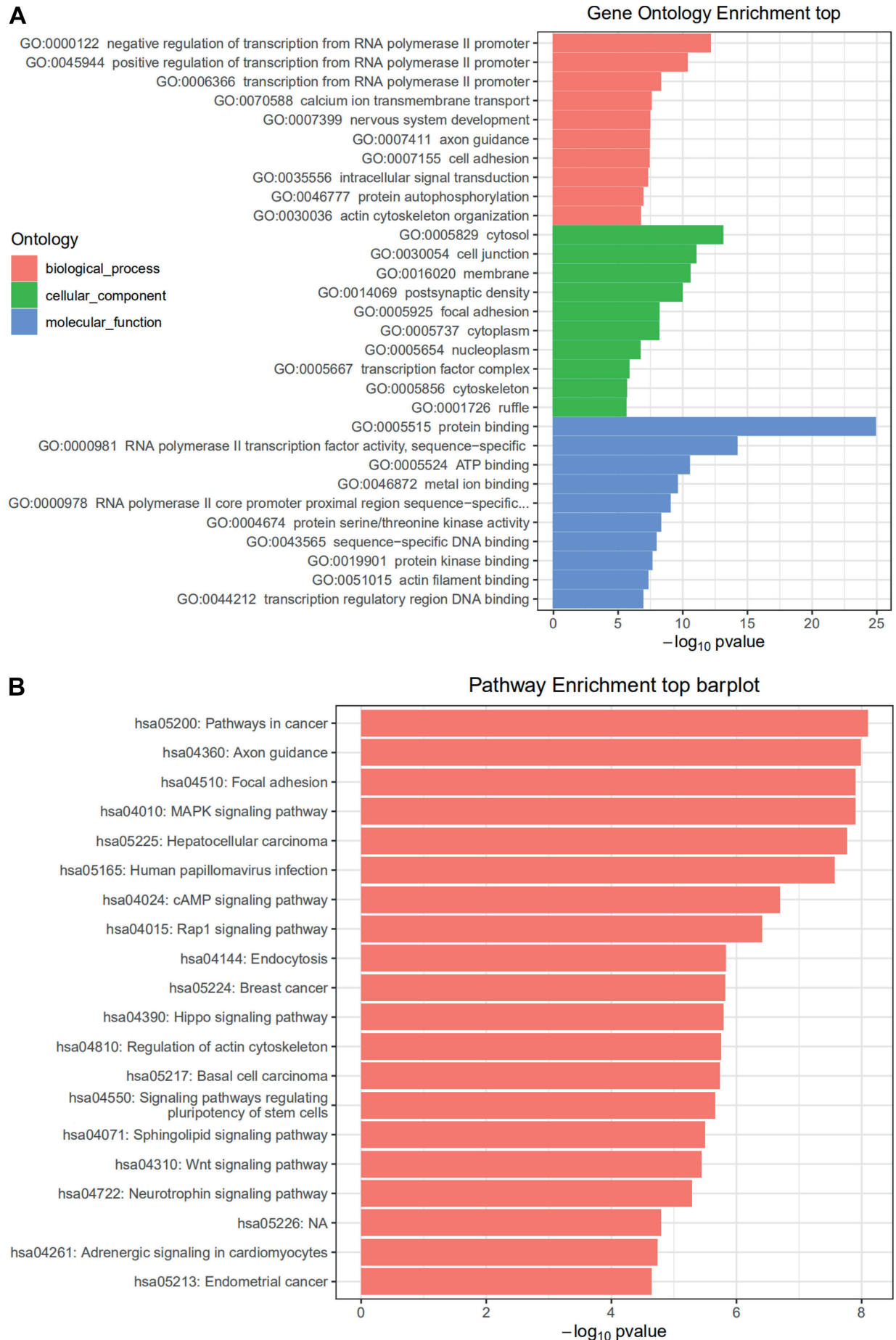
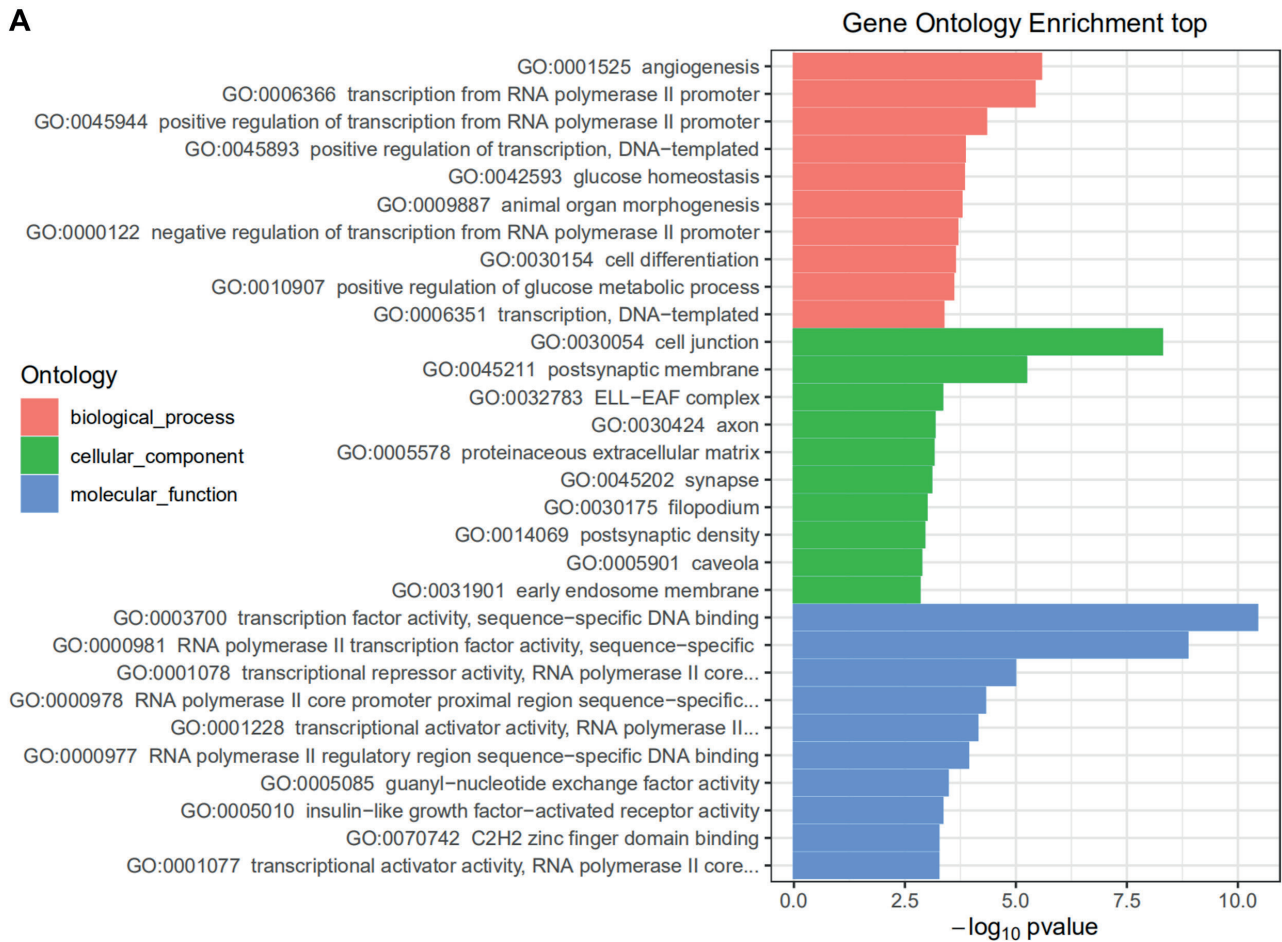
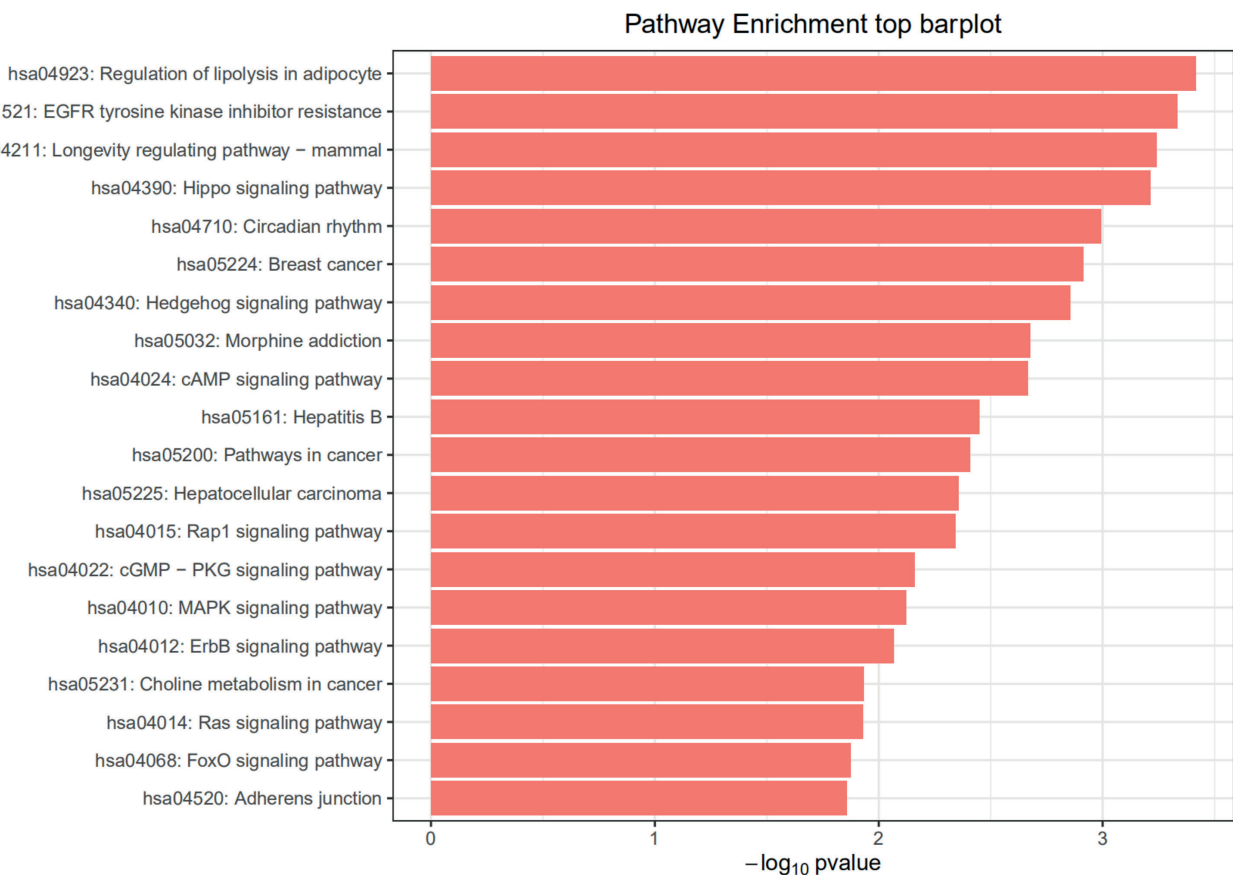
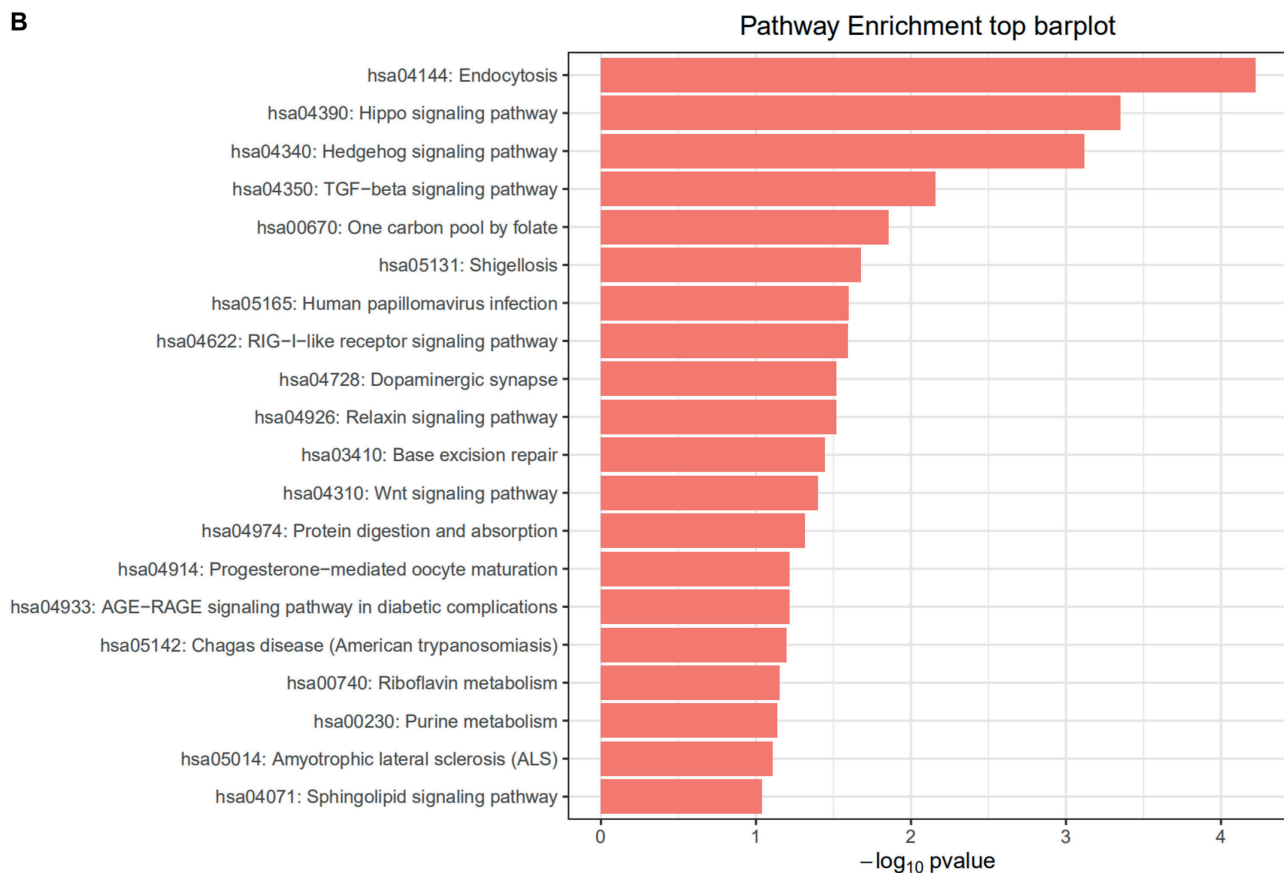
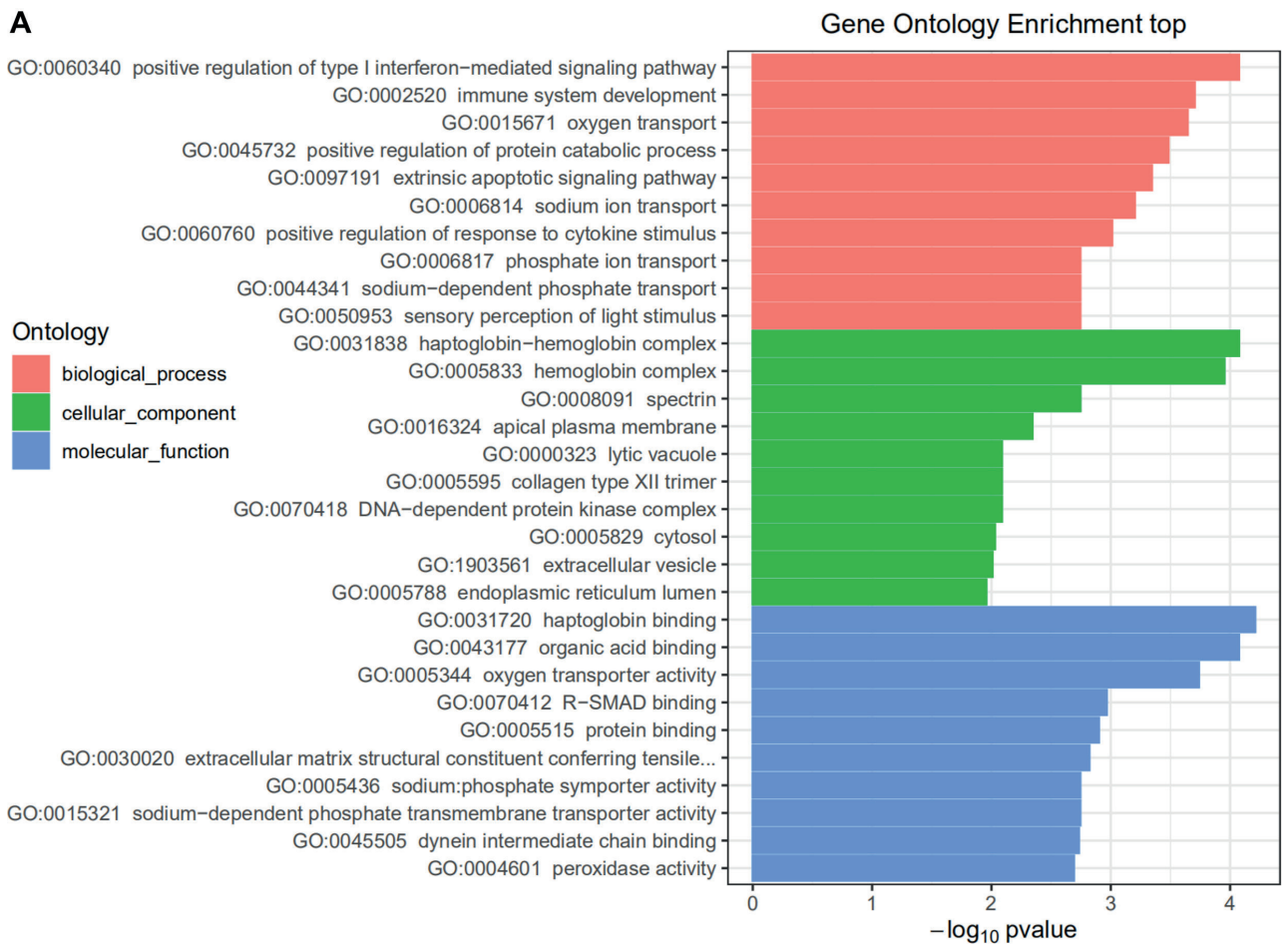


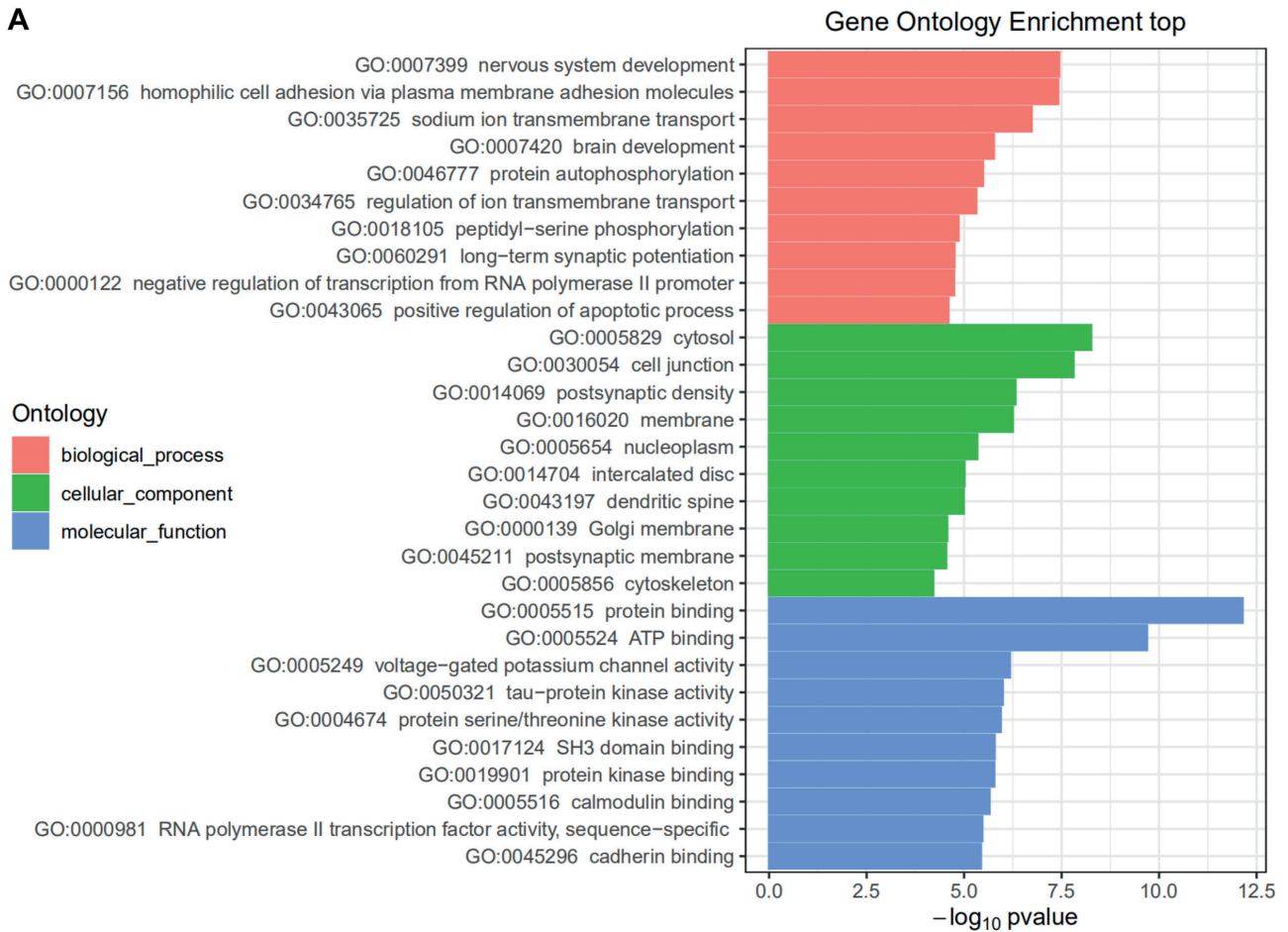
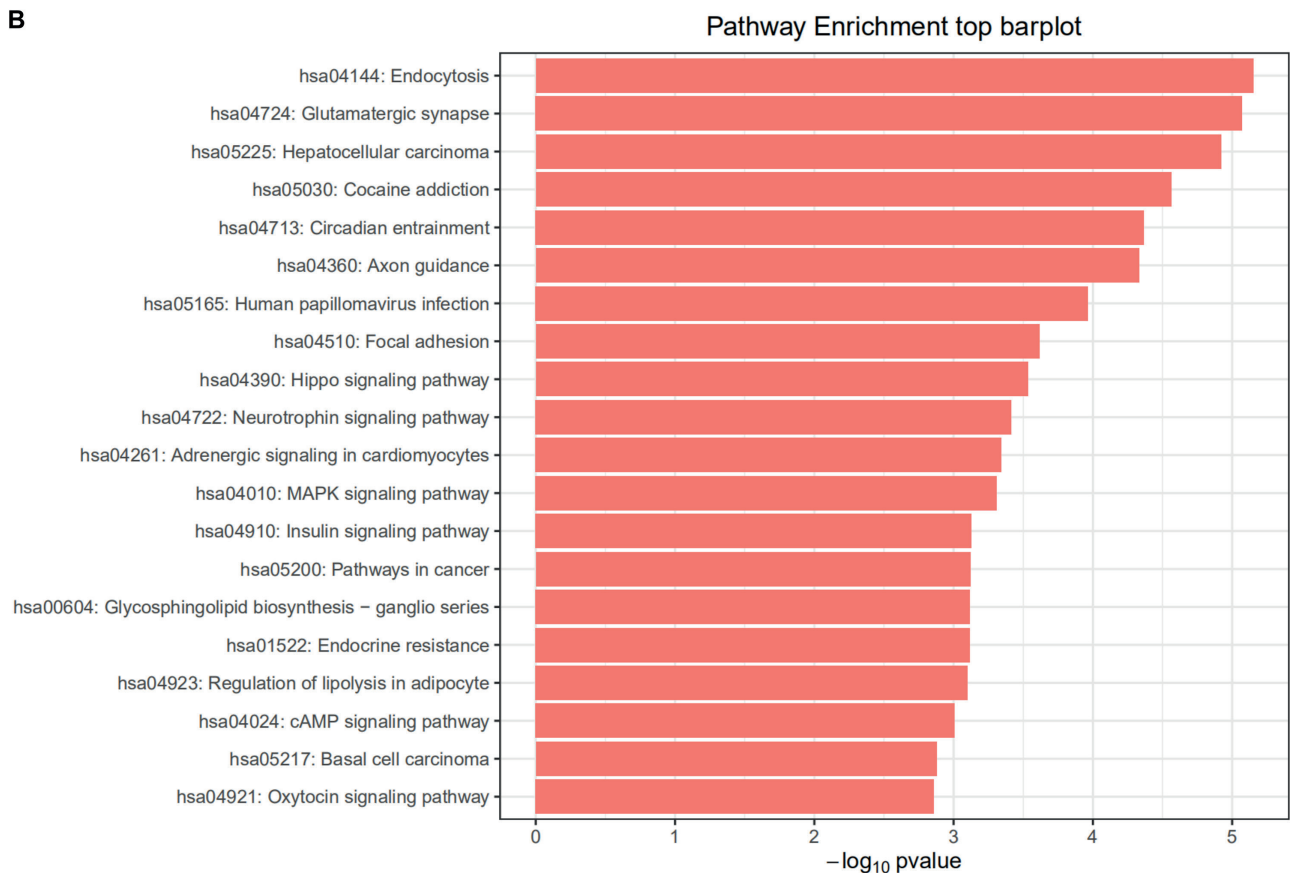
Fig. 5. HONE1\_M vs. CNE2\_M (A) Gene Ontology (GO) and (B) Kyoto Encyclopedia of Genes and Genomes (KEGG) pathway enrichment analyses

**A****B**

**Fig. 6.** CNE2\_M vs. CNE2\_C (A) Gene Ontology (GO) and (B) Kyoto Encyclopedia of Genes and Genomes (KEGG) pathway enrichment analyses. The GO analysis showed that CNE2\_M vs. CNE2\_C was mainly enriched in biological process such as angiogenesis (GO:0001525), cellular component such as cell junction (GO:0030054), and molecular function such as transcription factor activity, sequence-specific DNA binding (GO:0003700). In KEGG analysis, the genes that interact with miRNAs in the CNE2\_M vs. CNE2\_C group were enriched in the pathways in cancer (hsa05200), FoxO signaling pathway (hsa04068), MAPK signaling pathway (hsa04010), etc.



**Fig. 7.** HONE1\_M vs. HONE1\_C (A) Gene Ontology (GO) and (B) Kyoto Encyclopedia of Genes and Genomes (KEGG) pathway enrichment analyses. The GO analysis showed that HONE1\_M vs. HONE1\_C was mainly enriched in biological process such as positive regulation of type I interferon-mediated signaling pathway (GO:0060340), cellular component such as haptoglobin-hemoglobin complex (GO:0031838) and molecular function such as haptoglobin binding (GO:0031720). In KEGG analysis, the genes that interact with miRNAs in the HONE1\_M vs. HONE1\_C group were enriched in the endocytosis pathway (hsa04144), TGF- $\beta$  signaling pathway (hsa04350), etc.

**A****B**

**Fig. 8.** HONE1\_M vs. CNE2\_C (A) Gene Ontology (GO) and (B) Kyoto Encyclopedia of Genes and Genomes (KEGG) pathway enrichment analyses. The GO analysis showed that HONE1\_M vs. CNE2\_C was mainly enriched in biological process such as nervous system development (GO:0007399) and homophilic cell adhesion via plasma membrane adhesion molecules (GO:0007156), cellular component such as cytosol (GO:0005829), and molecular function such as protein binding (GO:0005515). In KEGG analysis, the endocytosis pathway (hsa04144), hepatocellular carcinoma pathway (hsa05225), cocaine addiction pathway (hsa05030), etc. were enriched

predicted the target genes. The miRNAs that interact with the cancer, TGF- $\beta$ , p53, PI3K-AKT, MAPK, and FoxO signaling pathways were selected and the network interaction maps were constructed (Fig. 3D, Fig. 4A–4E). The results showed that 9 genes were co-regulated by miRNA in various pathways. These results were also reflected in the GO and KEGG pathway enrichment analyses. Here, we discuss the functions of several genes that are closely related to cancer. The hsa-miR-17-5p and hsa-miR-20a-5p targeted *MAPK1*, *SOS1* and *TGF $\beta$ R2* genes. The *MAPK1* is an oncogene, and its expression is upregulated in various cancer tissues. The miR-511 targeting binding with *MAPK1* can inhibit the proliferation and invasion of osteosarcoma in nude mice.<sup>35</sup> The *SOS1* is a Ras-GEF family protein and an oncogene. Knockout of *SOS1* protein in mice can inhibit tumor growth and migration.<sup>36</sup> In NPC, miR-93 targets *TGF $\beta$ R2*, downregulates *TGF $\beta$ R2* expression, and promotes cancer cell proliferation, invasion and migration.<sup>37</sup> The hsa-let-7a-5p, hsa-let-7f-5p and hsa-let-7i-5p target and regulate the expression of tumor suppressor genes *TP53* and *CASP3* in the MAPK and p53 signaling pathways. Studies have found that tripartite motif-containing protein 21 (TRIM21) inhibits the expression of *TP53* and protects cancer cells from radiation-induced apoptosis by mediating the ubiquitination and degradation of guanine monophosphate synthase (GMPS).<sup>38</sup> The *CASP3*, also known as caspase 3, is an apoptotic protein, and its mutation can lead to cell carcinogenesis.<sup>39</sup> The hsa-miR-92a-3p, hsa-miR-26a-5p and hsa-miR-148b-3p targeted the *PTEN* gene. The *PTEN* signaling pathway is related to the resistance of NPC cells to radiotherapy. The inactivation of *PTEN* activates PI3K-AKT3 signaling pathway and inhibits cell apoptosis.<sup>23</sup> The hsa-miR-30e-5p, hsa-miR-92a-3p and hsa-miR-200c-3p targeted the *CCNE2* gene. In various cancers, many miRNAs can bind to *CCNE2* to inhibit the proliferation of cancer cells. For example, in glioma, miR-370 can downregulate the *CCNE2* expression and inhibit tumor growth.<sup>40</sup> These genes are directly or indirectly related to cancer proliferation, apoptosis and other physiological processes. They are the key genes for studying miRNA regulation of cancer cell resistance to X-rays.

### Limitations of the study





This study mainly investigated the miRNA profiling of HONE1 and CNE2 after X-ray therapy. Further studies may explore the mechanisms involved.

### Conclusions

Through an analysis of the miRNA expression and the cluster analysis of the regulatory pathway, 12 miRNAs and 9 genes which play an important role in X-ray radiation

resistance were identified. Among those with differential expression between the HONE1 and CNE2 cell lines, which played a regulatory role in multiple pathways, were hsa-miR-20a-5p, hsa-let-7a-5p, hsa-let-7f-5p, hsa-let-7i-5p, hsa-miR-30e-5p, hsa-miR-148b-3p, and hsa-miR-200c-3p. The corresponding genes were *MAPK1*, *SOS1*, *TGF $\beta$ R1*, *TGF $\beta$ R2*, *TP53*, *CASP3*, *CCNE2*, *PTEN*, and *CDK2*. We will conduct more in-depth research on these genes and miRNAs in follow-up studies to provide more experimental evidence for the mechanism of NPC resistance to radiotherapy.

### ORCID iDs

Hui Luo  <https://orcid.org/0000-0002-6285-5130>  
 Fangyan Zhong  <https://orcid.org/0000-0002-0766-5721>  
 Xiang Jing  <https://orcid.org/0000-0003-2026-7354>  
 Hong Lin  <https://orcid.org/0000-0001-9506-0994>  
 Yong Li  <https://orcid.org/0000-0003-1733-7569>

### References

- Sham JS, Wei WI, Zong YS, et al. Detection of subclinical nasopharyngeal carcinoma by fiberoptic endoscopy and multiple biopsy. *Lancet*. 1990;335(8686):371–374. doi:10.1016/0140-6736(90)90206-k
- Wei WI, Sham JS. Nasopharyngeal carcinoma. *Lancet*. 2005;365(9476):2041–2054. doi:10.1016/S0140-6736(05)66698-6
- Long M, Fu Z, Li P, Nie Z. Cigarette smoking and the risk of nasopharyngeal carcinoma: A meta-analysis of epidemiological studies. *BMJ Open*. 2017;7(10):e016582. doi:10.1136/bmjopen-2017-016582
- Tu C, Zeng Z, Qi P, et al. Genome-wide analysis of 18 Epstein-Barr viruses isolated from primary nasopharyngeal carcinoma biopsy specimens. *J Virol*. 2017;91(17):e00301-17. doi:10.1128/JVI.00301-17
- Chen W, Zheng R, Baade PD, et al. Cancer statistics in China, 2015. *CA Cancer J Clin*. 2016;66(2):115–132. doi:10.3322/caac.21338
- Zhang L, Chen QY, Liu H, Tang LQ, Mai HQ. Emerging treatment options for nasopharyngeal carcinoma. *Drug Des Devel Ther*. 2013;7:37–52. doi:10.2147/DDDT.S30753
- Tian Y, Tang L, Yi P, et al. miRNAs in radiotherapy resistance of nasopharyngeal carcinoma. *J Cancer*. 2020;11(13):3976–3985. doi:10.7150/jca.42734
- Huang T, Yin L, Wu J, et al. MicroRNA-19b-3p regulates nasopharyngeal carcinoma radiosensitivity by targeting TNFAIP3/NF- $\kappa$ B axis. *J Exp Clin Cancer Res*. 2016;35(1):188. doi:10.1186/s13046-016-0465-1
- Wang S, Zhang R, Claret FX, Yang H. Involvement of microRNA-24 and DNA methylation in resistance of nasopharyngeal carcinoma to ionizing radiation. *Mol Cancer Ther*. 2014;13(12):3163–3174. doi:10.1158/1535-7163.MCT-14-0317
- Lin SL, Kim H, Ying SY. Intron-mediated RNA interference and microRNA (miRNA). *Front Biosci*. 2008;13:2216–2230. doi:10.2741/2836
- Bartel DP. MicroRNAs: Target recognition and regulatory functions. *Cell*. 2009;136(2):215–233. doi:10.1016/j.cell.2009.01.002
- Xu T, Tang J, Gu M, Liu L, Wei W, Yang H. Recurrent nasopharyngeal carcinoma: A clinical dilemma and challenge. *Curr Oncol*. 2013;20(5):e406–e419. doi:10.3747/co.20.1456
- Wang S, Claret FX, Wu W. MicroRNAs as therapeutic targets in nasopharyngeal carcinoma. *Front Oncol*. 2019;9:756. doi:10.3389/fonc.2019.00756
- Bolger AM, Lohse M, Usadel B. Trimmomatic: A flexible trimmer for Illumina sequence data. *Bioinformatics*. 2014;30(15):2114–2120. doi:10.1093/bioinformatics/btu170
- Zheng Z, Qu JQ, Yi HM, et al. MiR-125b regulates proliferation and apoptosis of nasopharyngeal carcinoma by targeting A20/NF- $\kappa$ B signaling pathway. *Cell Death Dis*. 2017;8(6):e2855. doi:10.1038/cddis.2017.211
- Jiang N, Jiang X, Chen Z, et al. MiR-203a-3p suppresses cell proliferation and metastasis through inhibiting LASP1 in nasopharyngeal carcinoma. *J Exp Clin Cancer Res*. 2017;36(1):138. doi:10.1186/s13046-017-0604-3

17. Liu N, Jiang N, Guo R, et al. MiR-451 inhibits cell growth and invasion by targeting MIF and is associated with survival in nasopharyngeal carcinoma. *Mol Cancer*. 2013;12(1):123. doi:10.1186/1476-4598-12-123
18. Barker HE, Paget JT, Khan AA, Harrington KJ. The tumour microenvironment after radiotherapy: Mechanisms of resistance and recurrence. *Nat Rev Cancer*. 2015;15(7):409–425. doi:10.1038/nrc3958. Erratum in: *Nat Rev Cancer*. 2015;15(8):509. doi:10.1038/nrc3958
19. Yu Y, Liang H, Lv X, et al. Platinum-based concurrent chemotherapy remains the optimal regimen for nasopharyngeal carcinoma: A large institutional-based cohort study from an endemic area. *J Cancer Res Clin Oncol*. 2018;144(11):2231–2243. doi:10.1007/s00432-018-2721-6
20. Li Y, Yan L, Zhang W, et al. miR-21 inhibitor suppresses proliferation and migration of nasopharyngeal carcinoma cells through down-regulation of BCL2 expression. *Int J Clin Exp Pathol*. 2014;7(6):3478–3487. PMID:25031780. PMCID:PMC4097257.
21. Qu C, Liang Z, Huang J, et al. MiR-205 determines the radioresistance of human nasopharyngeal carcinoma by directly targeting PTEN. *Cell Cycle*. 2012;11(4):785–796. doi:10.4161/cc.11.4.19228
22. Mao Y, Wu S, Zhao R, Deng Q. MiR-205 promotes proliferation, migration and invasion of nasopharyngeal carcinoma cells by activation of AKT signalling. *J Int Med Res*. 2016;44(2):231–240. doi:10.1177/0300060515576556
23. Ou H, Li Y, Kang M. Activation of miR-21 by STAT3 induces proliferation and suppresses apoptosis in nasopharyngeal carcinoma by targeting PTEN gene. *PLoS One*. 2014;9(11):e109929. doi:10.1371/journal.pone.0109929
24. Yang GD, Huang TJ, Peng LX, et al. Epstein–Barr Virus\_ Encoded LMP1 upregulates microRNA-21 to promote the resistance of nasopharyngeal carcinoma cells to cisplatin-induced apoptosis by suppressing PDCD4 and Fas-L. *PLoS One*. 2013;8(10):e78355. doi:10.1371/journal.pone.0078355
25. Wong TS, Man OY, Tsang CM, et al. MicroRNA let-7 suppresses nasopharyngeal carcinoma cells proliferation through downregulating c-Myc expression. *J Cancer Res Clin Oncol*. 2011;137(3):415–422. doi:10.1007/s00432-010-0898-4
26. Chen ZX, Sun AM, Chen Y, et al. Effects of radiosensitivity and X-ray dose on miR-7 expression in nasopharyngeal carcinoma [in Chinese]. *Nan Fang Yi Ke Da Xue Xue Bao*. 2010;30(8):1810–1812,1816. PMID:20813671.
27. Liu Y, Li Z, Wu L, et al. MiRNA-125a-5p: A regulator and predictor of gefitinib's effect on nasopharyngeal carcinoma. *Cancer Cell Int*. 2014;14(1):24. doi:10.1186/1475-2867-14-24
28. Gao W, Chan JY, Wong TS. Curcumin exerts inhibitory effects on undifferentiated nasopharyngeal carcinoma by inhibiting the expression of miR-125a-5p. *Clin Sci (Lond)*. 2014;127(9):571–579. doi:10.1042/CS20140010
29. Lu J, He ML, Wang L, et al. MiR-26a inhibits cell growth and tumorigenesis of nasopharyngeal carcinoma through repression of EZH2. *Cancer Res*. 2011;71(1):225–233. doi:10.1158/0008-5472.CAN-10-1850
30. Yu L, Lu J, Zhang B, et al. miR-26a inhibits invasion and metastasis of nasopharyngeal cancer by targeting EZH2. *Oncol Lett*. 2013;5(4):1223–1228. doi:10.3892/ol.2013.1173
31. Wang S, Pan Y, Zhang R, et al. Hsa-miR-24-3p increases nasopharyngeal carcinoma radiosensitivity by targeting both the 3'UTR and 5'UTR of Jab1/CNS5. *Oncogene*. 2016;35(47):6096–6108. doi:10.1038/onc.2016.147
32. Kang M, Xiao J, Wang J, et al. MiR-24 enhances radiosensitivity in nasopharyngeal carcinoma by targeting SP1. *Cancer Med*. 2016;5(6):1163–1173. doi:10.1002/cam4.660
33. Huang D, Bian G, Pan Y, et al. MiR-20a-5p promotes radio-resistance by targeting Rab27B in nasopharyngeal cancer cells. *Cancer Cell Int*. 2017;17:32. doi:10.1186/s12935-017-0389-7
34. Zhao F, Pu Y, Qian L, Zang C, Tao Z, Gao J. MiR-20a-5p promotes radio-resistance by targeting NPAS2 in nasopharyngeal cancer cells. *Oncotarget*. 2017;8(62):105873–105881. doi:10.18632/oncotarget.22411
35. Wu J, Zhang C, Chen L. MiR-511 mimic transfection inhibits the proliferation, invasion of osteosarcoma cells and reduces metastatic osteosarcoma tumor burden in nude mice via targeting MAPK1. *Cancer Biomark*. 2019;26(3):343–351. doi:10.3233/CBM-190534
36. Licerias-Boillos P, Jimeno D, García-Navas R, et al. Differential role of the RasGEFs Sos1 and Sos2 in mouse skin homeostasis and carcinogenesis. *Mol Cell Biol*. 2018;38(16):e00049-18. doi:10.1128/MLB.00049-18
37. Lyu X, Fang W, Cai L, et al. TGFβR2 is a major target of miR-93 in nasopharyngeal carcinoma aggressiveness. *Mol Cancer*. 2014;13:51. doi:10.1186/1476-4598-13-51
38. Zhang P, Li X, He Q, et al. TRIM21-SERPINB5 aids GMPs repression to protect nasopharyngeal carcinoma cells from radiation-induced apoptosis. *J Biomed Sci*. 2020;27(1):30. doi:10.1186/s12929-020-0625-7
39. Lin J, Zhang Y, Wang H, et al. Genetic polymorphisms in the apoptosis-associated gene CASP3 and the risk of lung cancer in Chinese population. *PLoS One*. 2016;11(10):e0164358. doi:10.1371/journal.pone.0164358
40. Gong W, Zheng J, Liu X, et al. Knockdown of long non-coding RNA KCNQ10T1 restrained glioma cells' malignancy by activating miR-370/CNNE2 axis. *Front Cell Neurosci*. 2017;11:84. doi:10.3389/fncel.2017.00084





# Effect of different expression patterns of HAX-1 on the proliferation and apoptosis of human astrocyte

\*Xiaopeng Xia<sup>1,2,B,C,F</sup>, \*Xiaojian Zhu<sup>3,C,D,F</sup>, Shu Zhang<sup>4,C,D,F</sup>, Xiaoxia Zhang<sup>5,C,E,F</sup>, Yan Wang<sup>4,A,E,F</sup>

<sup>1</sup> Department of Orthopaedics, Affiliated Nantong Traditional Chinese Medical Hospital of Nantong University, China

<sup>2</sup> Department of Orthopaedics, Nantong Hospital of Traditional Chinese Medicine, China

<sup>3</sup> Department of Orthopaedics, Nantong Fourth People's Hospital, China

<sup>4</sup> Department of Pathology, Affiliated Hospital of Nantong University, China

<sup>5</sup> Department of Pathology, Maternal and Child Health Care Hospital of Nantong, China

A – research concept and design; B – collection and/or assembly of data; C – data analysis and interpretation;

D – writing the article; E – critical revision of the article; F – final approval of the article

Advances in Clinical and Experimental Medicine, ISSN 1899–5276 (print), ISSN 2451–2680 (online)

Adv Clin Exp Med. 2022;31(6):689–699

## Address for correspondence

Yan Wang

E-mail: yisheng\_wangyan@126.com

## Funding sources

Clinical Medicine Special Project of Nantong University (grant No. 2019JZ016); Nantong Science and Technology Program (grant No. JCZ19120).

## Conflict of interest

None declared

## Acknowledgements

We would like to gratefully acknowledge all the participants of the study, without whom the study would not have been possible.

\* Xiaopeng Xia and Xiaojian Zhu contributed equally to this research.

Received on November 8, 2021

Reviewed on December 15, 2021

Accepted on February 10, 2022

Published online on March 16, 2022

## Cite as

Xia X, Zhu X, Zhang S, Zhang X, Wang Y. Effect of different expression patterns of HAX-1 on the proliferation and apoptosis of human astrocyte. *Adv Clin Exp Med.* 2022;31(6):689–699. doi:10.17219/acem/146583

## DOI

10.17219/acem/146583

## Copyright

Copyright by Author(s)

This is an article distributed under the terms of the Creative Commons Attribution 3.0 Unported (CC BY 3.0) (<https://creativecommons.org/licenses/by/3.0/>)

## Abstract

**Background.** Spinal cord injury (SCI), a serious damage of the central nervous system, has become an extremely important issue that threatens the health of people worldwide. The proliferation of astrocytes plays an important role in the repair of SCI, which has typical two-sided effects. The HSI-associated protein X-1 (HAX-1), plays an important role in the physiological and pathological processes of cell apoptosis, proliferation, migration, and invasion. However, the specific role and mechanism of HAX-1 in human astrocyte HA1800 are still unclear.

**Objectives.** To explore the effect of HAX-1 on the proliferation and apoptosis of HA1800 cells and preliminarily explore its possible underlying mechanism.

**Materials and methods.** The HA1800 cell lines with high- and low-expression levels of HAX-1 were established using lentiviral vector pcDNA3.1. Quantitative reverse transcription polymerase chain reaction (qRT-PCR) and western blot were employed to determine the expression of HAX-1 after transfection. Cell viability and proliferation ability were estimated using MTT and 5-Ethynyl-2'-deoxyuridine (EdU) assay. The effects of HAX-1 on the HA1800 cell cycle and apoptosis were determined using flow cytometry. The BCL-2/BAX ratio and the expression of Ki67 and c-Myc in the transfected cells were detected using qRT-PCR. The Gene Expression Profiling Interactive Analysis (GEPIA) database was used to determine the relationships of HAX-1, BAX and BCL-2.

**Results.** The HA1800 cell lines with high and low expression of HAX-1 were obtained. The MTT, EdU and flow cytometry showed that elevated HAX-1 could inhibit the proliferation, reduce the viability and promote the apoptosis of HA1800 cells. The qRT-PCR showed that the mRNA levels of Ki67, c-Myc and the BCL-2/BAX ratio were significantly decreased in the HAX-1 high-expression group, but increased in the HAX-1 low-expression group. The results from the GEPIA database showed that HAX-1 was positively correlated with BAX and BCL-2 in the spinal cord.

**Conclusions.** The HAX-1 may influence the biological behavior of human HA1800 cells due to the progression of cell cycle and apoptosis associated with BCL-2/BAX.

**Key words:** HAX-1, HA1800, proliferation, apoptosis

## Background

Damage to the central nervous system, especially spinal cord injury (SCI), is a common and serious disease resulting in physical, psychological and social disorders.<sup>1</sup> In recent years, the morbidity and mortality of SCI have been increasing.<sup>2</sup> Among many possible causes of SCI, traffic accidents are not negligible. In 2015, the data from many countries have shown that approx. 12–60 cases of traffic accidents per million of population occur annually.<sup>3</sup> Spinal cord injury is classified as primary (acute phase) or secondary (recovery phase) injury, depending on the timing and mechanism of the nerve injury. The primary damage is mainly caused by a direct damage of the vertebrae, resulting in contusion or oppression of the spinal cord, and usually, the primary damage appears only at the injured site. In SCI, the neurons are directly damaged, and astrocyte and endothelial cell injuries are rare. The secondary injury may be the key factor in the damage that is difficult to repair and it results in the decline or loss of motor and sensory functions. The secondary damage occurs tens of seconds after the primary damage and lasts for several weeks. The various reactions caused by the damage appear not only at the injured and surrounding sites but also across the whole body. Some specific manifestations are ischemic dysfunction, changes in the electrolytes, accumulation of neurotransmitters, protein/lipid oxidation, DNA damage, inflammation, edema, oxidative stress necrosis, apoptosis of neurons, and glial hyperplasia.<sup>4,5</sup> Neuronal apoptosis is the most widely studied manifestation.<sup>6,7</sup> Under the stimulation of primary injury, the influence of secondary cytokines and chemical factors, reactive hyperplasia of astrocytes occurs at the injured and surrounding areas, and this process forms glial scar.<sup>8</sup> The occurrence of this scar in the acute stage may have more positive effects, such as the limitation of the scope of injury, protection of the ischemic penumbra, maintenance of local metabolism, and immune regulation.<sup>9</sup> However, in the subsequent recovery period, glial scar will hinder nerve repair. First, the scar in the damaged area directly acts as a physical barrier to the extension of newborn neuronal axons. Second, various cytokines secreted in the damaged area inhibit the regeneration of axons to varying degrees. Hence, astrocyte proliferation is typically double-sided for injury repair.<sup>10,11</sup> Effective target regulation of astrocyte proliferation at different time periods of injury may be beneficial for the regeneration of neurons and extension of axons, providing a new method for the treatment of SCI.

With the use of a system named yeast two-hybrid, Suzuki et al. discovered that HS1-associated protein X-1 (HAX-1) has an intracellular antiapoptotic effect and is homologous to the antiapoptotic protein – BCL2.<sup>12,13</sup> The HAX-1 mainly interacts with the hematopoietic cell-specific substrate protein 1 (HS1) and functions as a protein with molecular weight of 35 kD. The HAX-1 is the substrate of serine/tyrosine kinase located on the human chromosome

1q21.3, encoding 279 amino acid fragments.<sup>13</sup> This protein consists of a transmembrane domain, an acidic domain, and a proline, glutamic acid, serine and threonine (PEST) sequence.<sup>14</sup> The programmed pseudogenes are found on the human X chromosome, and similar pseudogenes are found in the rat and mouse genomes. The HAX-1 analogs have been found in many other species, including zebrafish (mackerel), rather than in more primitive organisms, such as nematodes and new rod-shaped nematodes. Also, the comparison and analysis of the mRNA expression data of human, rat and mouse HAX-1<sup>15</sup> have shown that HAX-1 is widely expressed in various tissues and organs of mammals (highly expressed in the skeletal muscle, cardiac muscle, colon, and other tissues), but lowly expressed in the nervous system and kidney.<sup>16</sup> As an antiapoptotic protein, HAX-1 has been confirmed to participate in the regulation of apoptosis through several signal pathways.<sup>17–19</sup> In the mitochondrial-related caspase apoptosis pathway, HAX-1 could inhibit the activation of caspase-3 and caspase-9 and then inhibit apoptosis. The HAX-1 also plays an antiapoptotic role by regulating the calcium ion homeostasis and improving calcium overload. In the serine protease Omi/HtrA2 signal transduction pathway in the mitochondria, HAX-1 is the substrate protein of Omi/HtrA2. The Omi/HtrA2 plays an enzymatic cleavage role in the apoptosis pathway. This effect can degrade HAX-1, thereby producing an antiapoptotic effect. In addition, HAX-1 interacts with the 2-pore channel of the endolysosome, which reduces the permeability of the lysosomal membrane and the release of enzymes, exerting an antiapoptotic effect. The HAX-1 also exerts antiapoptotic effects through the antioxidative stress response. The HAX-1 can affect the Ak1t/MDM2/p53 axis and the expression of p21, Bax and p53 proteins to participate in cell apoptosis. The HAX-1 can interact with the heat shock protein 90 (Hsp90) to affect the IRE-1 signal transduction, in order to regulate cell apoptosis.<sup>20</sup> However, studies have shown that HAX-1 may act not only as an antiapoptotic (human v1 isoform) but also as a proapoptotic (human v4 isoform) regulator through homodimerization or heterodimerization in cardiac cells.<sup>21,22</sup> The HAX1 is involved in many important physiological and pathological processes, such as the regulation of cell apoptosis, cell proliferation, motility, endocytosis, and mRNA transport.<sup>23,24</sup> Recent reports have shown that HAX-1 levels are elevated in various tumors, such as those in the esophagus, colorectal, nasopharynx, throat, prostate, ovary, breast, skin, and lymphoma.<sup>24–28</sup> In addition, by collecting clinical case studies, Deng et al. showed that HAX-1 was also expressed in gliomas and might be positively correlated with tumor malignancy. The role of HAX-1 in promoting tumor proliferation might be achieved through estrogen-related apoptosis pathways. However, whether a direct effect exists remains to be confirmed.<sup>29</sup> In the neurons, HAX-1 can interact through Rac1 and contraction to affect the formation of neuronal cells

and regulate the apoptosis and migration ability of tumor cells. Upregulated HAX-1 has been detected during brain damage caused by trauma or epilepsy.<sup>30,31</sup> The HAX-1 protein level was increased significantly in neurons after traumatic brain injury (TBI) but it was not expressed within glial cell population and microglia in the brain cortex. However, whether different subtypes of HAX-1 play distinct roles in the brain, especially in the astrocytes after TBI, has not been studied yet.<sup>31</sup> All the aforementioned studies showed that HAX-1 might be related to the regulation of astrocyte proliferation.

Apoptosis plays a key role in secondary SCI.<sup>32</sup> Lu et al. performed experiments on the effect of HAX-1 on neuronal apoptosis after SCI in rats. The results showed that HAX-1 expression was mainly upregulated in the local neurons after SCI but almost not expressed in the normal astrocytes. In addition, the upregulated HAX-1 was negatively correlated with neuronal apoptosis. The downregulation of HAX-1 in the reactive astrocytes in the experiments in vitro changed the cell viability of the primary cultured wild-type rat spinal cord astrocytes. Thus, HAX-1 might be related to the reduction in astrocyte proliferation.<sup>23</sup> These results suggested that HAX-1, as a multifunctional protein, may be involved in the proliferation of astrocytes after SCI. However, the experimental results failed to further verify the specific possible mechanism of activity, and whether HAX-1 had a certain regulatory effect on cell migration was not observed.<sup>23</sup> In conclusion, we speculate that HAX-1 may play a regulatory role in the growth, proliferation and migration of astrocytes. In this study, we constructed in vitro human HA1800 cell lines with high and low HAX-1 expression to verify the function of HAX-1 on the proliferation and apoptosis of human astrocytes. We also preliminarily explored the possible signal pathways to provide a certain experimental basis for clinically improving and regulating the formation of glial scars caused by injury and promoting the repair of nerve injury.

## Objectives

We examined the specific effects of HAX-1 expression on the proliferation, viability and apoptosis of human HA1800 cells by upregulating and downregulating its expression. We preliminarily explored the effects of HAX-1 on the cell proliferation and apoptosis-related factors to further clarify its possible underlying mechanism.

## Materials and methods

### Establishment of HA1800 cell lines with stable high and low HAX-1 expression

Lentiviral transfection was used to construct stable transfected HA1800 cell lines. The coding sequences

of HAX-1 and HAX-1 siRNAs were synthesized by Ribobio Biotech Company (Guangzhou, China). The interference sequences were as follows: HAX-1 siRNA1#, 5'GTACGAGATTTCAATAGCA3'; HAX-1 siRNA2#, 5'GGATACGTTTCCACGATAA3'; HAX-1 siRNA3#, 5'GGATACGTTTCCACGATAA3'; and NC-siRNA, 5'UUCUCCGAACGUUGACACACGUdTdT3'. The synthesized HAX-1 and HAX-1 siRNAs were integrated into the lentiviral vector pcDNA3.1 (+) (Invitrogen, Carlsbad, USA) vector, using BamHI and EcoRI (Thermo Fisher Scientific, Waltham, USA). The plasmids were confirmed by sequencing and then transfected into DH5a for amplification, screening of positive clones, identification, and sequencing, in order to obtain the recombinant retroviral vector. The plasmids were extracted according to the instructions provided by the manufacturer of Endo-free Plasmid Mini Kit I (Omega, Stanford, USA). Finally, plasmids with high HAX-1 expression and low HAX-1 expression (1#, 2# and 3#) were obtained.

Human HA1800 cells were purchased from the Shanghai GeneChem, Co., Ltd. (Shanghai, China). The cells were cultured in Dulbecco's Modified Eagle Medium (DMEM; Thermo-Life, Waltham, USA) with fetal bovine serum (FBS, 10%; Thermo Fisher Scientific), penicillin (100 µg/mL; Beyotime, Shanghai, China) and streptomycin (Beyotime). The cultivation environment was 37°C with 5% CO<sub>2</sub>. Approximately 1 × 10<sup>5</sup> cells were plated per well in a six-well plate. The following day, when the cell density reached 80% of the well, the plasmids were transfected with Lipofectamine™ 2000 (Invitrogen), according to the manufacturer's instructions. The empty lentiviral vector was used as the control group for the high-HAX-1 expression group, and NC-RNAi was used as the negative control (NC) group for the low-expression groups.

### Examination of HAX-1 mRNA and protein expression

Quantitative reverse transcription polymerase chain reaction (qRT-PCR) was performed to examine the HAX-1 mRNA expression. After the HA1800 cells were transfected with the plasmids (HAX-1, pcDNA3.1; NC and HAX-1 siRNAs (1#, 2#, and 3#)), the total RNA of each group of cells was extracted (UNIQ-10 Spin Column RNA Purification kit; Sangon Biotech Co., Ltd., Shanghai, China). The first-strand cDNA was synthesized (RevertAid First Strand cDNA Synthesis kit (Ferments; Thermo Fisher Scientific)) using the prepared total RNA (1 µg) and then analyzed in the Step One Plus™ real-time PCR system (Thermo Fisher Scientific), using the AceQ qPCR SYBR Green Master Mix (Vazyme, Piscataway, USA). The *GAPDH* was chosen as the control reference gene. The primers were as follows: HAX-1 (183 bp) forward, 5'-GGGGTCTTGGAGAGTGATG-3', and reverse, 5'-CTGGGGCTGTAGAACCG-3'; *GAPDH* (131 bp)

forward, 5'-GAAGGTCGGAGTCAACGGAT-3', and reverse, 5'-TCCCGTTCTCAGCCATGTAGTT-3'. The cycling parameters were as follows: 95°C for 5 min; 40 cycles of 95°C for 10 s and 60°C for 30 s. The  $2^{-\Delta\Delta C_q}$  method was used to calculate the expression levels.

Western blot was utilized to check the HAX-1 protein expression. The total proteins of the cultured groups of cells were extracted using the Tissue or Cell Total Protein Extraction kit (Sangon Biotech Co., Ltd.) and measured using the Enhanced BCA Protein Assay Kit (Beyotime, Haimen, China). Then, 10% sodium dodecyl-sulfate polyacrylamide gel electrophoresis (SDS-PAGE) was used to load and separate the total protein (30  $\mu$ g). After electrophoresis, the proteins were transferred to polyvinylidene fluoride membranes, and the membranes were blocked with skim milk (5%) for 1 h at room temperature. Then, the primary antibodies were incubated overnight at 4°C and washed thrice with 1× Tris-buffered saline and Tween-20 (TBST) solution (0.1% Tween; Sangon Biotech Co., Ltd.) (5 min each instance). The secondary antibody was incubated with the membranes for 4 h at room temperature. The following antibodies were used: rabbit anti- $\beta$ -actin (dilution, 1:1000; cat. No. ab8227; Abcam, Cambridge, UK); rabbit anti-HAX-1 (1:500; cat. No. ab137613; Abcam); horseradish peroxidase-conjugated goat anti-rabbit as the secondary antibody (1:3000; cat. No. ab205718; Abcam). Then, the membranes were washed thrice with TBST (5 min each instance) and detected using enhanced chemiluminescence reagent (cat. No. E411; Vazyme, Nanjing, China). Finally, the membranes were scanned using Chemidoc XRS system (Bio-Rad Laboratories, Inc., Hercules, USA), and the expression levels of the proteins were calculated using Image Lab software (Bio-Rad Laboratories, Inc.).

The best interfering group, referred to as HAX-1 siRNA, was chosen. Thus, the groups utilized for subsequent experiments contained pcDNA3.1-HA1800, HAX-1-HA1800, NC-HA1800, and HAX-1 siRNA-HA1800.

## MTT assay

Cells from each group were incubated in 96-well plates for 24 h and were added with MTT (0.5 mg/mL; Beyotime). After incubation at 37°C for 3 h, the cells were added with dimethyl sulfoxide (DMSO) (150  $\mu$ L). After incubation for 15 min, the absorbance was measured at 490 nm with a spectrophotometer (Tecan, Männedorf, Austria).

## 5-Ethynyl-2'-deoxyuridine (EdU) assay

Cells from each group were incubated in a 6-well plate for 24 h and treated with EdU (50  $\mu$ M) reagent. Then, the cells were treated with Apollo-567 reaction mixture for 30 min and washed thrice with phosphate-buffered saline (PBS). Finally, the cells were counterstained with Hoechst (dilution, 1:1000) for 10 min at room temperature for nuclear staining. The EVOS® FL imaging system (Thermo Fisher Scientific) was used to observe and count the cells. All materials in this assay were purchased from RiboBio Biotech Company.

## Cell cycle analysis

The cells were incubated, harvested, washed twice with PBS, and then fixed on ice-cold 75% ethanol for 30 min. After being washed twice successively with citrate phosphate buffer and PBS, the cells were treated with PBS containing 100  $\mu$ g/mL RNase A for 30 min at 37°C and then incubated in PBS containing 100  $\mu$ g/mL propidium iodide for 30 min at room temperature. Finally, flow cytometry (Becton Dickinson Biosciences, Franklin Lakes, USA) was used to ensure the cell cycle distribution of each sample (over 10,000 cells). The data were analyzed using ModFit software (Becton Dickinson Biosciences). The experiment was performed in triplicate.

## Measurement of Ki67, c-Myc, BCL-2, and Bax

The qRT-PCR was utilized to analyze the expression of Ki67, c-Myc, BCL-2, and Bax in the cells from each group. The specific method is as above. The primers applied are presented in Table 1.

## GEPIA analysis

The The Gene Expression Profiling Interactive Analysis (GEPIA)<sup>33</sup> (<http://gepia.cancer-pku.cn/index.html>) database was used to analyze the relationships between HAX-1 and BAX, as well as between HAX-1 and BCL-2, in the spinal cord.

## Statistical analyses

The IBM Statistical Package for the Social Sciences (SPSS) software v. 22.0 (IBM Corp., Armonk, USA) was applied

**Table 1.** The primer sequences applied in quantitative reverse transcription polymerase chain reaction (qRT-PCR) in this research

Gene	Forward primer (5'-3')	Reverse primer (5'-3')
Ki67 (72 bp)	TTGTTTGGGAAGGAGAAATGTGTT	GCAGAGCATTATCAGATGGC
c-Myc (136 bp)	CGCTTCTCTGAAAGGCTCTCCTTG	GAGTCGTAGTCGAGGTCATAGTTC
BCL-2 (141 bp)	GATTGTGGCCTTCTTTGAGTT	AGTTCACAAAGGCATCCCA
BAX (257 bp)	TCCACCAAGAAGCTGAGCGAG	GTCCAGCCCATGATGGTTCT

to count the data, which are presented as mean ± standard deviation (SD) (each experiment was repeated at least thrice, independently). Two sided Student's t-test (for parametric data set, meaning the data was suitable for parametric test) was used for double comparison and Pearson's correlation was applied to assess correlation. One-way analysis of variance (ANOVA) with Bonferroni's post test (for parametric data set, meaning the data suitable for parametric test) was performed for multiple comparisons. A value of  $p < 0.05$  was considered statistically significant. Graphs were drawn in GraphPad Prism software v. 5.0 (GraphPad Software, San Diego, USA).

## Results

### High and low expression of HAX-1 was established in the HA1800 cells

The HA1800 cells with either high or low expression of HAX-1 were established. The results from the qRT-PCR and western blot indicated that the mRNA and protein expression of HAX-1 were significantly upregulated in the high-HAX-1 expression group, which was transfected with pcDNA3.1-HAX-1 ( $p < 0.05$ ; t-test;  $t = 17.41$ ) (Fig. 1), compared with that in the control group (pcDNA3.1 transfected with empty lentiviral vector). The HAX-1 was obviously downregulated in the low-HAX-1 expression group,

which was transfected with HAX-1 siRNAs, compared with that in the NC group ( $p < 0.05$ ,  $p < 0.05$ ,  $p < 0.05$ ; ANOVA post tests;  $F$  (qRT-PCR) = 25.38,  $F$  (western blot) = 8.741) (Fig. 1). The HAX-1 siRNA3# was the best interfering group and was chosen for subsequent experiments.

### High HAX-1 expression reduced the HA1800 cell viability

The MTT assay was performed to determine the influence of HAX-1 on the cell viability of the HA1800 cells. The results showed that the viability of the high-HAX-1 expression group (HAX-1 transfected with pcDNA3.1-HAX-1) cells was significantly reduced, compared with that of the control group (pcDNA3.1) ( $p < 0.05$ ; ANOVA;  $F = 981.2$ ) (Fig. 2A), but was markedly enhanced in the low-HAX-1 expression group (HAX-1 siRNA transfected with HAX-1 siRNA3#) compared with the NC group ( $p < 0.05$ ; ANOVA;  $F = 79.14$ ) (Fig. 2B). These results indicated that the elevation of HAX-1 may play a key role in reducing the HA1800 cell viability.

### HAX-1 regulated the HA1800 cell proliferation

The EdU proliferation assay was applied to explore the influence of HAX-1 on the HA1800 cells. The proliferation rate of the cell lines in the HAX-1 group was decreased

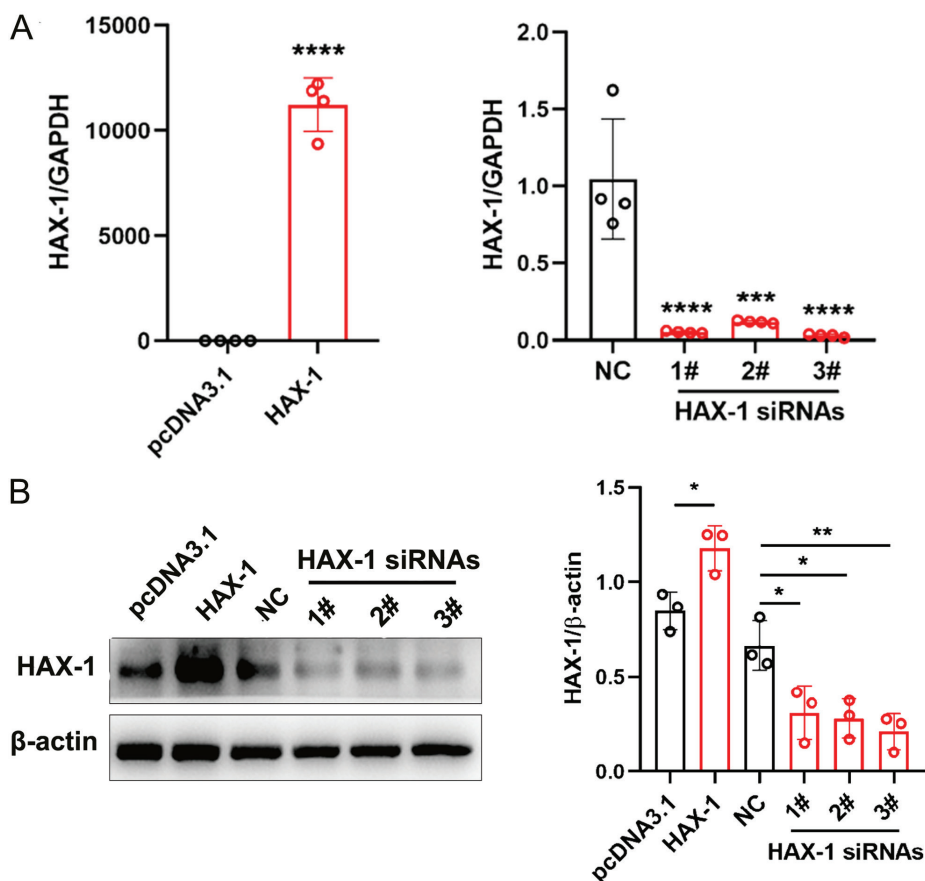
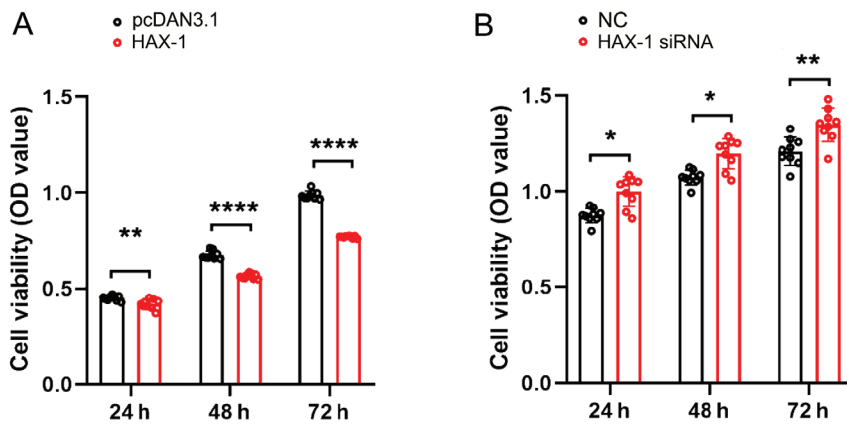
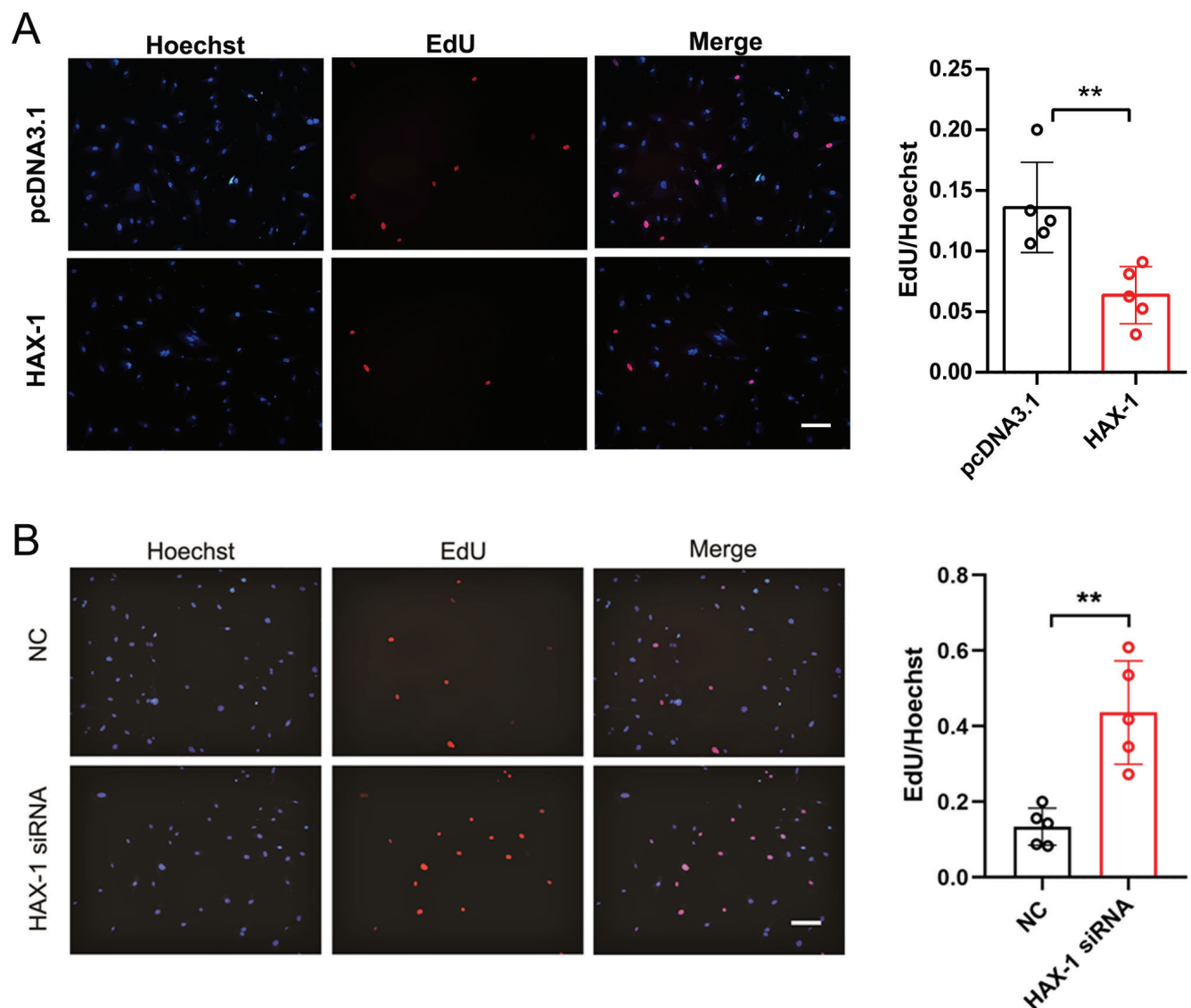


Fig. 1. Expressions of HAX-1-associated protein X-1 (HAX-1) mRNA (A) and protein (B) in HA1800 cell lines. The HAX-1 displayed an obvious upregulation in the HA1800 cells that were transfected with pcDNA3.1-HAX-1 (HAX-1 group), and a significant downregulation in the HA1800 cells transfected with HAX-1 siRNAs (HAX-1 siRNA 1#, 2# and 3# groups). The HAX-1 siRNA3# was the best interfering group. A. \*\*\*\* $p < 0.0001$  compared to control (pcDNA3.1 group) (t-test;  $t = 17.41$ ); \*\*\*\* $p < 0.0001$  (HAX-1 siRNA 1# group) compared to the negative control (NC) group (analysis of variance (ANOVA) post tests;  $q = 10.2$ ); \*\*\* $p = 0.0001$  (HAX-1 siRNA 2# group) compared to the NC group (ANOVA post tests;  $q = 9.513$ ); \*\*\*\* $p < 0.001$  (HAX-1 siRNA 3# group) compared to NC group (ANOVA post tests;  $q = 10.42$ ); B. \* $p < 0.05$  compared to control (pcDNA3.1 group) (t-test;  $t = 3.669$ ); \* $p < 0.05$  (HAX-1 siRNA 1# group) compared to NC group (ANOVA post tests;  $q = 5.169$ ); \* $p < 0.05$  (HAX-1 siRNA 2# group) compared to NC group (ANOVA post tests;  $q = 5.593$ ); \*\* $p < 0.01$  (HAX-1 siRNA 3# group) compared to NC group (ANOVA post tests;  $q = 6.605$ )



**Fig. 2.** The effect of HS1-associated protein X-1 (HAX-1) on HA1800 cell viability. The viability of HA1800 cells in the HAX-1 group was significantly lower than that in the pcDNA3.1 group (A), and the cell viability in the HAX-1 siRNA group was significantly stronger than that of the negative control (NC) group (B). A. \*\* $p < 0.01$  compared to control (pcDNA3.1 group) (24 h; t-test;  $t = 4.168$ ); \*\*\*\* $p < 0.0001$  compared to control (pcDNA3.1 group) (48 h; t-test;  $t = 14.6$ ); \*\*\*\* $p < 0.0001$  compared to control (pcDNA3.1 group) (72 h; t-test;  $t = 29.25$ ); B. \* $p < 0.05$  compared to NC group (24 h; t-test;  $t = 3.280$ ); \* $p < 0.05$  compared to NC group (48 h; t-test;  $t = 3.245$ ); \*\* $p < 0.01$  compared to NC group (72 h; t-test;  $t = 3.635$ )

OD – optical density.



**Fig. 3.** The influence of HS1-associated protein X-1 (HAX-1) on HA1800 cells checked with the EdU proliferation test. The proliferating cells of the HAX-1 group decreased (A), and the proliferating cells of the HAX-1 siRNA group increased (B). Red fluorescence labeled 5-Ethynyl-2'-deoxyuridine (EdU) and blue fluorescence stained the nucleus. Bar = 500  $\mu\text{m}$ . A. \*\* $p < 0.01$  compared to control (pcDNA3.1 group) (t-test;  $t = 3.676$ ); B. \*\* $p < 0.01$  compared to the negative control (NC) group (t-test;  $t = 4.648$ )

significantly compared with those in the pcDNA3.1 group ( $p < 0.01$ ; t-test;  $t = 3.676$ ) (Fig. 3A), and the proliferation rate of the cell lines in the HAX-1 siRNA group was increased,

compared with that in the NC group ( $p < 0.01$ , t-test;  $t = 4.648$ ) (Fig. 3B). These results indicated that the elevation of HAX-1 may cause slower proliferation of HA1800 cells.

## High HAX-1 expression inhibited the HA1800 cell cycle progression

Flow cytometry (TCM) was used to evaluate the cell cycle distribution of the HA1800 cells. The results showed more HA1800 cells in the G1 phase and less HA1800 cells in the S and G2 phases in the HAX-1 group, compared with those in the pcDNA3.1 group ( $p < 0.01$ ; t-test;  $t = 7.545$ ) (Fig. 4A). However, contrasting results were obtained from the HAX-1 siRNA group compared with the NC group ( $p < 0.05$ ; t-test;  $t = 3.632$ ) (Fig. 4B), demonstrating that the elevation of HAX-1 may suppress HA1800 cell cycle progression.

## HAX-1 participated in regulating the expression of genes related to cell proliferation and apoptosis

To study the possible mechanism of the expression of HAX-1 regulating the proliferation of HA1800 cells, the qRT-PCR analysis was used to examine the expressions of Ki67, c-Myc, BCL-2, and BAX. The results indicated that, compared with

the pcDNA3.1 group, the mRNA expression of Ki67 and c-Myc, and the BCL-2/BAX ratio were all significantly lower in the HAX-1 group ( $p < 0.01$ ; t-test;  $t = 4.889$ ,  $p < 0.05$ ; t-test;  $t = 3.524$ ,  $p < 0.005$ ; t-test;  $t = 8.759$ ) (Fig. 5A). By contrast, the expression of Ki67 mRNA and c-Myc, and the BCL-2/BAX ratio were all significantly higher in the HAX-1 siRNA group ( $p < 0.01$ ; t-test;  $t = 8.498$ ,  $p < 0.05$ ; t-test;  $t = 4.296$ ,  $p < 0.05$ ; t-test;  $t = 3.51$ ) (Fig. 5B) than in the NC group. Thus, high HAX-1 expression may inhibit the proliferation of human HA1800 cells and promote the apoptosis.

The results from the GEPIA online database displayed that BCL-2 and BAX were positively correlated with the HAX-1 in the spinal cord (both  $p < 0.001$ , Pearson’s correlation analysis) (Fig. 5C). Thus, BCL-2/BAX might constitute a possible mechanism for the effect of HAX-1 in HA1800.

## Discussion

As one of the diseases with high probability to cause human disability, SCI is a global medical problem. However, no reliable treatment for this disease is currently

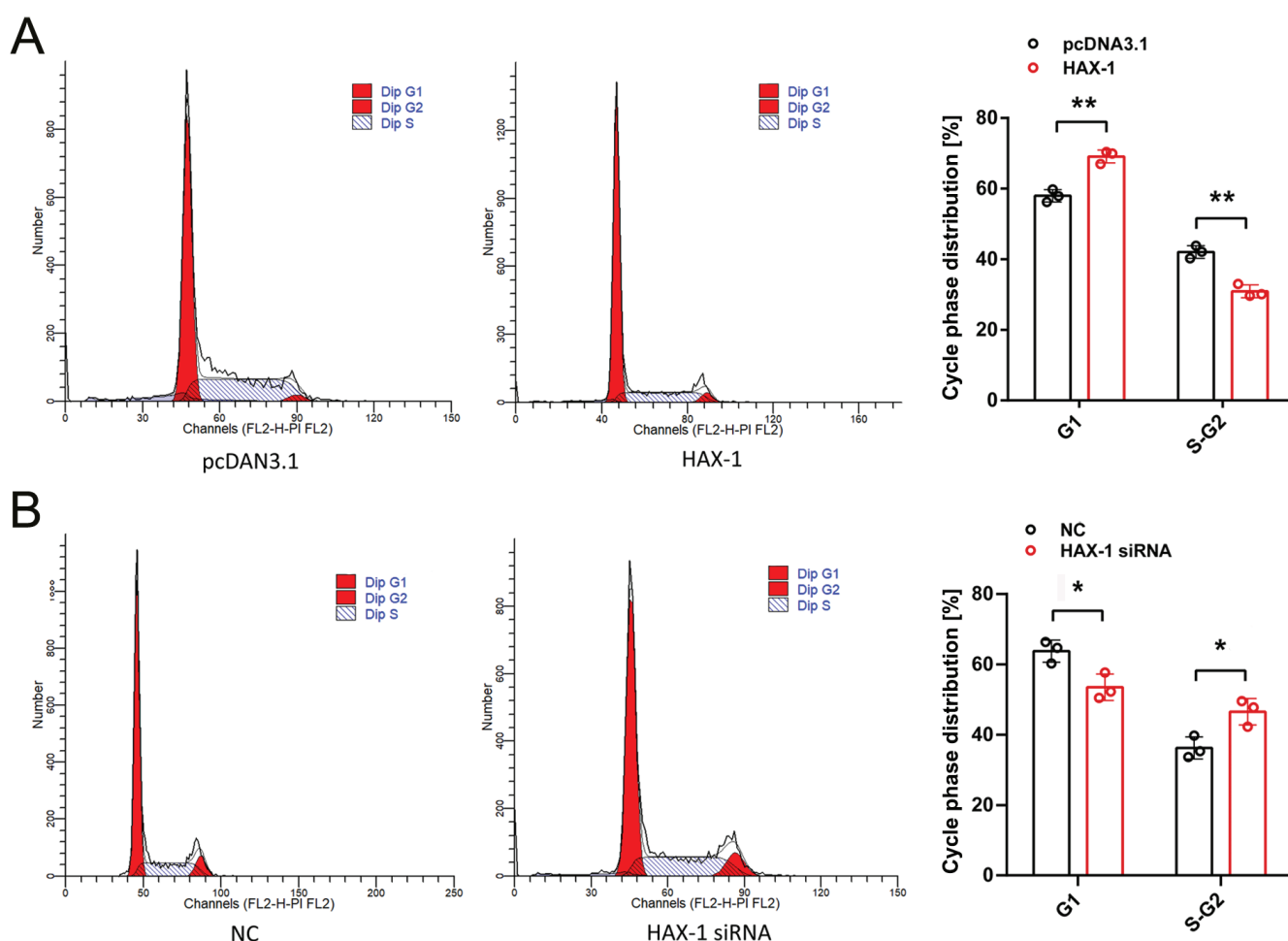


**Fig. 4.** The effect of HS1-associated protein X-1 (HAX-1) on cycle distribution of HA1800 cell. The results shown in the histograms demonstrated that there were more cells in the G1 phase and less cells in the S and G2 phases in the HAX-1 group (A), but in HAX-1 siRNA group the results were opposite (B). A.  $**p < 0.01$  compared to control (pcDNA3.1 group) (G1; t-test;  $t = 7.545$ );  $**p < 0.01$  compared to control (pcDNA3.1 group) (S-G2; t-test;  $t = 7.545$ ); B.  $*p < 0.05$  compared to the negative control (NC) group (G1; t-test;  $t = 3.632$ );  $*p < 0.05$  compared to NC group (S-G2; t-test;  $t = 3.632$ )

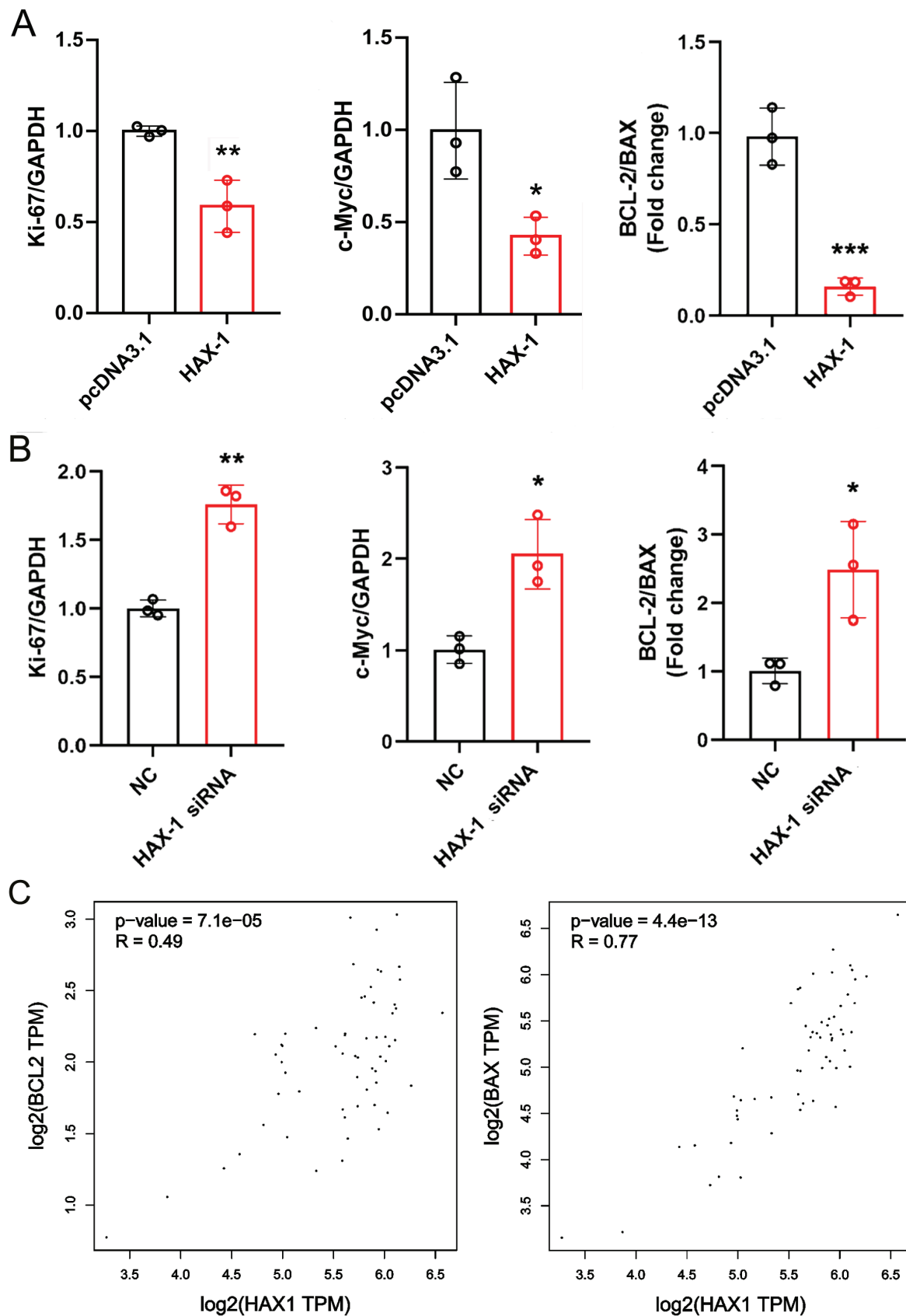


**Fig. 5.** The correlation between HSI-associated protein X-1 (HAX-1) and the expressions of Ki67, c-Myc, BCL-2, and BAX. **A.** In the HAX-1 group, Ki67 mRNA, c-Myc mRNA and BCL-2/BAX ratio were lower; **B.** In the HAX-1 siRNA group, Ki67 mRNA, c-Myc mRNA and BCL-2/BAX ratio were higher, compared to the control groups; **C.** BCL-2 and BAX were both positively correlated with HAX-1 in spinal cord; **A.** \*\* $p < 0.01$  compared to control (pcDNA3.1 group) (Ki67/GAPDH; t-test;  $t = 4.889$ ); \* $p < 0.05$  compared to control (pcDNA3.1 group) (c-Myc/GAPDH; t-test;  $t = 3.524$ ); \*\*\* $p < 0.001$  compared to control (pcDNA3.1 group) (BCL-2/BAX ratio; t-test;  $t = 8.759$ ); **B.** \*\* $p < 0.01$  compared to the negative control (NC) group (Ki67/GAPDH; t-test;  $t = 8.498$ ); \* $p < 0.05$  compared to the NC group (c-Myc/GAPDH; t-test;  $t = 4.296$ ); \* $p < 0.05$  compared to the NC group (BCL-2/BAX ratio; t-test;  $t = 3.513$ )



available.<sup>1,4</sup> The regeneration of the damaged axons after injury is very limited, resulting in a subsequent permanent dysfunction. Patients are disabled due to SCI caused by various reasons, leading to serious personal and social problems and heavy economic burden to patients and their families.<sup>1,34</sup> After SCI, the astrocytes become hypertrophic and proliferate, forming a dense network of astrocyte processes at the lesion site. This process builds a physical and biochemical barrier for axon regeneration.<sup>7</sup> Therefore, the inhibition of the activation and scar formation of the astrocytes will create a favorable environment for axon regeneration to promote recovery after SCI.<sup>10</sup>

Recent studies have shown that HAX-1 exists in numerous tissues and participates in or mediates the formation of cytoskeleton components by interacting with some proteins. This molecule also regulates the proliferation, adhesion and metastasis of many tumor cells.<sup>25,35,36</sup> The HAX-1 has been preferentially located in the mitochondria in the cell, and in a small part, on the endoplasmic reticulum and nuclear membrane, which was primarily inferred to be related to cell apoptosis.<sup>37</sup> However, some studies have demonstrated that the effect of HAX-1 on apoptosis was controversial. Human and rat HAX-1 genes have been severely spliced, resulting in at least 7 different variants, mainly due to the differences in the NH2 ends.<sup>38</sup> Different splice variants of HAX-1 have contrasting roles in regulating the apoptosis. The prototypical variant 1 has an antiapoptotic function, whereas HAX-1 variant 2 promotes cell death and abrogates the protective effect of variant 1.<sup>21</sup> The HAX-1 subtypes play different roles in apoptosis due to heterodimerization and homodimerization.<sup>22</sup> Based on this, HAX-1 has also been found to have an impact on cellular behaviors, such as the proliferation, migration and invasion of tumor cells (in particular, colorectal and nasopharyngeal cancer cell lines).<sup>39–41</sup> Qian et al. studied the expression and role of HAX-1 in cervical cancer and found that in the tumor cells, HAX-1 had an inhibitory effect on apoptosis and could promote the cell proliferation by reducing the formation of oxygen free radicals as well as protecting mitochondria through the P53 pathway. However, the effect of HAX-1 on cell migration is unknown.<sup>42</sup> A study on the effect of HAX-1 on the biological behavior of endothelial precursor cells showed that HAX-1 inhibited cell apoptosis and promoted proliferation of these cells by regulating the Akt signaling pathway and changing the interaction between Akt1 and HSP90.<sup>43</sup> The important role of HAX-1 in cell protection might also be related to the inhibition of mitochondrial and endoplasmic reticulum apoptosis pathways.<sup>37</sup> The HAX-1 also had certain effects on the nervous system. Studies have shown that HAX-1 had a neuroprotective effect against ischemic neuronal injury, and apoptosis after cerebral ischemia was induced by the downregulation of HAX-1 by NOX2-produced reactive oxygen species (ROS).<sup>17</sup> In addition, the lack of expression of HAX-1 had been associated with severe congenital neutropenia and the delayed and abnormal

neural development.<sup>44–46</sup> The HAX-1 might partially contribute to the formation of Lewy bodies and be associated with the occurrence and development of Parkinson's disease and dementia with Lewy bodies.<sup>47</sup> The HAX-1 expression was upregulated after hippocampal injury or traumatic brain injury induced by seizures.<sup>30</sup> In the current study, we successfully established HA1800 cell lines with high or low expression of HAX-1 to investigate the influence of HAX-1 on the proliferation and apoptosis of human astrocyte. The results showed that the cell activity and proliferation ability of HA1800 cells in the high-HAX-1 expression group were significantly weakened, and the cell cycle progress was decelerated, contrary to the results obtained from the low-HAX-1 expression group.

The Ki-67 is a nuclear protein that is also known as MKI-67, because it is encoded by the *MKI-67* gene, which is related to ribosomal RNA transcription and can be used as a marker of cell proliferation. The expression level of Ki67 is positively correlated with the activity of cell proliferation.<sup>48</sup> The *C-Myc* gene is one of the important members of the Myc proto-oncogene family. It is a translocation gene and an adjustable gene (regulated by various substances), which can promote cell division and make cells proliferate indefinitely and achieve immortalization. The level of *C-Myc* expression is closely related to the proliferation ability of cells.<sup>49</sup> The *BCL-2* gene family plays an important role in regulating cell apoptosis. The *BCL-2* and *BAX* belong to the *BCL-2* family and play, respectively, an anti-apoptotic and a proapoptotic effect on cells. The *BAX* has an antagonistic effect on *BCL-2*, which may lead to the loss of the proapoptotic effect of the *BCL-2* protein. The *BCL-2/BAX* ratio determines cell survival or death.<sup>50</sup> The results of this study showed that, in the low-HAX-1 expression HA1800 group, the expressions of Ki67 and c-Myc were upregulated, and the *BCL-2/BAX* ratio was increased. Contrasting results were obtained from the high-HAX-1 expression HA1800 group. Combined with the results from the GEPIA, these findings suggested that HAX-1 expression was closely related to the proliferation and apoptosis of human astrocytes, and the mechanism may be related to the *BCL-2/BAX* signaling pathway. Therefore, the level of HAX-1 at different stages of the SCI may be increased or decreased according to the double-sided role of glial cells in the process. The promotion of the repair of SCI may be achieved by silencing HAX-1 in the acute phase (promoting the formation of glial scars) and strengthening HAX-1 in the recovery phase (inhibiting the formation of glial scars). However, the specific mechanism and the involved signal pathway of HAX-1 in different injury stages need further studies and discussion.

## Limitations


In this study, the specific role of HAX-1 in the signaling pathway have not been clarified, which is a limitation of this study.

## Conclusions

This study shows that the high expression of HAX-1 could inhibit the proliferation, reduce cell viability and promote cell apoptosis of human HA1800 cells. In addition, the expression of Ki67 and c-Myc, and the ratio of BCL-2/BAX decreased in the high-HAX-1 expression group but significantly increased in the low-HAX-1 expression group. These results indicated that HAX-1 may promote the apoptosis of human HA1800 cells through the BCL-2/BAX signaling pathway, thereby inhibiting the cell proliferation. Further study on the specific role of HAX-1 in the signaling pathway should be performed.

### ORCID iDs

Xiaopeng Xia  <https://orcid.org/0000-0003-0534-8893>

Xiaojian Zhu  <https://orcid.org/0000-0001-7130-1749>

Shu Zhang  <https://orcid.org/0000-0001-8450-1627>

Xiaoxia Zhang  <https://orcid.org/0000-0003-3098-9553>

Yan Wang  <https://orcid.org/0000-0001-8759-5518>

### References

- Yousefifard M, Madani Neishaboori A, Rafiei Alavi S, et al. Active and passive immunization with myelin basic protein as a window for treatment of spinal cord injury: A systematic review and meta-analysis. *Int J Clin Pract*. 2021:e14406. doi:10.1111/ijcp.14406
- Casper DS, Zmistowski B, Schroeder G, et al. Preinjury patient characteristics and postinjury neurological status are associated with mortality following spinal cord injury. *Spine (Phila Pa 1976)*. 2018;43(13):895–899. doi:10.1097/brs.00000000000002533
- Rubiano AM, Carney N, Chesnut R, Puyana JC. Global neurotrauma research challenges and opportunities. *Nature*. 2015;527(7578):S193–S197. doi:10.1038/nature16035
- Sun X, Jones Z, Chen X, Zhou L, So K, Ren Y. Multiple organ dysfunction and systemic inflammation after spinal cord injury: A complex relationship. *J Neuroinflammation*. 2016;13(1):260. doi:10.1186/s12974-016-0736-y
- Anwar MA, Al Shehabi TS, Eid AH. Inflammogenesis of secondary spinal cord injury. *Front Cell Neurosci*. 2016;10:98. doi:10.3389/fncel.2016.00098
- Lee DY, Park YJ, Song SY, Hwang SC, Kim KT, Kim DH. The importance of early surgical decompression for acute traumatic spinal cord injury. *Clin Orthop Surg*. 2018;10(4):448–454. doi:10.4055/cios.2018.10.4.448
- Ahuja C, Martin A, Fehlings M. Recent advances in managing a spinal cord injury secondary to trauma. *F1000Res*. 2016;5:F1000. doi:10.12688/f1000research.7586.1
- Ahmed A, Patil AA, Agrawal DK. Immunobiology of spinal cord injuries and potential therapeutic approaches. *Mol Cell Biochem*. 2018;441(1–2):181–189. doi:10.1007/s11010-017-3184-9
- Rolls A, Shechter R, Schwartz M. The bright side of the glial scar in CNS repair. *Nat Rev Neurosci*. 2009;10(3):235–241. doi:10.1038/nrn2591
- Li G, Cao Y, Shen F, et al. Mdivi-1 inhibits astrocyte activation and astroglial scar formation and enhances axonal regeneration after spinal cord injury in rats. *Front Cell Neurosci*. 2016;10:241. doi:10.3389/fncel.2016.00241
- Cafferty W, Yang S, Duffy P, Li S, Strittmatter S. Functional axonal regeneration through astrocytic scar genetically modified to digest chondroitin sulfate proteoglycans. *J Neurosci*. 2007;27(9):2176–2185. doi:10.1523/jneurosci.5176-06.2007
- Klein C. Kostmann's disease and HCLS1-associated protein X-1 (HAX1). *J Clin Immunol*. 2017;37(2):117–122. doi:10.1007/s10875-016-0358-2
- Suzuki Y, Demoliere C, Kitamura D, Takeshita H, Deuschle U, Watanabe T. HAX-1, a novel intracellular protein, localized on mitochondria, directly associates with Hs1, a substrate of Src family tyrosine kinases. *J Immunol*. 1997;158(6):2736–2744. PMID:9058808.
- Li X, Jiang J, Yang R, et al. Expression of HAX-1 in colorectal cancer and its role in cancer cell growth. *Mol Med Report*. 2015;12(3):4071–4078. doi:10.3892/mmr.2015.3905
- Trebinska A, Högstrand K, Grandien A, Grzybowska E, Fadeel B. Exploring the anti-apoptotic role of HAX-1 versus BCL-XL in cytokine-dependent bone marrow-derived cells from mice. *FEBS Lett*. 2014;588(17):2921–2927. doi:10.1016/j.febslet.2014.05.042
- Deng X, Song L, Zhao W, Wei Y, Guo X. HAX-1 protects glioblastoma cells from apoptosis through the Akt1 pathway. *Front Cell Neurosci*. 2017;11:420. doi:10.3389/fncel.2017.00420
- Sui X, Yoshioka H, Fukumoto Y, Kanemaru K, Kinouchi H. Neuroprotective roles of HAX-1 in ischemic neuronal injury. *Exp Neurol*. 2021;339:113642. doi:10.1016/j.expneurol.2021.113642
- Lam A, Galione A, Lai F, Zissimopoulos S. Hax-1 identified as a two-pore channel (TPC)-binding protein. *FEBS Lett*. 2013;587(23):3782–3786. doi:10.1016/j.febslet.2013.10.031
- Lam CK, Zhao W, Liu GS, et al. HAX-1 regulates cyclophilin-D levels and mitochondria permeability transition pore in the heart. *Proc Natl Acad Sci U S A*. 2015;112(47):E6466–E6475. doi:10.1073/pnas.1508760112
- Chen J, Yang S, Wu C, et al. Novel role of HAX-1 in neurons protection after spinal cord injury involvement of IRE-1. *Neurochem Res*. 2020;45(10):2302–2311. doi:10.1007/s11064-020-03088-x
- Koontz J, Kontogianni-Konstantopoulos A. Competition through dimerization between antiapoptotic and proapoptotic HS-1-associated protein X-1 (Hax-1). *J Biol Chem*. 2014;289(6):3468–3477. doi:10.1074/jbc.M113.536151
- Wang K, Yuan Y, Liu X, et al. Cardiac specific overexpression of mitochondrial Omi/HtrA2 induces myocardial apoptosis and cardiac dysfunction. *Sci Rep*. 2016;6:37927. doi:10.1038/srep37927
- Lu X, Xue P, Fu L, et al. HAX1 is associated with neuronal apoptosis and astrocyte proliferation after spinal cord injury. *Tissue Cell*. 2018;54:1–9. doi:10.1016/j.tice.2018.07.001
- You B, Cao X, Shao X, et al. Clinical and biological significance of HAX-1 overexpression in nasopharyngeal carcinoma. *Oncotarget*. 2016;7(11):12505–12524. doi:10.18632/oncotarget.7274
- You B, Shan Y, Bao L, et al. The biology and function of extracellular vesicles in nasopharyngeal carcinoma (Review). *Int J Oncol*. 2018;52(1):38–46. doi:10.3892/ijo.2017.4202
- Baumann U, Fernández-Sáiz V, Rudelius M, et al. Disruption of the PRKCD-FBXO25-HAX-1 axis attenuates the apoptotic response and drives lymphomagenesis. *Nat Med*. 2014;20(12):1401–1409. doi:10.1038/nm.3740
- Sun S, Feng L, Zhao G, Dong Z. Retraction note: HAX-1 promotes the chemoresistance, invasion, and tumorigenicity of esophageal squamous carcinoma cells. *Dig Dis Sci*. 2019;64(8):2368. doi:10.1007/s10620-019-05728-x
- Wu H, Chen J, Wang Q, et al. Abnormal expression of HAX-1 is associated with cellular proliferation and migration in human hypopharyngeal squamous cell carcinoma. *Mol Med Rep*. 2017;16(4):4664–4670. doi:10.3892/mmr.2017.7155
- Deng X, Song L, Wei Y, Guo X. Analysis of the expression of HAX-1 gene in human glioma. *Neurosci Lett*. 2017;657(189–193). doi:10.1016/j.neulet.2017.07.039
- Shi W, Zhao W, Shen A, et al. Traumatic brain injury induces an up-regulation of Hs1-associated protein X-1 (Hax-1) in rat brain cortex. *Neurochem Res*. 2011;36(3):375–382. doi:10.1007/s11064-010-0332-y
- Rami A, Kim M, Niquet J, Langhagen A. Alterations in the expression of the anti-apoptotic factor HAX-1 upon seizures-induced hippocampal injury in the neonatal rat brain. *Neurochem Res*. 2012;37(1):116–125. doi:10.1007/s11064-011-0589-9
- Tran A, Warren P, Silver J. The biology of regeneration failure and success after spinal cord injury. *Physiol Rev*. 2018;98(2):881–917. doi:10.1152/physrev.00017.2017
- Tang Z, Li C, Kang B, Gao G, Li C, Zhang Z. GEPIA: A web server for cancer and normal gene expression profiling and interactive analyses. *Nucleic Acids Res*. 2017;45(W1):W98–W102. doi:10.1093/nar/gkx247
- Gooch CL, Pracht E, Borenstein AR. The burden of neurological disease in the United States: A summary report and call to action. *Ann Neurol*. 2017;81(4):479–484. doi:10.1002/ana.24897
- Meng L, Li J, Meng X, et al. *Sanguisorba parviflora* (Maxim.) Take-da alleviates cyclophosphamide-induced leukopenia by regulating haematopoietic cell-specific protein 1-associated protein X-1 gene expression. *J Clin Pharm Ther*. 2021;46(5):1373–1381. doi:10.1111/jcpt.13468

36. Li R, Zheng J, Huang X. Suppression of HAX-1 induced by miR-325 resensitizes bladder cancer cells to cisplatin-induced apoptosis. *Eur Rev Med Pharmacol Sci.* 2020;24(18):9303–9314. doi:10.26355/eur-rev\_202009\_23012
37. Fujino K, Horie M, Kojima S, et al. A human endogenous bornavirus-like nucleoprotein encodes a mitochondrial protein associated with cell viability. *J Virol.* 2021;95(14):e0203020. doi:10.1128/jvi.02030-20
38. Grzybowska E, Sarnowska E, Konopiński R, Wilczyńska A, Sarnowski T, Siedlecki J. Identification and expression analysis of alternative splice variants of the rat Hax-1 gene. *Gene.* 2006;371(1):84–92. doi:10.1016/j.gene.2005.11.035
39. Wu H, Chen J, Wang Q, et al. Abnormal expression of HAX-1 is associated with cellular proliferation and migration in human hypopharyngeal squamous cell carcinoma. *Mol Med Rep.* 2017;16(4):4664–4670. doi:10.3892/mmr.2017.7155
40. Yu L, Li H, Hou S, et al. Abnormal bone mineral density and bone turnover marker expression profiles in patients with primary spontaneous pneumothorax. *J Thorac Dis.* 2016;8(6):1188–1196. doi:10.21037/jtd.2016.04.52
41. Szwarz M, Sarnowska E, Grzybowska E. HAX-1 protein: Multifunctional factor involved in apoptosis, cell migration, endocytosis and mRNA transport [in Polish]. *Postepy Biochem.* 2007;53(3):218–227. PMID:18399350.
42. Qian B, Zhao LJ, Teng F, Gao LJ, Shen R. Role of the tumour protein P53 gene in human cervical squamous carcinoma cells: Discussing haematopoietic cell-specific protein 1-associated protein X-1-induced survival, migration and proliferation. *Oncol Lett.* 2018;16(2):2629–2637. doi:10.3892/ol.2018.8886
43. Guo X, Deng X, Wei Y. Hematopoietic substrate-1-associated protein X-1 regulates the proliferation and apoptosis of endothelial progenitor cells through akt pathway modulation. *Stem Cells.* 2018;36(3):406–419. doi:10.1002/stem.2741
44. Cetinkaya P, Cagdas D, Arikoglu T, Gumruk F, Tezcan I. Three patients with glucose-6 phosphatase catalytic subunit 3 deficiency. *J Pediatr Endocrinol Metab.* 2020;33(7):957–961. doi:10.1515/jpem-2019-0541
45. Ishikawa N, Okada S, Miki M, et al. Neurodevelopmental abnormalities associated with severe congenital neutropenia due to the R86X mutation in the HAX1 gene. *J Med Genet.* 2008;45(12):802–807. doi:10.1136/jmg.2008.058297
46. Yap S, Koontz J, Kontrogianni-Konstantopoulos A. HAX-1: A family of apoptotic regulators in health and disease. *J Cell Physiol.* 2011;226(11):2752–2761. doi:10.1002/jcp.22638
47. Kawamoto Y, Ayaki T, Urushitani M, Ito H, Takahashi R. Accumulation of HAX-1 and PARL in brainstem- and cortical-type Lewy bodies in Parkinson's disease and dementia with Lewy bodies. *J Neurol Sci.* 2020;415:116928. doi:10.1016/j.jns.2020.116928
48. Yamaguchi M, Takagi K, Sato M, et al. Androgens enhance the ability of intratumoral macrophages to promote breast cancer progression. *Oncol Rep.* 2021;46(3):188. doi:10.3892/or.2021.8139
49. Dang CV. MYC on the path to cancer. *Cell.* 2012;149(1):22–35. doi:10.1016/j.cell.2012.03.003
50. Li Y, Jing J, Dang W, et al. Effects of Notch2 on proliferation, apoptosis and steroidogenesis in bovine luteinized granulosa cells. *Theriogenology.* 2021;171:55–63. doi:10.1016/j.theriogenology.2021.05.009



# The functional and radiographic outcomes following distal radius fracture treatment in a cast for 4 and 6 weeks in the elderly: A randomized trial

Jarosław Olech<sup>1,A-F</sup>, Bartosz Kopczyński<sup>2,D-F</sup>, Łukasz Tomczyk<sup>3,C,D,F</sup>, Grzegorz Konieczny<sup>4,A,B,D,F</sup>, Krystian Kazubski<sup>2,D-F</sup>, Piotr Morasiewicz<sup>2,A,C-F</sup>

<sup>1</sup> Orthopedic Surgery Department, Provincial Specialist Hospital in Legnica, Poland

<sup>2</sup> Department of Orthopaedic and Trauma Surgery, Institute of Medical Sciences, University of Opole, Poland

<sup>3</sup> Department of Food Safety and Quality Management, Poznan University of Life Sciences, Poland

<sup>4</sup> Faculty of Health Sciences and Physical Education, The Witelton State University of Applied Sciences in Legnica, Poland

A – research concept and design; B – collection and/or assembly of data; C – data analysis and interpretation;

D – writing the article; E – critical revision of the article; F – final approval of the article

Advances in Clinical and Experimental Medicine, ISSN 1899–5276 (print), ISSN 2451–2680 (online)

*Adv Clin Exp Med.* 2022;31(6):701–706

## Address for correspondence

Piotr Morasiewicz

E-mail: morasp@poczta.onet.pl

## Funding sources

None declared

## Conflict of interest

None declared

Received on January 18, 2022

Reviewed on March 16, 2022

Accepted on May 13, 2022

Published online on June 2, 2022

## Cite as

Olech J, Kopczyński B, Tomczyk Ł, Konieczny G, Kazubski K, Morasiewicz P. The functional and radiographic outcomes following distal radius fracture treatment in a cast for 4 and 6 weeks in the elderly: A randomized trial. *Adv Clin Exp Med.* 2022;31(6):701–706. doi:10.17219/acem/150032

## DOI

10.17219/acem/150032

## Copyright

Copyright by Author(s)

This is an article distributed under the terms of the Creative Commons Attribution 3.0 Unported (CC BY 3.0) (<https://creativecommons.org/licenses/by/3.0/>)

## Abstract

**Background.** The optimal duration of cast immobilization following distal radius fractures (DRFs) in elderly patients has not been established.

**Objectives.** To assess the functional and radiological parameters following DRF treatment in elderly patients using 2 different periods of cast immobilization.

**Materials and methods.** We assessed 50 patients (33 women and 17 men). The mean age at the beginning of treatment was 71 years. The mean duration of follow-up was 1 year and 3 months. One subgroup (n = 26) included patients treated with a cast for 4 weeks, whereas the other subgroup (n = 24) included patients treated with a cast for 6 weeks. The following measures were assessed: union rate, radial inclination, volar tilt, radial height, Visual Analogue Scale (VAS) pain score, Mayo Wrist Score, and VAS activity score.

**Results.** The mean volar tilt was 9.13° in the group treated with a cast for 4 weeks and 3.29° in the group treated with a cast for 6 weeks (p = 0.043). There were no differences between the groups in terms of any other functional or radiological parameters.

**Conclusions.** The VAS pain score, Mayo Wrist Score and VAS activity score were similar between the 2 study groups. The greatest volar tilt angle was observed after 6 weeks of cast immobilization. The study groups showed no significant differences in terms of radial inclination, union rate, radial height, or bone union. A period of 4 weeks of cast treatment was sufficient for elderly patients with DRFs.

**Key words:** distal radius fracture, functional, radiographic, elderly

## Background

Distal radius fractures (DRFs) are among the top 3 fracture locations, which makes these fractures a considerable social problem and a major healthcare burden.<sup>1–12</sup> A closed reduction and immobilization using a forearm cast is indicated in simple fractures, in poor soft tissue condition around osteoporotic bone, and in less demanding patients, such as the elderly.<sup>11–15</sup> A closed reduction and immobilization including a forearm cast is the preferred method of treatment for DRFs in the elderly,<sup>13</sup> particularly since it is associated with good functional and clinical outcomes.<sup>11</sup>

There is no gold standard in terms of maintenance time for a plaster cast in patients with DRF.<sup>9,13–17</sup> Some studies recommend cast immobilization for 4 weeks,<sup>9,13</sup> some prefer a 5-week cast immobilization,<sup>13,14,17</sup> whereas others advocate a 6-week treatment.<sup>9,15</sup> To date, no studies have assessed the radiological and functional impact of cast immobilization time in DRF treatment in the elderly. Toon et al. noted a mean pain severity of 1.1 using the Visual Analogue Scale (VAS) after closed reduction and immobilization in a forearm cast, and 1.8 after open reduction and plate stabilization.<sup>9</sup> Kilic et al. and Yin et al. observed 100% bone union after closed reduction and immobilization in a forearm cast, without assessing the effects of the immobilization period on achieving bone union.<sup>13,18</sup> The studies which have analyzed nonsurgical treatment for DRF likewise did not consider the effects of the immobilization period on radiographic outcomes.<sup>9,13,15</sup>

A comparison of DRF treatment outcomes following cast immobilization for different periods of time may help in selecting the optimal duration of cast immobilization. The DRF treatment outcomes can be adequately compared via radiographic and functional assessment. Some studies have reported a correlation between good radiological and clinical outcomes.<sup>5,19,20</sup> A long period of immobilization in a cast may adversely affect the range of motion and hand function, and reduce muscle strength in patients with DRF.<sup>16,17,21,22</sup> These factors suggest the need for limiting the period of immobilization in elderly patients with DRFs. However, shortening the immobilization time may increase the frequency of bone fragment instability, bone nonunion and persistent pain. We hypothesized that the period of cast immobilization would affect radiographic and functional outcomes in the elderly patients treated for DRF.

The aim of our randomized trial was to perform functional and radiological evaluation of elderly patients after DRF treatment, depending on the period of cast immobilization.

## Materials and methods

Our study was a prospective evaluation of patients with DRF treated between June 2020 and November 2020. Within this period, 117 patients with DRF were treated

in our hospital. The following inclusion criteria were used: DRF with closed reduction and immobilization in a forearm cast; follow-up of at least 12 months after treatment completion; availability of radiological documentation; complete data on VAS-rated pain severity; VAS activity scores and Mayo Wrist Scores; age >65 years. The exclusion criteria included: bilateral upper limb injury; a multi-fragment fracture; surgery treatment; lack of complete medical and radiological documentation; age <65 years; incomplete medical and radiographic data; incomplete data on VAS pain scores, VAS activity scores or Mayo Wrist Scores. We assessed only the patients who initially qualified for conservative treatment, i.e., patients with simple fractures. In both groups, there were no patients with multi-fragment fractures, open fractures, intra-articular fractures, or initially unstable fractures eligible for surgery. The patients were informed about the voluntary nature of the study. All study protocols were approved by the Bioethics Committee at the Lower Silesian Medical Chamber in Wrocław, Poland (protocol No. 2/PNDR/2020, date of approval: June 10, 2020). Informed consent was obtained from all subjects. The study was conducted in accordance with the guidelines of the Declaration of Helsinki.

A total of 50 elderly patients (17 men and 33 women) met the study inclusion criteria. The mean age of the evaluated patients at the time of injury was 71 years (range: 65–86 years). The mean body mass index (BMI) was 27.4 kg/m<sup>2</sup> (range: 21.5–35.3 kg/m<sup>2</sup>). The mean follow-up period was 1 year and 3 months (range: 12–18 months). The patients who were diagnosed with DRF and provided informed consent were randomized. The randomization was carried out using numbered sealed envelopes, with patients allocated to one of the 2 subgroups, each with a different duration of cast immobilization. The 1<sup>st</sup> group (n = 26) consisted of patients who were to undergo cast treatment for 4 weeks and the 2<sup>nd</sup> group (n = 24) of patients slated for a 6-week treatment. The patients from both study groups underwent a closed reduction of their fracture in an emergency room and had their injured limb immobilized in a short arm cast. The first control X-rays were performed in the emergency department immediately after reduction and cast immobilization. The fracture was reduced with the arm stabilized by the assist, using traction, volar flexion and radialization of the hand and wrist. The limb was immobilized in a short arm cast in the volar flexion and wrist radialization. None of the patients developed a secondary displacement of reduced bone fragments which would require surgery.

All patients were periodically assessed radiographically and clinically during outpatient clinic visits. The casts were removed after 4 or 6 weeks, depending on the group. After cast removal, all patients were introduced to the identical exercise protocols for their hand and wrist. For 4–6 weeks, the patients were advised to use the affected hand sparingly. Based on clinical and radiological assessments, the use of the affected upper limb was gradually increased.

The following radiographic and functional parameters were evaluated: 1) union rate, 2) radial inclination, 3) volar tilt, 4) radial height, 5) VAS pain score, 6) Mayo Wrist Score, and 7) VAS activity score.

Bone union was assessed clinically and radiographically. Radiologically, bone union was found in the presence of 3 of the 4 cortical layers of bone, or with trabecular transition between fragments of the fractured bone on X-rays in 2 projections.<sup>7,23</sup> The clinical union was found in the absence of pathological mobility, pain and deformation during strong movement attempts around the wrist. The nonunion was found when the criteria of union were not met more than 6 months after the injury. The radial inclination was measured in anteroposterior radiographs of the wrist, and was defined as the angle between the line parallel to the distal radial articular surface and the line perpendicular to the long axis of the radius. The normal range for radial inclination of 16–29° was adopted based on previous studies.<sup>6,7,15,24</sup> Any deviation from the normal radial inclination was measured and presented in degrees.

The volar tilt was measured on lateral radiographs of the wrist, and was defined as the angle between the distal radial articular surface and the line perpendicular to the long axis of the radius. The normal range of volar tilt between 15° and 0° was adopted based on prior studies.<sup>6,7,15</sup> Any deviation from the normal range was measured and presented in degrees. Radial height, which was measured in postoperative anteroposterior radiographs, was defined as the distance between 2 parallel lines, both perpendicular to the long axis of the radius, with one of the lines passing through the tip of the radial styloid process, and the other through the distal ulnar articular surface. A normal radial height is 10–13 mm; these values, within a 5-mm range, were based on prior published studies.<sup>6,15</sup> Any deviation from normal values was presented in millimeters.

The pain severity was assessed using the VAS.<sup>7,9</sup> The Mayo Wrist Score was measured on a scale ranging from 0 to 100 points. The scores represent pain on active flexion/extension compared to the contralateral wrist,

and indicate the possibility of resuming work and the relative muscle strength.<sup>7,9,25</sup> Subjective physical activity was assessed by patients on a scale ranging from 0 to 10.<sup>26,27</sup> All patients were assessed clinically and radiographically at follow-up for more than 1 year after the end of treatment. The groups with immobilization in plaster cast for 4 weeks and for 6 weeks were compared. Statistical analyses were carried out using STATISTICA v. 13.1 (StatSoft Inc., Tulsa, USA). The Student’s t-test was used to compare quantitative variables between groups. The Bartlett’s test, Cochran’s test and Hartley’s test were used to evaluate homogeneity of variance between the groups. The Shapiro–Wilk test was used to assess the normality of the distributions (Table 1). A critical value of  $p \leq 0.05$  was used throughout this study.

## Results

The age of the patients in the 2 evaluation groups was comparable ( $p = 0.562$ ). There was no nonunion in any of the evaluated patients from both study groups (Table 1).

The radial inclination did not differ statistically between the study groups with the 2 different cast immobilization periods ( $p = 0.619$ ) (Table 1). Better outcomes were observed after 6-week cast immobilization, with the mean radial inclination 0.25° beyond the adopted normal range. Somewhat worse outcomes were observed after a 4-week immobilization period, with the mean radial inclination 0.55° beyond the adopted normal range (Table 1). The volar tilt values closer to normal were observed in the group treated for 6 weeks (with the mean value of 3.29° beyond the adopted normal range). Considerably worse results were achieved after 4 weeks of immobilization (9.13°). The difference was statistically significant ( $p = 0.043$ ) (Fig. 1, Table 1).

The group that achieved better post-treatment radial height values was the group treated for 4 weeks (with the final radial height differing from the normal by a mean of 1.9 mm). Somewhat worse radial height values were observed after

**Table 1.** Detailed results of the functional and radiological evaluation of individual subgroups

Analyzed variable (mean ±SD)	4-week group (n = 26)	6-week group (n = 24)	Shapiro–Wilk test – p-value		Bartlett’s test, Cochran’s test and Hartley’s test p-value	Student’s test p-value
			4-week group	6-week group		
Age of patients [years]	71.34 ±4.99	72.20 ±5.46	0.781	0.869	0.241	0.563
Radial height [mm]	0.55 ±2.84	0.25 ±1.03	0.054	0.050	0.672	0.619
Volar tilt [°]	9.13 ±7.12	3.29 ±5.11	0.074	0.094	0.522	0.043
Union	1 ±0	1 ±0	–	–	–	–
Radial height [°]	1.9 ±1.62	2.45 ±2.47	0.900	0.214	0.367	0.351
VAS pain score	2.53 ±3.06	3.58 ±2.56	0.087	0.064	0.472	0.199
VAS activity score	7.61 ±1.83	7.58 ±2.3	0.052	0.082	0.587	0.957
Mayo Wrist Score	58.46 ±21.24	61.87 ±22.97	0.300	0.147	0.687	0.588

SD – standard deviation; VAS – Visual Analogue Scale.

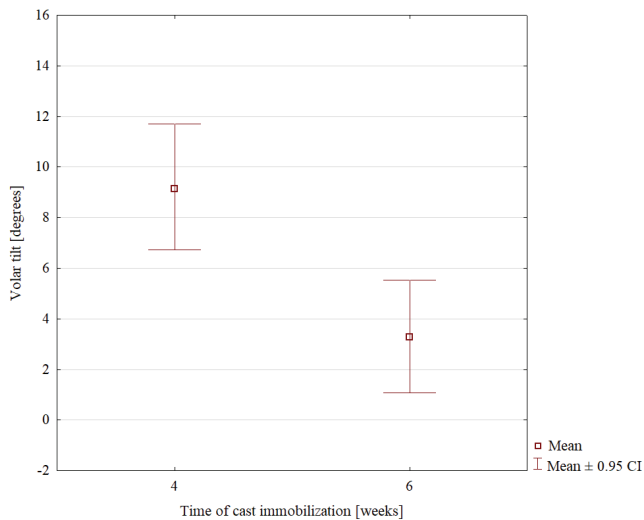


Fig. 1. Volar tilt in subgroups

CI – confidence interval.

6 weeks of cast immobilization (a mean of 2.45 mm beyond the normal value; Table 1). However, these differences were not significant ( $p = 0.351$ ). The patient-reported pain severity was lower in the 4-week group (VAS score of 2.53), with the moderately higher mean VAS pain score of 3.58 in the 6-week group. These differences were not significant ( $p = 0.199$ ) (Table 1). The mean Mayo Wrist Score was 58.46 in the subgroup treated for 4 weeks and 61.87 in the subgroup treated for 6 weeks (Table 1). This difference was not statistically significant ( $p = 0.588$ ). There were no statistical differences in the VAS activity score between the group with 4 weeks of immobilization (7.61) and the group with 6 weeks of immobilization (7.58) ( $p = 0.957$ ; Table 1).

## Discussion

Our study used functional and radiographic measures to assess whether elderly with DRF who undergo cast immobilization can complete their treatment earlier (after 4 weeks) and resume their normal activities without having to have their limb immobilized in a cast for 6 weeks. There have been no studies evaluating functional and radiographic parameters of elderly patients following DRF to determine which cast immobilization period (4 or 6 weeks) produces better outcomes. The outcomes achieved in patients whose fracture was immobilized for 6 weeks were significantly better only in terms of volar tilt. We observed no significant differences between the study groups in any of the other assessed parameters. Thus, our research hypothesis was only partially confirmed.

Distal radius fractures are among the top 3 fracture locations, which makes such fractures a considerable social problem and healthcare burden.<sup>1–12</sup> Distal radius fractures is often treated conservatively.<sup>11,13–15</sup> There is no gold standard regarding the maintenance time of a plaster cast for

DRF.<sup>9,13–17</sup> Some studies propose a 4-week immobilization period,<sup>9,13</sup> some propose a 5-week period,<sup>13,14,17</sup> while others advocate 6 weeks of cast immobilization.<sup>9,15</sup> A long maintenance time of a plaster cast may have a negative effect on the range of motion and hand function, and reduce muscle strength in patients with DRF.<sup>16,17,21,22</sup> These factors suggest that a shorter maintenance time of a plaster cast following DRFs would be more beneficial in elderly patients. A shorter maintenance time of a plaster cast in patients who have achieved bone union may allow for earlier exercises, limb rehabilitation and the return of limb function.<sup>15–17,21</sup> However, it should be noted that reducing the cast immobilization period in the elderly with osteoporosis may contribute to more complications in the form of bone fragment instability, nonunion and persistent pain.

The mean VAS pain score after treatment for DRFs was 1.1–1.8, which is comparable to the findings of prior studies.<sup>7,9,28</sup> No studies have compared the VAS pain scores following DRF treatment with a cast over time. In our study, we observed no differences in VAS pain scores between the 4-week group and the 6-week group. Our results were comparable to those of other researchers.<sup>7,9,28</sup> The mean Mayo Wrist Score was 82.4–85.3 in DRF patients stabilized with a plate.<sup>7,25</sup> Other measurements we obtained were similar, but lower in comparison to those reported by other authors.<sup>7,9,25</sup> The mean VAS activity scores in patients who underwent osteotomy with an Ilizarov fixator,<sup>26</sup> those with ankle joint arthrodesis with an Ilizarov fixator, and those with internal fixation were 5.98, 6.85 and 5.35, respectively.<sup>27</sup> In our study, VAS activity scores did not differ between the 4-week group and the 6-week group. These scores were somewhat better than those reported in prior studies.<sup>26,27</sup> Bone union was found in all patients after DRF treatment with plate stabilization or immobilization in plaster cast.<sup>13,18,29</sup> In our study, bone union was achieved in all patients from both study groups; this outcome was similar to those reported in prior studies.<sup>13,18,29</sup>

Katayama et al. reported a correlation between abnormal radial inclination and the development of arthritis; the mean radial inclination in the evaluated study group was 24.2°.<sup>7</sup> Radial inclination angles closer to normal were observed by Toon et al. in a group of patients with cast immobilization (16.9°).<sup>9</sup> Lameijer et al. observed a post-treatment radial inclination of 25.5° in patients without osteoporosis following DRFs.<sup>24</sup> Kilic et al. observed a radial inclination of 17  $\pm$  4.6° in patients after plaster cast immobilization.<sup>13</sup> Zengin et al. reported post-treatment radial inclination angles that were closer to normal in a group with a volar plate stabilization (mean radial inclination of 21.5°) than in patients with a cast immobilization (16.6°).<sup>15</sup> Arora et al. found a radial inclination of 19.2  $\pm$  6.5° in the cast immobilization group.<sup>14</sup> In our study, both groups achieved radial inclination angles close to normal, with no significant differences between the groups. Our radial inclination angles values were similar to those reported in earlier studies.<sup>7,9,13–15,24</sup>



Katayama et al. observed a correlation between abnormal volar tilt angles and the development of arthritis; the mean volar tilt angle in that study group was 6.4°.7 Toon et al. reported better mean volar tilt angles in a group of patients treated with plate fixation (5.6°) in comparison to those treated with plaster cast immobilization (0.1°).9 Kilic et al. observed a volar tilt of 5.6 ± 5.4° in a cast group.13 Arora et al. observed a volar tilt of -24.4 ± -12° in a group with cast immobilization.14 Zyluk et al. observed volar tilt angles closer to normal ones in a group with volar plate fixation and K-wire stabilization.19 The mean post-treatment volar tilt angles reported by Zengin et al. were within the adopted normal range in patients treated with volar plate fixation (6.9°) but fell outside of the normal range (-1°) in patients treated with cast immobilization.15 In our study, volar tilt values closer to normal were observed in the 6-week group, whereas values different from the normal ones were noticed in the 4-week group. The volar tilt angles were significantly better in the group with 6 weeks of cast immobilization. The volar tilt angle values in our study were similar to those of other studies.7,9,13–15,19

The mean radial height value in DRF patients treated with cast fixation was 3.9–9.0 mm, depending on the group.9,13–15 In our study, both groups achieved radial height values close to normal. The study subgroups did not differ significantly in terms of radial height and these values in our study were comparable to those of other studies.9,13–15 Some studies have found a correlation between good radiological and clinical outcomes after DRF treatment.5,19,20 In contrast, other studies reported good treatment outcomes even with poor radiographic outcomes.9,14,15 In our study, we achieved good radiographic and functional outcomes in both study groups, likely since patients experienced only mild pain following their treatment. Apart from volar tilt angle values in radiographic assessments, we have observed no differences between the study groups in either radiographic or functional parameters. These outcomes indicate the possibility of regaining full limb function by the elderly treated for DRF with 4 weeks of cast immobilization.


Our study showed that a period of 4 weeks was sufficient to achieve complete fracture remodeling and bone union in all patients. The similar radiographic and functional outcomes achieved in both evaluated groups encourage us to recommend a 4-week period of fracture immobilization. This duration of cast immobilization will help introduce earlier rehabilitation, earlier return to normal use of the injured arm and a more rapid return to normal daily functioning in older patients with DRF. One limitation of our study was the relatively small sample size. However, other studies have also used a similar or smaller group.7,9,13,25 The strengths of our study are patient randomization, the same rehabilitation protocol for all patients and the same examination protocol carried out by one orthopedist. We aim to perform a follow-up study in a larger group of patients.


## Conclusions


The study groups did not differ in terms of VAS pain scores, Mayo Wrist Scores or VAS activity scores. The highest volar tilt angle value was observed after 6 weeks of cast immobilization. All patients from both groups achieved bone union. The study groups showed no significant differences in terms of radial inclination, union rate or radial height. Both groups achieved good functional and radiographic outcomes. In summary, we found that cast immobilization for a period of 4 weeks is sufficient for DRF treatment in the elderly.

## ORCID iDs

Jarosław Olech  <https://orcid.org/0000-0001-8637-6882>

Bartosz Kopczyński  <https://orcid.org/0000-0002-8541-5824>

Łukasz Tomczyk  <https://orcid.org/0000-0002-4644-0111>

Krystian Kazubski  <https://orcid.org/0000-0002-0366-2371>

Piotr Morasiewicz  <https://orcid.org/0000-0002-7587-666X>

## References

- Hye-Young K, Hyun-Ho K, Yoon Kyoung S, Yound Chan H. Incidence and mortality of osteoporotic fracture in rheumatoid arthritis in South Korea using nationwide claims data. *J Bone Metab.* 2019; 26(2):97–104. doi:10.11005/jbm.2019.26.2.97
- Ogunleye AA, Mullner DF, Skochdopole A, Armstrong M, Herrera FA. Remote injuries and outcomes after distal radius fracture management. *Hand (N Y).* 2019;14(1):102–106. doi:10.1177/1558944718798838
- Ochi K, Go Y, Furuya T, et al. Risk factors associated with the occurrence of distal radius fractures in Japanese patients with rheumatoid arthritis: A prospective observational cohort study. *Clin Rheumatol.* 2014;33(4):477–483. doi:10.1007/s10067-013-2415-z
- Ali M, Eiriksdottir A, Murtadha M, Åkesson A, Atroshi I. Incidence of distal radius fracture in a general population in southern Sweden in 2016 compared with 2001. *Osteoporos Int.* 2020;31(4):715–720. doi:10.1007/s00198-020-05282-7
- Talmaç MA, Görgel MA, Kanar M, Tok O, Özdemir HM. Comparison of three surgical methods in the treatment of intraarticular comminuted distal radius fractures: Volar locking plate, non-bridging external fixator, and bridging external fixator. *Eklemler Hastalıkları Cerrahisi.* 2019;30(3):224–232. doi:10.5606/ehc.2019.66955
- Chung KC, Malay S, Shauver MJ, Kim HM; WRIST Group. Assessment of distal radius fracture complications among adults 60 years or older: A secondary analysis of the WRIST randomized clinical trial. *JAMA Netw Open.* 2019;2(1):e187053. doi:10.1001/jamanetworkopen.2018.7053
- Katayama T, Ono H, Omokawa S. Comparison of five years clinical and radiological outcomes between progressive and non-progressive wrist osteoarthritis after volar locking plate fixation of distal radius fractures. *J Hand Surg Asian Pac Vol.* 2019;24(1):30–35. doi:10.1142/S2424835519500061
- Lameijer CM, Ten Duis HJ, Dusseldorp IV, Dijkstra PU, van der Sluis CK. Prevalence of posttraumatic arthritis and the association with outcome measures following distal radius fractures in non-osteoporotic patients: A systematic review. *Arch Orthop Trauma Surg.* 2017;137(11):1499–1513. doi:10.1007/s00402-017-2765-0
- Toon DH, Premchand RAX, Sim J, Vaikunthan R. Outcomes and financial implications of intra-articular distal radius fractures: A comparative study of open reduction internal fixation (ORIF) with volar locking plates versus nonoperative management. *J Orthop Traumatol.* 2017;18(3):229–234. doi:10.1007/s10195-016-0441-8
- Rundgren J, Bojan A, Mellstrand Navarro C, Enocson A. Epidemiology, classification, treatment and mortality of distal radius fractures in adults: An observational study of 23,394 fractures from the national Swedish fracture register. *BMC Musculoskelet Disord.* 2020;21(1):88. doi:10.1186/s12891-020-3097-8

11. Hevonkorpi TP, Launonen AP, Huttunen TT, Kannus P, Niemi S, Mattila VM. Incidence of distal radius fracture surgery in Finns aged 50 years or more between 1998 and 2016: Too many patients are yet operated on? *BMC Musculoskelet Disord*. 2018;19(1):70. doi:10.1186/s12891-018-1983-0
12. Kelsey JL, Samelson EJ. Variation in risk factors for fractures at different sites. *Curr Osteoporos Rep*. 2009;7(4):127–133. doi:10.1007/s11914-009-0022-3
13. Kilic A, Ozkaya U, Kabukcuoglu Y, Sokucu S, Basilgan S. The results of non-surgical treatment for unstable distal radius fractures in elderly patients. *Acta Orthop Traumatol Turc*. 2009;43(3):229–234. doi:10.3944/AOTT.2009.229
14. Arora R, Gabl M, Gschwentner M, Deml C, Krappinger D, Lutz M. A comparative study of clinical and radiologic outcomes of unstable Colles type distal radius fractures in patients older than 70 years: Non-operative treatment versus volar locking plating. *J Orthop Trauma*. 2009;23(4):237–242. doi:10.1097/BOT.0b013e31819b24e9
15. Zengin EC, Ozcan C, Aslan C, Bulut T, Sener M. Cast immobilization versus volar locking plate fixation of AO type C distal radial fractures in patients aged 60 years and older. *Acta Orthop Traumatol Turc*. 2019;53(1):15–18. doi:10.1016/j.aott.2018.10.005
16. Filipova V, Lonžarić D, Jesenšek Papež B. Efficacy of combined physical and occupational therapy in patients with conservatively treated distal radius fracture: Randomized controlled trial. *Wien Klin Wochenschr*. 2015;127(Suppl 5):S282–S287. doi:10.1007/s00508-015-0812-9
17. Christensen OM, Kunov A, Hansen FF, Christiansen TC, Krasheninnikoff M. Occupational therapy and Colles' fractures. *Int Orthop*. 2001; 25(1):43–45. doi:10.1007/s002640000183
18. Yin SQ, Huang YP, Li MZ, Pan JD, Ding WQ, Wang X. Relationship between radiographic parameters and clinical outcomes of elderly patients with distal radius fractures [in Chinese]. *Zhongguo Gu Shang*. 2018;31(2):141–144. doi:10.3969/j.issn.1003-0034.2018.02.009
19. Zyluk A, Janowski P, Szlosser Z, Puchalski P. Percutaneous K-wires vs palmar locking plate fixation for different types of distal radial fractures: A comparison of the outcomes of two methods to control our guidelines. *Handchir Mikrochir Plast Chir*. 2018;50(5):319–325. doi:10.1055/a-0751-2886
20. Knirk JL, Jupiter JB. Intra-articular fractures of the distal end of the radius in young adults. *J Bone Joint Surg Am*. 1986;68:647–659. PMID:3722221.
21. Reid SA, Andersen JM, Vicenzino B. Adding mobilisation with movement to exercise and advice hastens the improvement in range, pain and function after non-operative cast immobilisation for distal radius fracture: A multicentre, randomised trial. *J Physiother*. 2020;66(2): 105–112. doi:10.1016/j.jphys.2020.03.010
22. Jakob M, Mielke S, Keller H, Metzger U. Results of therapy after primary conservative management of distal radius fractures in patients over 65 years of age. *Handchir Mikrochir Plast Chir*. 1999;31(4):241–247. doi:10.1055/s-1999-13532
23. Morasiewicz P, Dejneki M, Urbański W, Dragan S, Kulej M, Dragan SF. Radiological evaluation of ankle arthrodesis with Ilizarov fixation compared to internal fixation. *Injury*. 2017;48(7):1678–1683. doi:10.1016/j.injury.2017.04.013
24. Lameijer CM, Ten Duis HJ, Vrolijk D, Hartlief MT, El Moumni M, van der Sluis CK. Prevalence of posttraumatic arthritis following distal radius fractures in non-osteoporotic patients and the association with radiological measurements, clinician and patient-reported outcomes. *Arch Orthop Trauma Surg*. 2018;138(12):1699–1712. doi:10.1007/s00402-018-3046-2
25. Shimura H, Nimura A, Fujita K, Miyamoto T. Mid-term functional outcome after volar locking plate fixation of distal radius fractures in elderly patients. *J Hand Surg Asian Pac Vol*. 2018;23(2):238–242. doi:10.1142/S2424835518500273
26. Morasiewicz P, Konieczny G, Pawik Ł, Dragan S. Sport and physical activity in patients after derotational corticotomies with the Ilizarov method. *Acta Orthop Belg*. 2015;81(1):90–99. PMID:26280861.
27. Morasiewicz P, Dejneki M, Kulej M, et al. Sport and physical activity after ankle arthrodesis with Ilizarov fixation and internal fixation. *Adv Clin Exp Med*. 2019;28(5):609–614. doi:10.17219/acem/80258
28. Lutz M, Krappinger D, Wambacher M, Rieger M, Pechlaner S. Arthritis predicting factors in distal intraarticular radius fractures. *Arch Orthop Trauma Surg*. 2011;131(8):1121–1126. doi:10.1007/s00402-010-1211-3
29. Fan J, Jiang B, Yuan F, et al. Clinical effect of compound internal fixations in treating extreme distal radial fractures [in Chinese]. *Zhonghua Wai Ke Za Zhi*. 2016;54(10):766–771. doi:10.3760/cma.j.issn.0529-5815.2016.10.009

# Eculizumab treatment in pregnant women with paroxysmal nocturnal hemoglobinuria: A Polish experience

Jarosław Czyż<sup>1,A–D</sup>, Łukasz Szukalski<sup>1,B,C,E,F</sup>, Adriana Szukalska<sup>2,B,D</sup>, Bożena Katarzyna Budziszewska<sup>3,B,F</sup>, Ewa Lech-Marańda<sup>3,A,B,E</sup>, Joanna Zdziarska<sup>4,B,E</sup>, Tomasz Sacha<sup>4,A,B,E</sup>

<sup>1</sup> Clinic of Hematology, Ludwik Rydygier Collegium Medicum in Bydgoszcz, Nicolaus Copernicus University in Toruń, Poland

<sup>2</sup> Clinic of Hematology, Jan Biziel University Hospital No. 2 in Bydgoszcz, Poland

<sup>3</sup> Institute of Hematology and Transfusion Medicine, Warszawa, Poland

<sup>4</sup> Department of Hematology, Jagiellonian University Medical College, Kraków, Poland

A – research concept and design; B – collection and/or assembly of data; C – data analysis and interpretation;

D – writing the article; E – critical revision of the article; F – final approval of the article

Advances in Clinical and Experimental Medicine, ISSN 1899–5276 (print), ISSN 2451–2680 (online)

*Adv Clin Exp Med.* 2022;31(6):707–710

## Address for correspondence

Jarosław Czyż  
E-mail: jczyz@onet.pl

## Funding sources

None declared

## Conflict of interest

None declared

## Acknowledgements

We would like to thank Prof. Marek Hus for providing data of patients treated with eculizumab as a part of the Polish National Health Fund program.

Received on February 2, 2022

Reviewed on April 26, 2022

Accepted on June 1, 2022

Published online on June 14, 2022

## Abstract

**Background.** Eculizumab is an antibody targeting the C5 complement protein. Clinical trials suggest that eculizumab significantly reduces transfusion requirements and prevents disease complications in patients with paroxysmal nocturnal hemoglobinuria (PNH).

**Objectives.** To analyze the outcome of pregnancies among Polish women with PNH treated with eculizumab as a part of the Polish National Health Fund program.

**Materials and methods.** We report the outcomes of 3 pregnancies among women treated with eculizumab between 2017 and 2020. For 1 of these woman, it was the 1<sup>st</sup> pregnancy, while the remaining 2 patients had previously had 1 previous successful pregnancy each.

**Results.** All 3 mothers survived pregnancy, and all children were born alive. One of the patients had a vaginal delivery. Another required cesarean delivery at the 34<sup>th</sup> week due to a decreasing platelet count. In 1 case, premature rupture of the fetal membranes occurred at week 36, followed by artificial labor induction. All children were born without any inborn defects. The 2 prematurely born babies required a prolonged hospital stay.

**Conclusions.** Treatment with eculizumab seems to reduce the risk to a mother and a child associated with PNH. However, more data are necessary to confirm this notion.

**Key words:** pregnancy, eculizumab, PNH

## Cite as

Czyż J, Szukalski Ł, Szukalska A, et al. Eculizumab treatment in pregnant women with paroxysmal nocturnal hemoglobinuria: A Polish experience. *Adv Clin Exp Med.* 2022;31(6):707–710. doi:10.17219/acem/150600

## DOI

10.17219/acem/150600

## Copyright

Copyright by Author(s)

This is an article distributed under the terms of the Creative Commons Attribution 3.0 Unported (CC BY 3.0) (<https://creativecommons.org/licenses/by/3.0/>)

## Background

Paroxysmal nocturnal hemoglobinuria (PNH) is an uncommon, acquired clonal disorder characterized by venous and arterial thromboembolism, chronic hemolysis, and a broad spectrum of other symptoms related to terminal complement activation.<sup>1</sup> The progressive character of the disease seriously affects the prognosis, with a median survival varying from 1 to 3 decades.<sup>2,3</sup> Pregnancy among affected women has been universally discouraged due to the tendency for the disease to aggravate hemolysis, and because of transfusion requirements and an increased risk of thromboembolic complications.<sup>4</sup> In some reports, maternal mortality is as high as 20%, with most deaths observed postpartum.<sup>5</sup> Fetal morbidity and mortality are also high, reaching nearly 10%, primarily due to premature births.<sup>2–6</sup>

Eculizumab is a humanized IgG2/4 antibody targeting the C5 complement protein. It blocks complement cleavage to C5a and C5b.<sup>7</sup> Clinical trials suggest that eculizumab treatment in patients with PNH significantly reduces transfusion requirements, prevents disease complications and improves the quality of life.<sup>8–10</sup> There are limited data regarding the management of pregnant patients with eculizumab. The published series differ regarding the timing of the introduction of eculizumab, administered doses, infusion frequencies, and the type of anticoagulation used.<sup>11–18</sup>

## Objectives

Pregnancy among women with PNH has been discouraged due to the risk of thromboembolic complications in mothers and significant fetal morbidity and mortality. However, there are only sporadic reports describing the treatment results in pregnant women in the era of monoclonal antibody-controlled PNH. Therefore, this study aimed to assess the risks related to pregnancy pregnancy for mothers while being treated with eculizumab, as well as risks for babies, and to consider possible changes in the recommendations regarding pregnancy among affected women.

## Materials and methods

Information was collected from 3 patients who became pregnant during treatment with eculizumab or started treatment while pregnant between 2017 (the beginning of the Polish National Health Fund program) and 2020. They were selected from a total of 74 patients who qualified for the eculizumab treatment program. Among the treated patients, there were 46 females, 28 of whom were younger than 55 years. The treating physician provided detailed information about each patient. Eculizumab was administered using the standard treatment protocol: 600 mg intravenously weekly for the first 4 weeks, followed by 900 mg intravenously every 2 weeks.

Despite the retrospective nature of the study, the protocol had to receive approval from the Bioethics Committee of Collegium Medicum, Nicolaus Copernicus University in Toruń, Poland (approval No. KB 674/2021), and the study was performed in compliance with the Declaration of Helsinki.

## Results

The 1<sup>st</sup> patient was diagnosed with a mild form of aplastic anemia at the age of 26. At that time, the PNH granulocyte clone size was 3.8%. Before the treatment with eculizumab started, she had had 1 successful pregnancy. At the time of her 2<sup>nd</sup> pregnancy, her PNH clone increased to 38.9%; thus, the treatment with eculizumab was introduced at week 20. She was also receiving prophylactic enoxaparin. A drop in the platelet count occurred after the initiation of eculizumab, reaching a nadir of  $17 \times 10^9/L$  at the time of delivery. Otherwise, her pregnancy remained uncomplicated. She had a vaginal delivery in the 39<sup>th</sup> week with platelet transfusion support. No complications were observed during the postpartum period.

The 2<sup>nd</sup> patient was diagnosed with PNH with the presence of a 20.6% PNH clone at the 25 years of age. Soon after the diagnosis was established, the patient started treatment with eculizumab due to an aggravation of anemia. Later on, she developed immune thrombocytopenia that required steroid treatment. A bone marrow biopsy ruled out aplastic anemia. One year after diagnosis, she became pregnant and, at that time, the PNH clone increased to 24.1%. She continued the eculizumab infusions throughout her pregnancy. Artificial labor induction was necessary due to a premature rupture of the fetal membranes at week 36.

The 3<sup>rd</sup> patient was diagnosed before her pregnancy at the age of 30. Previously, she had had 1 successful pregnancy despite not being treated with eculizumab. At the time of her 2<sup>nd</sup> pregnancy, she had already started eculizumab treatment with the standard dose. She received anticoagulation prophylaxis with low-dose aspirin alone. At week 34, she had an uncomplicated cesarean section due to a falling platelet count. None of the above patients required blood transfusion during pregnancy.

All children were born without any inborn defects and scored 10 points on the Apgar scale. Two prematurely born babies (born at weeks 36 and 34) required a prolonged hospital stay. Their birth weight was 2650 g and 1920 g, respectively. The third baby (2830 g) born at week 39 was discharged as planned.

## Discussion

The introduction of eculizumab for the treatment of PHN allows affected patients to lead a relatively normal life and start a family. In this study, we confirm the safety

of eculizumab treatment during pregnancy both in mothers and their babies, with minimal morbidity observed. All our patients gave birth to healthy babies. No significant maternal mortality was observed in the patients treated with eculizumab, which means a certain progress in comparison with the pre-eculizumab era. De Guibert et al. observed 2 fatal postpartum thromboses among 27 pregnancies in 22 women at 10 French Society of Hematology centers between 1978 and 2008.<sup>5</sup> In other retrospective series, the percentage of fatalities among mothers related to thrombosis ranged from 11.6% to 22.2%.<sup>6,19</sup> Fetal mortality in the same groups varied from 4% to 7.2%. The introduction of eculizumab resulted in a substantial improvement in the pregnancies of affected mothers. Kelly et al. summarized a questionnaire survey investigating the outcome of pregnancies in 75 patients with PNH treated with eculizumab, which was reported to the International PNH Interest Group and Registry.<sup>11</sup> No maternal deaths occurred, and only 2 episodes of postpartum thrombosis were reported. Maternal thrombocytopenia and premature rupture of the fetal membranes were the leading causes of premature birth in 2 of our patients. In the report to the International PNH Interest Group and Registry, premature births occurred in 29% of cases (22 of 75 pregnancies). Thrombocytopenia that resulted in replacing enoxaparin with aspirin monotherapy did not cause any thrombotic complications. It resulted in premature cesarean sections, but otherwise was uncomplicated. Thrombocytopenia is common in pregnancy, affecting 27% of patients, and often requires platelet transfusions.<sup>19</sup> We did not observe any significant worsening of anemia with the aggravation of hemolysis that would have required an increase in the dose of eculizumab in any of the patients. No thrombotic complications were observed, possibly due to the decreased platelet count in our patients. The morbidity observed among babies was related to prematurity. According to data from the UK, the prevalence of premature births among patients with PNH is 4 times higher than in the normal population.<sup>11</sup> The most frequent causes of premature delivery were planned cesarean delivery, a decreased maternal platelet count, intrauterine growth retardation, and preeclampsia. In the group described by Kelly et al., fetal morbidity and mortality remained high despite eculizumab treatment, with 3 deaths (4%) and 2 stillbirths from the same mother, and the loss of a twin in another pregnancy.<sup>11</sup> In our study, 2 out of 3 babies were born prematurely and required a prolonged hospital stay.

## Limitations

Despite the fact that all the pregnant patients treated with eculizumab found by National Health Fund were included in the study, the number of patients remains limited. Only an international collaboration could provide more data regarding this critical subject. On the other hand, even a limited number of patients can provide vital information that will influence our clinical practice.

## Conclusions

Based on our observations and the previous data, we can assume that treatment with eculizumab can be used safely in pregnant women with PNH. This treatment reduces the risk of maternal morbidity and mortality. However, more evidence is required regarding the use of eculizumab and other C5 inhibitors in this setting.

## ORCID iDs

Jarosław Czyż  <https://orcid.org/0000-0002-4178-7837>  
 Łukasz Szukalski  <https://orcid.org/0000-0002-9885-5140>  
 Adriana Szukalska  <https://orcid.org/0000-0002-5533-4484>  
 Bożena Katarzyna Budziszewska  <https://orcid.org/0000-0002-9482-4099>  
 Ewa Lech-Marańda  <https://orcid.org/0000-0001-9592-0851>  
 Joanna Zdziarska  <https://orcid.org/0000-0001-6435-7613>  
 Sacha Tomasz  <https://orcid.org/0000-0002-7207-6595>

## References

- Hillmen P, Lewis SM, Bessler M, Luzzatto L, Dacie JV. Natural history of paroxysmal nocturnal hemoglobinuria. *N Engl J Med*. 1995;333(19):1253–1258. doi:10.1056/NEJM199511093331904
- de Latour RP, Mary JY, Salanoubat C, et al. Paroxysmal nocturnal hemoglobinuria: Natural history of disease subcategories. *Blood*. 2008;112(8):3099–3106. doi:10.1182/blood-2008-01-133918
- Nishimura JI, Kanakura Y, Ware RE, et al. Clinical course and flow cytometric analysis of paroxysmal nocturnal hemoglobinuria in the United States and Japan. *Medicine (Baltimore)*. 2004;83(3):193–207. doi:10.1097/01.md.0000126763.68170.46
- Bais J, Pel M, von dem Borne A, van der Lelie H. Pregnancy and paroxysmal nocturnal hemoglobinuria. *Eur J Obstet Gynecol Reprod Biol*. 1994;53(3):211–214. doi:10.1016/0028-2243(94)90121-x
- de Guibert S, de Latour RP, Varoquaux N, et al. Paroxysmal nocturnal hemoglobinuria and pregnancy before the eculizumab era: The French experience. *Haematologica*. 2011;96(9):1276–1283. doi:10.3324/haematol.2010.037531
- Fieni S, Bonfanti L, Gramellini D, Benassi L, Delsignore R. Clinical management of paroxysmal nocturnal hemoglobinuria in pregnancy: A case report and updated review. *Obstet Gynecol Surv*. 2006;61(9):593–601. doi:10.1097/01.ogx.0000234794.27485.59
- Parker C. Eculizumab for paroxysmal nocturnal haemoglobinuria. *Lancet*. 2009;373(9665):759–767. doi:10.1016/S0140-6736(09)60001-5
- Hillmen P, Hall C, Marsh JCW, et al. Effect of eculizumab on hemolysis and transfusion requirements in patients with paroxysmal nocturnal hemoglobinuria. *N Engl J Med*. 2004;350(6):552–559. doi:10.1056/NEJMoa031688
- Brodsky RA, Young NS, Antonioli E, et al. Multicenter phase 3 study of the complement inhibitor eculizumab for the treatment of patients with paroxysmal nocturnal hemoglobinuria. *Blood*. 2008;111(4):1840–1847. doi:10.1182/blood-2007-06-094136
- Hillmen P, Young NS, Schubert J, et al. The complement inhibitor eculizumab in paroxysmal nocturnal hemoglobinuria. *N Engl J Med*. 2006;355(12):1233–1243. doi:10.1056/NEJMoa061648
- Kelly RJ, Höchsmann B, Szer J, et al. Eculizumab in pregnant patients with paroxysmal nocturnal hemoglobinuria. *N Engl J Med*. 2015;373(11):1032–1039. doi:10.1056/NEJMoa1502950
- Sharma R, Keyzner A, Liu J, Bradley T, Allen SL. Successful pregnancy outcome in paroxysmal nocturnal hemoglobinuria (PNH) following escalated eculizumab dosing to control breakthrough hemolysis. *Leuk Res Rep*. 2015;4(1):36–38. doi:10.1016/j.lrr.2015.05.001
- Patriquin C, Leber B. Increased eculizumab requirements during pregnancy in a patient with paroxysmal nocturnal hemoglobinuria: Case report and review of the literature. *Clin Case Rep*. 2015;3(2):88–91. doi:10.1002/ccr3.161
- Gesson G, Canistro R, Bergamini L, et al. Postpartum thrombotic complication in a patient with paroxysmal nocturnal hemoglobinuria. *Blood Coagul Fibrinolysis*. 2015;26(4):458–463. doi:10.1097/MBC.0000000000000250

15. Miyasaka N, Miura O, Kawaguchi T, et al. Pregnancy outcomes of patients with paroxysmal nocturnal hemoglobinuria treated with eculizumab: A Japanese experience and updated review. *Int J Hematol*. 2016;103(6):703–712. doi:10.1007/s12185-016-1946-x
16. Patel A, Unnikrishnan A, Murphy M, et al. Paroxysmal nocturnal hemoglobinuria in pregnancy: A dilemma in treatment and thromboprophylaxis. *Case Rep Hematol*. 2017;2017:7289126. doi:10.1155/2017/7289126
17. Vekemans MC, Lambert C, Ferrant A, et al. Management of pregnancy in paroxysmal nocturnal hemoglobinuria on long-term eculizumab. *Blood Coagul Fibrinolysis*. 2015;26(4):464–466. doi:10.1097/MBC.0000000000000248
18. Kelly R, Arnold L, Richards S, et al. The management of pregnancy in paroxysmal nocturnal haemoglobinuria on long term eculizumab. *Br J Haematol*. 2010;149(3):446–450. doi:10.1111/j.1365-2141.2010.08099.x
19. Ray JG, Burows RF, Ginsberg JS, Burrows EA. Paroxysmal nocturnal hemoglobinuria and the risk of venous thrombosis: Review and recommendations for management of the pregnant and nonpregnant patient. *Haemostasis*. 2000;30(3):103–117. doi:10.1159/000022532